Removal of Dimethyl Phthalate, Diethyl Phthalate, Bisphenol-A, and Dimethyl Sulfoxide from Water by Ozone Microbubbles

A thesis submitted in

partial fulfilment of the requirement for the degree of

DOCTOR OF PHILOSOPHY

by

Abdisa Jabesa

Department of Chemical Engineering

Indian Institute of Technology Guwahati

Guwahati – 781039, Assam, India

April 2021

Removal of Dimethyl Phthalate, Diethyl Phthalate, Bisphenol-A, and Dimethyl Sulfoxide from Water by Ozone Microbubbles

A thesis submitted in

partial fulfilment of the requirement for the degree of

DOCTOR OF PHILOSOPHY

by

Abdisa Jabesa

Department of Chemical Engineering

Indian Institute of Technology Guwahati

Guwahati – 781039, Assam, India

April 2021

Dedicated

to

My Mother

Indian Institute of Technology Guwahati

Department of Chemical Engineering

STATEMENT

I hereby declare that the content embodied in this thesis titled **"Removal of Dimethyl Phthalate, Diethyl Phthalate, Bisphenol-A, and Dimethyl Sulfoxide from Water by Ozone Microbubbles"** is the result of investigations carried out by me at the Department of Chemical Engineering, Indian Institute of Technology Guwahati, Guwahati, India, under the supervision of **Prof. Pallab Ghosh**.

In keeping with the general practice of reporting scientific observations, due acknowledgments have been made on the findings of other investigators, wherever the work described is based.

Guwahati
April 2021

Abdisa Jabesa

Indian Institute of Technology Guwahati

Department of Chemical Engineering

CERTIFICATE

It is certified that the work described in this thesis titled **"Removal of Dimethyl Phthalate, Diethyl Phthalate, Bisphenol-A, and Dimethyl Sulfoxide from Water by Ozone Microbubbles"** by Mr. Abdisa Jabesa for the award of the degree of Doctor of Philosophy is an authentic record of the results obtained from research work carried out under my supervision at the Department of Chemical Engineering, Indian Institute of Technology Guwahati, Guwahati, India, and this work has not been submitted elsewhere for a degree.

Dr. Pallab Ghosh
Professor
Department of Chemical Engineering
IIT Guwahati, Guwahati – 781039
Assam, India

ACKNOWLEDGMENTS

Primarily, I am grateful to the Almighty God for His love and help in all aspects of my life. This doctoral thesis was completed under the devoted guidance and supervision of **Prof. Pallab Ghosh.** I would like to express my sincere gratitude to him for introducing me to work in such a fascinating area of research. I am also grateful also for his continuous guidance and immense support, scientific discussions, important bits of advice, and encouragements, which helped me to finish this work. I am very thankful to him for his enormous efforts on correcting all my mistakes, and making my work and research publications more valuable.

I would also like to thank **Prof. Pughazenti G., Prof. Mahuya De, Prof. Bishnupada Mandal, Prof. Dipankar Bandyopadhyay, and Prof. Ramgopal Uppaluri** for their research-oriented teaching during my coursework. I also thank **Prof. Bishnupada Mandal** and **Prof. Anugrah Singh**, Heads, Department of Chemical Engineering, for their administrative support. Furthermore, I must thank all the technical staffs of my department, especially, **Mr. Harsaraj Biswanath**, **Mr. Prasun Bhattacharjee**, **Dr. Kaustavmoni Deka**, **and Dr. Lukumani Borah** for their kind help.

I would like to thank my friends at IIT Guwahati for helping me out on several occasions. I deeply acknowledge my research-group members **Dr. Snigdha Khuntia**, **Dr. Badri Vishal**, **Dr. Shailesh Varade**, **Mr. Jinesh Machale**, **and Mr. Awadh Kishor Kumar**. Particularly, the professional help of **Dr. Khuntia**, my senior, was invaluable during the early stages of my research work. I would also like to thank my friends, **Dr. Ali Shemsedin**, **Dr. Melakuu Tesfaye**, **Dr. Kibrom Alebel**, **Dr. Abdulkerim Bedawi**,

Dr. Randeep Singh, **Mr. Abebe Moges**, **Mr. Fekadu Mosissa**, **and Mr. Habtom Teklu**, who have made my stay pleasant at IIT Guwahati.

Saving the best for the last, I am forever indebted to my parents, and friends in Ethiopia, **Jabu and Daa**, **Getch and Daa**, **Tade and Tg**, **Toli and Dare**, **Waktol and Kaku**, **Tiba and Dure**, **Fiqe and Ebo**, **Dr. Endalu (General)**, **Dr. Abdi (Boss)**, **and Dr. Habtish (Boss)**, who are the reason behind my great education. They have been a source of love and encouragement for me, and without their emotional support, it would have been impossible for me to stay away from home all this time. Finally, I would like to thank my beloved wife **Mrs. Barkot Tadesse** for her love and support, which kept my morale high during this long journey with ups and downs. It would also be unfair to forget mentioning the precious gift of my life, my baby boy, **Master Anhanis Abdisa**, who has joined us during this long journey. Praise to God for all His help and His blessing gift.

Abdisa Jabesa

ABSTRACT

Ozone microbubbles (OMBs) have been widely used nowadays for water/wastewater treatment. Properties of ozone, its applications in water/wastewater treatment, properties of the ozone microbubbles, and their applications in water/wastewater treatment have been discussed in this thesis.

The environmental fate of the phthalates is considerably important due to their effects on the health of human beings and animals. Dimethyl phthalate (DMP) and diethyl phthalate (DEP) are among the most frequently identified phthalates in diverse environments. The removals of DMP and DEP from water using OMBs were studied in an experimental setup with a reactor of 20 dm^3 capacity. Experiments were performed under various reaction conditions to examine the effects of the initial concentration of the pollutants, pH of the medium, and ozone generation rate. The DMP present in water was effectively removed by the OMBs. The removal was effective in neutral and alkaline media. Increase in the initial concentration of the DMP adversely affected its removal efficiency. The removal efficiency dramatically increased from 1 to 99% when the ozone generation rate was increased from 0.28 to 1.94 mg s^{-1} at pH 7. The total organic carbon (TOC) measurements revealed that complete mineralization of DMP was achieved within 1.8 ks at the high ozone feed rate. The use of *tert*-butanol (*t*-BuOH) as the hydroxyl radical (·OH) scavenger confirmed that the reaction between DMP and ·OH dominated over its direct reaction with ozone. The reaction between DMP and ozone followed an overall second-order kinetics. The volumetric mass transfer coefficient of ozone in the reacting system and the enhancement factor increased with increasing initial concentration of DMP. The Hatta number was low, which proves that the mass transfer resistance was negligible, implying that the rate of mass transfer was enhanced by the

OMBs. The removal of DEP by the OMBs was very effective at the high pH and high ozone generation rates. Almost complete mineralization of DEP could be achieved at the high pH. In neutral and alkaline media, the reaction of DEP with ·OH dominated over its direct reaction with ozone. The overall oxidation reaction fitted a second-order kinetic model. The optimal addition of H_2O_2 increased the rate of removal of the pollutants by augmenting the generation of the ·OH.

Oxidation of bisphenol-A (BPA) in the aqueous medium was performed using OMBs. The removal efficiency of BPA was improved from 41 to 98% within 600 s of ozonation when the initial pH of the medium was increased from 3 to 7. Further increase of pH led to an insignificant improvement in the ozonation time (i.e., it did not significantly lessen the ozonation time to achieve the same removal efficiency). The stoichiometric ratio of the moles of ozone consumed to the moles of BPA removed was found to be in the range of 0.228 – 0.276 at pH 7 and 0.125 mol m^{-3} initial concentration of BPA. A considerably high range of ozone utilization efficiency (i.e., 52.4 – 86.3%) for the complete removal of BPA was achieved by using the OMBs. Based on the TOC removal, three stages of ozonation (i.e., 0 – 0.6, 0.6 – 2.5, and 2.5 – 3.0 ks) were observed. Their corresponding observed reaction rate constants were 294.1, 1365.3, and 2477.7 dm^3 mol^{-1} s^{-1}, respectively. The reaction between ozone and BPA followed an overall second-order kinetics, and first-order with respect to both ozone and BPA.

The potential of the OMBs for the oxidation of DMSO was investigated in detail, and the results were compared with those of the conventional ozonation using the ozone millibubbles (OMLBs). Keeping constant other operational parameters for both the oxidation systems, the OMLBs needed a longer time for complete removal of DMSO, and hence necessitated a higher consumption of ozone. Therefore, a higher stoichiometric

ratio of ozone consumed to the DMSO removed (i.e., a factor of 10) was observed for the OMLBs. Higher ozone utilization efficiencies were observed for the OMBs (i.e., 65 – 79%) than the OMLBs (i.e., 21 – 48%). The degradation of DMSO to methane sulfonic acid (MSA) was achieved via two possible pathways (i.e., direct conversion to MSA by the reaction with ·OH, and a two-stage conversion via the formation of $DMSO_2$ by molecular ozone, followed by further oxidation of $DMSO_2$ to MSA by the ·OH). In terms of the TOC removal efficiency, the effectiveness was in the following order: OMLBs < OMLBs/H_2O_2 < OMBs < OMBs/H_2O_2. Oxidation of DMSO by ozone followed an overall second-order kinetics for the OMBs, and first-order kinetics for the OMLB system. Higher ozone volumetric mass transfer coefficient, enhancement factor, and volumetric ozone transfer rate were obtained for the OMBs as compared to the OMLBs.

CONTENTS	Page no.

LIST OF FIGURES

LIST OF TABLES

CHAPTER 1

INTRODUCTION

This chapter presents a general discussion on ozone and its application in water/wastewater treatment. The properties of the microbubbles and their applications in water/wastewater treatment are also discussed. A brief review of the literature for each target pollutant (studied in this work) is presented. The objectives of the research work and the organization of the thesis are also outlined in this chapter.

1.1 Background

In recent times, new advances in the diverse technologies for meeting the ever-increasing human needs have led to the emergence of new pollutants in the effluent streams of the process industries, which are not easily degraded by the conventional wastewater treatment methods. Industrial wastewaters are becoming more and more complex due to the presence of these emerging contaminants. Among these emerging contaminants, the organic pollutants are more recalcitrant and pose serious problems. These pollutants bring severe problems even at low concentrations and lead to comprehensive chemical, physical, and biological changes in the quality of water. Organic compounds released from various industries (e.g., dyes, pharmaceuticals, and food products), farmlands (e.g., pesticides), and domestic applications (e.g., surfactants and detergents) have attracted high attention. The removal of organic compounds from aqueous solutions has become an important goal in the treatment of water and wastewater because of increased industrial production of waste streams containing harmful organic compounds (Shin et al., 1999). With rapid growth of population and diminishing water resources, the need of treated

drinking water and safe environment has become an important issue. Hence, researchers are inclined towards environment-friendly technologies in which such toxic and harmful organic compounds are either totally eliminated or degraded to less harmful intermediates/end products. New technologies have been developed in the last couple of decades to degrade such pollutants as a result of the inadequacies of the conventional wastewater treatment methods. In these aspects, emerging treatment technologies such as the advanced oxidation processes (AOPs) hold great promise as alternative and efficient methods (Comninellis et al., 2008; Cuerda-Correa et al., 2020).

Among the common disinfectants, chlorine has been widely used all over the world in the conventional water and wastewater treatment to prevent waterborne transmission of infectious diseases. However, chlorine reacts readily with a wide variety of organics to form organic by products, mainly trihalomethanes and haloacetic acids (Li, 2006; Von Gunten, 2003b; Yang et al., 2005b). These chlorination by products have been associated with adverse health effects related to cancer and reproductive health concerns (Nieuwenhuijsen et al., 2000). Most of the conventional wastewater treatment methods are reported to be incapable of removing many biorecalcitrant organic pollutants (Saravanan et al., 2009), which means that new efficient alternative treatment technologies are needed for degrading such pollutants.

Ozone, an allotropic form of oxygen, has long been used in wastewater treatment and came into use as a drinking water disinfectant more than a century ago (Glaze, 1987). Since then, several water treatment plants have been developed all over the world using ozone. Some have used ozone as the primary or sole disinfectant. Others have used it as an oxidant for the control of odor, color, and flora, and for reducing the manganese and iron in drinking water. Moreover, ozone can be used as a natural water coagulant (e.g., a pre-oxidant) to improve the efficiency of other unit operations such as coagulation,

flocculation, sedimentation, and carbon filtration. It can also be used to remove biological or toxic compounds for improving the biological oxidation units (i.e., reducing the amount of sludge generated) (Glaze, 1987; Hoigne and Bader, 1979).

It has been reported (Tiwari et al., 2010) that ozone is one of best green alternatives to the conventional fumigants in grain processing. Ozone is known for its considerable potential for the treatment of water and wastewater since it is a very powerful eco-friendly (i.e., residue free) oxidant (Gottschalk et al., 2010; Loeb et al., 2012; von Sonntag and von Gunten, 2012). It has a standard redox potential of +2.07 V, and can react with many organic chemicals with the exception of a few, which react very slowly with molecular ozone (e.g., chloro alkanes) (Glaze, 1986). For those chemicals, more effective AOPs are used, some of which consist of a combination of single oxidants and involve the generation of the hydroxyl radicals. AOPs are the aqueous phase oxidation processes, which are primarily based on the involvement of the hydroxyl radicals in the mechanism leading to the destruction of the target pollutant or xenobiotic or contaminant compound. The hydroxyl radical is an extremely strong and nonselective oxidant with a standard redox potential of +2.80 V (Masten and Davies, 1994). They react with most organic compounds with rate constants in the range of 10^{7}–10^{10} dm^{3} mol^{-1} s^{-1} (Buxton et al., 1988).

It has been reported by various researchers (Gurol, 1985; Shin et al., 1999; Zhou and Smith, 2000) that ozonation in the water and wastewater treatment systems is controlled by mass transfer, and the most effective way to overcome this limitation is to increase the gas–liquid interfacial area available for mass transfer by decreasing the size of the ozone bubbles dispersed in the aqueous medium. Transfer of ozone to water is a very important step in the water and wastewater treatment reactors, such as the bubble column reactors. Usually ozone is introduced into the reactors as a dilute gas mixture in

oxygen. Ozone is sparingly soluble in water (Johnson and Davis, 1996; Silva and Jardim, 2006). Because of their less ability of dissolving ozone in water, millibubbles used in the bubble column reactors require a considerable amount of ozone, which requires high-energy consumption. The excess ozone passed into the column remains unused, which is finally destructed or released into the atmosphere as is. Therefore, a better gas–liquid contactor is required that can enhance the solubility of ozone in water, perform rapid oxidation of the organic compounds, and decrease the loss of ozone. In this regard, microbubbles can offer an alternative to the millibubbles. They are very effective in increasing the rate of transfer of ozone to water (i.e., enhance the solubility of ozone), and decrease its loss. A small amount of ozone is sufficient to produce a large number of microbubbles that are capable of oxidizing the organic compounds present in water. The dissolved ozone in the dispersion of ozone microbubbles (OMBs) generates the hydroxyl radicals that are highly effective in decomposing the organic molecules (Sumikura et al., 2007; Takahashi et al., 2007a). The hydroxyl radicals are generated in the solutions by the collapse of the OMBs (Chu et al., 2008b). During the decomposition of ozone, the generation of the hydroxyl radicals is an advantage, because it is a more powerful oxidant than ozone.

Daughton (2004) has reported that nearly 23 million organic and inorganic substances have been indexed by the Chemical Abstracts Service of The American Chemical Society, excluding the biosequences such as proteins and nucleotides. From approximately 3000 different estimated substances used as pharmaceutical ingredients, only a small subset has been investigated in environmental studies so far (Richardson and Ternes, 2014). This shows that further investigations are necessary. Several studies have confirmed the efficiency of oxidation processes, such as ozonation and advanced oxidation for the transformation/degradation/removal of micropollutants. In recent years,

microbubble technologies have become a key aspect of improving ozonation and ozone-based advanced oxidation processes. Although several research works have been performed in the past few decades on the ozonation of water/wastewater containing various organic pollutants, most of these works have been done by using conventional millibubbles. The size of the millibubbles depends on the gas sparger used, and it usually varies in the range of 2 – 5 mm. On the other hand, a few works have used microbubbles. The microbubbles have diameter less than 100 μm (Tsuge, 2014). A few fundamental issues related to the ozone-based microbubble technology have remained as a subject of further research.

1.2 Ozone and its application in wastewater treatment

Ozone has a high redox potential, due to which it a strong oxidizing agent. It is widely applied in water treatment as an oxidizing agent. The main uses of ozonation are decolorization, elimination of taste and odor, degradation of organics, and disinfection. The potential application points of ozone in the municipal wastewater treatment plants, which include odor control, pre-oxidation of primary effluent, disinfection of secondary effluent, and sludge conditioning are shown in a generalized process flow diagram in Figure 1.1 (Oneby et al., 2010).

Ozone spontaneously self-decomposes to oxygen within a short time so that it does not remain dissolved in water. This feature has rendered ozone a desirable oxidizing agent for removing the impurities present in water. However, factors such as the cost of ozone production and the expenditure incurred in the maintenance of equipment (due to heavy corrosion caused by ozone) have restricted its use in the developing countries. Because of its instability, ozone must be generated at the point of use. An overview of various types ozone generation methods are summarized in Table 1.1 (Gottschalk et al.,

2010). Any method of generation of ozone relies on the energy required to break the bonds holding the oxygen atoms in the O_2 molecule, allowing them to dissociate and then re-form as ozone molecule (i.e., O_3).

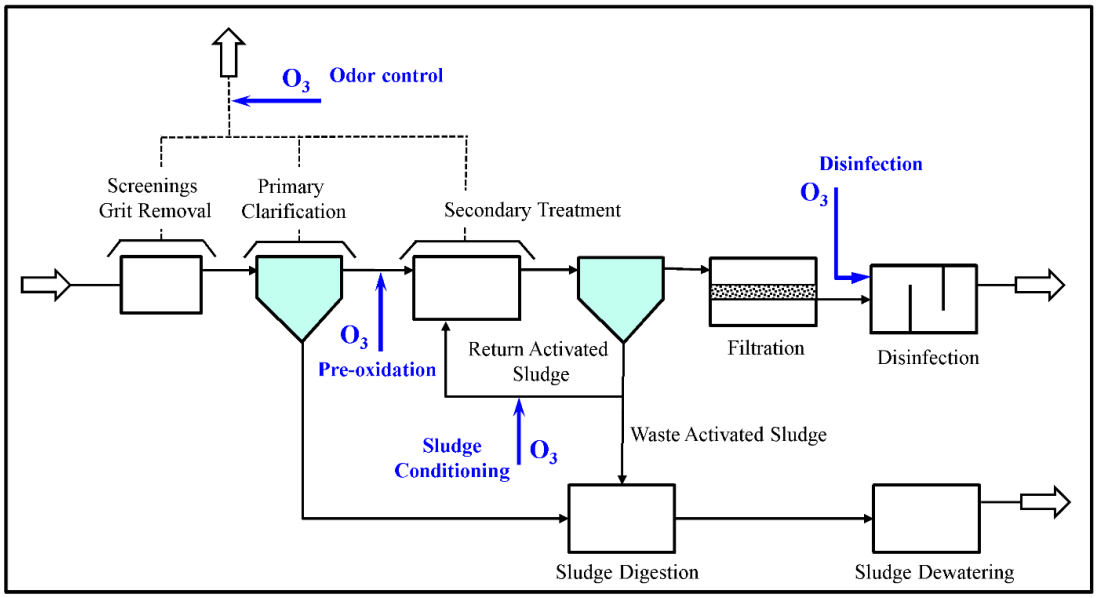

Figure 1.1: Potential ozone application points in municipal wastewater plants (Oneby et al., 2010).

For industrial consumption, ozone is usually generated from an oxygen-containing gas by the silent electric discharge method (Magara et al., 1995), which is also known as *corona discharge*. In this method (Ciambrone, 1976; Gottschalk et al., 2010; Shin et al., 1999), pure oxygen is subjected to an electrical discharge (Figure 1.2). The oxygen molecules in the gas are dissociated and form ozone molecules by the electrons that are created from the electrical discharge. Power is supplied in the form of high alternating current, creating ionized gas in the space between the two electrodes. Currently, this method is the most widely used method for commercial ozone production.

Table 1.1: An overview of the ozone generation methods, working principles, and fields of application

Method of ozone generation	Ozone source	Working principle	Field of application
Electrical	Air or oxygen	Electrical discharge	Common standard from laboratory to full-scale
Electrochemical	Highly purified water	Electrolysis	Mainly for pure water applications, and laboratory to small industrial scale
Photochemical ($\lambda < 185$ nm)	Oxygen (air) and water (drinking water or highly purified water)	Irradiation (abstraction of electrons)	New technology, laboratory to full-scale
Radiation Chemistry	Highly purified water	X - rays, γ - rays, and radioactive	Laboratory scale
Thermal	Water	Light arc ionization	Laboratory scale

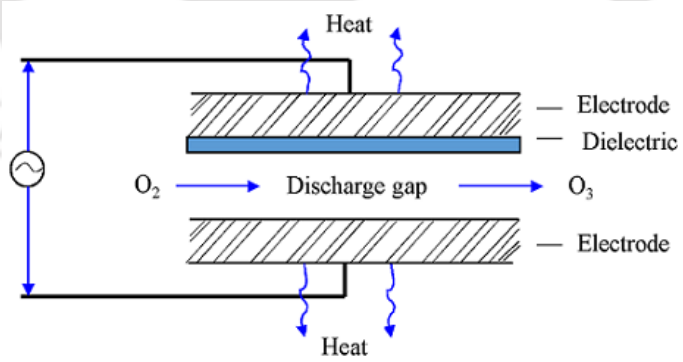

Figure 1.2: Schematic diagram of ozone generation by corona discharge.

The other recognized methods are electrochemical, photochemical, and radiochemical methods. In the photochemical generation method, ozone is generated by

means of ultraviolet light ($\lambda < 200$ nm), which is generated by arc discharge lamps, in a similar fashion as the formation of ozone in the upper atmosphere. This method of ozone generation may be used only for small-scale systems inasmuch as it cannot generate ozone concentration as much as the corona-discharge ozone generators (Glaze, 1987). An electrochemical ozone generator is used to generate highly concentrated ozone dissolved in water by applying a direct current, for small scale application, which is simple and safe for the users (Nishiki et al., 2011). Ozone has a wide range of applications, which varies from destroying microorganisms, improving ventilation of buildings, and cleaning and sterilizing drinking water and wastewater (Gonçalves, 2009; Gottschalk et al., 2010).

The reaction between ozone and a target pollutant in the aqueous phase is known to be a complex process. It involves direct reaction with molecular ozone and/or an indirect reaction in which hydroxyl radicals form during the auto-decomposition of ozone (Magara et al., 1995; Staehelin and Hoigne, 1985; von Gunten, 2003a), and react with the pollutant. Classification of wastewater components in terms of reactivity with ozone is not an easy task. Generally, a high concentration of pollutants may lead to a high reactivity with ozone, which is an indication of a fast kinetic regime, and direct reaction with ozone. Low concentration of pollutants usually means low ozone reactivity, and hence, a factor that favors the development of indirect reactions of ozone (Beltrán, 2004). It is apparent that whenever conclusions are to be made on the formation of products of ozonation, it is absolutely necessary to consider the extent of direct reaction of ozone with the pollutant, and the indirect reactions by the hydroxyl radicals, which are generated *in situ* (Staehelin and Hoigne, 1985). The decomposition of ozone in water takes place via a series of initiation, propagation, and termination steps. The mechanism of

decomposition of ozone in pure water is summarized in Table 1.2 (Beltrán, 2004; Kasprzyk-Hordern et al., 2003; Khuntia et al., 2012a).

Table 1.2: Mechanism of decomposition of ozone in pure water

	Reaction	Rate constant
Initiation	$O_3 + OH^- \rightarrow HO_2^- + O_2^- \cdot$	70 $dm^3\ mol^{-1}\ s^{-1}$
Propagation	$HO_2 \cdot \rightarrow O_2^- \cdot + H^+$	$7.9\times10^5\ s^{-1}$
	$O_2^- \cdot + H^+ \rightarrow HO_2 \cdot$	$5.0\times10^{10}\ dm^3\ mol^{-1}\ s^{-1}$
	$O_3 + O_2^- \cdot \rightarrow O_3^- \cdot + O_2$	$1.6\times10^9\ dm^3\ mol^{-1}\ s^{-1}$
	$O_3^- \cdot + H^+ \rightarrow HO_3 \cdot$	$5.2\times10^{10}\ dm^3\ mol^{-1}\ s^{-1}$
	$HO_3 \cdot \rightarrow O_3^- \cdot + H^+$	$3.3\times10^2\ s^{-1}$
	$HO_3 \cdot \rightarrow \cdot OH + O_2$	$1.1\times10^5\ s^{-1}$
	$O_3 + \cdot OH \rightarrow HO_4 \cdot$	$2.0\times10^9\ dm^3\ mol^{-1}\ s^{-1}$
	$HO_4 \cdot \rightarrow HO_2 \cdot + O_2$	$2.8\times10^4\ s^{-1}$
Termination	$HO_4 \cdot + HO_4 \cdot \rightarrow H_2O_2 + 2O_3$	$5.0\times10^9\ dm^3\ mol^{-1}\ s^{-1}$
	$HO_4 \cdot + HO_3 \cdot \rightarrow H_2O_2 + O_2 + O_3$	$5.0\times10^9\ dm^3\ mol^{-1}\ s^{-1}$

Ozone can be useful or harmful for health and environment depending on where it is found in the atmosphere (EPA, 2015). Stratospheric ozone is useful because it protects the living beings from ultraviolet radiation from the sun. Near the surface, ozone is harmful because it can trigger a variety of health problems, particularly for children, the elderly, and people of all ages who have lung diseases such as asthma. According to the United States Environmental Protection Agency, exposure to ozone levels of > 137 μg m^{-3} for eight hours or longer is unsafe. Therefore, the excess ozone coming out of any ozonation process should be converted to oxygen by the ozone destructor before it is sent to the environment. In this regard, processes such as the OMB system, which involves a

very small amount of ozone, are advantageous as they minimize its leakage to the environment.

1.3 Advanced oxidation processes

AOPs are a class of oxidation techniques, which involve two stages of oxidation processes, i.e., the formation of hydroxyl radicals, and the reaction of these radicals with organic pollutants present in water. Nevertheless, the term *AOP* refers specifically to processes in which oxidation of organic pollutants occurs predominantly through reactions with hydroxyl radicals (Glaze, 1987). David (1993) has given a broad definition of AOPs as the aqueous phase oxidation processes, which are based primarily on the intermediacy of the hydroxyl radical in the mechanism, leading to the destruction of the target pollutant or xenobiotic or contaminant compound. The commonly known AOPs are treatment processes, which include ozone with UV, ozone with hydrogen peroxide, hydrogen peroxide and ultraviolet light, Fenton's reagent, and photocatalysis that uses titanium dioxide in combination with UV light and oxygen (David, 1993; Esplugas et al., 2002). The same chemical feature, i.e. the production of nonselective oxidants (viz. hydroxyl radicals), characterizes all these AOPs.

As hydroxyl radicals are stronger oxidants compared to the milder ozone, one may expect that simple ozonation dominated by the direct ozone–organic reactions may degrade reactant but complete mineralization to carbon dioxide and water may not be achieved. On the other hand, hydroxyl radicals lead to mineralization. This shows both ozone and ozone-based advanced oxidation processes may provide similar rates of disappearance of targeted organic pollutants, but the latter leads to complete disappearance of total organic carbon due to the hydroxyl radicals produced *in situ*. The reaction between most of organic pollutants and ozone produces intermediates, which are

less reactive than the reactant. This leads to a slower conversion of these compounds. The benefit of the ozone-based AOPs is thus a realization of complete mineralization (David, 1993). Table 1.3 gives the oxidation power of different common oxidation species. A species with a higher reduction potential (i.e., higher reduction potential has a more positive value) possesses a higher tendency to acquire electrons and be reduced, whereas, a species with a higher oxidation potential (i.e., higher oxidation potential has a more negative value) possesses a higher tendency to lose electrons and be oxidized (Zanello et al., 2011).

Table 1.3: Standard redox potentials of common oxidation species

Oxidation species	Standard redox potential (V)	Reference
Oxygen	+1.23	
Chlorine	+1.36	Zhou and Smith (2002)
Permanganate	+1.69	
Hydrogen peroxide	+1.78	
Ozone	+2.07	Masten and Davies (1994)
Hydroxyl radical	+2.80	
Fluorine	+3.03	Zhou and Smith (2002)

1.4 Microbubbles

Microbubbles are defined as tiny spherical bubbles with an average diameter of ≤ 100 µm. Tsuge (2014) has reported that the diameter range of microbubbles is 10–40 µm for bioactivity, and less than 100 µm for fluid physics. Agarwal et al. (2011) have defined

microbubbles as tiny bubbles having diameter in the range of 10–50 µm. Other researchers have classified microbubbles as bubbles having diameter in the range of 30–100 µm (Pérez-Garibay et al., 2012). Temesgen et al. (2017) have suggested the minimum and maximum diameter of the microbubbles as 10 and 100 µm, respectively. Therefore, there is a disagreement among the researchers regarding the size of the microbubbles. The Reynolds number of a microbubble of 100 µm diameter is nearly unity (Tsuge, 2014).

Microbubbles are different from the ubiquitous macrobubbles, both in terms of their size and physicochemical properties, which have made them particularly useful in various water and wastewater treatment applications (Agarwal et al., 2011; Tsuge, 2014). These important features include large gas–liquid interfacial area, low rising velocity through water, surface having high curvature, and electrically-charged gas–liquid interface. These characteristics are of great importance in the enhancement of mass transfer between the two phases (Takahashi et al., 2003).

1.4.1. Applications of microbubbles

Microbubbles have been used in the water/wastewater treatment such as degradation of phenol (Li et al., 2009b; Shin et al., 1999), oxidation of dimethyl sulfoxide (Li et al., 2009d), ozonation of practical textile wastewater (Chu et al., 2008a), treatment of wastewater containing dyestuff (Chu et al., 2007), sludge solubilization (Chu et al., 2008b), disinfection of *Bacillus subtilis* spores (Zhang et al., 2013), disinfection of hydroponic culture solutions (Kobayashi et al., 2011), removal of residual pesticides (Ikeura et al., 2011b; Li et al., 2020), removal of soluble organics like BTEX (i.e., benzene, toluene, ethylbenzene, and xylenes) from simulated seawater (Walker et al., 2001), removal of ammonia from water (Khuntia et al., 2012b; Ryskie et al., 2020), oxidation of As(III) to As(V) (Khuntia et al., 2014a), degradation of dyes in water

(Khuntia et al., 2014b), degradation of benzo[a]pyrene and toxicity reduction (Nam et al., 2019), organics contaminated wastewater (Xia and Hu, 2019), degradation of atrazine in water (Liu et al., 2020), pre-treatment of peat water (Qadafi et al., 2020), treatment of high concentration acid plasticizer wastewater (Wan et al., 2020), oxidation of pharmaceutical drugs (Patel et al., 2020), and petrochemical wastewater treatment (Jothinathan et al., 2021; Sun et al., 2020).

Apart from water treatment, microbubbles have exhibited a great potential in various engineering and medical applications due to their extremely high bioactivity and mass transfer efficiency. For instance, in medical applications, microbubbles are used for scanning body organs, drug delivery, and as a gene carrier and ultrasound contrast agent (Dijkmans et al., 2004; Geis et al., 2012; Kaufmann and Lindner, 2007; Kurup and Naik, 2010; Sirsi and Borden, 2009; Xu et al., 2011). Agarwal et al. (2011) have reviewed several works and concluded that the ability of generating free radicals without using any toxic chemical has proved that the use of microbubbles is a good technique for controlling membrane fouling and cleaning conducting surfaces. Microbubbles have got a great role in the dissolved air flotation (DAF) technique for the removal of oil from water (Al-Shamrani et al., 2002; Zouboulis and Avranas, 2000). Terasaka and Shinpo (2007) have reported that microbubbles are effective in the separation processes, e.g., removal of volatile contaminants and particulate matters from aqueous solutions. Enzyme extraction and protein recovery are some other applications of the microbubble technology (Jauregi and Varley, 1999; Xu et al., 2011).

1.4.2 Properties of microbubbles

The long residence time in the water and the high gas dissolution ability of the microbubble are the most significant characteristics, which help it to decrease its volume

gradually and subsequently collapse in water (Liu et al., 2010). The ordinary bubbles (i.e., macrobubbles) rise rapidly through water and burst at the surface of water (Figure 1.3). Hence, the solubility of the gas in water is very low. Whereas, the microbubbles gradually decrease in size and ultimately collapse under the water and disappear (Takahashi, 2009). A lower rising velocity of the microbubble ensures its longer residence time in the column, allowing more opportunities for interaction between the target molecules of the pollutant and the ozone molecules (Al-Shamrani et al., 2002). For instance, a 10 μm diameter microbubble rises only 20 cm in an hour in water (Tsuge, 2014). The gas inside the microbubble has a very good solubility in water due to the high internal pressure. Bubble diameter is inversely proportional to the pressures difference between the inside of the bubble and its outside. It can be expressed by the Young–Laplace equation (Ghosh, 2009)

$$P_g - P_l = \Delta P = \frac{4\gamma}{d} \tag{1.1}$$

The pressurized gas gets efficiently dissolved in the surrounding water and obeys Henry's law $\left(\tilde{p} = k_H C\right)$. According to Henry's law, the amount of dissolved gas around the shrinking bubble increases with increasing gas pressure inside the bubble. Li et al. (2009c) have reported that when the gas dissolves in a solution, the bubble shrinks further as the gas pressure inside the bubble increases due to the increase in the curvature. The rate of shrinkage also increases with time, which leads to the collapse of the microbubble (Takahashi, 2010). Several minutes may be required for the collapse of microbubbles (Takahashi, 2010). From Equation (1.1), very small bubbles are expected to have a very high internal gas pressure. The size of bubbles formed by single-pore nozzle and rotating-flow type of microbubble generators was compared by Tsuge et al. (2009). Smaller-size microbubbles were formed with the rotating-flow microbubble generator as the bubbles

were sheared and crushed by the rotating flow. When the outlet pressure of the pump was large, which implies that the change in pressure (i.e., ΔP) was greater, smaller bubbles were produced with both the generators, which agrees with Young–Laplace equation [i.e., Equation (1.1)].

The rate of mass transfer is higher for the microbubble process due to the slow rising velocity, large gas–liquid interfacial area, and high internal pressure. Therefore, the concentration of ozone in the aqueous phase would be high, which can generate more hydroxyl radicals. This can lead to a faster rate of reaction with the target pollutant and a quicker oxidation of the latter. Microbubbles enhance the formation of hydroxyl radicals in two ways. The microbubble surface is negatively charged due to the preferential accumulation of the hydroxyl ions at the gas–liquid interface (Liu et al., 2020). Consequently, the ozone molecules can readily react with the hydroxyl ions and decompose into the hydroxyl radicals through the series of reactions shown in Table 1.2. Besides, hydroxyl radicals are also generated by the self-shrinkage and collapse of the microbubbles. To summarize, the use of microbubbles can significantly increase the efficiency of the ozonation process due to the high rate of mass transfer, less ozone requirement, and generation of the hydroxyl radicals.

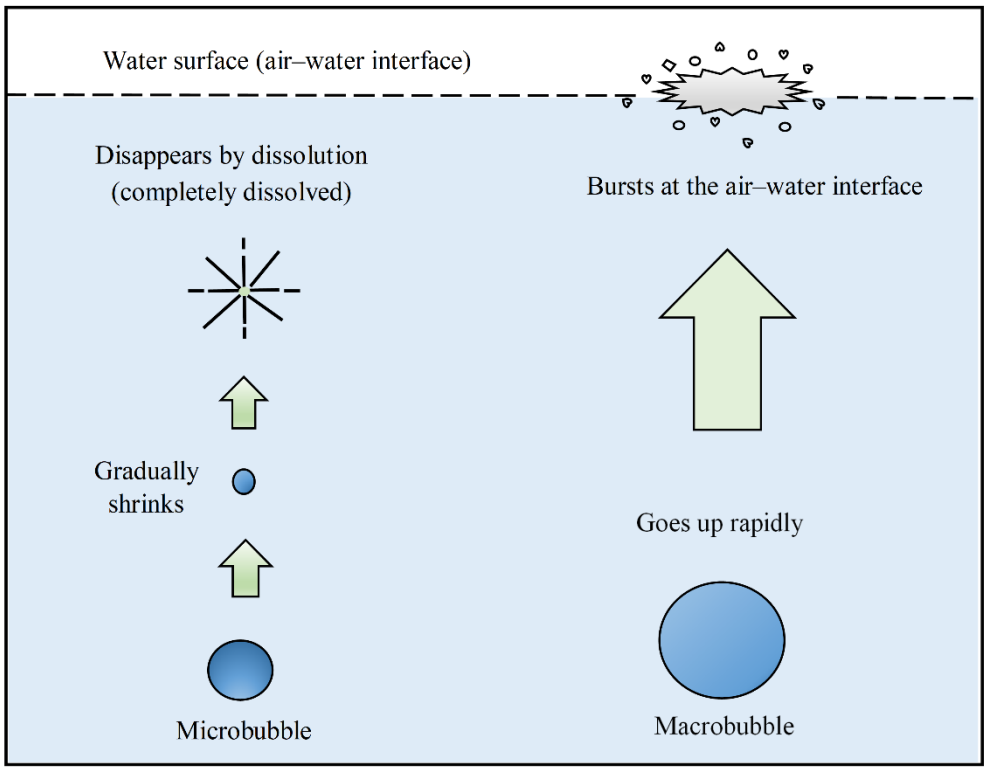

Figure 1.3: The difference between microbubbles and macrobubbles.

Various factors such as the presence of surface-active impurities and electrolytes can have significant effects on the size of the microbubbles. Increase in the salt concentration (e.g., NaCl) in the solution decreases the size of the microbubbles (Walker et al., 2001). Some authors (Hofmeier et al., 1995) have suggested that the surface elasticity plays an important role on the size of the bubbles in the presence of NaCl. In general, pure liquids or solutions with a smaller surface elasticity give rise to large bubbles through the coalescence of the smaller bubbles. In the aqueous solutions with a high values of surface elasticity, bubble size is reduced by the inhibition of coalescence.

Several methods are available for measuring the size of microbubbles. Digital cameras (such as CCD cameras and microscopes) are used for simple visualization of the microbubbles (Kawahara et al., 2009; Sadatomi et al., 2005; Zhang et al., 2000). Bubble diameter up to 1μm can be digitally processed and measured by this technique. Some of

the other available technologies for measuring the size of the microbubbles are dynamic light scattering (Berne and Pecora, 2000), laser light scattering using single particle optical sizing apparatus (Pelssers et al., 1990), phase Doppler anemometry (Hosokawa et al., 2009), and X-ray particle tracking velocimetry (Lee and Kim, 2005). The laser light scattering technique is more sophisticated where a laser beam is shone on the dispersion containing the microbubbles, and the scattered light is detected by a photomultiplier tube detector. The intensity of the scattered light is proportional to the bubble diameter. Dynamic light scattering, which is based on the Brownian motion, is another sophisticated technique used for the measurement of micro-nanobubbles (Berne and Pecora, 2000). The velocity of the Brownian motion is defined by the translational diffusion coefficient, and the Brownian motion becomes slower with the increase in the size of the bubble. For large bubbles $(>1\ \mu m)$, this method is not suitable.

The size of a spherical micro-nanobubble can be calculated by using the Stokes–Einstein equation (Ghosh, 2009).

$$d = \frac{RT}{3\pi\mu N_A D_b} \tag{1.2}$$

As the bubbles produced from the microbubble generators have a broad size distribution, the average diameter of the microbubbles is often expressed as a function of the number of the bubbles (n_i) and the bubble diameter (d_{bi}). The Satuer bubble diameter (d_{32}) is defined as (Majumder, 2016)

$$d_{32} = \frac{\sum_{i=1}^{n} n_i d_{bi}^3}{\sum_{i=1}^{n} n_i d_{bi}^2} \tag{1.3}$$

The kinetic properties (i.e., rising velocity of the microbubbles) are the other important characteristics. The motion of the microbubbles in water under gravity is similar to that

of a hard colloid particle. The balance of the buoyancy and drag forces acting on it determines the rising velocity of a microbubble through a liquid. From different experimental results on the rising velocity of microbubbles, it has been reported that they follow the Stokes equation (Tsuge, 2014), i.e., the rising velocity can be expressed by the following equation (Ghosh, 2009).

$$u = \frac{gd^2\rho_l}{18\mu} \tag{1.4}$$

The experimental works of Takahashi (2005) have shown that the rising velocity of the microbubbles closely obeyed the Stokes law. The average rising velocity of the microbubbles has been expressed in terms of the fractional gas hold-up and the superficial gas velocity (Kawahara et al., 2009).

The surface of the microbubbles dispersed in water is charged. This surface charge can be measured in terms of zeta potential, which is the potential at the plane of shear. Various scientists have reported that the zeta potential of the microbubbles is negative (Hasegawa et al., 2009; Qu et al., 2009; Takahashi, 2005). The zeta potential strongly depends on the pH of the medium but does not significantly vary with the bubble diameter. It has been reported (Tsuge, 2014) that the average zeta potential at the microbubble surface is in the range of –30 to –40 mV. However, when the microbubbles shrink in water, the transient value of zeta potential shows a significant variation with time, and hence, with bubble diameter. When the microbubble collapses, an ionic field of very high ion concentration is created that helps the formation of hydroxyl radicals, which are the main reactive species in the oxidative treatment of wastewater (Takahashi, 2010; Takahashi et al., 2007a). The presence of surface active compounds in water, such as surfactants and alcohols, have a significant effect on the zeta potential of microbubbles. These compounds have a high concentration at the air–water interface even when they

are present in trace amounts. Hence, they easily displace the OH^- and H^+ ions from the interface, because the surface activity of the latter ions is much smaller (Khuntia et al., 2012a).

1.4.3 Mass transfer in the microbubble systems

The primary objective of using the microbubble technology in ozonation for the treatment of water and wastewater is to improve the mass transfer to enhance the reaction. In this process, the gas present in the microbubbles must dissolve in the surrounding aqueous phase before reacting with the target pollutants.

The general two film-theory of gas absorption was demonstrated first by Whitman (Whitman, 1962). Based on the assumptions of no deviation from the Henry's law, local steady-state in the films, little temperature variation, one dimensional concentration gradients in the film, and local equilibrium between the gas and liquid phases at the gas–liquid interface, the two-film theory can be expressed as shown in Figure 1.4 (Whitman, 1962)

$$\frac{dC}{dt} = k_g \left(P_g - P_i \right) = k_l \left(C_i - C_l \right) \tag{1.5}$$

From Equation (1.5), it is observed that the concentration of the gas in the liquid phase increases as it is dissolved in the liquid phase. The rate of increase in concentration of the gas in the liquid phase is expressed in terms of the volumetric mass transfer coefficient $(k_l a)$, which is the product of mass transfer coefficient (k_l) and the interfacial area per unit volume (a). The rate of change of concentration is given by (Khuntia et al., 2012a)

$$\frac{dC}{dt} = k_l a \left(C^* - C_l \right) \tag{1.6}$$

where C^* is the saturation concentration of the gas in water. The interfacial area per unit volume is related to the fractional gas hold-up (ε_g) and Sauter mean diameter as

$$a = \frac{6\varepsilon_g}{d_{32}} \tag{1.7}$$

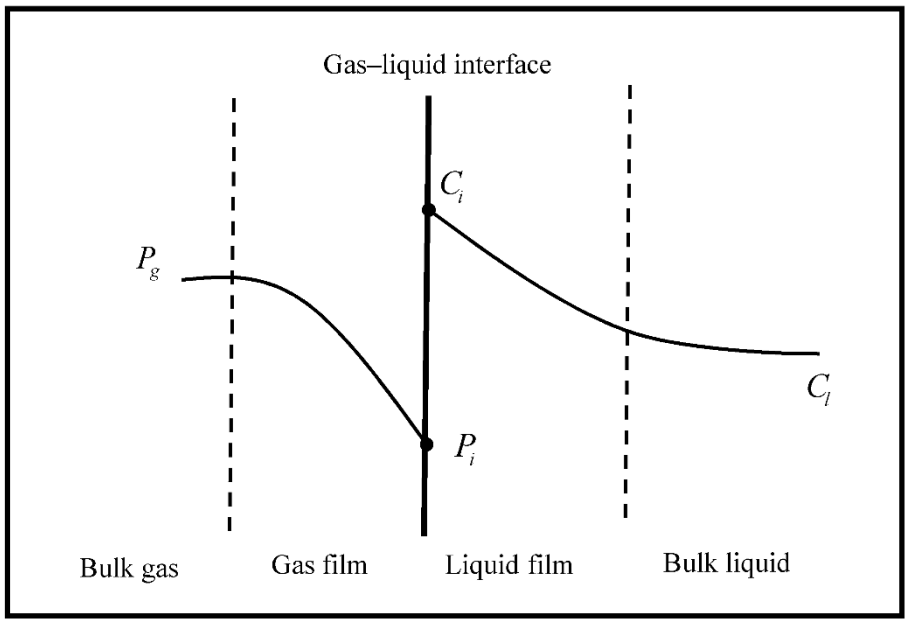

Figure 1.4: Mass transfer in the gas–liquid systems according to the two-film theory.

The overall mass transfer coefficients in the liquid (K_l) and gas phases (K_g) are given by the following relation (Cussler, 1997).

$$\frac{1}{K_l} = \frac{1}{K_g H} = \frac{1}{k_l} + \frac{1}{k_g H} \tag{1.8}$$

In Equation (1.8), the gas phase mass transfer resistance term can be neglected because, for small bubbles, k_g is large, since the gas molecules need to diffuse through a small distance (Motarjemi and Jameson, 1978). In addition to this, the gas phase mass transfer resistance can be ignored due to the relatively less solubility of ozone in water, and the mass transfer resistance mainly lies in the liquid phase (Johnson and Davis, 1996). Thus,

it is reasonable to approximate $(K_l \gg k_l)$. For a microbubble rising in water following the Stokes law given by Equation (1.4), the following correlation can be used to estimate the mass transfer coefficient (Clift et al., 2005):

$$k_l = \frac{D}{d}\left[1+\left\{1+\frac{du}{D}\right\}^{1/3}\right] \tag{1.9}$$

Several researchers (Waslo and Gal-or, 1971) have proposed different correlations, such as Equation (1.10), to estimate the mass transfer coefficient for different systems, which are applicable for industrial dispersions containing small bubbles and microbubbles having rigid surface. Equation (1.11) (Motarjemi and Jameson, 1978) is applicable for the microbubbles whose surfaces are immobile, and hence the microbubbles behave like solid particles.

$$k_l = 0.55\left(\frac{1-\varepsilon_g^{5/3}}{3+2\varepsilon_g^{5/3}}\right)^{1/3}\left(\frac{\Delta\rho g}{\mu}\right)^{1/3} \tag{1.10}$$

$$k_l = 0.6\left(\frac{D}{d}\right)\left(\frac{du\rho_l}{\mu}\right)^{1/2}\left(\frac{\mu}{\rho_l D}\right)^{1/3} \tag{1.11}$$

It has been reported (Khuntia et al., 2012a) that Equation (1.12) (Calderbank and Moo-Young, 1961) is applicable for bubbles of diameter of < 100 μm having a rigid surface.

$$k_l = 0.31\left(\frac{\Delta\rho g}{\mu}\right)^{1/3} D^{2/3} \tag{1.12}$$

Johnson and Davis (1996) have reported that the temperature dependence of the diffusivity of ozone in water, D_{O_3}, can be expressed by an Arrhenius function, as shown by Equation (1.13).

$$D_{O_3} = 1.1\times10^{-6}\exp\left(-\frac{1896}{T}\right) \tag{1.13}$$

1.4.4 Microbubble generators

There are various methods for generating microbubbles, and the principles of generation have their own effects on the microbubble properties (Ikeura et al., 2011a; Parmar and Majumder, 2013; Terasaka et al., 2011). Since efficiency and performance of microbubble systems depend on the diameter and number density of the microbubbles, it is important to understand the mechanism of their generation and optimize them in the design of the microbubble generators (Maeda et al., 2015). Microbubbles, formed by any method, have a wide size distribution, which can be unimodal or bimodal. The microbubble generation technique has a significant effect on the width and shape distribution of the microbubbles (Li, 2006).

In general microbubble generators can be classified into two major types i.e. gas–water circulation and pressurization–decompression types. In the former type, gas is introduced into the water vortex, bubbles are formed, and they are broken into microbubbles by breaking the vortex. In the second type of microbubble generator, a supersaturated solution is formed by dissolving a sufficient amount of gas in water under moderately high pressure. The supersaturated solution thus formed is unstable and the gas escapes from water generating a large number of microbubbles (Ikeura et al., 2011a; Khuntia et al., 2012a; Takahashi, 2009). Maeda et al. (2015), in their review, have classified methods of microbubble generators into four types, i.e., bubble breakup, ultrasonic wave, microfluidic devices, and pressurized dissolution. Table 1.4 summarizes these methods.

Table 1.4: Summary of the microbubble generation methods

Method	Principle	Unique properties	Reference

Bubble breakup	Bubble breakup due to shear flow/pressure wave	Generates microbubbles at a high void fraction but relatively larger diameters	Sadatomi et al. (2005)
Ultrasonic	Ultrasonic waves	Can generate monodisperse fine microbubbles, but the number density of the microbubbles is low	Makuta et al. (2006)
Microfluidic	Microfluidic technology	Can generate monodisperse fine microbubbles but the number density of the microbubbles is low	Xu et al. (2006)
Pressurized-dissolution	Depressurization/ decompression	Can generate fine microbubbles with a high number density	Hosokawa et al. (2009)

Sadatomi et al. (2012) have invented and developed the orifice type of microbubble generator. Their generator has an orifice in a flowing water tube. When pressurized water is introduced into the generator, the velocity of water through the orifice becomes several times of that at the exit of the generator. Thus, from the energy conservation principle, the pressure at a little downstream of the orifice becomes negative. With the aid of the negative pressure, air is automatically sucked through a porous pipe embedded inside the pipe, and this air is converted to a huge number of microbubbles by a high-shear water flow with strong turbulence. Thus, the generator can discharge a water jet with microbubbles from the exit.

Terasaka et al. (2011) have discussed the principles of four types of microbubble generators, i.e., spiral liquid flow, venturi, ejector, and pressurized-dissolution. In the spiral liquid flow type microbubble generators, the pumped water is tangentially

introduced from a side hole into a cylinder. The spiral liquid flow is produced, and it forms a maelstrom-like cavity in the cylinder. Then the gas is sucked from an orifice on the bottom, and it spouts out with the liquid from a hole situated at the top of the cylinder, where the gas is reduced to very fine bubbles (i.e., microbubbles) as a result of the centrifugation effect caused by the flow of high-speed rotating liquid. In the venturi type microbubble generator, a liquid stream involving conventional macrobubbles flows from the inlet of a venturi tube to its throat. As the two-phase flow is accelerated through the throat of the venturi tube, the dynamic pressure changes very rapidly and microbubbles are formed by reducing the millibubbles and/or by cavitation. In the typical ejector type microbubble generator, liquid flow-channels in the cylindrical generator are designed to shrink and stepwise expand, so that a complex pressure profile is produced along the stream. The gas is self-sucked from the most reduced pressure point, and reduced to a number of microbubbles by cavitation. In the pressurized-dissolution type of microbubble generator, a mixture of liquid and gas is pressurized in the tank. The gas is dissolved at (or near) the saturation condition. When this saturated liquid is flashed using a reducing valve, the microbubbles are generated. The pressure in the pressurized tank and the decompression process determine the size and population of the microbubbles.

Terasaka et al. (2011) have concluded that the microbubble generators are much more efficient for transferring oxygen into the aqueous phase than the conventional gas distributors (e.g., perforated plate and constant-flow nozzle). The spiral liquid-flow type of microbubble generator had shown the highest oxygen transfer coefficient even at a low air flow rate. However, it consumed more energy than the typical distributors. Both spiral liquid-flow and pressurization–decompression types of microbubble generators showed a high gas hold-up. They proposed a new aeration system utilizing a spiral liquid flow type of microbubble generator for improving an industrial wastewater treatment system.

In general, the power requirement of the microbubble generators is relatively higher because of the necessity of the pump, which is not required for the conventional gas distributors. Therefore, when the microbubble generators are used, the disadvantage of a high power consumption and the advantage of a better performance should be weighed before taking a decision.

1.5 Ozone millibubbles and microbubbles

Transfer of ozone to water is a very important task in water and wastewater treatment reactors (such as the bubble column reactors). Usually ozone, which is used in dilute gas mixtures, is transferred to the aqueous phase inside the bubble columns by spargers. Study of bubble size is very important in these reactors. The following paragraphs describe some works reported on the effectiveness of using ozone microbubbles for water and wastewater treatment. Some of the works have also given a comparative study with that of the conventional millibubbles.

Shin et al. (1999) have reported ozonation using microbubbles formed by an electrostatic ozonation reactor. This reactor produced fine microbubbles via electrostatic spraying. They focused on the behavior and the characteristics of their reactor. They had investigated the electrostatic spraying of ozone into water as a method of improving the rate of mass transfer, which enhanced phenol degradation. They have determined that the rate of mass transfer had increased by as much as 40% when the applied voltage was increased from 0 to 4 kV as a result of the smaller bubbles generated by electrostatic spraying. The comparative study with medium pore size bubble diffuser indicated that electrostatic spraying was more effective.

Chu et al. (2007) have presented a comparative study of ozonation of a simulated wastewater containing the dye, Reactive Black 5, by using both microbubble generator

and the conventional bubble contactor. They had qualitatively tested the concentration of hydroxyl radicals produced from ozone using terephthalic acid as the chemical probe. They measured the size of microbubbles using a microscope equipped with a CCD camera. The bubble size was analyzed by using the Image-Pro Plus® software. The microbubble generator produced a milky and high-intensity dispersion in which the bubbles had a mean diameter of 58 μm. Their work included a comparative study of the total mass transfer coefficient, rate constant, amount of TOC removed per gram of ozone consumed, and decolorization. In all the cases, they concluded that the microbubble system was a more promising process than the conventional bubble contactor system. They suggested that in addition to the enhancement of mass transfer, microbubbles, which had higher inner pressure, could accelerate the formation of the hydroxyl radicals, and hence improve the oxidation of the dye molecules.

Chu et al. (2008a) have reported another comparative study of enhanced treatment of textile wastewater by the microbubbles and conventional bubble contactor. Similar to their previous report, higher oxygen transfer rate was observed at lower gas flow rate. Volumetric oxygen transfer rate of 0.024–0.115 mg dm^{-3} s^{-1} and total mass transfer coefficient of 0.002–0.008 s^{-1} were obtained at the air flow rates of 0.0003–0.025 dm^3 s^{-1} using the microbubble system. Almost complete utilization of the input ozone was observed, and the rates of decolorization and organic reduction were much faster than those of the conventional bubble contactor. Their results verified that the time required to remove 80% of the color from the textile wastewater by the microbubble system was about 8.4 ks, which showed 50% improvement compared to that of the conventional bubble contactors (i.e., 16.8 ks). The COD removal efficiency also improved by almost 20%. They concluded that the microbubbles improved the oxidation of textile wastewater in addition to the enhancement of the mass transfer of ozone.

Chu et al. (2008b) compared the performance of sludge solubilization and reduction using microbubble-based ozonation and conventional ozonation using a bubble contactor. Their study corroborated the earlier works that microbubble-aided ozonation was more effective in increasing ozone utilization and improving sludge solubilization than the conventional bubble contactor. For the same contact time of 4.8 ks, more than 99% ozone utilization efficiency was obtained using the microbubbles, while the same was only about 72% for the conventional bubble contactor. Their results showed that the microbubble system showed better performance than the conventional bubble contactor in most cases (e.g., rate of microbial inactivation, removal of COD, and removal of total nitrogen and phosphorous).

Li et al. (2009b) studied decomposition of phenol by collapsing air microbubbles. They have reported up to 60% degradation during a 3.6 ks test period using air microbubbles. The main parameters studied by them were the pH of the solution and the type of gas used as the source of microbubbles. Their results showed that the degradation of phenol was favored by a more acidic solution. The reduction of phenol greatly increased when the pH of the solution decreased from 4 to 2. The use of oxygen microbubbles showed a better reduction rate than their nitrogen counterpart. Using *t*-BuOH (a well-known hydroxyl radical scavenger), they verified that the hydroxyl radicals were mainly responsible for phenol decomposition in both the cases. Their analysis included the effect of the degree of ionization of phenol in aqueous solution, since ion distribution on the gas–water interface has a vital effect on the decomposition reaction.

Li et al. (2009d) studied oxidation of dimethyl sulfoxide (DMSO) using ozone microbubbles. They have reported that it is a first-order reaction controlled by mass transfer. They have also studied the dependence of degradation of DMSO on liquid and gas flow rates. Their results show that the increase in gas superficial velocity enhanced

the reaction rate, and the ozone transfer ratio decreased with the gas flow rate. In addition, they have also observed that no changes in DMSO concentration and TOC occurred with the air microbubbles at the pH range of 4.3–9.5, and different salt concentrations (i.e., 0–0.1%), which suggested that free hydroxyl radicals were not generated under these conditions.

Ikeura et al. (2011b) studied the removal of the residues of a pesticide [i.e., fenitrothion (FT)] from lettuce and fruity vegetables (such as cherry tomatoes and strawberries) using ozone microbubbles. They have reported that the removal was fast and very effective. A comparison with the ozone millibubbles indicated that the former were more effective than the latter because of the generation of the hydroxyl radicals. In another research article (Ikeura et al., 2011a), they have reported a comparative study between two ozone microbubble generation methods (i.e., decompression and gas–water circulation types), and analyzed their effectiveness for the removal of similar residual pesticides. Their results suggest that the microbubbles generated from the decompression type were more effective than those from the gas–water circulation type of generators for removing the residual pesticide in vegetables, which was attributed to the larger number of fine bubbles that could easily penetrate into the vegetables.

Kobayashi et al. (2011) have reported the effectiveness of ozone microbubbles in disinfection i.e., inactivation of two phytopathogens found in plant roots (i.e., *Fusarium oxysporum* f. sp. *melonis* and *Pectobacterium carotovorum* subsp. *carotovorum*) in hydroponic culture solutions. They proposed that it was a new disinfectant method having a good potential. Higher solubility and longer durability of the ozone microbubbles in water was the reason behind its consideration as the best disinfectant against both the phytopathogens. Increase in the initial dose of ozone improved the disinfection process.

They had done a comparative study with ozone millibubbles and concluded that the microbubbles had a higher disinfectant activity than the ozone millibubbles.

Wen et al. (2012b) designed and tested an environment-friendly physical separation method employing microbubbles, as an alternative to the conventional DAF systems. They had tested the effectiveness of a microbubble system that employed air and ozone microbubbles for the treatment of three types of common industrial wastewater, i.e., oily wastewater, hotel laundry water, and fish pond wastewater. Without addition of any chemical, they concluded that microbubbles were simple yet effective for the removal/reduction of oil and grease, ammonia, TSS, BOD and COD. Their test results revealed that both air and ozone microbubble systems achieved large reductions in the TSS, BOD, and COD, and these methods were cost effective.

Zhang et al. (2013), investigated the effect of inlet ozone concentration on the disinfection performance of an ozone microbubble system for inactivation of a selected model microorganism (i.e. *Bacillus subtilis* spores). They have reported that in the microbubble ozonation system, for 3 min of contact time, the log reduction (i.e. 90% reduction in numbers of live microorganism) under high inlet ozone concentration was much higher than that under low inlet ozone concentration. For the same contact time, nearly about ten times log reduction improvement was observed when the initial ozone concentration increased from 40 to 140 mg dm^{-3}. Moreover, they have verified that increase in the inlet ozone concentration enhanced the ozone utilization efficiency, as it was a potential reason to reduce the bubble size. It significantly improved interfacial area per unit volume of the microbubble and increased the mass-transfer coefficient.

Summary of applications of oxygen and ozone microbubbles for water/wastewater treatments is given in Table 1.5.

Table 1.5: Applications of oxygen and ozone microbubbles for water/wastewater treatment

Target pollutant	Type of waste	Method of microbubble generation	Type of gas	*d* (μm)	% removal	Time (min)	Reference
p-xylene	Organic	Spinning-disk generator	Oxygen	–	BDL	120	Jenkins et al. (1993)
Phenol	Organic	Electrostatic spraying	Ozone	40–60	100	10	Shin et al. (1999)
BTEX organics	organic	Electrostatic spraying	Ozone	10−80	83	10	Walker et al. (2001)
E. coli	Microorganism	Pressurized solution	Ozone	30−60	Significant	10	Sumikura et al. (2007)
Reactive black 5	Dye	Spiral liquid flow	Ozone	< 58	99	30	Chu et al. (2007)
Sludge	Sludge	Spiral liquid flow	Ozone	< 58	80	20	Chu et al. (2008b)
DMSO	Detergent (odor)	Rotating flow	Ozone	50	70	10	Li et al. (2009d)
Methyl orange	Color	Shirasu porous glass membranes	Oxygen	5.8	94.1	20	Tasaki et al. (2009)
Microorganism*	Microorganism	Spiral liquid flow	Ozone	–	100	3	Kobayashi et al. (2011)
Fenitrothion	Pesticide	Decompression	Ozone	10	55	10	Ikeura et al. (2011a)
		Gas–water circulation	Ozone	40	45	10	
Bacillus subtilis	Microorganism	Decompression	Ozone	40−60	100	3	Zhang et al. (2013)
		Rotary flow type nozzle	Ozone	–	Significant	15	Tsuge et al. (2009)
Ammonia	Odor	Pressurized dissolution	Ozone	25	>99	120	Khuntia et al. (2012b)
Arsenic (III)	Arsenic	Pressurized dissolution	Ozone	25	98	30	Khuntia et al. (2014a)

* "Microorganism" stands for *Fusarium oxysporum* f. sp. *melonis* and *Pectobacterium carotovorum* subsp. *Carotovorum*.
Corona discharge ozone generation method was used for all cases.

1.6 Literature survey on the removal of target pollutants

1.6.1 Removal of dimethyl and diethyl phthalate

Nowadays, industrial wastewaters are becoming more and more complex due to the presence of emerging contaminants. Among these emerging contaminants, the organic pollutants are more recalcitrant and pose serious problems. Plasticizer is one such category, which includes the phthalates. These are synthetic compounds used predominantly as additives in plastics to improve their mechanical properties during post-processing (Cadogan, 1991; Staples et al., 1997). Due to their wide production and utilization, phthalates are ubiquitous and persistent organic pollutants in the environment. They are also present in the cosmetics, solvents, lubricants, toys, disposable medical packages and insecticide carriers (Abdel daiem et al., 2012; Khan et al., 2015). The environmental fate of phthalates is considerably important due to their effects on the health of human beings and animals. They were classified as "priority pollutants" and "endocrine-disrupting" compounds by the United States Environmental Protection Agency and other similar international agencies (Chang et al., 2005; EPA, 2014). The annual worldwide production of phthalates is about 6–8 million tons (Net et al., 2015; Xie et al., 2007). Figure 1.5 shows the significant increment of annual productions of phthalates over the last four decades (Huang et al., 2013; Net et al., 2015; Peijnenburg and Struijs, 2006). Most of the phthalates can easily escape into the environment during manufacturing, use, and/or after the disposal of the product, because they are not chemically bonded to the polymeric matrix (Bauer et al., 1998; Fromme et al., 2002; Huang et al., 2013; Roslev et al., 2007). Biodegradation is generally the desired removal method for these phthalates. However, some studies have indicated that some phthalates are poorly degraded

and some of them are considered as resistant to biological treatment (Maldonado et al., 2006; Staples et al., 1997).

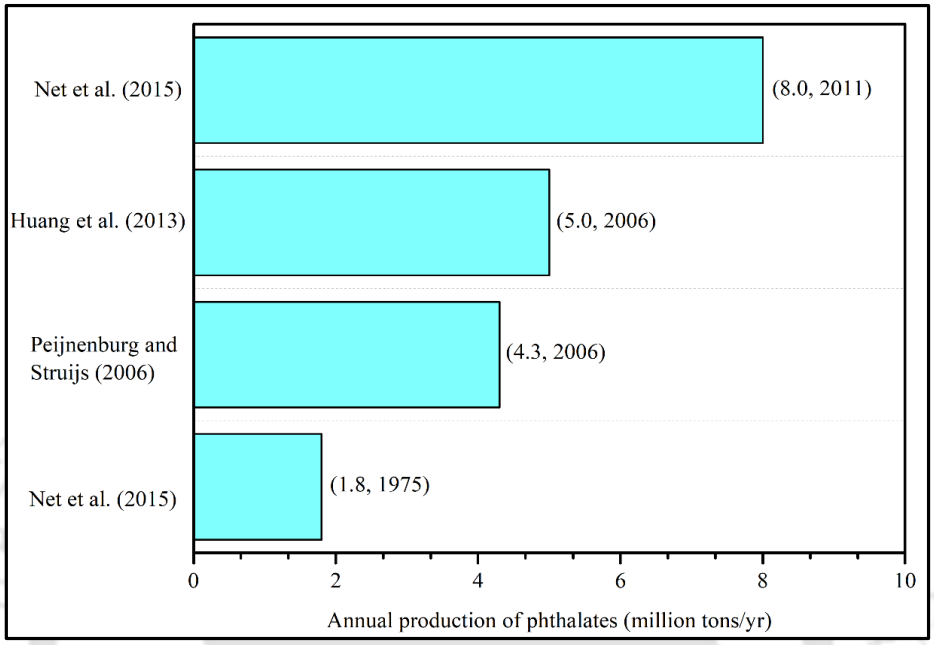

Figure 1.5: Annual production of phthalates.

Dimethyl phthalate (DMP) and diethyl phthalate (DEP) are among the most frequently identified phthalates in the environment. They were selected as model target pollutants in this research to investigate their removal from water by using ozone microbubbles. DMP is commonly encountered in the environment because of its high mobility and widespread usage in the aquatic systems (Abdel daiem et al., 2012). DEP is used as a plasticizer in various products such as in plastic packaging and as an ingredient in more than 60 cosmetic formulations (Api, 2001). The DEP molecule has a non-dissociating structure (Mansouri et al., 2013). The chemical identifications and physicochemical properties of DMP and DEP are given in Table 1.6.

Table 1.6: Chemical identifications and physicochemical properties of DMP and DEP

Chemical identifications	Physicochemical properties (Staples et al., 1997)
Chemical name: Dimethyl phthalate Molecular formula: $C_{10}H_{10}O_4$ Molecular weight: 194.2 g mol^{-1} CASRN: 131-11-3 Chemical structure: 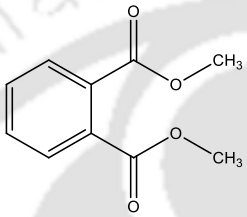	Physical state: colorless, oily liquid Density: 1190 kg m^{-3} at 293 K Solubility in water: 4200 mg dm^{-3} at 298 K Boiling point: 556 K Melting point: 268 K Vapor pressure: 0.27 Pa at 298 K Henry's constant: 1.24×10^{-2} Pa m^3 mol^{-1}
Chemical name: Diethyl phthalate Molecular formula: $C_{12}H_{14}O_4$ Molecular weight: 222.23 g mol^{-1} CASRN: 84-66-2 Chemical structure: 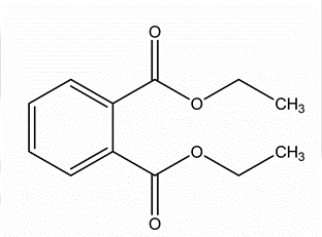	Physical state: colorless, oily liquid Density: 1120 kg m^{-3} at 298 K Solubility in water: 1080 mg dm^{-3} at 298 K Boiling point: 568 K Melting point: 233 K Vapor pressure: 0.28 Pa at 298 K Henry's constant: 6.2×10^{-2} Pa m^3 mol^{-1}

The common methods employed for the removal of DMP are based on metabolic degradation by microorganism under aerobic or anaerobic conditions (i.e., biological treatment) (Brar et al., 2009; Liang et al., 2007; Roslev et al., 2007; Shelton et al., 1984; Staples et al., 1997; Vega and Bastide, 2003). However, previous studies have indicated that most phthalates are poorly degraded and some of them are considered as "refractory" (i.e.,

resistant) to biological treatment (Bauer et al., 1998; Chen et al., 2008). Most of the works reported on the removal of DMP from water are based on catalytic ozonation. For instance, high-silica zeolites (Chen et al., 2008), ruthenium supported on alumina (Ru/Al_2O_3) (Yunrui et al., 2007), RuO_2/Al_2O_3 (Wang et al., 2013), cerium supported on activated carbon (AC) (Ce/AC) (Li et al., 2009a), TiO_2/Al_2O_3 (Chen et al., 2011), TiO_2 (Jing et al., 2011), and ruthenium/AC (Wang et al., 2009a) are some of the catalysts and supports, which have been used for the catalytic ozonation of DMP. The primary objective of applying catalytic ozonation for DMP degradation was to enhance the formation of reactive hydroxyl radicals in the aqueous medium.

Several methods have been reported the removal of DEP from water and wastewater. Some of them are ozonation (Jung et al., 2010; Legube et al., 1983), ozonation with UV irradiation (Oh et al., 2006), ozonation in the presence of H_2O_2 (Wen et al., 2011), treatment with UV irradiation and H_2O_2 (Xu et al., 2007), ozonation in the presence of activated carbon (de Oliveira et al., 2011; Mansouri et al., 2013; Nahum et al., 2013), electro-peroxone process (Hou et al., 2016), photo-Fenton process (Yang et al., 2005a), sonophotolysis and sonophotocatalysis (Na et al., 2012), and membrane filtration (Bodzek et al., 2004). Most of the ozonation processes have used conventional bubbles or millibubbles. Some works (Yuan et al., 2002) show that DEP is difficult to degrade by the biological and photo-chemical methods. Hence, there is a strong need to search for effective treatment processes for the removal of DEP from water and wastewater. The conventional ozonation plants use millibubbles. The size of the bubbles depends on the sparger used in these setups. In the conventional reactors, a considerable amount of ozone is wasted, which leads to the loss of

energy. Therefore, a better gas–liquid contactor is required that can perform rapid oxidation of the organic compounds, and also reduce the ozone loss.

In recent years, microbubble technology has been extensively used for improving ozone-based advanced oxidation processes for water and wastewater treatment due to their important physicochemical properties (Agarwal et al., 2011; Gurol, 1985; Khuntia et al., 2012a; Sadatomi et al., 2012; Shin et al., 1999; Takahashi, 2005; Takahashi et al., 2007b; Takahashi et al., 2012). These include large gas–liquid interfacial area, low rising velocity through water, surface with a high curvature, and electrically charged gas–liquid interface (see Section 1.4.2). These features are of great importance in the enhancement of transfer of ozone to the aqueous phase and generation of hydroxyl radicals (Takahashi et al., 2003). The hydroxyl radical is a strong oxidant with a standard redox potential of +2.8 V (Masten and Davies, 1994). Hence, application of ozone microbubbles may be an efficient alternative method for the complete removal of DMP and DEP from water. To the best of our information, hardly any work has addressed the use of ozone microbubbles for the removal of these two phthalates from water/wastewater.

1.6.2 Oxidation of bisphenol-A

Endocrine-disrupting chemicals (EDCs) are among top emerging contaminants. They are subclasses of the ubiquitous organic pollutants in the various waters (i.e., streams, drinking waters, seawater, groundwater, wastewaters) at very low concentrations. They have become the focus of environmental research in recent years, which implies that they are still unregulated, or in the process of regularization. EDCs are exogenous chemicals, or a mixture of chemicals, that can interfere with any aspect of hormone action (Zoeller et al., 2012). Such

compounds include bisphenols, alkylphenols, phthalates, pesticides, organotin compounds, polychlorinated biphenyls, polycyclic aromatic hydrocarbons, pharmaceuticals, natural hormones, and heavy metals (Umar et al., 2013). Literature shows that they often survive the conventional wastewater treatment processes, eventually entering water resources or water supplies. These compounds have adverse impacts on both human beings and natural organisms at trace/low concentrations, which may cause disruption of the endocrine systems, and affect the hormonal control of development in aquatic organisms and wildlife. Thus, it is desirable to remove these chemicals from water.

Bisphenol-A (BPA) is primarily used as an intermediate-monomer in the production of epoxy resins and polycarbonates (Kang et al., 2006; Umar et al., 2013). It is produced in high volumes. The worldwide production of BPA is about 2.7×10^9 kg every year (Burridge, 2003; Vandenberg et al., 2007). The United States Environmental Protection Agency has classified BPA as an EDC (Crisp et al., 1998). Due to the use of BPA for manufacturing products used in many applications, it is expected that human exposure to BPA may be widespread, and these exposures may reach high levels (Dekant and Völkel, 2008). BPA has been released into the environment because of its widespread use, and it is frequently detected in the influent, effluent, and sludge of the wastewater treatment plants (Fürhacker et al., 2000; Vethaak et al., 2005), treated drinking water (Rodriguez-Mozaz et al., 2004), surface water (Kolpin et al., 2002), hazardous waste landfill leachates (Yamamoto et al., 2001), tissues of aquatic animals (Hayashi et al., 2008; Vethaak et al., 2005), and sediment samples from rivers and lakes (Fromme et al., 2002; Vethaak et al., 2005).

Wastewater treatment plants are considered to be one of the major secondary sources of BPA pollution due to its incomplete degradation by the physico-chemical and biological

treatments (Tan et al., 2007; Umar et al., 2013). A comprehensive review by Umar et al. (2013) on BPA indicates that there is a lack of knowledge of the effect of BPA on humans, however, its harmful effects on animals suggest that there are potentially serious impacts on humans. BPA is believed to cause neurochemical and behavioral effects (Vom Saal and Hughes, 2005), obesity-promoting effects, type II diabetes (Rubin and Soto, 2009; Wetherill et al., 2002), reproduction and developmental effects such as ovarian diseases and miscarriages, human prostate cancer, cardiovascular disease, hormonal imbalance, and liver enzyme abnormalities (Sugiura-Ogasawara et al., 2005; Takeuchi et al., 2004).

The extensive detection of BPA in the environment, and its serious health effects (Onundi et al., 2017) have caused great concern among public health agencies and researchers. Consequently, a considerable amount of work has been done in the last two decades investigating its degradation in water and wastewater using various treatment techniques such as chemical oxidation (Cui et al., 2009; Li et al., 2008), sonochemical reaction (Inoue et al., 2008; Torres et al., 2007), Fenton and sono-Fenton (Ioan et al., 2007), photodegradation (Barbieri et al., 2008), photocatalysis (Wang et al., 2009b), UV/H_2O_2 (Mehrabani-Zeinabad et al., 2015; Xie and Li, 2006), conventional ozonation (Ahmad et al., 2015; Deborde et al., 2008; Garoma et al., 2010; Isil et al., 2009; Kusvuran and Yildirim, 2013; Mehrabani-Zeinabad et al., 2015; Mutseyekwa et al., 2017; Zhang et al., 2008), catalytic ozonation (Liu et al., 2015; Luo et al., 2018; Yang et al., 2016; Zhang et al., 2020; Zhang et al., 2019), O_3/UV/H_2O_2 (Liu et al., 2018), O_3/H_2O_2 (Mehrabani-Zeinabad et al., 2016), and O_3/UV (Irmak et al., 2005; Mehrabani-Zeinabad et al., 2015). Treatment of BPA is difficult by conventional wastewater treatment methods because of its ring structure, which

enables the molecules to escape from the primary and secondary treatment facilities (Mutseyekwa et al., 2017).

From the aforementioned extensive literature, it is observed that the ozone-based removal techniques can be more efficient for reducing the concentration of BPA in water to practically insignificant values. Conventional ozonation, which uses ozone millibubbles, has been effective to varied degrees of success for the BPA removal. In order to enhance its effectiveness, researchers have coupled it with other processes, such as catalysts, UV light, and hydrogen peroxide. The purpose of the catalyst and hydrogen peroxide is to enhance the formation of the highly-reactive hydroxyl radical in the aqueous medium, which is a more powerful oxidant than ozone. The hydroxyl radical readily reacts with various organic compounds through electrophilic addition, electron transfer, hydrogen abstraction, and radical–radical reactions, which can lead to complete mineralization of the organic compound. Most of the works based on the catalytic ozonation process have reported that it is effective in the removal of BPA. However, the major drawback of this process is the preparation of the catalyst, which is complicated and expensive. Hence, the application of the ozone microbubbles (OMBs) would be a very good alternative, and an efficient method for complete degradation of BPA inasmuch as the reaction between ozone and the organic compound is expected to be accelerated by the use of the microbubbles, and the hydroxyl radicals would be formed *in situ* without using any catalyst. As far as we are aware, hardly any work has addressed the use of OMBs for removing BPA from water/wastewater. The chemical identifications and physicochemical properties of BPA are given in Table 1.7. Table 1.8 shows a summary of the literature for oxidation of BPA in water/wastewater by ozonation and ozone-based advanced oxidation processes.

Table 1.7: Chemical identifications and physicochemical properties of bisphenol-A

Chemical identifications	Physicochemical properties (Staples et al., 1998)
Chemical name: Bisphenol-A Molecular formula: $C_{15}H_{16}O_2$ Molecular weight: 228.29 g mol^{-1} CASRN: 80-05-7 Chemical structure: 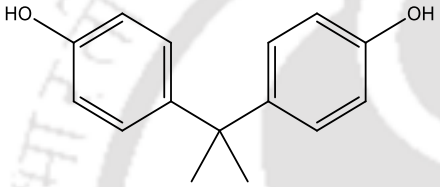 	Physical state: white crystalline solid Density: 1200 kg m^{-3} at 298 K Solubility in water: 120 – 300 mg dm^{-3} at 295 K Boiling point: 493 K at 4 mmHg Melting point: 431 – 432 K Vapor pressure: 87 Pa at 463 K Henry's constant: 1.0×10^{-7} Pa m^3 mol^{-1} at 298 K $\log(K_{ow})$: 2.20 – 3.82 at 298 K (K_{ow} is octanol–water partition coefficient)

Table 1.8: Oxidation of BPA in water/wastewater by ozonation and ozone-based advanced oxidation processes

Method	Medium	pH	Ozone dose ($mol\ m^{-3}$)	$[BPA]_0$ ($mol\ m^{-3}$)	Time* (s)	Removal (%)		Reference
						BPA	TOC	
O_3/H_2O_2	Water	2–12	0.521–0.625	0.004–0.044	4200	100	–	Lee et al. (2003)
O_3	Deionized water	2–10	0.025–0.106	0.023–0.057	840	84–99	–	Garoma and Matsumoto (2009)
O_3/TiO_2	Water	7	0.625	0.099	7200	100	80	Rivas et al. (2009)
O_3	Deionized water	7	0.208	0.051	5400	> 99	21.5	Garoma et al. (2010)
O_3/Al_2O_3	Milli-Q water	5	0.094	0.044	3600	100	35, 90	Keykavoos et al. (2013)
O_3	Distilled water	3–10	11.08	0.051–0.509	1500	100	30	Kusvuran and Yildirim (2013)
O_3	Water	3–10	0.458–0.583	0.438	5400	100	52	Mutseyekwa et al. (2017)
$O_3/H_2O_2/UV$	Demineralized water	3–11	0.002–0.021	8.76×10^{-4}	1200	> 99	–	Liu et al. (2018)

*maximum ozonation time required for the oxidation

1.6.3 Removal of dimethyl sulfoxide

Dimethyl sulfoxide (DMSO) is a widely-used detergent and photoresist stripping solvent in the manufacturing of semiconductor and liquid crystal displays. The chemical identifications and physicochemical properties of DMSO are given in Table 1.9. Its good solvent property, stability, and water miscibility have increased its industrial use. As a result of these numerous applications, wastewater containing large quantities of DMSO are discharged from the washing and rinsing processes (Glindemann et al., 2006; Lee et al., 2004; Park et al., 2001; Wu et al., 2006).

Table 1.9: Chemical identifications and physicochemical properties of dimethyl sulfoxide

Chemical identifications	Physicochemical properties (MacGregor, 1967)
Chemical name: Dimethyl sulfoxide Molecular formula: C_2H_6OS Molecular weight: 78.13 g mol^{-1} CASRN: 67-68-5 Chemical structure: 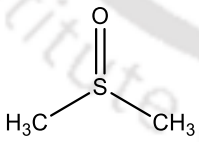 	Physical state: colorless liquid, slightly sulfurous odor, very hygroscopic Density: 1100 kg m^{-3} at 293 K Solubility in water: very soluble Boiling point: 462 K Melting point: 292 K Vapor pressure: 0.08 kPa at 298 K Acid dissociation constant (pKa): 35.1

Degradation of DMSO by the conventional biological methods is known to be difficult, because of the odor problems caused by intermediate products such as dimethyl sulfide (DMS), methyl mercaptan, and hydrogen sulfide, which makes it difficult to carry out the treatment process (Park et al., 2001). Incubation of activated sludge with the

DMSO concentration in the range of 1–10 mg dm^{-3} produces the odorous DMS gas at concentrations exceeding the odor threshold by approximately four orders of magnitude (Glindemann et al., 2006). In case the DMSO is incompletely recycled and/or inappropriately disposed into the sewage plants, the annual worldwide industrial production of DMSO about 5×10^7 kg could result in a significant formation of DMS (Glindemann et al., 2007). Cheng et al. (2009) have reported that the amount of DMSO discharged from the industry can exceeded the handling capacity of the wastewater treatment plants. This could result in the "canned corn-like" odor when the DMSO concentration exceeds ~0.5 mg dm^{-3} in the incoming wastewater.

The maximum allowable concentration of DMSO in the discharge wastewater, set by the United States Environmental Protection Agency, is less than 0.05 mg dm^{-3} (Chen et al., 2016). Scientists, in their effort to develop a cost-efficient treatment of wastewater containing DMSO, have studied a combination of conventional biological processes and the AOPs. DMSO can be oxidized promptly by chemical oxidation, such as the AOPs, and dimethyl sulfone [$DMSO_2$, i.e., $(CH_3)_2\ SO_2$] is formed (Baldoni-Andrey et al., 2005; Koito et al., 1998). In this oxidation process, no noxious compound is generated since there is no reducing decomposition. However, another method is necessary to treat the $DMSO_2$ because it is extremely stable against chemical oxidation. Ozone-based AOPs such as O_3/UV and O_3/H_2O_2, and photochemical degradation (i.e., UV/H_2O_2) have been reported as effective methods for DMSO removal (Koito et al., 1998; Lee et al., 2004; Wu et al., 2007). In the photochemical degradation (UV/H_2O_2) system, first DMSO is decomposed to methane sulfonic acid (MSA) by the hydroxyl radicals generated *in situ*, and the MSA is further degraded easily by conventional biological treatment without producing any reduced and harmful sulfur-containing byproducts, as shown in Figure 1.6 (Koito et al., 1998).

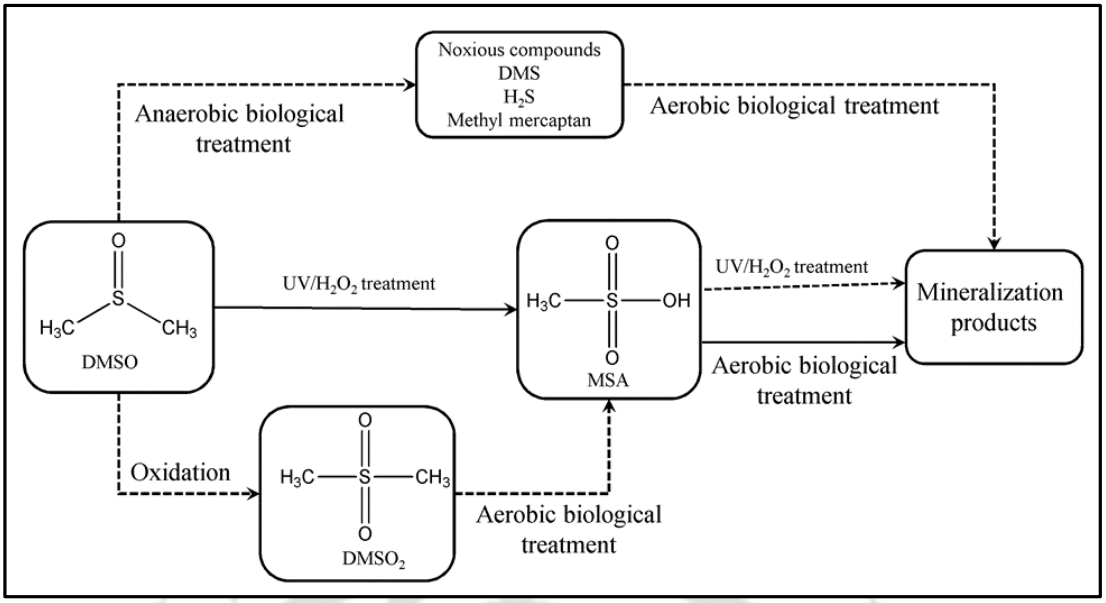

Figure 1.6: Possible oxidation routes of DMSO by different AOPs and biological treatments.

Oxidation of DMSO by the hydroxyl radicals primarily gives methane sulfonic acid (Scaduto, 1995). DMSO is very stable in pure water or in solutions containing H_2O_2, and it reacts very rapidly with the hydroxyl radicals (k = 4.5 × 10^9 dm^3 mol^{-1} s^{-1}) (Bardouki et al., 2002). Large scale treatment of organic compounds with UV irradiation is disadvantageous due to their quite high cost. The feasibility of the Fenton oxidation process was studied for the removal of DMSO from aqueous solutions (Wen et al., 2012a). A fluidized-bed Fenton process was reported as an effective method for the degradation of DMSO in synthetic wastewater (Chen et al., 2016). Wu et al. (2006) have proposed a combination of hydrogen peroxide and goethite (a heterogeneous catalyst) as an alternative for the expensive Fenton-type degradation of DMSO. Lee et al. (2006) have demonstrated a streamer corona discharge process, which produced locally-concentrated hydroxyl radicals for the oxidative degradation of DMSO, and reported a high efficiency for the DMSO removal, albeit less TOC reduction. Figure 1.7 shows the comparison of

some AOPs for the degradation and mineralization of DMSO in water/wastewater (Abellán et al., 2009; Lee et al., 2004; Park et al., 2001; Wu et al., 2007).

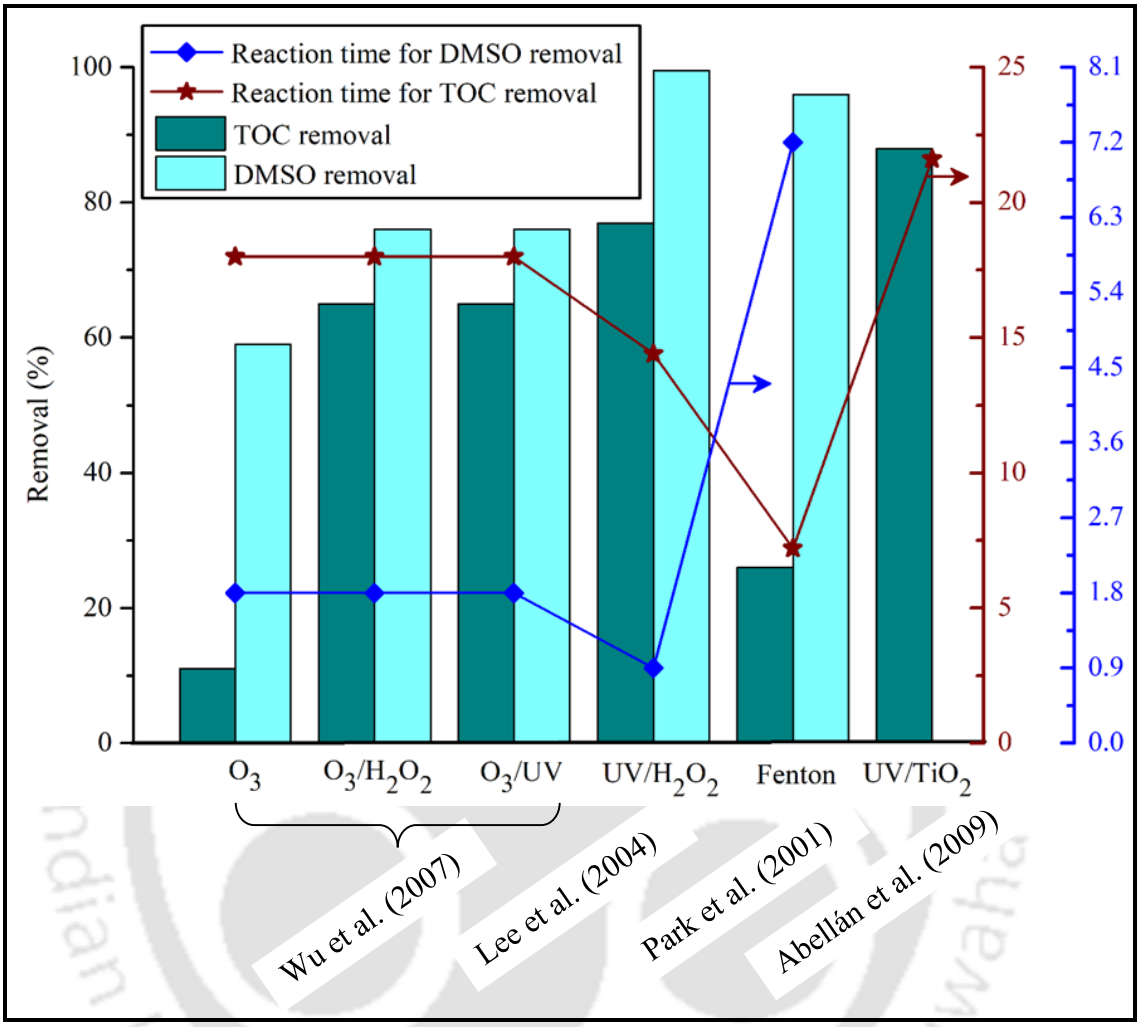

Figure 1.7: Comparison of different AOPs for degradation and mineralization of DMSO in water/wastewater.

From these reports, it is observed that DMSO removal could be achieved through most of AOPs. Nevertheless, the rate of mineralization of DMSO was too slow, and it required extended oxidation time. Therefore, more efficient methods are required for faster mineralization of DMSO. Recently, ozone-based microbubble-aided technology has attracted much attention as a new potential candidate for DMSO oxidation in wastewater. For instance, Li et al. (2009d) have found that DMSO could be efficiently

decomposed into MSA by the OMBs without producing any noxious sulfur-containing by-products. They have suggested that the stimulant-enhanced ozonation is an effective treatment method for the DMSO-containing wastewater. Their result has revealed that ozonation of DMSO is a mass-transfer-controlled reaction, and the experimental results fitted the first-order kinetic model. The free hydroxyl radicals generated *in situ* lead to the efficient degradation, and they are responsible for the decomposition of DMSO into biodegradable intermediates.

1.7 Scopes of the work

This thesis has investigated the removal of two phthalates (i.e., DMP and DEP), BPA, and DMSO from water using the OMBs in a reactor of 20 dm^3 capacity. The effects of the operational parameters such as the initial concentrations of the pollutant, pH of the medium, ozone generation rate (i.e., the concentration of ozone in the inlet gas), and the addition of using H_2O_2 in the presence of the OMBs on the removal of these pollutants were investigated in detail. The contribution of the hydroxyl radical in the oxidation was investigated by using the well-known scavenger of the hydroxyl radicals, i.e., *tert*-butanol (*t*-BuOH). The effects of addition of bicarbonate ions were also studied. Important parameters such as TOC reduction, stoichiometric ratio of ozone consumed to the target pollutant removed, ozone utilization efficiency, reaction kinetics, volumetric mass transfer coefficient of ozone in the reacting system, enhancement factor, and Hatta number were determined at different reaction conditions. The performance of the ozone microbubbles was compared with the same of the ozone millibubbles, based on these parameters.

1.8 Objectives of the work

The main objective of this thesis was to investigate the effectiveness of the OMBs for the removal of selected organic pollutants. The main objectives of this work are as follows:

[1] Study the removal of DMP and DEP from water using OMBs at different operational conditions.

[2] Investigate the degradation efficiency of BPA and its selected major oxidation intermediates.

[3] Compare the removal of dimethyl sulfoxide from water using ozone microbubbles with the same by the ozone millibubbles.

[4] Check the effectiveness of the OMB process by determining the ozone utilization efficiency and the stoichiometric ratio of ozone consumed to the pollutant removed.

[5] Study the effect of hydrogen peroxide in the presence of the OMBs, and the contribution of the hydroxyl radicals on the degradation of the target pollutant.

[6] Determine the extent of mineralization of the target pollutant by the OMB process.

[7] Determine the mass transfer and the kinetic parameters of the process, such as the volumetric mass transfer coefficient of ozone, Hatta number, self-decomposition rate constant of ozone, and overall rate constant.

1.9 Outline of the thesis

This thesis deals with the removal of two phthalates (i.e., DMP and DEP), BPA, and DMSO from water by the OMBs, focusing on the effectiveness of their removal under different reaction conditions. The literature relevant to these processes has been reviewed. The chapter-wise structure of the thesis is described below.

Chapter 1 **(Introduction):** This chapter presents a discussion on ozone and its application in water/wastewater treatment. The properties of the OMBs and their applications in water/wastewater treatment are also discussed. A brief review of the literature for each target pollutant is presented. The objectives of the research work are also given in this chapter.

Chapter 2 **(Materials and Experimental Methods)**: This chapter presents the details of the experimental setup used in this work. The list of chemicals used, their source, and purity are given. A detailed description of the equipment used, preparation of the samples, and the experimental procedures are provided. The procedure for conducting the experiments and analyzing the samples is also described.

Chapter 3 **(Removal of Dimethyl Phthalate from Water by the Ozone Microbubbles)**: This chapter presents the work on the removal of DMP from water using the OMBs. The effects of the initial concentration of DMP, pH of the medium, ozone generation rate, and the role of H_2O_2 on the removal of DMP are described and analyzed. The TOC analysis is provided to estimate the mineralization of DMP. *t*-BuOH is used as the hydroxyl radical scavenger to examine the effect of hydroxyl radicals on the oxidation of DMP. The self-decomposition rate constant of ozone is determined from the experimental results. The overall kinetics of the reaction between DMP and ozone is studied and the kinetic parameters are reported. The Hatta number is computed to find out the relative importance of mass transfer and chemical reaction.

Chapter 4 **(Removal of Diethyl Phthalate from Water by the Ozone Microbubbles)**: This chapter presents the use of OMBs to remove DEP from water, and the mineralization

efficiency is discussed under various reaction conditions. The contribution of hydroxyl radicals is determined by using a hydroxyl radical scavenger (i.e., *t*-BuOH). The effect of addition of H_2O_2 on the removal of DEP is investigated by adding 1 – 8 mol m^{-3} H_2O_2 at pH 7. The overall kinetic parameters of the oxidation of DEP by ozone are computed from mass balance and experimental results.

Chapter 5 **(Oxidation of Bisphenol-A by Ozone Microbubbles)**: This chapter presents the use of the OMBs for the oxidation of BPA in water. The effect of some major operational parameters that influence the removal of BPA are investigated. The stoichiometric ratio of ozone consumed to BPA removed, and the ozone utilization efficiency are computed from the experimental results. The degradation efficiency of BPA and its selected major reaction-intermediates (i.e., catechol and hydroquinone) are studied in aqueous solution by the OMBs at the optimal reaction conditions. The effects of bicarbonate ion and the contribution of hydroxyl radicals on the degradation of BPA are reported. The extent of mineralization of BPA and its oxidation-intermediates at the optimal conditions are estimated by TOC measurements. The overall kinetic parameters of the reaction between BPA and ozone are reported at different initial concentrations of BPA and pH.

Chapter 6 **(A Comparative Study on the Removal of Dimethyl Sulfoxide from Water using Microbubbles and Millibubbles of Ozone):** In this chapter, the potential of the OMBs for the oxidation of DMSO is investigated in detail, and the results are compared with those of the conventional ozonation using millibubbles (i.e., OMLBs). The main operational parameters that influence the removal of DMSO are studied. In addition, the contribution of hydroxyl radicals to the removal of DMSO is investigated for both OMBs

and OMLBs. Ozone utilization and the stoichiometric ratio of ozone consumed to DMSO removed are computed and compared. The effectiveness of OMBs and OMLBs in terms of the extent of mineralization of DMSO is investigated and compared. Formation and depletion of the two main oxidation intermediates of DMSO (i.e., $DMSO_2$ and MSA) are investigated for both OMBs and OMLBs. The overall kinetic parameters of the reaction between DMSO and ozone, and their variation with the pH of the medium is determined from the experimental results, and the values are compared.

Chapter 7 **(Summary and Scope for Future Work):** This chapter provides a summary of the work, and suggests ideas for future research.

Notations

a	specific gas–liquid interfacial area ($m^2\ m^{-3}$)
C	concentration (mol m^{-3})
C^*	saturation concentration of the gas in water (mol m^{-3})
D	mean diameter of microbubbles (m)
d_{32}	Sauter mean diameter (m)
D	diffusivity of gas in liquid ($m^2\ s^{-1}$)
D_b	translational diffusion coefficient of microbubble ($m^2\ s^{-1}$)
D_{O_3}	diffusivity of ozone in water ($m^2\ s^{-1}$)
G	acceleration due to gravity (m s^{-2})
k_g	gas phase mass transfer coefficient (mol $N^{-1}\ s^{-1}$)
K_g	overall gas-side mass transfer coefficient (mol $N^{-1}\ s^{-1}$)
k_H	Henry's law constant (Pa m^3 mol^{-1})
k_l	liquid phase mass transfer coefficient (m s^{-1})
K_l	overall liquid-side mass transfer coefficient (m s^{-1})
$k_L a$	volumetric mass transfer coefficient (s^{-1})
K_{ow}	octanol–water partition coefficient
n	number of bubbles
N_A	Avogadro's number (mol^{-1})
$\tilde{p}$	partial pressure of gas (Pa)
P	pressure (Pa)
P_g	gas pressure (Pa)

P_l	liquid pressure (Pa)
R	gas constant (J mol^{-1} K^{-1})
t	time (s)
T	temperature (K)
u	rising velocity of bubble (m s^{-1})
V	volume (m^3)

Greek symbols

γ	surface tension of liquid (N m^{-1})
$\Delta\rho$	density difference between the gas and liquid phases (kg m^{-3})
ΔP	pressure difference between gas and liquid phases (Pa)
ε_g	fractional gas hold-up
λ	wavelength (nm)
μ	viscosity of liquid (Pa s)
ρ_l	density of liquid (kg m^{-3})

Abbreviations

AC	activated carbon
AOPs	advanced oxidation processes
BDL	below detection limit
BOD	biological oxygen demand
BPA	bisphenol–A
BTEX	benzene, toluene, ethylbenzene, and xylenes
CASRN	chemical abstracts service registry number
CCD	charge-coupled device
COD	chemical oxygen demand

DAF	dissolved air flotation
DEP	diethyl phthalate
DMP	dimethyl phthalate
DMS	dimethyl sulfide
DMSO	dimethyl sulfoxide
$DMSO_2$	dimethyl sulfone
E. coli	*Escherichia coli*
EDCs	endocrine-disrupting chemicals
FT	fenitrothion
OMBs	ozone microbubbles
OMLBs	ozone millibubbles
MSA	methane sulfonic acid
t-BuOH	*tert*-butyl alcohol
TOC	total organic carbon
TSS	total suspended solids
UV	ultraviolet

References

Abdel daiem, M.M., Rivera-Utrilla, J., Ocampo-Pérez, R., Méndez-Díaz, J.D., Sánchez-Polo, M., **2012**. Environmental impact of phthalic acid esters and their removal from water and sediments by different technologies – a review. *J. Environ. Manage.*, *109*, 164–178.

Abellán, M.N., Dillert, R., Giménez, J., Bahnemann, D., **2009**. Evaluation of two types of TiO_2-based catalysts by photodegradation of DMSO in aqueous suspension. *J. Photochem. Photobiol. A*, *202*, 164–171.

Agarwal, A., Ng, W.J., Liu, Y., **2011**. Principle and applications of microbubble and nanobubble technology for water treatment. *Chemosphere*, *84*, 1175–1180.

Ahmad, N.A., Yuzir, M.A., Yong, E.L., Abdullah, N., Salim, M.R., **2015**. Removal of bisphenol A (BPA) in surface water by ozone oxidation process. *Appl. Mech. Mater.*, *735*, 210–214.

Al-Shamrani, A.A., James, A., Xiao, H., **2002**. Separation of oil from water by dissolved air flotation. *Colloids Surf., A*, *209*, 15–26.

Api, A., **2001**. Toxicological profile of diethyl phthalate: a vehicle for fragrance and cosmetic ingredients. *Food Chem. Toxicol.*, *39*, 97–108.

Baldoni-Andrey, P., Commarieu, A., Plisson-Saune, S., **2005**. Treatment of Wastewater Containing Dimethyl Sulfoxide (DMSO), in: Lichtfouse, E., Schwarzbauer, J., Robert, D. (Eds.), *Environmental Chemistry: Green Chemistry and Pollutants in Ecosystems*. Springer Berlin Heidelberg, Berlin (Germany), pp. 615–620.

Barbieri, Y., Massad, W.A., Díaz, D.J., Sanz, J., Amat-Guerri, F., García, N.A., **2008**. Photodegradation of bisphenol A and related compounds under natural-like conditions in the presence of riboflavin: kinetics, mechanism and photoproducts. *Chemosphere*, *73*, 564–571.

Bardouki, H., da Rosa, M.B., Mihalopoulos, N., Palm, W.U., Zetzsch, C., **2002**. Kinetics and mechanism of the oxidation of dimethylsulfoxide (DMSO) and methanesulfinate (MSI^-) by OH radicals in aqueous medium. *Atmos. Environ.*, *36*, 4627–4634.

Bauer, M.J., Herrmann, R., Martin, A., Zellmann, H., **1998**. Chemodynamics, transport behaviour and treatment of phthalic acid esters in municipal landfill leachates. *Water Sci. Technol.*, *38*, 185–192.

Beltrán, F.J., **2004**. Ozone Reaction Kinetics for Water and Wastewater Systems, 1st ed. Lewis Publishers, Boca Raton (USA).

Berne, B.J., Pecora, R., **2000**. Dynamic Light Scattering with Applications to Chemistry, Biology, and Physics, 2nd ed. Courier Corporation, New York (USA).

Bodzek, M., Dudziak, M., Luks-Betlej, K., **2004**. Application of membrane techniques to water purification. Removal of phthalates. *Desalination, 162*, 121–128.

Brar, S.K., Verma, M., Tyagi, R.D., Valéro, J.R., Surampalli, R.Y., **2009**. Concurrent degradation of dimethyl phthalate (DMP) during production of *Bacillus thuringiensis* based biopesticides. *J. Hazard. Mater., 171*, 1016–1023.

Burridge, E., **2003**. Bisphenol A: product profile. *Eur. Chem. News, 17*, 14–20.

Buxton, G.V., Greenstock, C.L., Helman, W.P., Ross, A.B., **1988**. Critical review of rate constants for reactions of hydrated electrons, hydrogen atoms and hydroxyl radicals (·OH /·O^-) in aqueous solution. *J. Phys. Chem. Ref. Data, 17*, 513–886.

Cadogan, D.F., **1991**. Plasticizers: a consideration of their impact on health and the environment. *J. Vinyl Technol., 13*, 104 –108.

Calderbank, P.H., Moo-Young, M.B., **1961**. The continuous phase heat and mass-transfer properties of dispersions. *Chem. Eng. Sci., 16*, 39–54.

Chang, B.V., Liao, C.S., Yuan, S.Y., **2005**. Anaerobic degradation of diethyl phthalate, di-n-butyl phthalate, and di-(2-ethylhexyl) phthalate from river sediment in Taiwan. *Chemosphere, 58*, 1601–1607.

Chen, T.C., Matira, E.M., Lu, M.C., Dalida, M.L.P., **2016**. Degradation of dimethyl sulfoxide through fluidized-bed Fenton process: kinetic analysis. *Int. J. Environ. Sci. Technol., 13*, 1017–1028.

Chen, Y.-H., Hsieh, D.-C., Shang, N.-C., **2011**. Efficient mineralization of dimethyl phthalate by catalytic ozonation using TiO_2/Al_2O_3 catalyst. *J. Hazard. Mater., 192*, 1017–1025.

Chen, Y.H., Shang, N.C., Hsieh, D.C., **2008**. Decomposition of dimethyl phthalate in an aqueous solution by ozonation with high silica zeolites and UV radiation. *J. Hazard. Mater., 157*, 260–268.

Cheng, X., Wodarczyk, M., Lendzinski, R., Peterkin, E., Burlingame, G.A., **2009**. Control of DMSO in wastewater to prevent DMS nuisance odors. *Water Res., 43*, 2989–2998.

Chu, L.-B., Xing, X.-H., Yu, A.-F., Sun, X.-L., Jurcik, B., **2008a**. Enhanced treatment of practical textile wastewater by microbubble ozonation. *Process Saf. Environ. Prot., 86*, 389–393.

Chu, L.B., Xing, X.H., Yu, A.F., Zhou, Y.N., Sun, X.L., Jurcik, B., **2007**. Enhanced ozonation of simulated dyestuff wastewater by microbubbles. *Chemosphere, 68*, 1854 –1860.

Chu, L.B., Yan, S.T., Xing, X.H., Yu, A.F., Sun, X.L., Jurcik, B., **2008b**. Enhanced sludge solubilization by microbubble ozonation. *Chemosphere, 72*, 205–212.

Ciambrone, D.F., **1976**. Corona discharge ozone generator. United States Patent US3942020 A, 1976–03–02.

Clift, R., Grace, J.R., Weber, M.E., **2005**. Bubbles, Drops, and Particles, 1st ed. Courier Corporation, Chelmsford (UK).

Comninellis, C., Kapalka, A., Malato, S., Parsons, S.A., Poulios, I., Mantzavinos, D., **2008**. Advanced oxidation processes for water treatment: advances and trends for R&D. *J. Chem. Technol. Biotechnol., 83*, 769–776.

Crisp, T.M., Clegg, E.D., Cooper, R.L., Wood, W.P., Anderson, D.G., Baetcke, K.P., Hoffmann, J.L., Morrow, M.S., Rodier, D.J., Schaeffer, J.E., **1998**. Environmental endocrine disruption: an effects assessment and analysis. *Environ. Health Perspect., 106*, 11–56.

Cuerda-Correa, E.M., Alexandre-Franco, M.F., Fernández-González, C., **2020**. Advanced oxidation processes for the removal of antibiotics from water. an overview. *Water, 12*, 102–153.

Cui, Y.-h., Li, X.-y., Chen, G., **2009**. Electrochemical degradation of bisphenol A on different anodes. *Water Res., 43*, 1968–1976.

Cussler, E.L., **1997**. Diffusion: Mass Transfer in Fluid Systems, 1st ed. Cambridge University Press, Cambridge (UK)

Daughton, C.G., **2004**. Non-regulated water contaminants: emerging research. *Environ. Impact Assess. Rev., 24*, 711–732.

David, F.O., **1993**. Comparative Aspects of Advanced Oxidation Processes, *Emerging Technologies in Hazardous Waste Management III*. American Chemical Society, pp. 18–34.

de Oliveira, T.F., Chedeville, O., Fauduet, H., Cagnon, B., **2011**. Use of ozone/activated carbon coupling to remove diethyl phthalate from water: influence of activated carbon textural and chemical properties. *Desalination, 276*, 359–365.

Deborde, M., Rabouan, S., Mazellier, P., Duguet, J.-P., Legube, B., **2008**. Oxidation of bisphenol A by ozone in aqueous solution. *Water Res., 42*, 4299–4308.

Dekant, W., Völkel, W., **2008**. Human exposure to bisphenol A by biomonitoring: methods, results and assessment of environmental exposures. *Toxicol. Appl. Pharmacol., 228*, 114–134.

Dijkmans, P.A., Juffermans, L.J., Musters, R.J., van Wamel, A., ten Cate, F.J., van Gilst, W., Visser, C.A., de Jong, N., Kamp, O., **2004**. Microbubbles and ultrasound: from diagnosis to therapy. *Eur. J. Echocardiogr., 5*, 245–256.

EPA **2014**: Toxic and priority pollutants under the clean water act. https://www.epa.gov/eg/toxic-and-priority-pollutants-under-clean-water-act (accessed 23 Nov 2020).

EPA **2015**: National Ambient Air Quality Standards (NAAQS) for Ozone. https://www.epa.gov/ground-level-ozone-pollution/ozone-national-ambient-air-quality-standards-naaqs (accessed 20 March 2021).

Esplugas, S., Giménez, J., Contreras, S., Pascual, E., Rodríguez, M., **2002**. Comparison of different advanced oxidation processes for phenol degradation. *Water Res., 36*, 1034 –1042.

Fromme, H., Küchler, T., Otto, T., Pilz, K., Müller, J., Wenzel, A., **2002**. Occurrence of phthalates and bisphenol A and F in the environment. *Water Res., 36*, 1429–1438.

Fürhacker, M., Scharf, S., Weber, H., **2000**. Bisphenol A: emissions from point sources. *Chemosphere, 41*, 751–756.

Garoma, T., Matsumoto, S., **2009**. Ozonation of aqueous solution containing bisphenol A: effect of operational parameters. *J. Hazard. Mater., 167*, 1185–1191.

Garoma, T., Matsumoto, S.A., Wu, Y., Klinger, R., **2010**. Removal of bisphenol A and its reaction-intermediates from aqueous solution by ozonation. *Ozone Sci. Eng., 32*, 338–343.

Geis, N.A., Katus, H.A., Bekeredjian, R., **2012**. Microbubbles as a vehicle for gene and drug delivery: current clinical implications and future perspectives. *Curr. Pharm. Des., 18*, 2166–2183.

Ghosh, P., **2009**. Colloid and Interface Science, 1st ed. PHI Learning, New Delhi (India).

Glaze, W.H., **1986**. Reaction products of ozone: a review. *Environ. Health Perspect., 69*, 151–157.

Glaze, W.H., **1987**. Drinking-water treatment with ozone. *Environ. Sci. Technol., 21*, 224–230.

Glindemann, D., Novak, J., Witherspoon, J., **2006**. Dimethyl sulfoxide (DMSO) waste residues and municipal waste water odor by dimethyl sulfide (DMS): the north-east WPCP plant of Philadelphia. *Environ. Sci. Technol., 40*, 202–207.

Glindemann, D., Novak, J.T., Witherspoon, J., **2007**. Aeration tank odour by dimethyl sulphoxide (DMSO) waste in sewage. *Water Sci. Technol., 55*, 319–326.

Gonçalves, A.A., **2009**. Ozone: an emerging technology for the seafood industry. *Braz. Arch. Biol. Technol., 52*, 1527–1539.

Gottschalk, C., Libra, J.A., Saupe, A., **2010**. Ozonation of Water and Waste Water: A Practical Guide to Understanding Ozone and its Applications, 2nd ed. Wiley-VCH, Weinheim (Germany).

Gurol, M.D., **1985**. Factors controlling the removal of organic pollutants in ozone reactors. *J. Am. Water Works Assoc., 77*, 55–60.

Hasegawa, H., Kataoka, H., Asano, K., **2009**. Effect of electrical potential of microbubbles on ozone dissolution. *J. Phys.: Conf. Ser., 147*, 1–9.

Hayashi, O., Kameshiro, M., Masuda, M., Satoh, K., **2008**. Bioaccumulation and metabolism of [^{14}C] bisphenol A in the brackish water bivalve *Corbicula japonica*. *Biosci., Biotechnol., Biochem.*, 3219–3224.

Hofmeier, U., Yaminsky, V.V., Christenson, H.K., **1995**. Observations of solute effects on bubble formation. *J. Colloid Interface Sci., 174*, 199–210.

Hoigne, J., Bader, H., **1979**. Ozonation of water: selectivity and rate of oxidation of solutes. *Ozone Sci. Eng., 1*, 73–85.

Hosokawa, S., Tanaka, K., Tomiyama, A., Maeda, Y., Yamaguchi, S., Ito, Y., **2009**. Measurement of micro bubbles generated by a pressurized dissolution method. *J. Phys.: Conf. Ser., 147*, 1–10.

Hou, M., Chu, Y., Li, X., Wang, H., Yao, W., Yu, G., Murayama, S., Wang, Y., **2016**. Electro-peroxone degradation of diethyl phthalate: cathode selection, operational parameters, and degradation mechanisms. *J. Hazard. Mater., 319*, 61–68.

Huang, J., Nkrumah, P.N., Li, Y., Appiah-Sefah, G., **2013**. Chemical behavior of phthalates under abiotic conditions in landfills. *Rev. Environ. Contam. Toxicol., 224*, 39–52.

Ikeura, H., Kobayashi, F., Tamaki, M., **2011a**. Removal of residual pesticide, fenitrothion, in vegetables by using ozone microbubbles generated by different methods. *J. Food Eng., 103*, 345–349.

Ikeura, H., Kobayashi, F., Tamaki, M., **2011b**. Removal of residual pesticides in vegetables using ozone microbubbles. *J. Hazard. Mater., 186*, 956–959.

Inoue, M., Masuda, Y., Okada, F., Sakurai, A., Takahashi, I., Sakakibara, M., **2008**. Degradation of bisphenol A using sonochemical reactions. *Water Res., 42*, 1379–1386.

Ioan, I., Wilson, S., Lundanes, E., Neculai, A., **2007**. Comparison of Fenton and sono-Fenton bisphenol A degradation. *J. Hazard. Mater., 142*, 559–563.

Irmak, S., Erbatur, O., Akgerman, A., **2005**. Degradation of 17β-estradiol and bisphenol A in aqueous medium by using ozone and ozone/UV techniques. *J. Hazard. Mater., 126*, 54–62.

Isil, G., Valko, M., Nilsun, H.I., **2009**. Degradation of bisphenol-A by ozonation. *J. Adv. Oxid. Technol., 12*, 242–248.

Jauregi, P., Varley, J., **1999**. Colloidal gas aphrons: potential applications in biotechnology. *Trends Biotechnol., 17*, 389–395.

Jenkins, K.B., Michelsen, D.L., Novak, J.T., **1993**. Application of oxygen microbubbles for *in situ* biodegradation of p-xylene-contaminated groundwater in a soil column. *Biotechnol. Progr., 9*, 394–400.

Jing, Y., Li, L., Zhang, Q., Lu, P., Liu, P., Lü, X., **2011**. Photocatalytic ozonation of dimethyl phthalate with TiO_2 prepared by a hydrothermal method. *J. Hazard. Mater., 189*, 40–47.

Johnson, P.N., Davis, R.A., **1996**. Diffusivity of ozone in water. *J. Chem. Eng. Data, 41*, 1485–1487.

Jothinathan, L., Cai, Q.Q., Ong, S.L., Hu, J.Y., **2021**. Organics removal in high strength petrochemical wastewater with combined microbubble-catalytic ozonation process. *Chemosphere, 263*, 127980.

Jung, Y.J., Oh, B.S., Kim, K.S., Koga, M., Shinohara, R., Kang, J.W., **2010**. The degradation of diethyl phthalate (DEP) during ozonation: oxidation by-products study. *J. Water Health, 8*, 290–298.

Kang, J.H., Kondo, F., Katayama, Y., **2006**. Human exposure to bisphenol A. *Toxicology, 226*, 79–89.

Kasprzyk-Hordern, B., Ziółek, M., Nawrocki, J., **2003**. Catalytic ozonation and methods of enhancing molecular ozone reactions in water treatment. *Appl. Catal. B, 46*, 639–669.

Kaufmann, B.A., Lindner, J.R., **2007**. Molecular imaging with targeted contrast ultrasound. *Curr. Opin. Biotechnol., 18*, 11–16.

Kawahara, A., Sadatomi, M., Matsuyama, F., Matsuura, H., Tominaga, M., Noguchi, M., **2009**. Prediction of micro-bubble dissolution characteristics in water and seawater. *Exp. Therm. Fluid Sci., 33*, 883–894.

Keykavoos, R., Mankidy, R., Ma, H., Jones, P., Soltan, J., **2013**. Mineralization of bisphenol A by catalytic ozonation over alumina. *Sep. Purif. Technol., 107*, 310–317.

Khan, N.A., Jung, B.K., Hasan, Z., Jhung, S.H., **2015**. Adsorption and removal of phthalic acid and diethyl phthalate from water with zeolitic imidazolate and metal–organic frameworks. *J. Hazard. Mater., 282*, 194–200.

Khuntia, S., Majumder, S.K., Ghosh, P., **2012a**. Microbubble-aided water and wastewater purification: a review. *Rev. Chem. Eng., 28*, 191–221.

Khuntia, S., Majumder, S.K., Ghosh, P., **2012b**. Removal of ammonia from water by ozone microbubbles. *Ind. Eng. Chem. Res., 52*, 318–326.

Khuntia, S., Majumder, S.K., Ghosh, P., **2014a**. Oxidation of As(III) to As(V) using ozone microbubbles. *Chemosphere, 97*, 120–124.

Khuntia, S., Majumder, S.K., Ghosh, P., **2014b**. A pilot plant study of the degradation of Brilliant Green dye using ozone microbubbles: mechanism and kinetics of reaction. *Environ. Technol., 36*, 336–347.

Kobayashi, F., Ikeura, H., Ohsato, S., Goto, T., Tamaki, M., **2011**. Disinfection using ozone microbubbles to inactivate *Fusarium oxysporum* f. sp. *melonis* and *Pectobacterium carotovorum* subsp. *carotovorum*. *J. Crop Prot., 30*, 1514–1518.

Koito, T., Tekawa, M., Toyoda, A., **1998**. A novel treatment technique for DMSO wastewater. *IEEE Trans. Semicond., 11*, 3–8.

Kolpin, D.W., Furlong, E.T., Meyer, M.T., Thurman, E.M., Zaugg, S.D., Barber, L.B., Buxton, H.T., **2002**. Pharmaceuticals, hormones, and other organic wastewater contaminants in US streams, 1999− 2000: a national reconnaissance. *Environ. Sci. Technol.*, *36*, 1202–1211.

Kurup, N., Naik, P., **2010**. Microbubbles: a novel delivery system. *Asian J. Pharmaceut. Res. Health Care*, *2*, 228–234.

Kusvuran, E., Yildirim, D., **2013**. Degradation of bisphenol A by ozonation and determination of degradation intermediates by gas chromatography–mass spectrometry and liquid chromatography–mass spectrometry. *Chem. Eng. J.*, *220*, 6–14.

Lee, C., Lee, Y., Yoon, J., **2006**. Oxidative degradation of dimethylsulfoxide by locally concentrated hydroxyl radicals in streamer corona discharge process. *Chemosphere*, *65*, 1163–1170.

Lee, J., Park, H., Yoon, J., **2003**. Ozonation characteristics of bisphenol A in water. *Environ. Technol*, *24*, 241–248.

Lee, S., Kim, S., **2005**. Simultaneous measurement of size and velocity of microbubbles moving in an opaque tube using an X-ray particle tracking velocimetry technique. *Exp Fluids*, *39*, 492–497.

Lee, Y., Lee, C., Yoon, J., **2004**. Kinetics and mechanisms of DMSO (dimethylsulfoxide) degradation by UV/H_2O_2 process. *Water Res.*, *38*, 2579–2588.

Legube, B., Guyon, S., Sugimitsu, H., Dore, M., **1983**. Ozonation of some aromatic compounds in aqueous solution: styrene, benzaldehyde, naphthalene, diethylphthalate, ethyl and chloro benzenes. *Ozone Sci. Eng.*, *5*, 151–170.

Li, C., Li, X., Graham, N., Gao, N., **2008**. The aqueous degradation of bisphenol A and steroid estrogens by ferrate. *Water Res.*, *42*, 109–120.

Li, C., Yuan, S., Jiang, F., Xie, Y., Guo, Y., Yu, H., Cheng, Y., Qian, H., Yao, W., **2020**. Degradation of fluopyram in water under ozone enhanced microbubbles: kinetics, degradation products, reaction mechanism, and toxicity evaluation. *Chemosphere*, *258*, 127216.

Li, L., Ye, W., Zhang, Q., Sun, F., Lu, P., Li, X., **2009a**. Catalytic ozonation of dimethyl phthalate over cerium supported on activated carbon. *J. Hazard. Mater.*, *170*, 411–416.

Li, P. **2006.** Development of advanced water treatment technology using micro bubbles. *PhD Thesis*, Keio University, Japan.

Li, P., Takahashi, M., Chiba, K., **2009b**. Degradation of phenol by the collapse of microbubbles. *Chemosphere, 75*, 1371–1375.

Li, P., Takahashi, M., Chiba, K., **2009c**. Enhanced free-radical generation by shrinking microbubbles using a copper catalyst. *Chemosphere, 77*, 1157–1160.

Li, P., Tsuge, H., Itoh, K., **2009d**. Oxidation of dimethyl sulfoxide in aqueous solution using microbubbles. *Ind. Eng. Chem. Res., 48*, 8048–8053.

Liang, D.-W., Zhang, T., Fang, H.H.P., **2007**. Anaerobic degradation of dimethyl phthalate in wastewater in a UASB reactor. *Water Res., 41*, 2879–2884.

Liu, S., Wang, Q., Ma, H., Huang, P., Li, J., Kikuchi, T., **2010**. Effect of micro-bubbles on coagulation flotation process of dyeing wastewater. *Sep. Purif. Technol., 71*, 337–346.

Liu, Y., Wang, S., Shi, L., Lu, W., Li, P., **2020**. Enhanced degradation of atrazine by microbubble ozonation. *Environ. Sci. Water Res. Technol., 6*, 1681–1687.

Liu, Y., Zhao, J., Li, Z., Li, G., Li, W., Gao, X., **2015**. Catalytic ozonation of bisphenol A in aqueous solution using Mn-Ce/HZSM-5 as catalyst. *Water Sci. Technol., 72*, 696–703.

Liu, Z., Wardenier, N., Hosseinzadeh, S., Verheust, Y., De Buyck, P.-J., Chys, M., Nikiforov, A., Leys, C., Van Hulle, S., **2018**. Degradation of bisphenol A by combining ozone with UV and H_2O_2 in aqueous solutions: mechanism and optimization. *Clean Technol. Environ. Policy, 20*, 2109–2118.

Loeb, B.L., Thompson, C.M., Drago, J., Takahara, H., Baig, S., **2012**. Worldwide ozone capacity for treatment of drinking water and wastewater: a review. *Ozone Sci. Eng., 34*, 64–77.

Luo, K., Zhao, S.X., Wang, Y.F., Zhao, S.J., Zhang, X.H., **2018**. Synthesis of petal-like δ-MnO_2 and its catalytic ozonation performance. *New J. Chem., 42*, 6770–6777.

MacGregor, W.S., **1967**. The chemical and physical properties of DMSO. *Ann. N. Y. Acad. Sci., 141*, 3–12.

Maeda, Y., Hosokawa, S., Baba, Y., Tomiyama, A., Ito, Y., **2015**. Generation mechanism of micro-bubbles in a pressurized dissolution method. *Exp. Therm. Fluid Sci., 60*, 201–207.

Magara, Y., Itoh, M., Morioka, T., **1995**. Application of ozone to water treatment and power consumption of ozone generating systems. *Prog. Nucl. Energy, 29 (Supplement)*, 175–182.

Majumder, S.K., **2016**. Hydrodynamics and Transport Processes of Inverse Bubbly Flow, 1st ed. Elsevier, Amsterdam (the Netherlands).

Makuta, T., Takemura, F., Hihara, E., Matsumoto, Y., Shoji, M., **2006**. Generation of micro gas bubbles of uniform diameter in an ultrasonic field. *J. Fluid Mech., 548*, 113–131.

Maldonado, M.I., Malato, S., Pérez-Estrada, L.A., Gernjak, W., Oller, I., Doménech, X., Peral, J., **2006**. Partial degradation of five pesticides and an industrial pollutant by ozonation in a pilot-plant scale reactor. *J. Hazard. Mater., 138*, 363–369.

Mansouri, L., Mohammed, H., Tizaoui, C., Bousselmi, L., **2013**. Heterogeneous catalytic ozonation of diethyl phthalate. *Desalination Water Treat., 51*, 6698–6710.

Masten, S.J., Davies, S.H.R., **1994**. The use of ozonation to degrade organic contaminants in wastewaters. *Environ. Sci. Technol., 28*, 180A–185A.

Mehrabani-Zeinabad, M., Achari, G., Langford, C.H., **2015**. Advanced oxidative degradation of bisphenol A and bisphenol S. *J. Environ. Eng. Sci., 10*, 92–102.

Mehrabani-Zeinabad, M., Achari, G., Langford Cooper, H., **2016**. Degradation of bisphenol S using O_3 and/or H_2O_2 with UV in a flow-through reactor. *J. Environ. Eng., 142*, 0601–6004.

Motarjemi, M., Jameson, G.J., **1978**. Mass transfer from very small bubbles: the optimum bubble size for aeration. *Chem. Eng. Sci., 33*, 1415–1423.

Mutseyekwa, M.E., Doğan, Ş., Pirgalıoğlu, S., **2017**. Ozonation for the removal of bisphenol A. *Water Sci. Technol., 76*, 2764–2775.

Na, S., Ahn, Y.G., Cui, M., Khim, J., **2012**. Significant diethyl phthalate (DEP) degradation by combined advanced oxidation process in aqueous solution. *J. Environ. Manage., 101*, 104–110.

Nahum, M.C., Raúl, O.P., Roberto, L.R., Manuel, S.P., José, R.U., José D., M.D., **2013**. Removal of diethyl phthalate from water solution by adsorption, photo-oxidation, ozonation and advanced oxidation process (UV/H_2O_2, O_3/H_2O_2 and O_3/activated carbon). *Sci. Total Environ., 442*, 26–35.

Nam, G., Mohamed, M.M., Jung, J., **2019**. Enhanced degradation of benzo[a]pyrene and toxicity reduction by microbubble ozonation. *Environ. Technol, 41*, 1–8.

Net, S., Sempéré, R., Delmont, A., Paluselli, A., Ouddane, B., **2015**. Occurrence, fate, behavior and ecotoxicological state of phthalates in different environmental matrices. *Environ. Sci. Technol., 49*, 4019–4035.

Nieuwenhuijsen, M.J., Toledano, M.B., Eaton, N.E., Fawell, J., Elliott, P., **2000**. Chlorination disinfection byproducts in water and their association with adverse reproductive outcomes: a review. *Occup Environ Med, 57*, 73–85.

Nishiki, Y., Kitaori, N., Nakamuro, K., **2011**. Performances of small-sized generator of ozone-dissolved water using boron-doped diamond electrodes. *Ozone Sci. Eng., 33*, 114–120.

Oh, B.S., Jung, Y.J., Oh, Y.J., Yoo, Y.S., Kang, J.W., **2006**. Application of ozone, UV and ozone/UV processes to reduce diethyl phthalate and its estrogenic activity. *Sci. Total Environ., 367*, 681–693.

Oneby, M.A., Bromley, C.O., Borchardt, J.H., Harrison, D.S., **2010**. Ozone treatment of secondary effluent at U.S. municipal wastewater treatment plants. *Ozone Sci. Eng., 32*, 43–55.

Onundi, Y., Drake, B.A., Malecky, R.T., DeNardo, M.A., Mills, M.R., Kundu, S., Ryabov, A.D., Beach, E.S., Horwitz, C.P., Simonich, M.T., **2017**. A multidisciplinary investigation of the technical and environmental performances of TAML/peroxide elimination of bisphenol A compounds from water. *Green Chem., 19*, 4234–4262.

Park, S.J., Yoon, T.I., Bae, J.H., Seo, H.J., Park, H.J., **2001**. Biological treatment of wastewater containing dimethyl sulphoxide from the semi-conductor industry. *Process Biochem., 36*, 579–589.

Parmar, R., Majumder, S.K., **2013**. Microbubble generation and microbubble-aided transport process intensification: a state-of-the-art report. *Chem. Eng. Process., 64*, 79–97.

Patel, S., Agarwal, R., Majumder, S.K., Das, P., Ghosh, P., **2020**. Kinetics of ozonation and mass transfer of pharmaceuticals degraded by ozone fine bubbles in a plant prototype. *Heat Mass Transfer, 56*, 385–397.

Peijnenburg, W.J.G.M., Struijs, J., **2006**. Occurrence of phthalate esters in the environment of the Netherlands. *Ecotoxicol. Environ. Saf., 63*, 204–215.

Pelssers, E.G.M., Cohen Stuart, M.A., Fleer, G.J., **1990**. Single particle optical sizing (SPOS): I. Design of an improved SPOS instrument and application to stable dispersions. *J. Colloid Interface Sci., 137*, 350–361.

Pérez-Garibay, R., Martínez-Ramos, E., Rubio, J., **2012**. Gas dispersion measurements in microbubble flotation systems. *Miner. Eng., 26*, 34–40.

Qadafi, M., Notodarmojo, S., Zevi, Y., **2020**. Effects of microbubble pre-ozonation time and pH on trihalomethanes and haloacetic acids formation in pilot-scale tropical peat water treatments for drinking water purposes. *Sci. Total Environ., 747*, 141540.

Qu, X., Wang, L., Karakashev, S.I., Nguyen, A.V., **2009**. Anomalous thickness variation of the foam films stabilized by weak non-ionic surfactants. *J. Colloid Interface Sci., 337*, 538–547.

Richardson, S.D., Ternes, T.A., **2014**. Water analysis: emerging contaminants and current issues. *Anal. Chem., 86*, 2813–2848.

Rivas, F.J., Encinas, Á., Acedo, B., Beltrán, F.J., **2009**. Mineralization of bisphenol A by advanced oxidation processes. *J. Chem. Technol. Biotechnol., 84*, 589–594.

Rodriguez-Mozaz, S., de Alda, M.J.L., Barceló, D., **2004**. Monitoring of estrogens, pesticides and bisphenol A in natural waters and drinking water treatment plants by solid-phase extraction–liquid chromatography–mass spectrometry. *J. Chromatogr. A, 1045*, 85–92.

Roslev, P., Vorkamp, K., Aarup, J., Frederiksen, K., Nielsen, P.H., **2007**. Degradation of phthalate esters in an activated sludge wastewater treatment plant. *Water Res., 41*, 969–976.

Rubin, B.S., Soto, A.M., **2009**. Bisphenol A: perinatal exposure and body weight. *Mol. Cell. Endocrinol., 304*, 55–62.

Ryskie, S., Gonzalez-Merchan, C., Neculita, C.M., Genty, T., **2020**. Efficiency of ozone microbubbles for ammonia removal from mine effluents. *Miner. Eng., 145*, 106071.

Sadatomi, M., Kawahara, A., Kano, K., Ohtomo, A., **2005**. Performance of a new micro-bubble generator with a spherical body in a flowing water tube. *Exp. Therm. Fluid Sci., 29*, 615–623.

Sadatomi, M., Kawahara, A., Matsuura, H., Shikatani, S., **2012**. Micro-bubble generation rate and bubble dissolution rate into water by a simple multi-fluid mixer with orifice and porous tube. *Exp. Therm. Fluid Sci., 41*, 23–30.

Saravanan, P., Pakshirajan, K., Saha, P., **2009**. Degradation of phenol by TiO_2-based heterogeneous photocatalysts in presence of sunlight. *J. Hydro-envron. Res., 3*, 45–50.

Scaduto, R.C., **1995**. Oxidation of DMSO and methanesulfinic acid by the hydroxyl radical. *Free Radical Biol. Med., 18*, 271–277.

Shelton, D.R., Boyd, S.A., Tiedje, J.M., **1984**. Anaerobic biodegradation of phthalic acid esters in sludge. *Environ. Sci. Technol., 18*, 93–97.

Shin, W.T., Mirmiran, A., Yiacoumi, S., Tsouris, C., **1999**. Ozonation using microbubbles formed by electric fields. *Sep. Purif. Technol., 15*, 271–282.

Silva, L.M.d., Jardim, W.F., **2006**. Trends and strategies of ozone application in environmental problems. *Quim. Nova, 29*, 310–317.

Sirsi, S., Borden, M., **2009**. Microbubble compositions, properties and biomedical applications. *Bubble Sci. Eng. Technol., 1*, 3–17.

Staehelin, J., Hoigne, J., **1985**. Decomposition of ozone in water in the presence of organic solutes acting as promoters and inhibitors of radical chain reactions. *Environ. Sci. Technol., 19*, 1206–1213.

Staples, C.A., Dome, P.B., Klecka, G.M., Oblock, S.T., Harris, L.R., **1998**. A review of the environmental fate, effects, and exposures of bisphenol A. *Chemosphere, 36*, 2149–2173.

Staples, C.A., Peterson, D.R., Parkerton, T.F., Adams, W.J., **1997**. The environmental fate of phthalate esters: a literature review. *Chemosphere, 35*, 667–749.

Sugiura-Ogasawara, M., Ozaki, Y., Sonta, S., Makino, T., Suzumori, K., **2005**. Exposure to bisphenol A is associated with recurrent miscarriage. *Hum. Reprod., 20*, 2325–2329.

Sumikura, M., Hidaka, M., Murakami, H., Nobutomo, Y., Murakami, T., **2007**. Ozone micro-bubble disinfection method for wastewater reuse system. *Water Sci. Technol., 56*, 53–61.

Sun, Z., Xia, F., Lou, Z., Chen, X., Zhu, N., Yuan, H., Shen, Y., **2020**. Innovative process for total petroleum hydrocarbons reduction on oil refinery sludge through microbubble ozonation. *J. Cleaner Prod., 256*, 120337.

Takahashi, M., **2005**. ζ potential of microbubbles in aqueous solutions: electrical properties of the gas–water interface. *J. Phys. Chem. B, 109*, 21858–21864.

Takahashi, M., **2009**. Base and technological application of micro-bubble and nano-bubble (article written in Japanese) *Mater. Integration 22*, 2–9.

Takahashi, M., **2010**. Water treatment based on microbubble technology (article written in Japanese). *Bull. Soc. Sea Water Sci. Jpn. , 64*, 19–23.

Takahashi, M., Chiba, K., Li, P., **2007a**. Formation of hydroxyl radicals by collapsing ozone microbubbles under strongly acidic conditions. *J. Phys. Chem. B, 111*, 11443–11446.

Takahashi, M., Chiba, K., Li, P., **2007b**. Free-radical generation from collapsing microbubbles in the absence of a dynamic stimulus. *J. Phys. Chem. B, 111*, 1343–1347.

Takahashi, M., Ishikawa, H., Asano, T., Horibe, H., **2012**. Effect of microbubbles on ozonized water for photoresist removal. *J. Phys. Chem. C, 116*, 12578–12583.

Takahashi, M., Kawamura, T., Yamamoto, Y., Ohnari, H., Himuro, S., Shakutsui, H., **2003**. Effect of shrinking microbubble on gas hydrate formation. *J. Phys. Chem. B, 107*, 2171–2173.

Takeuchi, T., Tsutsumi, O., Ikezuki, Y., Takai, Y., Taketani, Y., **2004**. Positive relationship between androgen and the endocrine disruptor, bisphenol A, in normal women and women with ovarian dysfunction. *Endocr. J., 51*, 165–169.

Tan, B.L., Hawker, D.W., Müller, J.F., Leusch, F.D., Tremblay, L.A., Chapman, H.F., **2007**. Modelling of the fate of selected endocrine disruptors in a municipal wastewater treatment plant in South East Queensland, Australia. *Chemosphere, 69*, 644–654.

Tasaki, T., Wada, T., Fujimoto, K., Kai, S., Ohe, K., Oshima, T., Baba, Y., Kukizaki, M., **2009**. Degradation of methyl orange using short-wavelength UV irradiation with oxygen microbubbles. *J. Hazard. Mater., 162*, 1103–1110.

Temesgen, T., Bui, T.T., Han, M., Kim, T.-i., Park, H., **2017**. Micro and nanobubble technologies as a new horizon for water-treatment techniques: a review. *Adv. Colloid Interface Sci., 246*, 40–51.

Terasaka, K., Hirabayashi, A., Nishino, T., Fujioka, S., Kobayashi, D., **2011**. Development of microbubble aerator for waste water treatment using aerobic activated sludge. *Chem. Eng. Sci., 66*, 3172–3179.

Terasaka, K., Shinpo, Y., **2007**. Separation of fine particles suspended in water using microbubble flotation. *Jpn. J. Multiphase Flow*, *21*, 77–83.

Tiwari, B.K., Brennan, C.S., Curran, T., Gallagher, E., Cullen, P.J., O' Donnell, C.P., **2010**. Application of ozone in grain processing. *J. Cereal Sci.*, *51*, 248–255.

Torres, R.A., Abdelmalek, F., Combet, E., Pétrier, C., Pulgarin, C., **2007**. A comparative study of ultrasonic cavitation and Fenton's reagent for bisphenol A degradation in deionised and natural waters. *J. Hazard. Mater.*, *146*, 546–551.

Tsuge, H., **2014**. Micro- and Nanobubbles: Fundamentals and Applications, 1st ed. CRC Press, Boca Raton, FL.

Tsuge, H., Li, P., Shimatani, N., Shimamura, Y., Nakata, H., Ohira, M., **2009**. Fundamental study on disinfection effect of microbubbles (article written in Japanese). *Kagaku Kogaku Ronbun.*, *35*, 548–552.

Umar, M., Roddick, F., Fan, L., Aziz, H.A., **2013**. Application of ozone for the removal of bisphenol A from water and wastewater – a review. *Chemosphere*, *90*, 2197–2207.

Vandenberg, L.N., Hauser, R., Marcus, M., Olea, N., Welshons, W.V., **2007**. Human exposure to bisphenol A (BPA). *Reprod. Toxicol.*, *24*, 139–177.

Vega, D., Bastide, J., **2003**. Dimethylphthalate hydrolysis by specific microbial esterase. *Chemosphere*, *51*, 663–668.

Vethaak, A.D., Lahr, J., Schrap, S.M., Belfroid, A.C., Rijs, G.B., Gerritsen, A., de Boer, J., Bulder, A.S., Grinwis, G.C., Kuiper, R.V., **2005**. An integrated assessment of estrogenic contamination and biological effects in the aquatic environment of The Netherlands. *Chemosphere*, *59*, 511–524.

Vom Saal, F.S., Hughes, C., **2005**. An extensive new literature concerning low-dose effects of bisphenol A shows the need for a new risk assessment. *Environ. Health Perspect.*, *113*, 926–933.

von Gunten, U., **2003a**. Ozonation of drinking water: part I. Oxidation kinetics and product formation. *Water Res.*, *37*, 1443–1467.

Von Gunten, U., **2003b**. Ozonation of drinking water: part II. Disinfection and by-product formation in presence of bromide, iodide or chlorine. *Water Res.*, *37*, 1469–1487.

von Sonntag, C., von Gunten, U., **2012**. Chemistry of Ozone in Water and Wastewater Treatment: From Basic Principles to Applications. *Water Intelligence Online*, *11*.

Walker, A.B., Tsouris, C., DePaoli, D.W., Thomas, K.K., **2001**. Ozonation of soluble organics in aqueous solutions using microbubbles. *Ozone Sci. Eng.*, *23*, 77–87.

Wan, X., Zhang, L., Sun, Z., Yu, W., Xie, H., **2020**. Treatment of high concentration acid plasticizer wastewater by ozone microbubble oxidation. *Water, Air, Soil Pollut.*, *231*, 367.

Wang, J., Cheng, J., Wang, C., Yang, S., Zhu, W., **2013**. Catalytic ozonation of dimethyl phthalate with RuO_2/Al_2O_3 catalysts prepared by microwave irradiation. *Catal. Commun.*, *41*, 1–5.

Wang, J., Zhou, Y., Zhu, W., He, X., **2009a**. Catalytic ozonation of dimethyl phthalate and chlorination disinfection by-product precursors over Ru/AC. *J. Hazard. Mater.*, *166*, 502–507.

Wang, R., Ren, D., Xia, S., Zhang, Y., Zhao, J., **2009b**. Photocatalytic degradation of Bisphenol A (BPA) using immobilized TiO_2 and UV illumination in a horizontal circulating bed photocatalytic reactor (HCBPR). *J. Hazard. Mater.*, *169*, 926–932.

Waslo, S., Gal-or, B., **1971**. Boundary layer theory for mass and heat transfer in clouds of moving drops, bubbles or solid particles. *Chem. Eng. Sci.*, *26*, 829–838.

Wen, C.C., Wang, C.T., Chou, W.L., Chang, W.C., Lee, S.R., **2012a**. Degradation of DMSO in aqueous solutions by the Fenton reaction based advanced oxidation processes. *Fresenius Environ. Bull.*, *21*, 644–650.

Wen, G., Ma, J., Liu, Z.Q., Zhao, L., **2011**. Ozonation kinetics for the degradation of phthalate esters in water and the reduction of toxicity in the process of O_3/H_2O_2. *J. Hazard. Mater.*, *195*, 371–377.

Wen, L.H., Ismail, A.B., Menon, P.M., Saththasivam, J., Thu, K., Choon, N.K., **2012b**. Case studies of microbubbles in wastewater treatment. *Desalination Water Treat.*, *30*, 10–16.

Wetherill, Y.B., Petre, C.E., Monk, K.R., Puga, A., Knudsen, K.E., **2002**. The xenoestrogen bisphenol A induces inappropriate androgen receptor activation and mitogenesis in prostatic adenocarcinoma cells. *Mol. Cancer Ther.*, *1*, 515–524.

Whitman, W.G., **1962**. The two film theory of gas absorption. *Int. J. Heat Mass Transfer*, *5*, 429–433.

Wu, J.J., Muruganandham, M., Chen, S.H., **2007**. Degradation of DMSO by ozone-based advanced oxidation processes. *J. Hazard. Mater.*, *149*, 218–225.

Wu, J.J., Muruganandham, M., Yang, J.S., Lin, S.S., **2006**. Oxidation of DMSO on goethite catalyst in the presence of H_2O_2 at neutral pH. *Catal. Commun.*, *7*, 901–906.

Xia, Z., Hu, L., **2019**. Treatment of organics contaminated wastewater by ozone micro-nano-bubbles. *Water*, *11*, 55–65.

Xie, Y.-B., Li, X.-Z., **2006**. Degradation of bisphenol A in aqueous solution by H_2O_2-assisted photoelectrocatalytic oxidation. *J. Hazard. Mater.*, *138*, 526–533.

Xie, Z., Ebinghaus, R., Temme, C., Lohmann, R., Caba, A., Ruck, W., **2007**. Occurrence and air-sea exchange of phthalates in the Arctic. *Environ. Sci. Technol.*, *41*, 4555–4560.

Xu, B., Gao, N.Y., Sun, X.F., Xia, S.J., Rui, M., Simonnot, M.O., Causserand, C., Zhao, J.F., **2007**. Photochemical degradation of diethyl phthalate with UV/H_2O_2. *J. Hazard. Mater.*, *139*, 132–139.

Xu, J.H., Li, S.W., Chen, G.G., Luo, G.S., **2006**. Formation of monodisperse microbubbles in a microfluidic device. *AIChE J.*, *52*, 2254–2259.

Xu, Q., Nakajima, M., Liu, Z., Shiina, T., **2011**. Biosurfactants for microbubble preparation and application. *Int. J. Mol. Sci.*, *12*, 462–475.

Yamamoto, T., Yasuhara, A., Shiraishi, H., Nakasugi, O., **2001**. Bisphenol A in hazardous waste landfill leachates. *Chemosphere*, *42*, 415–418.

Yang, G.-P., Zhao, X.-K., Sun, X.-J., Lu, X.-L., **2005a**. Oxidative degradation of diethyl phthalate by photochemically-enhanced Fenton reaction. *J. Hazard. Mater.*, *126*, 112–118.

Yang, X., Shang, C., Huang, J.-C., **2005b**. DBP formation in breakpoint chlorination of wastewater. *Water Res.*, *39*, 4755–4767.

Yang, Y., Guo, H., Zhang, Y., Deng, Q., Zhang, J., **2016**. Degradation of bisphenol A using ozone/persulfate process: kinetics and mechanism. *Water, Air, Soil Pollut.*, *227*, 53.

Yuan, S.Y., Liu, C., Liao, C.S., Chang, B.V., **2002**. Occurrence and microbial degradation of phthalate esters in Taiwan river sediments. *Chemosphere*, *49*, 1295–1299.

Yunrui, Z., Wanpeng, Z., Fudong, L., Jianbing, W., Shaoxia, Y., **2007**. Catalytic activity of Ru/Al_2O_3 for ozonation of dimethyl phthalate in aqueous solution. *Chemosphere*, *66*, 145–150.

Zanello, P., Nervi, C., De Biani, F.F., **2011**. Inorganic Electrochemistry: Theory, Practice and Application. Royal Society of Chemistry, Cambridge (UK).

Zhang, F., Xi, J., Huang, J.-J., Hu, H.-Y., **2013**. Effect of inlet ozone concentration on the performance of a micro-bubble ozonation system for inactivation of *Bacillus subtilis* spores. *Sep. Purif. Technol., 114*, 126–133.

Zhang, H., He, Y., Lai, L., Yao, G., Lai, B., **2020**. Catalytic ozonation of bisphenol A in aqueous solution by Fe_3O_4-MnO_2 magnetic composites: performance, transformation pathways and mechanism. *Sep. Purif. Technol., 245*, 116–449.

Zhang, H., Yamada, H., Tsuno, H., **2008**. Removal of endocrine-disrupting chemicals during ozonation of municipal sewage with brominated byproducts control. *Environ. Sci. Technol., 42*, 3375–3380.

Zhang, R., Hayama, S., Fujikawa, S., Takasugi, N., **2000**. A study of the measurement of bubbles in microbubble generation device (article written in Japanese). *Jpn. J. Multiphase Flow, 14*, 329–338.

Zhang, X., Shen, T., Ding, Y., Tong, S., **2019**. Graphite felt supported MgO catalytic ozonation of bisphenol A. *Ozone Sci. Eng., 41*, 541–550.

Zhou, H., Smith, D.W., **2000**. Ozone mass transfer in water and wastewater treatment: experimental observations using a 2D laser particle dynamics analyzer. *Water Res., 34*, 909–921.

Zhou, H., Smith, D.W., **2002**. Advanced technologies in water and wastewater treatment. *J. Environ. Eng. Sci., 1*, 247–264.

Zoeller, R.T., Brown, T.R., Doan, L.L., Gore, A.C., Skakkebaek, N.E., Soto, A.M., Woodruff, T.J., Vom Saal, F.S., **2012**. Endocrine-disrupting chemicals and public health protection: a statement of principles from The Endocrine Society. *Endocrinology, 153*, 4097–4110.

Zouboulis, A.I., Avranas, A., **2000**. Treatment of oil-in-water emulsions by coagulation and dissolved-air flotation. *Colloids Surf., A, 172*, 153–161.

CHAPTER 2

MATERIALS AND EXPERIMENTAL METHODS

This chapter presents the details of the experimental setups used for the removal of dimethyl phthalate, diethyl phthalate, bisphenol-A, and dimethyl sulfoxide. The list of chemicals used in this work and their sources are given. The experimental methods employed for the ozonation of the targeted pollutants are described. The details of the instruments used for the analysis of the samples are also given.

2.1. Experimental setup

2.1.1 Ozone microbubbles

The experimental setup for the ozone microbubbles (OMBs) was assembled from a number of units, which included an oxygen concentrator, an ozone generator, a microbubble generator (MBG), a polycarbonate reactor, an external circulatory water bath, and a destructor of excess ozone (Khuntia et al., 2012). Figure 2.1 shows a photograph of the experimental setup, whereas Figure 2.2 shows the schematic of the experimental setup for the OMBs, and the analysis of the samples. The ozonation was carried out in a polycarbonate reactor of 20 dm^3 capacity. The reactor was connected to the pressurized-dissolution/decompression type MBG [make: Riverforest Corporation (USA), model: AS MK-III], which operated in a continuous recirculation mode and generated the microbubbles. The oxygen concentrator [make: Oz-Air (India), model: HG 03], which employs the pressure swing adsorption technique (Grande, 2012; Sircar and Kratz, 1989), was used to isolate oxygen from air.

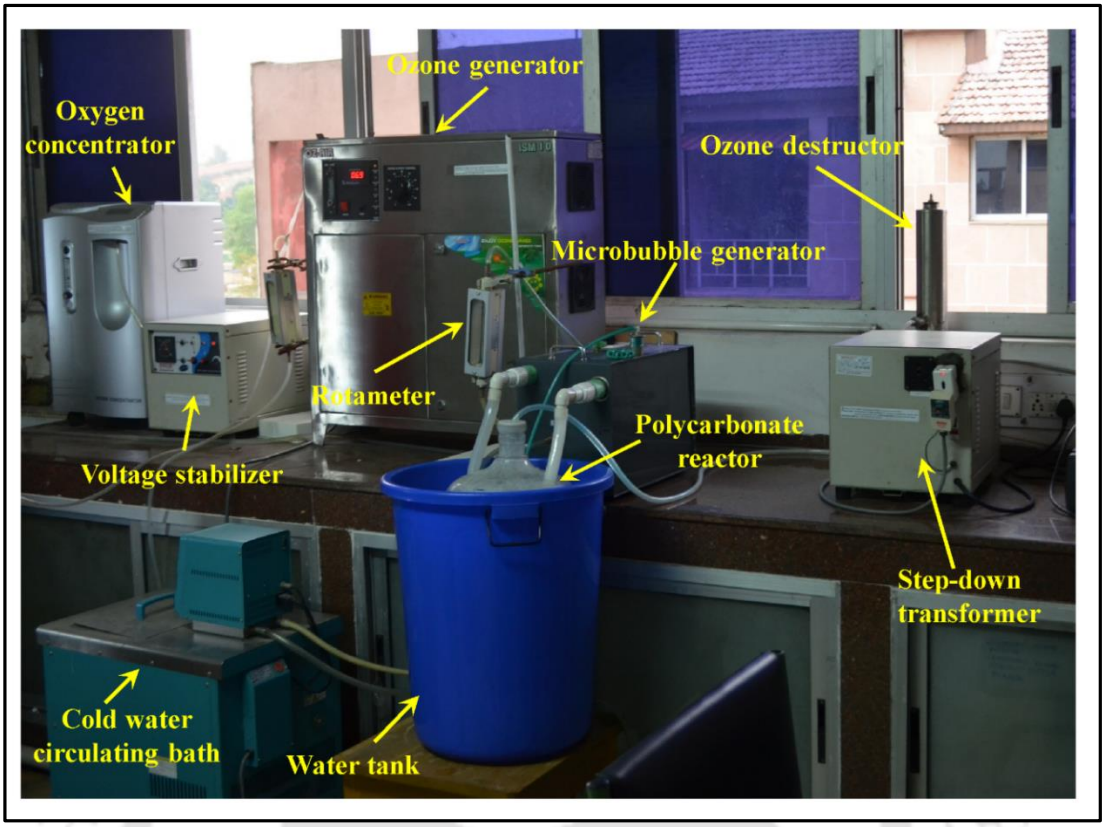

Figure 2.1: Photograph of the experimental setup for the OMBs.

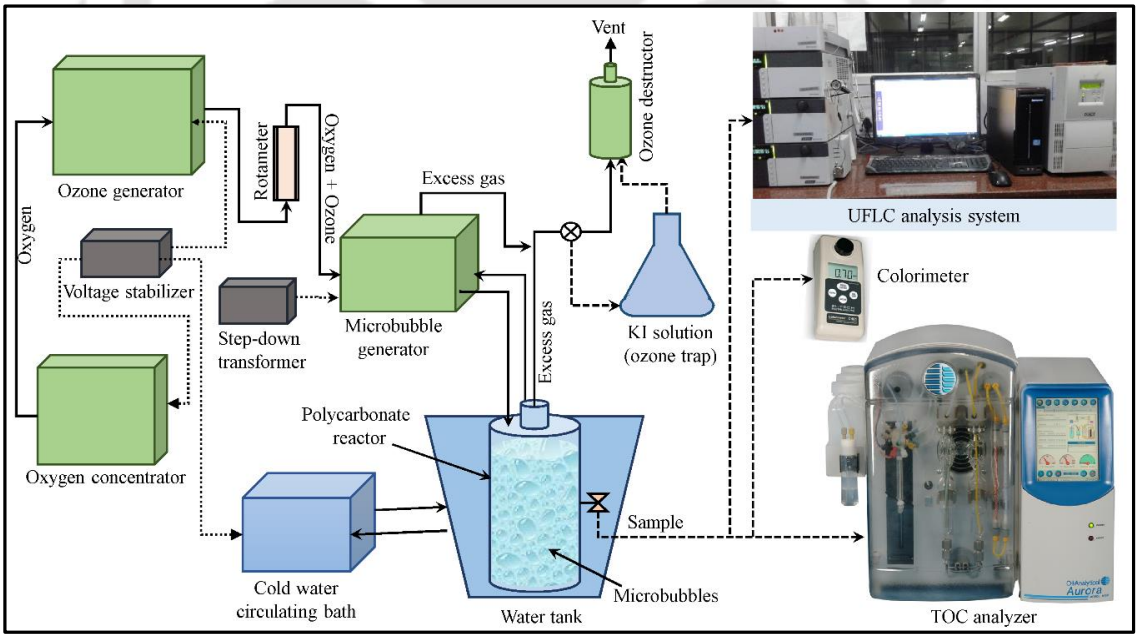

Figure 2.2: Schematic of the experimental setup for the OMBs, and analysis of the samples.

It generated high-purity oxygen from air (> 98%). Its oxygen output capacity was 0–83 $cm^3\ s^{-1}$. This oxygen was fed to the ozone generator [make: Oz-Air (India), model: ISM 10 Oxy], which converted oxygen to ozone by the corona-discharge method (Ciambrone, 1976). The ozone generation rate varied in the range of 0.5–3.0 mg s^{-1}, as per the recommendation of the manufacturer. A rotameter [make: Instrumentation Engineers Pvt. Ltd. (India), model: 1114C] was used to measure the flow rate of the gas mixture (i.e., oxygen and ozone) coming out of the ozone generator. Its range was 8–80 $cm^3\ s^{-1}$. The gas mixture from the ozonator was sent to the MBG, which had an intake capacity of 1.7 $cm^3\ s^{-1}$. The percentage of ozone in the gas mixture that was fed to the MBG was varied in the range of 0.7–3.4% (which is equivalent to the ozone generation rate of 0.6–2.8 mg s^{-1}). The MBG, which was connected to a polycarbonate reactor, operated in a continuous recirculation mode. The gas was dissolved in the aqueous phase under high pressure applied by the pump inside the MBG. The liquid became saturated with the gas at the high pressure. This saturated liquid was subjected to throttling by the discharge valve. Upon passing the pressurized gas–liquid mixture through the discharge valve, the excess gas came out of the liquid phase in the form of microbubbles due to shearing and decompression at the valve throttle (Kim et al., 2011). A milky dispersion of the microbubbles, with a mean diameter of ~ 30 μm was continuously generated by this method. The bubble size distribution in pure water is shown in Figure 2.3. From this figure, it can be seen that about 65% of the bubbles had diameter less than 30 μm. The excess ozone coming out of the reactor (and the MBG) was catalytically converted to oxygen by the ozone destructor [make: Oz-Air (India), model: Dest-50]. The temperature of the aqueous solution within the reactor was controlled at 298 (± 1 K) by an external circulatory water bath [make: Jeio Tech (Korea), model: RW-2025G].

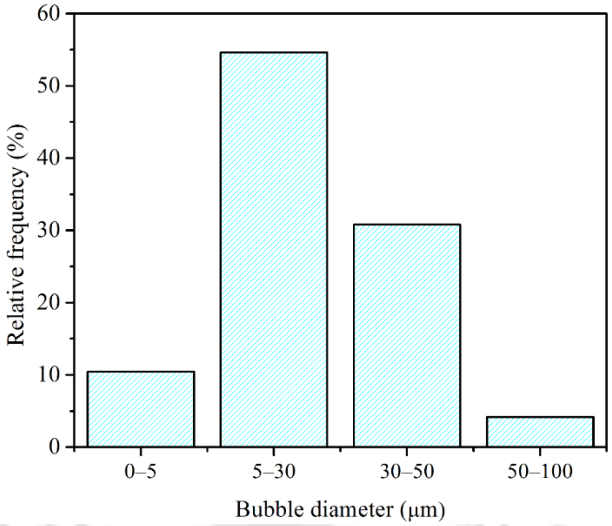

Figure 2.3: Size distribution of the microbubbles [courtesy: Riverforest Corporation (USA)].

2.1.2 Ozone millibubbles

The experimental setup for the millibubbles is shown in Figure 2.4. The methods of isolation of oxygen from air, generation of ozone, and its destruction, and controlling the temperature of the aqueous solution within the reactor were the same as that for the OMBs (Section 2.1.1). The gas mixture from the ozone generator was sparged into the polycarbonate reactor of 20 dm^3 capacity by an ozone-compatible rectangular gas diffuser [make: Ozone Solutions (USA), model: CD-3KB] having fine pores and the dimensions of 3.81 cm × 1.91 cm × 1.91 cm. The gas was supplied at a constant flow rate. This gas diffuser generated the OMLBs.

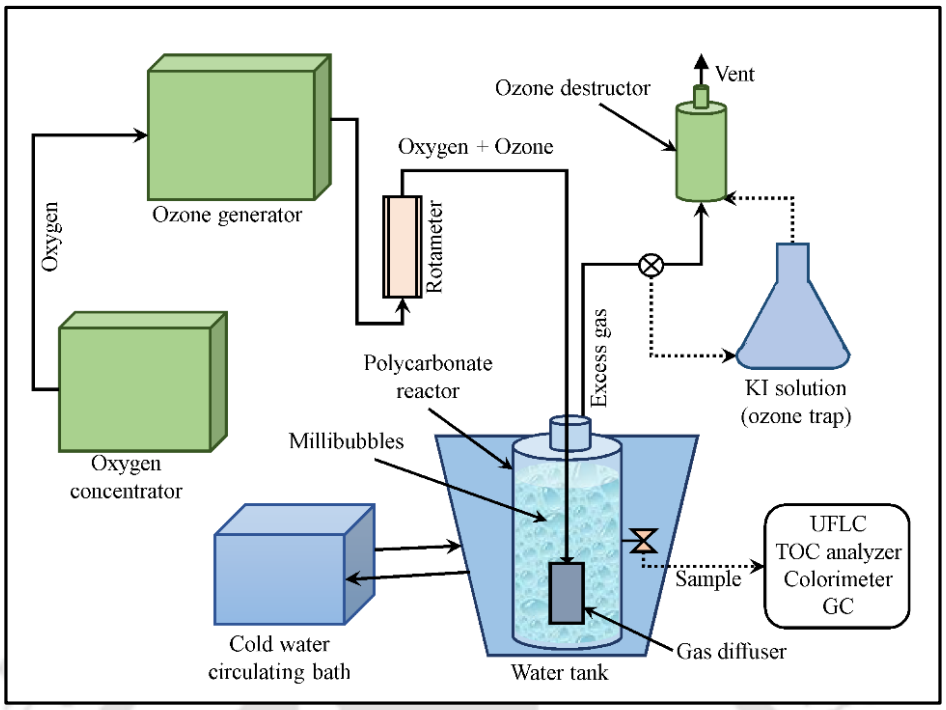

Figure 2.4: Schematic of the experimental setup for the OMLBs.

2.2 Chemicals used

The detailed list of chemicals used in this work, including their source and purity, are given in Table 2.1. All chemicals were of analytical grade, and they were used as received from their respective manufacturers. Milli-Q water [make: Millipore (USA), model: Elix-3] having a conductivity of 5.5 μS m^{-1} (at 298 K) was used to prepare the stock solutions for the analysis. These solutions were diluted further as per the requirements. The aqueous media in the reactor were prepared using the tap water. The tap water was filtered using an iron removal cartridge [make: Eureka Forbes (India), model: Iron-Nil]. Controlled experiments were also conducted using Milli-Q water. There was no difference in the results obtained by using the filtered tap water and the Milli-Q water. Therefore, the effect of the ions present in the filtered tap water was negligible.

Table 2.1: List of chemicals and reagents used in this work

Chemicals	Purity (%)	Source
Acetonitrile	99.9	Spectrochem (India)
Bisphenol-A	97	Alfa Aesar (England)
Catechol	99	Merck (India)
Dimethyl phthalate	99	Alfa Aesar (England)
Dimethyl sulfone	99.5	Alfa Aesar (England)
Dimethyl sulfoxide	99	Alfa Aesar (England)
Diethyl phthalate	99	Alfa Aesar (England)
Hydrogen peroxide	50	Merck (India)
Hydrochloric acid	> 35	Merck (India)
Hydroquinone	99	Merck (India)
Methane sulfonic acid	98	Alfa Aesar (England)
Methanol (HPLC grade)	99.9	Spectrochem (India)
Oxalic acid	99	Merck (India)
Phosphoric acid	85	Spectrochem (India)
Potassium dihydrogen phosphate	99.9	Merck (India)
Potassium hydrogen phthalate	99	Merck (India)
Potassium iodide	99.8	Merck (India)
Potassium periodate	99	Merck (India)
Sodium bicarbonate	99	Merck (India)
Sodium hydroxide	> 98	Rankem (India)
Sodium hydrogen phosphate	99.5	Merck (India)
Sodium thiosulfate	99.5	Merck (India)

Standard pH solutions	–	Oakton (USA)
Sulfuric acid	98	Merck (India)
t-butanol	99.5	Spectrochem (India)
Zinc iodide starch solution	Laboratory reagent grade	Merck (India)

2.3 Analysis methods

The pH of the aqueous medium was measured by a pH meter [make: Eutech (Singapore), model: pH 2700, electrode: 93X218819]. Necessary pH adjustment of the aqueous solution was made before starting the experiment by using 1.0 μmol m^{-3} HCl and 0.5 μmol m^{-3} NaOH solutions. The samples were withdrawn at regular time intervals during the reaction for analyzing the concentration of the pollutant, its reaction intermediates, and the concentration of dissolved ozone. Most of the experiments/analyses were repeated at least three times and the average values are reported in the thesis. The error bars were obtained from the standard deviations in the data obtained from the experiments/analyses carried out in triplicate. Sample uncertainty analysis of retention time and measured concentration are given in Appendix A1. All experiments on ozonation and analysis of the samples were performed in an air-conditioned room where the temperature was maintained at 298 (± 1 K).

2.3.1 Removal of DMP and DEP from water by the OMBs

2.3.1.1 Measurement of the concentrations of DMP and DEP

Stock solutions of the DMP and DEP were prepared by using Milli-Q water. Aqueous solutions of DMP and DEP for the reactor were prepared by using filtered tap-water, after removing iron from it, as discussed in Section 2.1. Quantitative analysis of the

concentrations of DMP and DEP were made by an ultra-fast liquid chromatography (UFLC) [make: Shimadzu (Japan), model: LC-20AD] equipped with a UV detector and an Eclipse XDB – C18 column [make: Agilent (USA)] having the dimensions of 250 mm × 4.6 mm, packed with 5 μm particles. A mixture of 30% (v/v) Milli-Q water and 70% (v/v) acetonitrile was used as the mobile phase for both DMP and DEP at the flow rates of 0.012 and 0.013 $cm^3\ s^{-1}$, respectively, in the isocratic elution mode. The sample injection volume was 20 mm^3 for both DMP and DEP analyses. DMP and DEP were detected at the wavelengths of 275 and 276 nm, respectively. The experiments were repeated at least three times. The detection limits of DMP and DEP were 5.15×10^{-5} and 4.5×10^{-4} mol m^{-3}, respectively. The average retention time of DMP was 220 s, whereas it was 297 s for DEP. The standard deviations of the retention times were less than 10 s. Figure 2.5 shows the UFLC peaks and standard calibration curves of DMP and DEP.

2.3.1.2 UV–Vis absorption spectra of DMP and DEP

The UV–Vis absorption spectra of the DMP and DEP before and after ozonation were measured by using a spectrophotometer [make: Perkin Elmer (Switzerland), model: Lambda 35].

2.3.1.3 Measurement of dissolved ozone concentration

The concentration of dissolved ozone in the reactor was measured by a colorimeter [make: Eutech (Singapore), model: C 105] using the ozone-specific reagent (i.e., the DPD method) (Eaton et al., 2005; Khuntia et al., 2012). The measurements were made immediately after the samples were collected, as per the standard procedure (Eaton et al., 2005). The colorimeter gave readings in the range of 0–4.1 mg dm^{-3} of dissolved ozone. In the case of higher dissolved ozone concentrations, appropriate dilutions were made

with Milli-Q water, as per the recommendation of the colorimeter supplier and the standard procedure (Eaton et al., 2005).

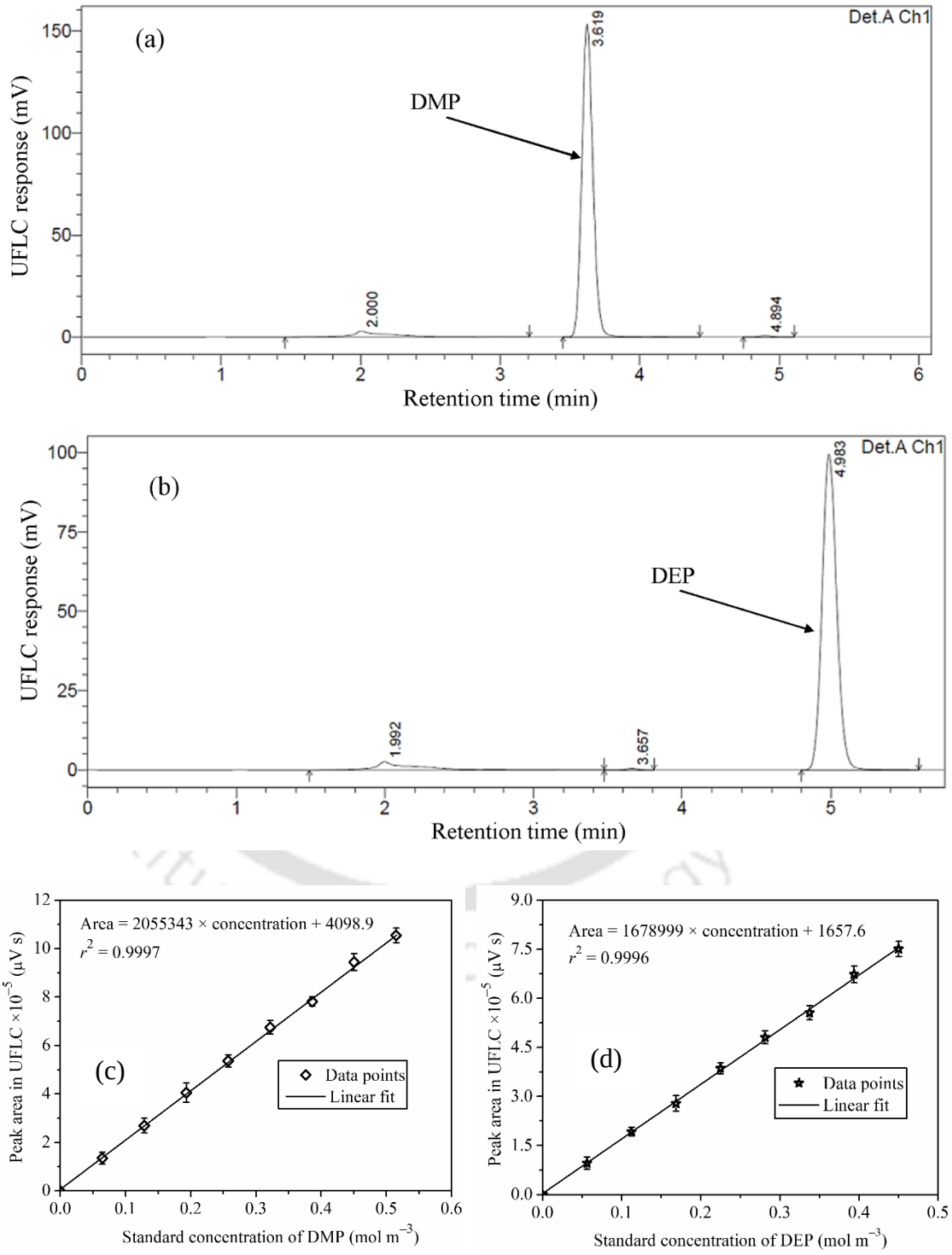

Figure 2.5: UFLC peaks of **(a)** DMP and **(b)** DEP, and UFLC calibration curves of **(c)** DMP and **(d)** DEP.

2.3.2 Oxidation of BPA in water by the OMBs

The samples were withdrawn from the reactor at regular time intervals during the reaction for the analyses of BPA and its reaction-intermediates, and the measurement of the dissolved ozone concentration.

2.3.2.1 UV–Vis absorption spectra of BPA, catechol, and hydroquinone

The UV–Vis absorption spectra of the BPA, catechol, and hydroquinone were measured by using a spectrophotometer [make: Shimadzu (Singapore), model: UV-2600]. The spectra are shown in Figure 2.6 to identify the detection wavelength for the UFLC analysis.

2.3.2.2 Measurement of the concentrations of BPA, catechol, and hydroquinone

Quantitative analysis of the concentrations of BPA, catechol, and hydroquinone were made by a UFLC equipped with a ternary pump system and UV detector. 20 mm^3 sample was injected into the C18 column [make: Varian (The Netherlands), model: Hypersil ODS, 250 mm length, 4.6 mm ID, 5 μm particle size]. A mobile phase consisting of 50% (v/v) methanol and 50% (v/v) Milli-Q water containing 0.1% (v/v) phosphoric acid was used for the detection of BPA, catechol, and hydroquinone at a flow rate of 0.013 $cm^3\ s^{-1}$. The chromatography was carried out in the isocratic elution mode. BPA, catechol, and hydroquinone were detected at the wavelength of 275 nm using the C18 column, since low concentrations of hydroquinone (formed after the reaction with the OMBs) were well-detected at the wavelength of 290 nm (which is its maximum wavelength, as

depicted in Figure 2.6). The detection limits, retention times, and relative standard deviations (% RSD) of BPA, catechol, and hydroquinone for the UFLC analysis are given in Table 2.2. Figure 2.8 shows the standard calibration curves of BPA, catechol, and hydroquinone in Milli-Q water.

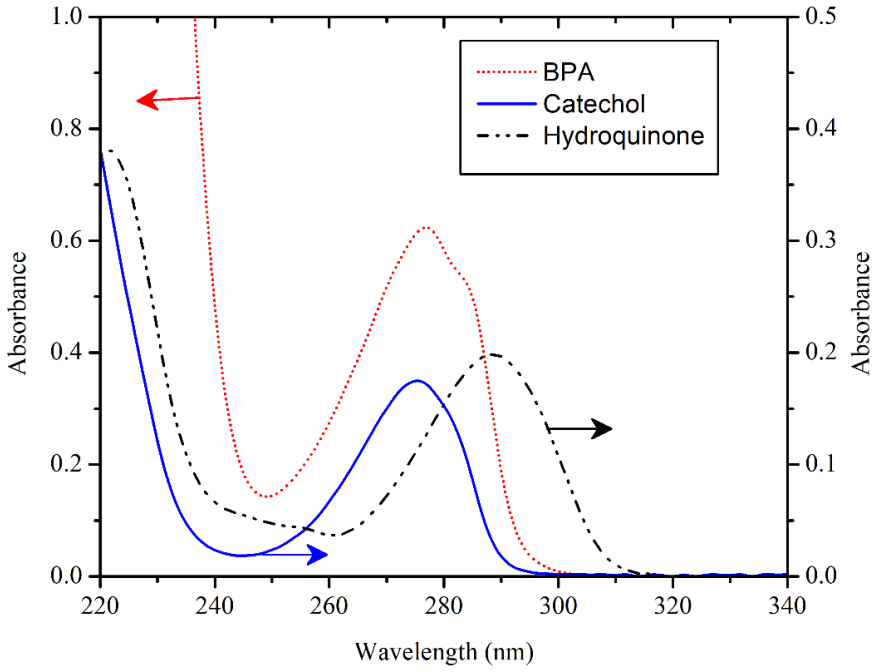

Figure 2.6: UV–Vis spectra of the standard solutions of BPA, catechol, and hydroquinone in Milli-Q water.

Table 2.2: UFLC analysis conditions for BPA and its oxidation intermediates

Compound name	UFLC analysis conditions				
	Wavelength (nm)	Detection limits (mol m^{-3})	RSD (%)	Retention time (s)	RSD (%)
Bisphenol-A	276	4.38×10^{-5}	0.58	313	0.34
Catechol	275	9.08×10^{-5}	1.58	245	1.80
Hydroquinone	290	1.81×10^{-4}	1.85	212	1.88

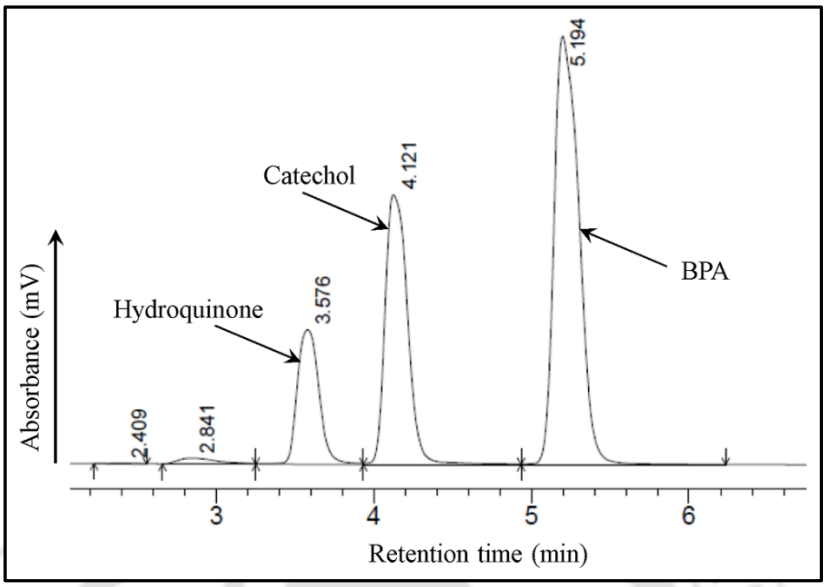

Figure 2.7: UFLC chromatogram of the standard solutions of BPA, catechol, and hydroquinone.

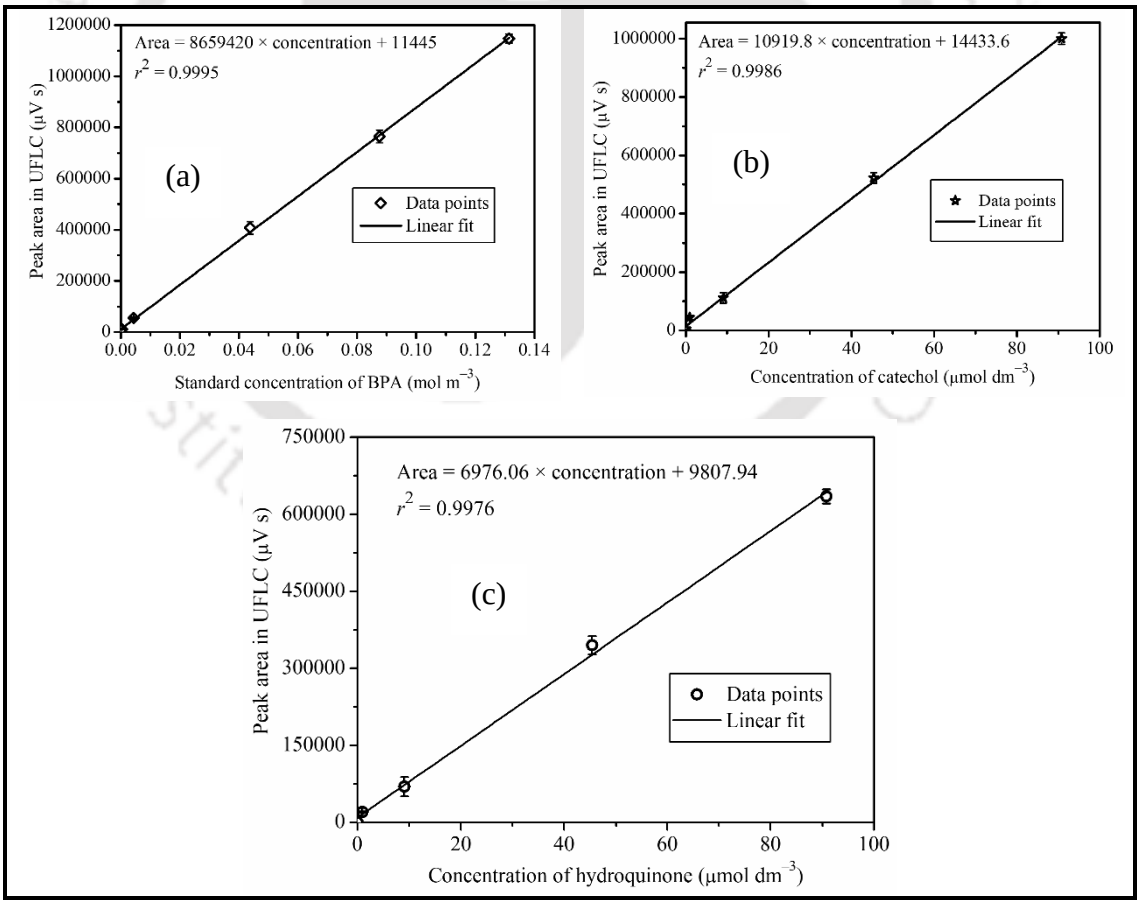

Figure 2.8: UFLC calibration curves of **(a)** BPA, **(b)** catechol, and **(c)** hydroquinone.

2.3.2.3 Measurement of dissolved and excess ozone concentrations

The concentration of dissolved ozone in the reactor was measured by a colorimetric method as explained in Section 2.3.1.3. The excess ozone coming out of the reactor was monitored under selected experimental conditions to determine the stoichiometry of the ozone consumed and the BPA removed by using the potassium iodide (KI) wet-chemistry method (i.e., the iodometric method) following a standard procedure (Kusvuran et al., 2010; Rakness et al., 1996a; Rakness et al., 1996b), before it was sent to the ozone destructor. Ozone traps containing 0.5 dm^3 of 20 g dm^{-3} KI solution were used, as recommended in the standard procedure (Kusvuran et al., 2010). The trap-contents were titrated with 10 mol m^{-3} sodium thiosulfate ($Na_2S_2O_3$) (Rakness et al., 1996b). The excess ozone concentration was determined by the amount of titrant volume.

2.3.3 Removal of DMSO from water using the OMBs and OMLBs

2.3.3.1 UV–Vis absorption spectrum of DMSO

To determine the optimal wavelength for UV-detection of DMSO in the UFLC, the UV-Visible spectrum of DMSO in a mixture of acetonitrile and Milli-Q water [acetonitrile : water = 80 : 20 (v/v)] was generated in the wavelength range of 200 to 400 nm by using a UV–visible spectrophotometer (Section 2.3.2.1). The UV–Vis absorption spectrum of DMSO is shown in Figure 2.9 (a).

2.3.3.2 Measurement of the concentration of DMSO and its oxidation intermediates

The quantitative analysis of the concentration of DMSO was made by a UFLC as explained in Section 2.3.1.1. A mixture of 80% acetonitrile and 20% Milli-Q water (v/v) was used as the mobile phase for the detection of DMSO at the flow rate of 0.013 cm^3 s^{-1} in isocratic elution. The sample injection volume was 20 mm^3. DMSO was detected at

the wavelength of 207 nm. The experiments were repeated at least three times. The detection limit for DMSO was 4.5×10^{-4} mol m^{-3}. The retention time was 185 s [Figure 2.9 (a)]. The standard deviation of the retention time was lower than 5 s.

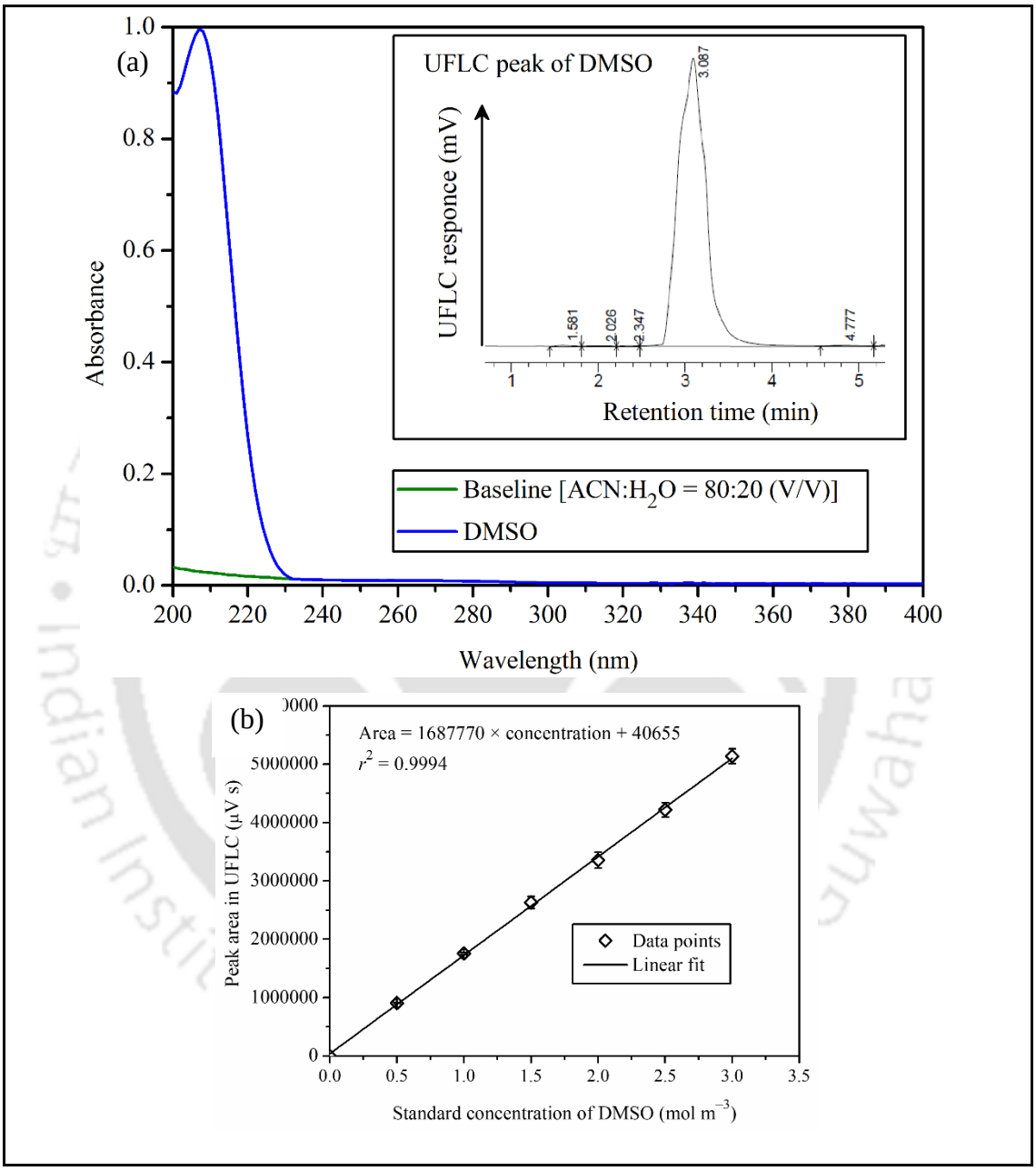

Figure 2.9: (a) UV–Vis absorption spectrum and UFLC chromatogram (inset) and **(b)** UFLC calibration curve of the standard aqueous DMSO solutions in a mixture of ACN and water [ACN : water = 80 : 20 (v/v)].

Concentrations of the two major oxidation intermediates of DMSO in the aqueous samples (i.e., MSA and $DMSO_2$) were measured by a gas chromatography [make: Bruker (Germany), model: 450-GC] equipped with a CP-Sil 8 CB (60 m × 0.32 mm × 0.45 mm) column and a pulsed-flame photometric detector. The GC was operated at 333 – 473 K. The injection volume in the GC was 0.001 cm^3 with 1:80 split ratio. Helium, hydrogen, and nitrogen were used as the carrier gases at the flow rate of 0.17 cm^3 s^{-1}. The filament temperature was 323 K, and its limit was 663 K. The oven temperature was in the range of 323 – 493 K, with ramping at 0.17 K/s. Calibration curves were plotted from the known standard solutions of the compounds for the quantitative determination of MSA and $DMSO_2$ (Figure 2.10) (Chou and Chang, 2007; Sahle-Demessie and Devulapelli, 2008).

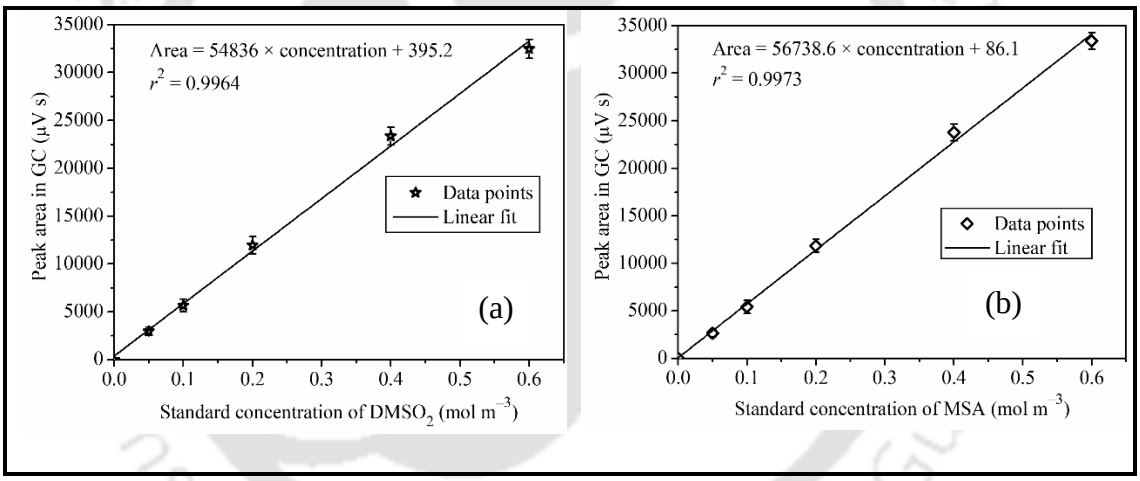

Figure 2.10: Calibration curves of **(a)** $DMSO_2$ and **(b)** MSA for GC.

2.3.4 TOC measurement

The effectiveness of any water/wastewater treatment method should be based not only on its organic pollutant removal efficiency but also on the extent of mineralization of the intermediate organic compounds, which are formed during the course of reaction. The overall degree of mineralization of the target pollutants was determined by analyzing the TOC before and during the course of ozonation. The TOC analyses were performed in a

TOC analyzer [make: O. I. Analytical (USA), model: Aurora 1030] equipped with a non-dispersive infrared (NDIR) detector following the procedure given in the literature (Szabo and Hall, 2014). The sample was acidified with phosphoric acid (5% v/v, in Milli-Q water) and sparged to convert the total inorganic carbon (TIC) in the sample to CO_2. The TIC-free sample was then oxidized using heated (i.e., 373 K) sodium persulfate (10% v/v, in Milli-Q water), where the organic compounds were oxidized and converted the carbon to CO_2. It was then analyzed and quantified by the NDIR detector. The result was reported as the TOC content in terms of the concentration of carbon. The TOC standards for the calibration were prepared from high-purity potassium hydrogen phthalate following the procedure described in the ASTM Standard D7573-09 (2009). Figure 2.11 shows the TOC calibration curve. For every new experiments, the TOC content of the filtered tap water was checked. The results were varied within the range of 0.1 to 0.7 mg dm^{-3}. These baseline values were subtracted from the respective TOC readings of samples, and the difference is reported in this work.

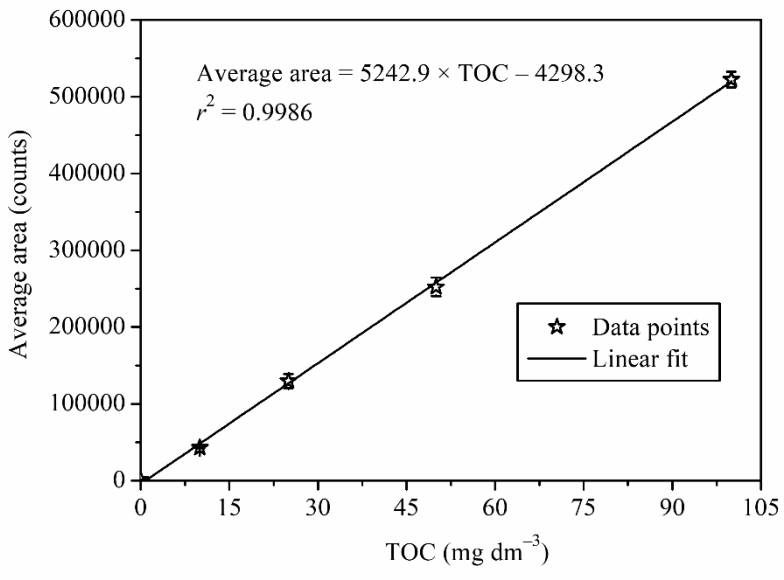

Figure 2.11: TOC calibration curve.

Abbreviations

ACN	acetonitrile
BPA	bisphenol–A
DEP	diethyl phthalate
DMP	dimethyl phthalate
DMSO	dimethyl sulfoxide
$DMSO_2$	dimethyl sulfone
DPD	N, N-diethyl-*p*-phenylenediamine
GC	gas chromatography
HPLC	high performance liquid chromatography
MSA	methane sulfonic acid
NDIR	non-dispersive infrared
OMBs	ozone microbubbles
OMLBs	ozone millibubbles
RSD	relative standard deviation
TIC	total inorganic carbon
TOC	total organic carbon
UFLC	ultra-fast liquid chromatography
UV	Ultraviolet

References

Chou, M.S., Chang, K.L., **2007**. Oxidation of aqueous dimethyl sulfoxide (DMSO) using UV, O_3, and UV/O_3. *Ozone Sci. Eng.*, *29*, 391–397.

Ciambrone, D.F., **1976**. Corona discharge ozone generator. United States Patent US3942020 A, 1976–03–02.

Eaton, A.D., Clesceri, L.S., Rice, E.W., Greenberg, A.E., **2005**. Standard Methods for the Examination of Water & Wastewater, 21st ed. American Public Health Association, New York (USA).

Grande, C.A., **2012**. Advances in pressure swing adsorption for gas separation. *ISRN Chem. Eng.*, *2012*, 1–13.

Khuntia, S., Majumder, S.K., Ghosh, P., **2012**. Removal of ammonia from water by ozone microbubbles. *Ind. Eng. Chem. Res.*, *52*, 318–326.

Kim, C.N., Madhav, M.P., Jayaprakash, S., **2011**. A microbubble generator. European Patent EP2558189A1, 2011–04–18.

Kusvuran, E., Gulnaz, O., Samil, A., Erbil, M., **2010**. Detection of double bond-ozone stoichiometry by an iodimetric method during ozonation processes. *J. Hazard. Mater.*, *175*, 410–416.

Rakness, K., Gordon, G., Langlais, B., Masschelein, W., Matsumoto, N., Richard, Y., Robson, C.M., Somiya, I., **1996a**. Guideline for measurement of ozone concentration in the process gas from an ozone generator. *Ozone Sci. Eng.*, *18*, 209–229.

Rakness, K.L., DeMers, L.D., Blank, B.D., Henry, D.J., **1996b**. Gas phase ozone concentration comparisons from a commercial UV meter and KI wet-chemistry tests. *Ozone Sci. Eng.*, *18*, 231–249.

Sahle-Demessie, E., Devulapelli, V.G., **2008**. Vapor phase oxidation of dimethyl sulfide with ozone over V_2O_5/TiO_2 catalyst. *Appl. Catal. B*, *84*, 408–419.

Sircar, S., Kratz, W.C., **1989**. Oxygen production by pressure swing adsorption. *Sep. Sci. Technol.*, *24*, 429–440.

Szabo, J., Hall, J., **2014**. On-line Water Quality Monitoring for Drinking Water Contamination, in: Ahuja, S. (Ed.), *Comprehensive Water Quality and Purification*. Elsevier, Waltham, pp. 266–282.

CHAPTER 3

REMOVAL OF DIMETHYL PHTHALATE FROM WATER BY OZONE MICROBUBBLES

This chapter presents the work on the removal of dimethyl phthalate (DMP) from water using ozone microbubbles (OMBs). The effects of the initial concentration of DMP, pH of the medium, ozone generation rate, hydroxyl radicals, and the role of H_2O_2 on the removal of DMP have been studied. The TOC analysis has also been carried out to study the extent of mineralization of DMP. The self-decomposition rate constant of ozone for the OMB system was determined from the experimental results. The overall kinetics of the reaction between DMP and ozone has been studied. The Hatta number has been computed to study the roles of mass transfer of ozone and the kinetics of the reaction.

3.1 Introduction

DMP is the simplest phthalic acid ester. It was selected as a representative phthalate in this work to investigate its removal from water by using OMBs. Most of the works reported on the removal of DMP from water are based on catalytic ozonation (Section 1.6.1). The primary objective of applying catalytic ozonation for DMP degradation was to enhance the formation of reactive hydroxyl radicals in the aqueous media. Therefore, application of OMBs may be an efficient alternative method for effective removal of DMP from water.

The objective of this work was to investigate the removal efficiency of DMP by the OMBs using a commercial microbubble generator. This work focused on the main

parameters that influence the removal rate of DMP such as the initial concentration of DMP, pH of the reaction medium and the ozone generation rate. Furthermore, the effect of H_2O_2 on ozonation and the contribution of hydroxyl radicals to the removal of DMP have been investigated. The total organic carbon (TOC) was measured to find out the extent of mineralization. The results show that the use of OMBs is a promising technology for removing DMP from water.

3.2 Results and discussion

3.2.1 UV–Vis spectra of DMP

The UV–Vis spectra of DMP before and after the reaction are shown in Figure 3.1. From these spectra, it is observed that there are two maxima at 229 and 276 nm. This is similar to that reported in the literature (Liao and Wang, 2009). Under the reaction conditions, these peaks almost vanished after 1.8 ks of ozonation. The aromatic ring of DMP was possibly destroyed by direct and indirect reactions with the ozone molecules, which was manifested in the decline of these peaks.

3.2.2 Effect of initial concentration of DMP

The concentration of phthalates in water and wastewater varies over a wide range, e.g. 0.0001–300 μg dm^{-3} (Yuan et al., 2002). Thus, it is necessary to study the effect of concentration of DMP on its rate of removal by the OMBs. The concentration profiles are shown in Figure 3.2. It is clearly observed that the concentration profiles followed a similar trend for all initial concentrations of DMP. The rate of oxidation of DMP increased with the increasing initial concentration of DMP in the reactor. This is apparent because the reaction follows second-order kinetics (first-order with respect to both DMP and ozone, as demonstrated later in the Section 3.2.9. Therefore, the rate of reaction

increased with the increasing concentration of DMP. However, the extent of the removal of DMP decreased with increasing initial concentration. For instance, for the lowest initial concentration (i.e., 0.052 mol m^{-3}), almost 99% of DMP was removed within 300 s of ozonation.

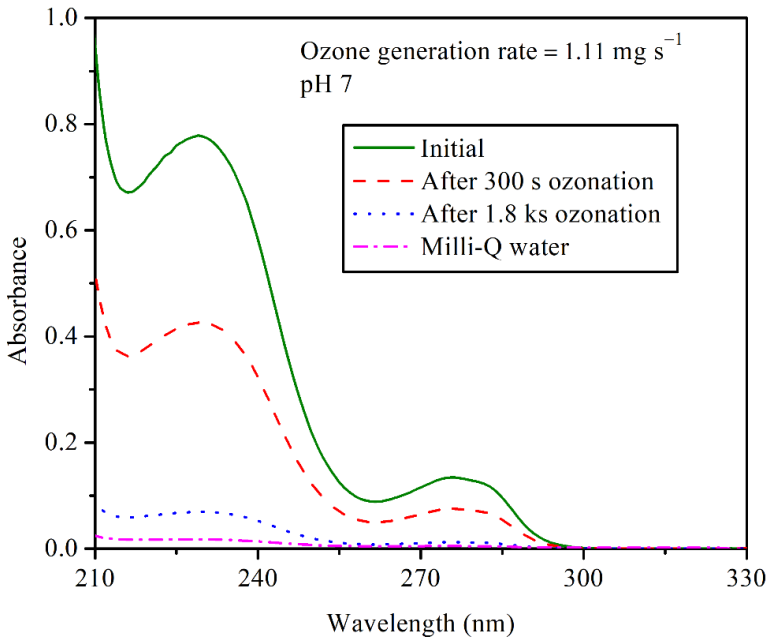

Figure 3.1: UV–Vis absorption spectra of DMP before and after ozonation.

On the other hand, only 95% removal was achieved for the highest initial concentration of DMP (i.e., 1.029 mol m^{-3}) at 1.8 ks. This indicates that the OMBs achieved a less extent of oxidation of DMP, within a given time, as its concentration was increased. An increase in the initial concentration of DMP led to an increase in the concentration of the main and intermediate compounds formed during the course of ozonation. Thus, the ozone available in the reaction medium and the hydroxyl radicals produced *in situ* were both consumed in the oxidation of DMP and the intermediates produced during the course of reaction.

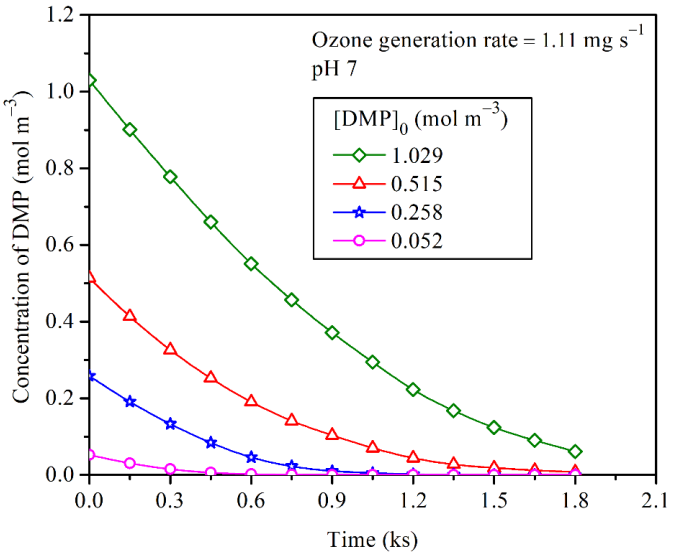

Figure 3.2: Effect of initial concentration of DMP on its removal by the OMBs.

3.2.3 Effect of initial pH of the aqueous solution

The pH of the aqueous medium controls the mechanism and rate of ozonation. Therefore, it is important to study the effect of pH on the oxidation of DMP. The H^+ or OH^- ions present in the ozonation system may either impede or promote the generation of free radicals. Therefore, the pH of the aqueous solution plays an important role in the decomposition of ozone into hydroxyl radicals (Beltrán, 2004). The effect of pH on ozone treatment of DMP is shown in Figure 3.3. It is seen from Figure 3.3 that the neutral and alkaline media were more suitable than the acidic medium for the degradation of DMP. The degradation condition was better at pH 9 because the concentration of free radicals increased with increasing pH, which favored the indirect reaction. This conclusion is in accordance with the results reported in the literature (Beltrán, 2004; Gottschalk et al., 2010; Huang, 2010).

At every time interval, the pH of the solution was measured immediately after the sample was collected from the reactor. It is observed from Figure 3.4 that the pH of the

solution decreased slightly at all initial concentrations. On the basis of the results reported by Chen et al. (2008), it is likely that organic acids were formed during the ozonation of DMP, which lowered the pH of the medium.

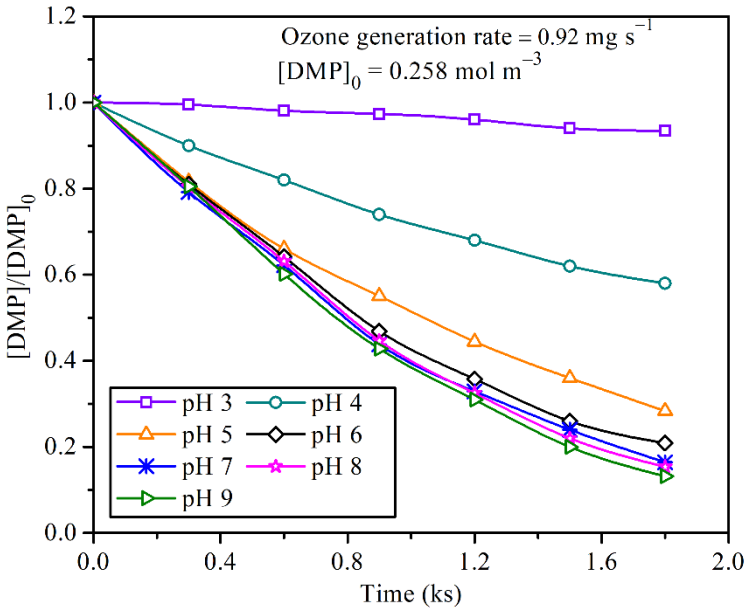

Figure 3.3: Effect of pH on the removal of DMP by the OMBs.

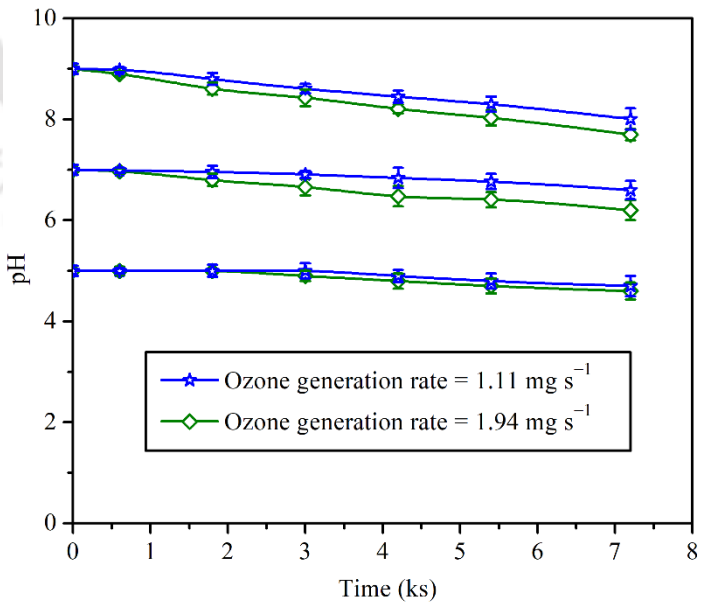

Figure 3.4: Variation of pH of the solution with time during ozonation.

3.2.4 Effect of ozone concentration

Increase in the ozone generation rate increases the partial pressure of ozone in the gas mixture released from the ozonator, which increases the concentration of ozone in the aqueous phase due to enhanced mass transfer. The concentration profiles of dissolved ozone in the aqueous solution at different ozone generation rates are given in Figure 3.5. The concentration of ozone in the aqueous phase had a profound effect on the rate of oxidation of DMP. Oxidation of DMP increased with increasing ozone generation rate. This is expected because the ozone either directly reacted with the organic compounds or decomposed to produce ·OH, which reacted with these compounds.

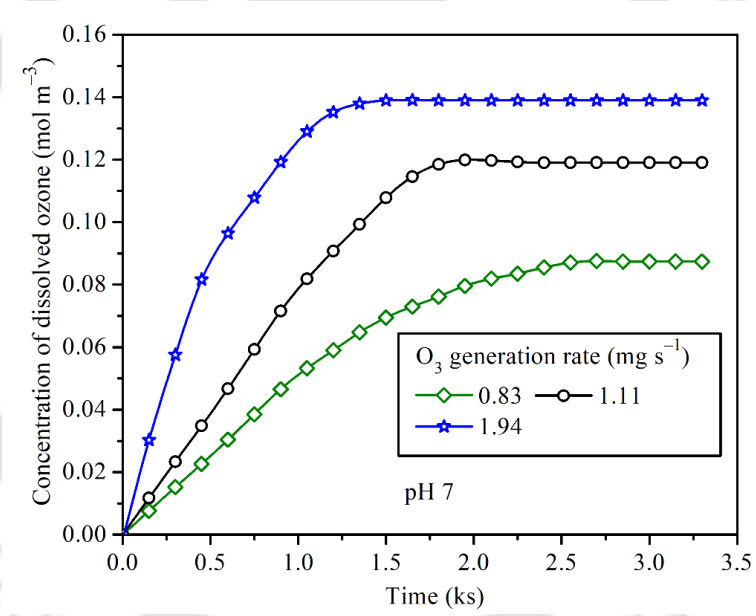

Figure 3.5: Concentration profiles of dissolved ozone in the aqueous phase at different ozone generation rates.

In order to investigate the effect of ozone concentration (in the gas present in the microbubbles) on the removal efficiency of DMP, the ozonation experiments were conducted with seven different ozone generation rates ranging from 0.28 to 1.94 mg s^{-1}. The experimental results shown in Figure 3.6 indicate that the extent of removal of DMP

increased with increasing ozone concentration in the feed gas. It is clearly seen that increase in the ozone flow rate from 0.28 to 1.94 mg s^{-1} highly improved the removal of DMP from 1 to 99% within 900 s of the reaction time. These trends are in good agreement with the results reported in the literature (Chen et al., 2008). The increase in the ozone concentration in the aqueous phase may enhance the electrophilic reaction of DMP with ozone as well as its reaction with the hydroxyl radicals. The contribution of the hydroxyl radicals is reported in Section 3.2.6 to verify whether the direct reaction (i.e., electrophilic attack of O_3) or the indirect reaction (i.e., the attack of ·OH radicals) predominated.

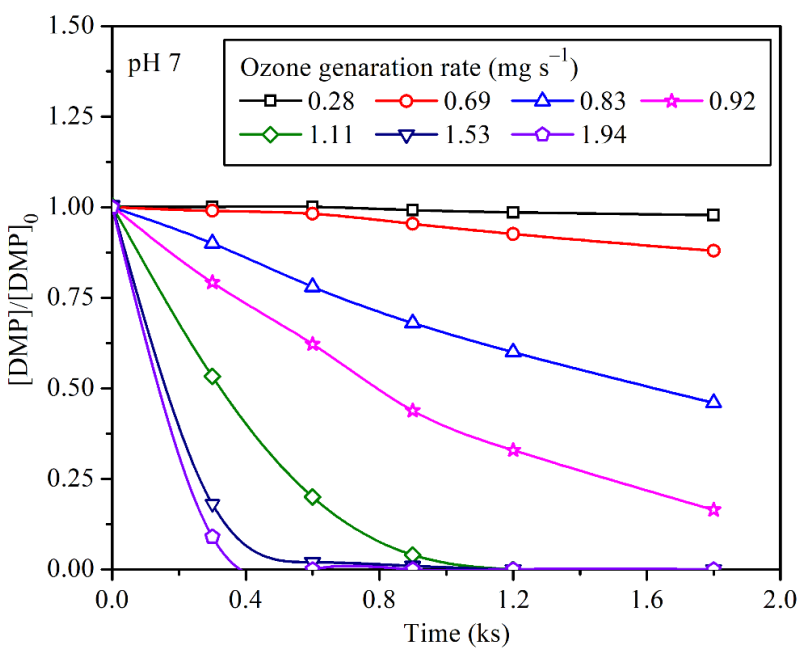

Figure 3.6: Effect of ozone generation rate on the removal of DMP.

3.2.5 Effect of ozone generation rate on TOC removal

The ozonation of DMP produces various intermediate compounds, which partly mineralize to H_2O and CO_2. The measurement of TOC before and during ozonation gives the extent of the oxidation of DMP (and the intermediate organic compounds) to the mineralized products. The initial TOC of the solutions was ~26 mg dm^{-3}. Figure 3.7

shows the TOC removal with time at different ozone generation rates. It is observed that the TOC removal was enhanced with increasing ozone generation rate, and the trend was similar to that of DMP oxidation (shown in Figure 3.6).

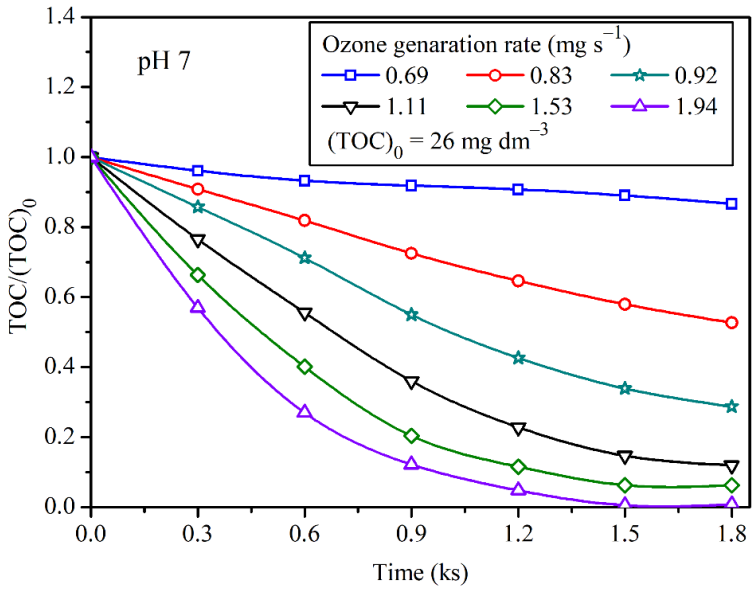

Figure 3.7: Effect of ozone generation rate on the removal of TOC.

Complete mineralization of DMP was achieved within 1.8 ks at the highest ozone generation rate (i.e., 1.94 mg s^{-1}) at pH 7. For the same condition, the TOC removal was only about 46% (Figure 3.7), although more than 94% of the DMP was removed within 300 s (Figure 3.6). Similarly, for all ozone feed rates, the TOC removal rates were less than the corresponding DMP removal rates. This was due to the formation of intermediates during the course of reaction, and complete mineralization of them needed a longer time. The degradation pathway and the identification of the intermediate compounds, however, was not investigated in this work.

3.2.6 Effect of addition of H_2O_2

It is known (Hoigné, 1998; Mansouri et al., 2013) that the addition of H_2O_2 to the ozonation system greatly promotes the decomposition of ozone and augments the generation of ·OH radicals. This would increase the reaction rate, which would make it possible to enhance the removal of the pollutants more effectively.

To investigate the effect of H_2O_2 in the presence of OMBs on the removal of DMP, experiments were conducted by using 2.0, 4.0, and 8.0 mol m^{-3} H_2O_2 at the ozone generation rate of 0.92 mg s^{-1}. It is evident from the results presented in Figure 3.8 that a slight enhancement in the removal of DMP was achieved for the 2.0 mol m^{-3} dose of H_2O_2. It can be observed from Figure 3.8 that at 1.8 ks reaction time, addition of 2.0 mol m^{-3} H_2O_2 improved the removal of DMP from 84 to 90%. However, further increase in the dosage of H_2O_2 adversely affected the degradation rate of DMP. The removal rate decreased to 81 and 73% for the H_2O_2 dosages of 4 and 8 mol m^{-3}, respectively. In the earlier studies (Gottschalk et al., 2010), it was reported that an increase in the ratio of H_2O_2 to O_3 might produce more hydroxyl radicals. However, these radicals may recombine, and therefore, may lead to a low reaction rate, which is not helpful for the oxidation of the target pollutant. The works of Beltrán (2004) have shown that H_2O_2 is not only an initiator and promoter of ozonation, but it can also act as an inhibitor of ozone decomposition when its concentration is so high that the reaction between H_2O_2 and O_3 becomes controlled by mass transfer. Huang (2010) has reported that increasing the H_2O_2/O_3 mole ratio beyond 1:2 did not lead to a pro-rata improvement in the removal rate of DMP.

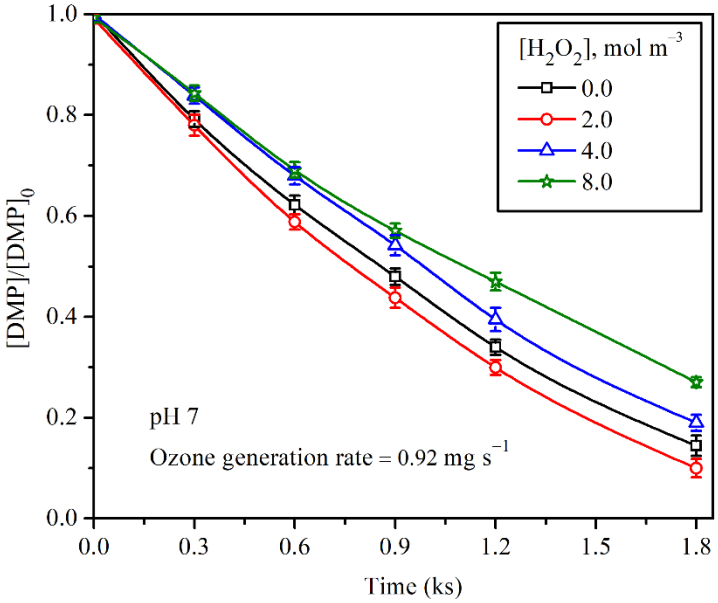

Figure 3.8: Effect of using H_2O_2 along with OMBs for DMP degradation.

3.2.7 Effect of t-BuOH on DMP removal

The contribution of hydroxyl radicals to the degradation of organic pollutants by OMBs can be investigated by adding radical scavengers. In this study, a well-known scavenger (i.e., *t*-BuOH) was used to study the contribution of ·OH in the oxidation. *t*-BuOH reacts very rapidly with the hydroxyl radicals (i.e., the rate constant is 6×10^8 dm^3 mol^{-1} s^{-1}), but very slowly with ozone (i.e., the rate constant is 3×10^{-3} dm^3 mol^{-1} s^{-1}) (de Oliveira et al., 2011; Hoigné and Bader, 1983; Mansouri et al., 2013). The experiments were conducted with 1.0, 2.5, 5, 10.0 and 15.0 mol m^{-3} *t*-BuOH. The results are shown in Figure 3.9 (a). The experimental results from Figure 3.9 (a) reveal that almost 100% removal was observed after 1.8 ks reaction time in the absence of *t*-BuOH, as compared to only 13% in the presence of 10 mol m^{-3} *t*-BuOH.

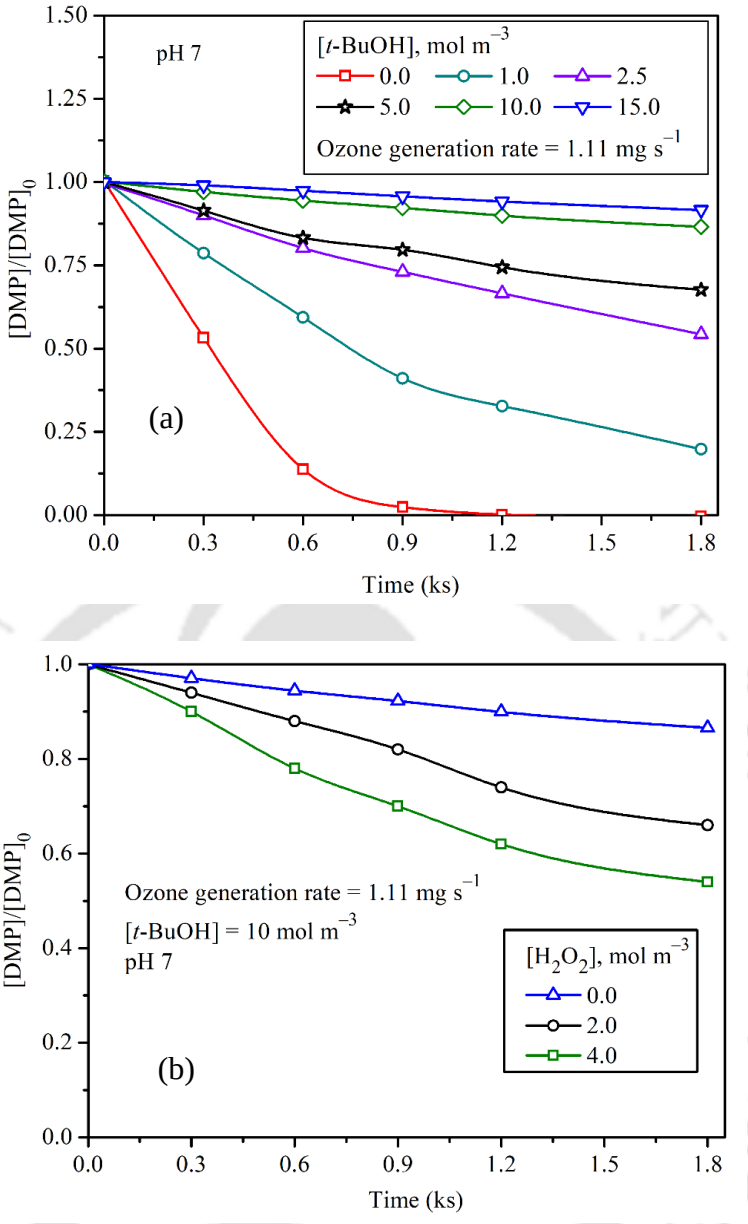

Figure 3.9: Effect of *t*-BuOH on the removal of DMP **(a)** without H_2O_2 and **(b)** in the presence of H_2O_2.

This indicates that the reaction between DMP and ·OH dominated over the direct reaction with the ozone molecules. Furthermore, the effect of *t*-BuOH in the presence of H_2O_2 was also studied. As the addition of H_2O_2 enhanced the generation of the ·OH radicals, the DMP removal rate increased with the increasing concentration of H_2O_2 at a

given concentration of *t*-BuOH [Figure 3.9 (b)**]**. This confirms that the reactions with the ·OH indeed played an important role in the ozonation of DMP.

3.2.8 Estimation of self-decomposition rate constant of ozone

Mass transfer of ozone in the aqueous phase by the microbubbles for the non-reacting systems has been reported earlier (Khuntia et al., 2012). In this work, the self-decomposition rate constant of ozone was determined by kinetic studies in our experimental setup. The dissolved ozone concentration in water was measured as a function of time, and the experiment was continued until the aqueous phase was saturated, which is termed as the *steady state ozone concentration*, $[O_3]_{ss}$. Then, the supply of ozone in the reactor was stopped and the decrease in concentration of ozone in the reactor was measured with time. Several researchers have reported that the decomposition of ozone in water depends on the pH of the solution, and it follows a first-order kinetics (Beltrán, 2004; Sotelo et al., 1987; Sotelo et al., 1989). The reaction rate equation for the self-decomposition of ozone can be written as (Gao et al., 2005; Kukuzaki et al., 2010; Rosal et al., 2006)

$$-\frac{d[O_3]}{dt} = k_d[O_3] \tag{3.1}$$

where $[O_3]$ is the concentration of ozone in the aqueous solution and k_d is the ozone self-decomposition rate constant. Equation (3.1) can be integrated with the boundary condition: at $t = 0, [O_3] = [O_3]_{ss}$. This gives

$$\ln\left(\frac{[O_3]_{ss}}{[O_3]}\right) = k_d t \tag{3.2}$$

Equation (3.2) predicts that a plot of $\ln\left(\frac{[O_3]_{ss}}{[O_3]}\right)$ versus time, *t*, should be a straight line passing through the origin, and the slope of this line would be k_d (Figure 3.10).

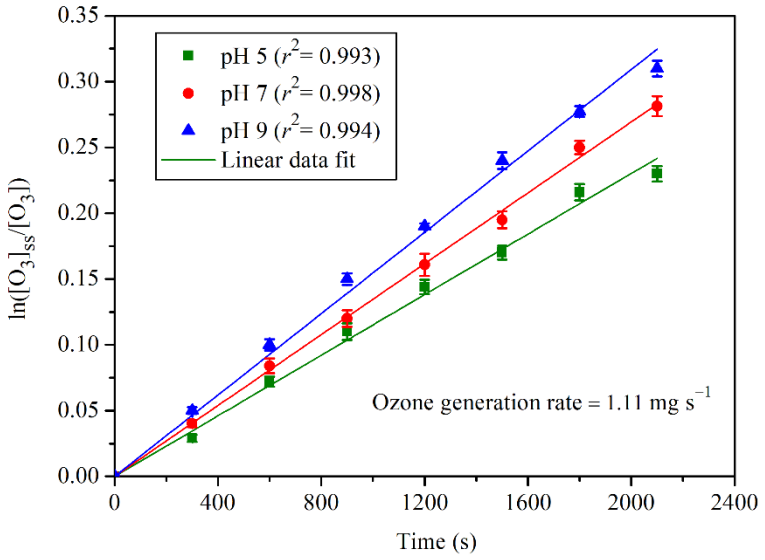

Figure 3.10: Linear fit of the data for the determination of the self-decomposition rate constant of ozone.

Table 3.1 summarizes the experimental values of k_d at different pH. k_d is a fundamental kinetic parameter, and it should be independent of the type of reactor. However, the values reported in the literature (Gao et al., 2005; Hsu et al., 2002; Kukuzaki et al., 2010; Sotelo et al., 1987) show wide variations. For instance, k_d values of 4.0 × 10^{-5} s^{-1} (at pH 7) (Gao et al., 2005), 2.1 × 10^{-4} – 4.2 × 10^{-4} s^{-1} (at pH 2.5 – 9) (Sotelo et al., 1987), 2.1 × 10^{-4} – 5.4 × 10^{-4} s^{-1} (at pH 2.6 – 7) (Hsu et al., 2002), and 4.2 × 10^{-4} s^{-1} (pH unspecified) (Kukuzaki et al., 2010) have been reported. The values of k_d obtained in this study fall in the range of these values. It is observed that k_d increased with increasing pH, which agrees with the results in literature (Sotelo et al., 1987). The

estimated errors (i.e., the relative uncertainties as per Equation A1.5 in the Appendix A1) of these results were less than 1%.

Table 3.1: Values of the self-decomposition rate constant of ozone

pH	$k_d \times 10^3$ (s^{-1})	Relative uncertainty (%)
5	0.12	0.49
7	0.13	0.63
9	0.15	0.59

3.2.9 Overall kinetics of DMP ozonation

In literature, a few kinetic data are available for the oxidation of DMP by ozone. A pseudo-first-order kinetics for the DMP oxidation using ozone was reported in the literature (Yu et al., 2013) whereas, a second-order kinetics has been reported by other researchers (David Yao and Haag, 1991; Li et al., 2009; Wen et al., 2011). In this work, the kinetic parameters of the overall reaction between DMP and ozone were determined from the experimental results by using a mass balance.

When ozone is absorbed into water from a gas mixture and it simultaneously undergoes self-decomposition in a completely mixed reactor, the mass balance equation is given by

$$\frac{\mathrm{d}[\mathrm{O_3}]}{\mathrm{d}t} = k_L a\left([\mathrm{O_3}]^* - [\mathrm{O_3}]\right) - k_d[\mathrm{O_3}] \tag{3.3}$$

where $[\mathrm{O_3}]^*$ is the equilibrium concentration of ozone in the aqueous phase and $k_L a$ is the volumetric mass transfer coefficient of ozone in the reacting system. The diffusivity

of ozone in the gas phase is much larger than that in water, so the resistance to mass transfer in the gas phase is negligible, compared to that in the liquid phase. The equilibrium concentration of ozone in the aqueous phase and its steady state concentration can be related by the following equation (Roth and Sullivan, 1981):

$$[O_3]_{ss} = \left(\frac{k_L a}{k_L a + k_d} \right) [O_3]^* \tag{3.4}$$

From Equations (3.3) and (3.4), the following equation is obtained.

$$\frac{d[O_3]}{dt} = (k_L a + k_d)([O_3]_{ss} - [O_3]) \tag{3.5}$$

In the reactor of our experimental setup, ozone gradually dissolved in water and reacted with DMP. The rate equation for the reaction between ozone and DMP is expressed by

$$\frac{d[DMP]}{dt} = -k[DMP]^m[O_3]^n \tag{3.6}$$

In the presence of DMP, the mass balance of ozone contains three terms, i.e., the mass transfer of ozone from gas to liquid, the self-decomposition of ozone, and the reaction of DMP with ozone. Therefore, incorporating Equation (3.6) into Equation (3.5) we get the overall mass balance of ozone as

$$\frac{d[O_3]}{dt} = (k_L a + k_d)([O_3]_{ss} - [O_3]) - k[DMP]^m[O_3]^n \tag{3.7}$$

The ordinary differential equations given by Equations (3.6) and (3.7) were simultaneously solved by the Runge–Kutta method using Polymath® (version 6.0), and the concentration profiles were fitted to the experimental data to obtain the best-fit values of the kinetic parameters. The best-fit values of the unknown parameters (i.e., k, $k_L a$, m, and n) are presented in Table 3.2. The data were fitted well with $r^2 > 0.99$. The values of k_d reported in Table 3.1 were used in these computations. The

concentration profiles of DMP and ozone are shown in Figures 3.11 (a) and (b), respectively. The volumetric mass transfer coefficient of ozone slightly increased with increasing initial concentration of DMP. $k_L a$ depends on the type of reactor used. The value of $k_L a$ obtained in this study are close to those reported for similar systems (Chu et al., 2008; Chu et al., 2007), and more than ten times higher than those of conventional ozonation systems (Kukuzaki et al., 2010). The overall reaction rate constant (k) did not significantly vary with the initial concentration of DMP, which is expected.

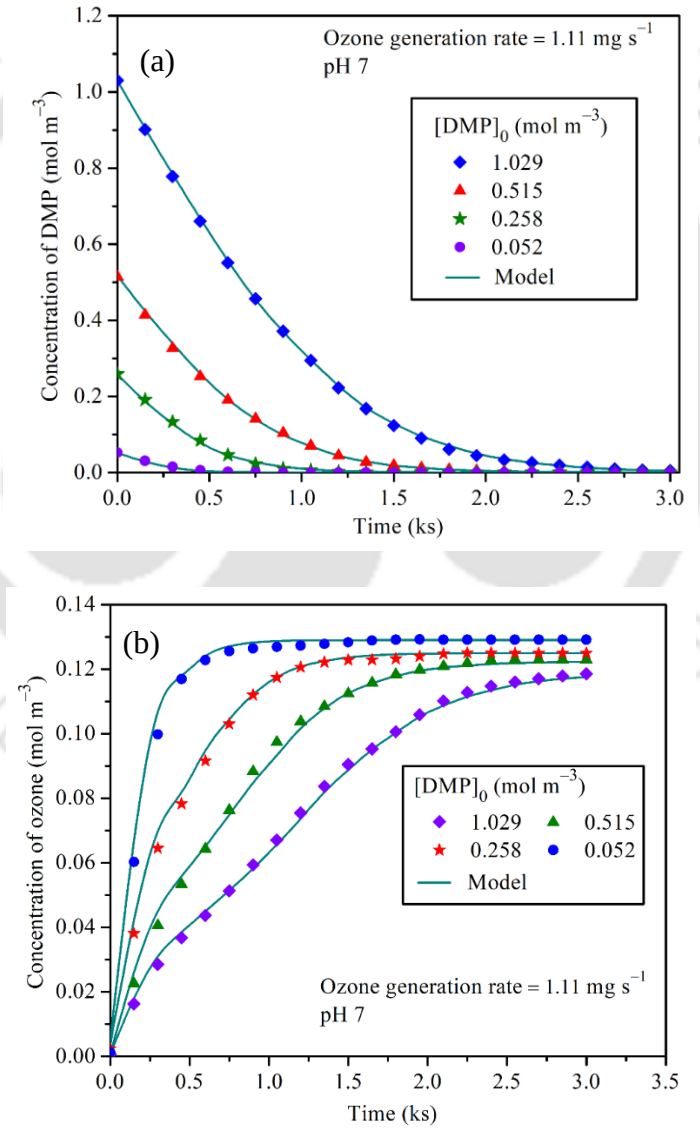

Figure 3.11: Concentration profiles of **(a)** DMP and **(b)** ozone in the reactor, and the fit of the model.

The enhancement factor (E) is a measure of the increase in the rate of mass transfer of ozone due to chemical reaction. It is defined as the ratio of the volumetric mass transfer coefficients in the reacting and non-reacting systems [i.e., $k_L a$ and $(k_L a)_0$] (Chang et al., 2005; Khuntia et al., 2014; Wu and Wang, 2001).

$$E = \frac{k_L a}{(k_L a)_0} \tag{3.8}$$

The values of volumetric mass transfer coefficient of ozone in the non-reacting systems were taken from the work of Khuntia et al. (2012). As shown in Table 3.2, the enhancement factor increased with the increasing initial concentration of DMP.

Table 3.2: Kinetic and mass transfer parameters (at the ozone generation rate of 1.11 mg s^{-1})

$[DMP]_0$ (mol m^{-3})	$[O_3]_{ss}$ (mol m^{-3})	$k_L a \times 10^3$ (s^{-1})	k [(mol $dm^{-3})^{1-m-n}$ s^{-1}]	m (–)	n (–)	E (–)	Ha (–)
0.052	0.129	7.98	0.94	1.07	0.55	3.63	0.002
0.258	0.125	8.06	0.93	1.01	0.60	3.66	0.003
0.515	0.123	8.12	0.90	1.04	0.63	3.69	0.005
1.029	0.119	9.92	0.93	1.02	0.66	4.51	0.007

3.2.10 Calculation of Hatta number

Hatta number (Ha) indicates the relative importance of chemical reaction and mass transfer rates in the gas–liquid reaction system (Beltrán, 2004). For the second-order reaction, it can be computed from Equation (3.9), given below.

$$\mathrm{Ha} = \frac{\sqrt{k[\mathrm{DMP}]_0 D_{\mathrm{O_3}}}}{k_l} \tag{3.9}$$

where k is the rate constant for the reaction of DMP with ozone, k_l is the mass transfer coefficient and $D_{\mathrm{O_3}}$ is the diffusivity of ozone in water. The temperature dependence of $D_{\mathrm{O_3}}$ can be expressed by an Arrhenius-type equation, as shown by Equation (1.13) (Johnson and Davis, 1996). For microbubbles rising in water following Stokes' law [Equation (3.10)] (Ghosh, 2009), the mass transfer coefficient can be calculated from Equation (3.11) (Clift et al., 2005).

$$u = \frac{gd^2}{18\nu} \tag{3.10}$$

where u is the average rising velocity of the microbubbles in water, d is their mean diameter, ν is the kinematic viscosity of water, and g is the acceleration due to gravity.

$$k_l = \frac{D_{\mathrm{O_3}}}{d}\left[1+\left\{1+\frac{du}{D_{\mathrm{O_3}}}\right\}^{1/3}\right] \tag{3.11}$$

From Equation (1.13), at 298 K, $D_{\mathrm{O_3}}$ is calculated to be 1.89×10^{-9} m^2 s^{-1}. From Equation (3.10), with $g = 9.81$ m s^{-2}, d = 30 µm, and $\nu = 8.9\times10^{-7}$ m^2 s^{-1} (Perry and Green, 1997), the average rising velocity of the microbubbles is calculated to be 5.5×10^{-4} m s^{-1}. From Equation (3.11), the value of k_l is calculated to be 1.975×10^{-4} m s^{-1}. Using these values and the data given in Table 3.2, Ha was computed from Equation (3.9) at different initial concentrations of DMP. These values are given in Table 3.2. Ha was calculated at different pH by following the same procedure. These results are given in Table 3.3.

Table 3.3: Calculated values of Ha at different pH (ozone generation rate = 0.92 mg s^{-1}, $[DMP]_0$ = 0.258 mol m^{-3})

pH	k (m^3 mol^{-1} s^{-1})	Ha (–)	Relative uncertainty (%)
5	2.4	0.0017	0.44
7	9.3	0.0034	0.67
9	10.6	0.0036	0.29

We have determined the values of k at different pH by using our experimental data on mass transfer with chemical reaction (similar to the Section 3.2.9). The k_l used in the calculation of Ha was computed from Equation (3.11), which does not include the effect of pH. Accordingly, the values of Ha depend on the reaction rate constant, which varied slightly with the pH. From these results, it can be seen that Ha < 0.02, which shows that the reaction was very slow (i.e., slow reaction regime) (Levenspiel, 1999) for all initial concentrations of DMP and pH. Due to their high curvature, and consequently, high internal pressure, the rate of transfer of ozone to water was higher for the microbubble process. The low values of Ha found in this study prove that the mass transfer resistance, $(1/k_l)$, was negligible. This implies that the rate of mass transfer was high. As a result of enhanced transfer of ozone into the aqueous phase, the concentration of ozone in the aqueous phase was high. This led to the generation of the hydroxyl radicals, and the organic pollutant was efficiently oxidized. Therefore, this reactor was efficient for the oxidation of DMP by ozone.

3.3 Conclusions

The following conclusions were reached based on the experimental studies and the analysis of the results.

- DMP present in water was effectively removed by the OMBs. Neutral and alkaline solutions were good media for the generation of hydroxyl radicals as compared to the acidic solutions.
- Increase in the initial concentration of DMP had an adverse impact on its extent of removal.
- Increase in the ozone generation rate dramatically improved the removal of DMP.
- Increase in the ozone generation rate enhanced the efficiency of TOC removal. The rate of TOC removal was less than the corresponding DMP removal rate, which was possibly due to the formation of reaction intermediates during the course of ozonation. Complete mineralization of these compounds required a longer time.
- The addition of H_2O_2 slightly increased the rate of removal of DMP by augmenting the generation of ·OH radicals. However, a large dosage of H_2O_2 had an adverse effect on the rate of removal of DMP.
- The use of *t*-BuOH as the hydroxyl radical scavenger confirmed the contribution of hydroxyl radicals to the degradation of DMP. These results clearly reveal that the reaction between DMP and ·OH was dominant over the direct reaction of DMP with ozone at pH 7.
- The value of the ozone self-decomposition rate constant increased with the pH.
- The reaction between DMP and ozone followed an overall second-order kinetics, and first-order with respect to both DMP and ozone. The volumetric mass transfer coefficient and the enhancement factor for the reacting system increased with

increasing initial concentration of DMP. The steady state concentration of ozone in the reactor decreased with increasing initial concentration of DMP.

- The values of Ha revealed that the reaction was very slow (i.e., it was in the slow reaction regime), and the mass transfer resistance was negligible.

Notations

a	specific gas–liquid interfacial area ($m^2\ m^{-3}$)
d	mean diameter of microbubbles (μm)
[DMP]	concentration of dimethyl phthalate in the reactor during the reaction (mol m^{-3})
$[DMP]_0$	initial concentration of dimethyl phthalate in the reactor (mol m^{-3})
D_{O_3}	diffusivity of ozone in water ($m^2\ s^{-1}$)
E	enhancement factor (–)
g	acceleration due to gravity (m s^{-2})
Ha	Hatta number (–)
k	rate constant for the reaction of DMP with ozone [$(mol\ dm^{-3})^{1-m-n}\ s^{-1}$]
k_d	self-decomposition rate constant of ozone (s^{-1})
k_l	mass transfer coefficient (m s^{-1})
k_La	volumetric mass transfer coefficient of ozone in the reacting system (s^{-1})
$(k_La)_0$	volumetric mass transfer coefficient of ozone in the non-reacting system (s^{-1})
m	order of reaction with respect to DMP (–)
n	order of reaction with respect to ozone (–)
$[O_3]$	concentration of ozone during the reaction (mol m^{-3})
$[O_3]^*$	saturation concentration of ozone in water (mol m^{-3})
$[O_3]_{ss}$	steady state concentration of ozone in the aqueous phase (mol m^{-3})
r	correlation coefficient (–)
t	ozonation time (s)

T	temperature (K)
$[TOC]_0$	initial total organic carbon (mg dm^{-3})
u	average rising velocity of the microbubbles (m s^{-1})

Greek symbols

ν	kinematic viscosity of water (m^2 s^{-1})

Abbreviations

DMP	dimethyl phthalate
OMB	ozone microbubble
TOC	total organic carbon
UV	ultraviolet

References

Beltrán, F.J., **2004**. Ozone Reaction Kinetics for Water and Wastewater Systems, 1st ed. Lewis Publishers, Boca Raton (USA).

Chang, B.V., Liao, C.S., Yuan, S.Y., **2005**. Anaerobic degradation of diethyl phthalate, di-n-butyl phthalate, and di-(2-ethylhexyl) phthalate from river sediment in Taiwan. *Chemosphere, 58*, 1601–1607.

Chen, Y.H., Shang, N.C., Hsieh, D.C., **2008**. Decomposition of dimethyl phthalate in an aqueous solution by ozonation with high silica zeolites and UV radiation. *J. Hazard. Mater., 157*, 260–268.

Chu, L.-B., Xing, X.-H., Yu, A.-F., Sun, X.-L., Jurcik, B., **2008**. Enhanced treatment of practical textile wastewater by microbubble ozonation. *Process Saf. Environ. Prot., 86*, 389–393.

Chu, L.B., Xing, X.H., Yu, A.F., Zhou, Y.N., Sun, X.L., Jurcik, B., **2007**. Enhanced ozonation of simulated dyestuff wastewater by microbubbles. *Chemosphere, 68*, 1854 –1860.

Clift, R., Grace, J.R., Weber, M.E., **2005**. Bubbles, Drops, and Particles, 1st ed. Courier Corporation, Chelmsford (UK).

David Yao, C.C., Haag, W.R., **1991**. Rate constants for direct reactions of ozone with several drinking water contaminants. *Water Res., 25*, 761–773.

de Oliveira, T.F., Chedeville, O., Fauduet, H., Cagnon, B., **2011**. Use of ozone/activated carbon coupling to remove diethyl phthalate from water: influence of activated carbon textural and chemical properties. *Desalination, 276*, 359–365.

Gao, M., Hirata, M., Takanashi, H., Hano, T., **2005**. Ozone mass transfer in a new gas–liquid contactor – Karman contactor. *Sep. Purif. Technol., 42*, 145–149.

Ghosh, P., **2009**. Colloid and Interface Science, 1st ed. PHI Learning, New Delhi (India).

Gottschalk, C., Libra, J.A., Saupe, A., **2010**. Ozonation of Water and Waste Water: A Practical Guide to Understanding Ozone and its Applications, 2nd ed. Wiley-VCH, Weinheim (Germany).

Hoigné, J., **1998**. Chemistry of aqueous ozone and transformation of pollutants by ozonation and advanced oxidation processes, in: Hrubec, J. (Ed.), *Quality and Treatment of Drinking Water II*. Springer-Verlag, Berlin (Germany), pp. 83–141.

Hoigné, J., Bader, H., **1983**. Rate constants of reactions of ozone with organic and inorganic compounds in water–I: non-dissociating organic compounds. *Water Res., 17*, 173–183.

Hsu, Y.C., Chen, T.Y., Chen, J.H., Lay, C.W., **2002**. Ozone transfer into water in a gas-inducing reactor. *Ind. Eng. Chem. Res., 41*, 120–127.

Huang, Y. **2010.** Degradation of waterborne contaminants by ozone and hydrogen peroxide. *Doctor of Philosophy Thesis*, Civil & Environmental Engineering, University of Utah, Utah.

Johnson, P.N., Davis, R.A., **1996**. Diffusivity of ozone in water. *J. Chem. Eng. Data, 41*, 1485–1487.

Khuntia, S., Majumder, S.K., Ghosh, P., **2012**. Removal of ammonia from water by ozone microbubbles. *Ind. Eng. Chem. Res., 52*, 318–326.

Khuntia, S., Majumder, S.K., Ghosh, P., **2014**. A pilot plant study of the degradation of Brilliant Green dye using ozone microbubbles: mechanism and kinetics of reaction. *Environ. Technol., 36*, 336–347.

Kukuzaki, M., Fujimoto, K., Kai, S., Ohe, K., Oshima, T., Baba, Y., **2010**. Ozone mass transfer in an ozone–water contacting process with Shirasu porous glass (SPG) membranes – a comparative study of hydrophilic and hydrophobic membranes. *Sep. Purif. Technol., 72*, 347–356.

Levenspiel, O., **1999**. Chemical Reaction Engineering, 3rd ed. Wiley, New York (USA).

Li, L., Ye, W., Zhang, Q., Sun, F., Lu, P., Li, X., **2009**. Catalytic ozonation of dimethyl phthalate over cerium supported on activated carbon. *J. Hazard. Mater., 170*, 411–416.

Liao, W., Wang, P., **2009**. Microwave-assisted photocatalytic degradation of dimethyl phthalate using a microwave discharged electrodeless lamp. *J. Braz. Chem. Soc., 20*, 866–872.

Mansouri, L., Mohammed, H., Tizaoui, C., Bousselmi, L., **2013**. Heterogeneous catalytic ozonation of diethyl phthalate. *Desalination Water Treat., 51*, 6698–6710.

Perry, R.H., Green, D.W., **1997**. Perry's Chemical Engineers' Handbook, 7th ed. McGraw-Hill, New York (USA).

Rosal, R., Rodríguez, A., Zerhouni, M., **2006**. Enhancement of gas–liquid mass transfer during the unsteady-state catalytic decomposition of ozone in water. *Appl. Catal. A, 305*, 169–175.

Roth, J.A., Sullivan, D.E., **1981**. Solubility of ozone in water. *Ind. Eng. Chem. Fundam.*, *20*, 137–140.

Sotelo, J.L., Beltran, F.J., Benitez, F.J., Beltran-Heredia, J., **1987**. Ozone decomposition in water: kinetic study. *Ind. Eng. Chem. Res.*, *26*, 39–43.

Sotelo, J.L., Beltrán, F.J., Benitez, F.J., Beltrán-Heredia, J., **1989**. Henry's law constant for the ozone–water system. *Water Res.*, *23*, 1239–1246.

Wen, G., Ma, J., Liu, Z.Q., Zhao, L., **2011**. Ozonation kinetics for the degradation of phthalate esters in water and the reduction of toxicity in the process of O_3/H_2O_2. *J. Hazard. Mater.*, *195*, 371–377.

Wu, J., Wang, T., **2001**. Ozonation of aqueous azo dye in a semi-batch reactor. *Water Res.*, *35*, 1093–1099.

Yu, L., Zhang, P., Pang, L., Li, Y., Hou, J., Jia, S., **2013**. Degradation efficiency and kinetics of dimethyl phthalate in aqueous solution by ozonation (article written in Chinese). *CIESC J.*, *64*, 1408–1414.

Yuan, S.Y., Liu, C., Liao, C.S., Chang, B.V., **2002**. Occurrence and microbial degradation of phthalate esters in Taiwan river sediments. *Chemosphere*, *49*, 1295–1299.

CHAPTER 4

REMOVAL OF DIETHYL PHTHALATE FROM WATER BY OZONE MICROBUBBLES

This chapter presents the use of ozone microbubbles to remove diethyl phthalate (DEP) from water. The removal of DEP and the mineralization efficiency have been discussed under various reaction conditions. The contribution of ·OH has been determined by using a hydroxyl radical scavenger (i.e., t-BuOH). The effect of addition of H_2O_2 on the removal of DEP has also been investigated. The overall kinetic parameters of oxidation of DEP by ozone have been computed from the experimental results.

4.1 Introduction

DEP is one of the most frequently-identified phthalates in diverse environments. It is used as a plasticizer in various products. It was chosen as a model target pollutant in this work because of its high solubility in water and toxicity. As discussed in Section 1.6.1, DEP is difficult to degrade by the biological and photo-chemical methods. Therefore, there is a strong need for effective treatment processes for the removal of DEP from water and wastewater. The use of ozone microbubbles (OMBs) may be a good alternative method for complete degradation and mineralization of DEP present in water.

The aim of this work was to investigate the removal efficiency of DEP by the OMBs. The major parameters which influence the removal of DEP, such as its initial concentration, ozone generation rate (i.e., concentration of ozone in the feed gas), and the pH of reaction medium, have been studied. In addition, the contribution of hydroxyl

radicals to the removal of DEP and the effect of H_2O_2 on ozonation have been investigated. The total organic carbon (TOC) of the solutions was analyzed to determine the extent of mineralization. The overall kinetic parameters of the reaction between DEP and ozone, and their variation with the pH of the medium have been determined from the experimental results. Microbubbles enhanced mass transfer as compared to the conventional bubbling process. Therefore, the microbubble-based ozonation process is expected to provide a better efficiency for the removal of DEP and mineralization.

4.2 Results and discussion

4.2.1 UV–Vis spectra of DEP

The experiments for OMBs were conducted at the ozone generation rate of 1.94 mg s^{-1}. The UV–Vis spectra of DEP before and after ozonation are shown in Figure 4.1. From these spectra, it is observed that initially, there were two maxima at 230 and 276 nm. The absorption spectrum of DEP at both maxima almost vanished after 1.2 ks of ozonation. This shows that the aromatic ring of DEP was destroyed by direct and indirect reactions with ozone. Similar spectra of DEP have been reported by Oh et al. (2006). However, they have reported that the peak at 275 nm had somewhat weakened and the nearby bands showed a slight increase, whereas the peak at 230 nm was slightly reduced after 1.8 ks of ozonation using millibubbles. From these observations, they concluded that the slight increase of absorbance at 275 nm indicated the formation of the intermediate products.

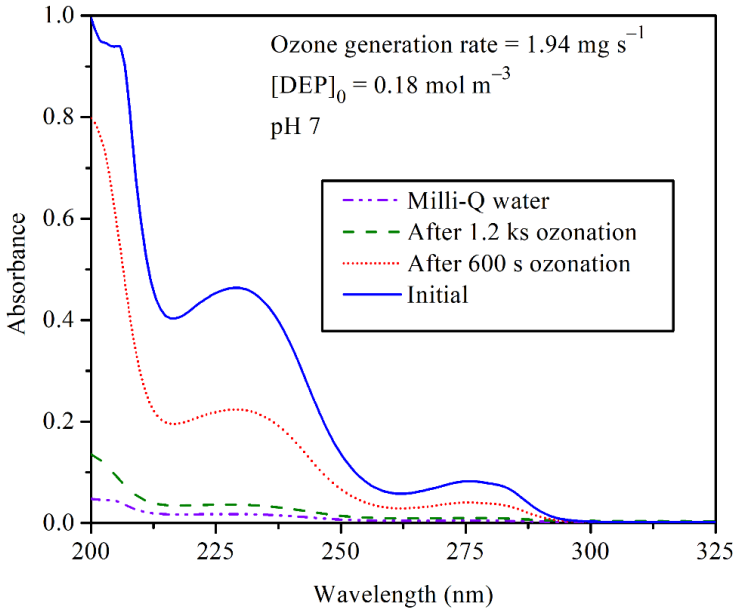

Figure 4.1: UV–Vis absorption spectra of DEP before and after ozonation.

4.2.2 Effect of hydroxyl radicals on the removal of DEP

Molecular ozone can directly participate in the oxidation of organic and inorganic compounds. In addition, ozone decomposes in water through a series of chain reactions (Beltrán, 2004). The mechanism of decomposition in the acidic medium differs from that in the alkaline medium (Khuntia et al., 2015).

The decomposition of ozone leads to the generation of ·OH during the initiation and propagation reactions (see Table 1.2). Thus, the oxidation of a compound by ozone may occur via two mechanisms (i.e., by direct reaction with molecular ozone and by indirect reaction with the ·OH) (Staehelin et al., 1984; Tomiyasu et al., 1985; von Gunten, 2003). In order to account for the contribution of each of the two pathways, radical scavengers have been used to gain information on the nature of the reactions. Similar to Section 3.2.7, *t*-BuOH was used to study the contribution of ·OH in the oxidation of DEP. After scavenging the ·OH by *t*-BuOH, only the reaction by molecular ozone would prevail

in the system. In this work, the experiments were conducted with 2.5, 5, and 10 mol m^{-3} *t*-BuOH at the ozone generation rate of 1.94 mg s^{-1} and pH 7. The experimental results shown in Figure 4.2 (a) reveal that in the absence of *t*-BuOH, almost all of the DEP was removed within 1.8 ks reaction time, whereas only 9% removal was achieved in the presence of 10 mol m^{-3} *t*-BuOH. This clearly indicates that the reaction involving ·OH dominated over the reaction with the ozone molecules.

The effects of *t*-BuOH in the acidic and alkaline media were investigated by the addition of 5 mol m^{-3} *t*-BuOH at the ozone generation rate of 1.94 mg s^{-1}. The results shown in Figure 4.2 (b) indicate that DEP was mainly oxidized by the indirect reaction in alkaline solutions, where the effect of *t*-BuOH was more pronounced (see Section 4.2.3 for the effect of pH in absence of *t*-BuOH). Our results agree with the previous studies (Na et al., 2012b). This may be due to the more favorable reaction of ·OH with DEP in the alkaline medium. The experimental results reported in this study clearly demonstrate that the reactions with ·OH indeed play a very important role in the oxidation of DEP.

4.2.3 Effect of pH of the aqueous solution

The mechanism of decomposition of ozone in the acidic and alkaline solutions has been proposed by several researchers (Gardoni et al., 2012; Sehested et al., 1991; Sehested et al., 1984; Staehelin et al., 1984; Tomiyasu et al., 1985) and summarized in the work of Khuntia et al. (2015). The effect of pH on the oxidation of DEP is shown in Figure 4.3 (a). The experiments were conducted at the ozone generation rate of 1.94 mg s^{-1}. The initial DEP concentration was 0.18 mol m^{-3} and the pH was varied from 3 to 9. It is seen from Figure 4.3 (a) that the acidic medium (i.e., pH 3) was not suitable for the oxidation of DEP by the OMBs. On the other hand, when the pH was increased, the removal of DEP increased significantly.

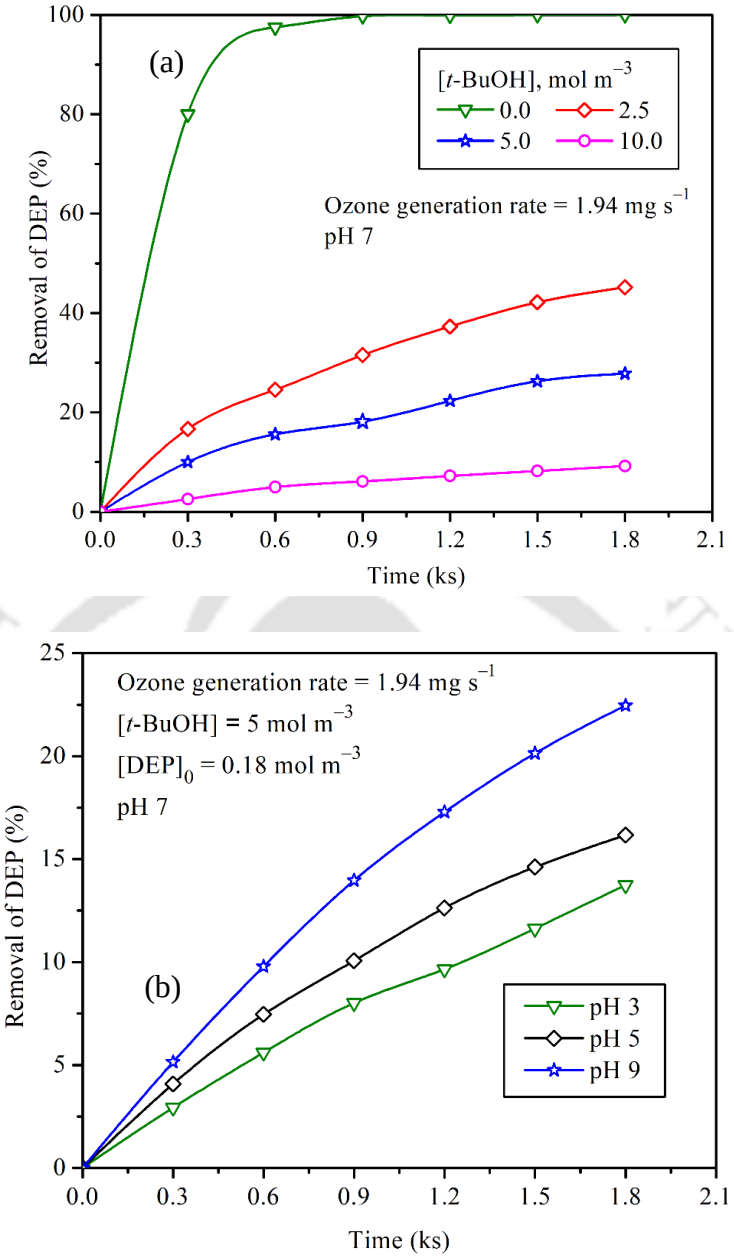

Figure 4.2: (a) Effect of concentration of *t*-BuOH (at pH 7) and **(b)** effect of pH in the presence of 5 mol m^{-3} *t*-BuOH on the removal of DEP.

After performing ozonation for 1.8 ks, the removal of DEP was 35 and 98% at pH 3 and 7, respectively. Thus, it is apparent that the concentration of ·OH increased with increasing pH, which favored the indirect reaction (Beltrán, 2004; Gottschalk et al., 2010; Hoigné and Bader, 1983). This conclusion is in good agreement with the results reported

in the literature (Mansouri et al., 2013; Tay et al., 2010). At low pH (i.e., pH 3), the oxidation of DEP was less due to the lower decomposition of ozone, and hence a lower concentration of ·OH (Mansouri et al., 2013; Staehelin and Hoigne, 1982).

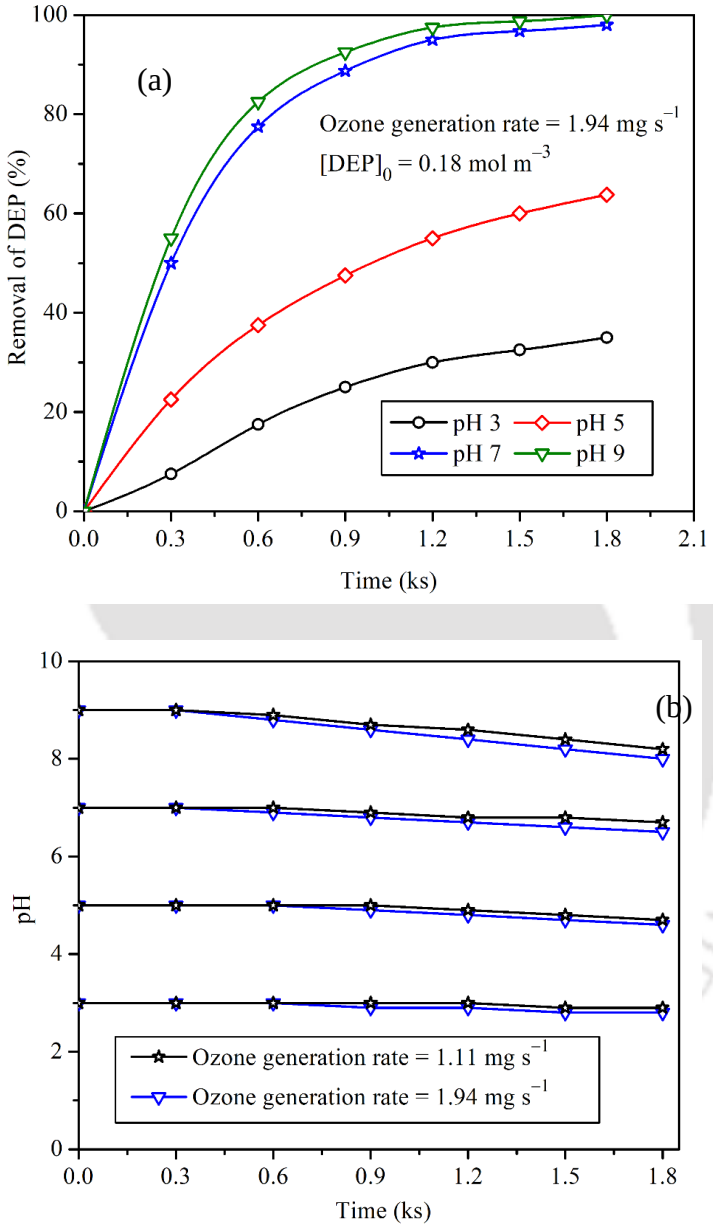

Figure 4.3: (a) Effect of pH of the aqueous solution on the removal of DEP and **(b)** variation of pH of the solution with time during ozonation.

The pH of the solution slightly decreased with time [Figure 4.3 (b)], which is likely due to the formation of organic acid intermediates during the oxidation of DEP (Hou et al., 2016; Jung et al., 2010). This lowered the pH of the medium.

4.2.4 Effect of initial concentration of DEP

Figure 4.4 shows the effect of initial concentration of DEP on its removal by the OMBs at 1.94 mg s^{-1} ozone generation rate. The concentration profiles followed a similar trend at the different initial concentrations of DEP. It is clearly seen that the extent of removal of DEP decreased as the initial concentration of DEP increased. The times required to achieve 50% removal (i.e., half-life time) were 180, 300, 420, 600, and 1500 s, when the initial concentrations of DEP were 0.045, 0.09, 0.18, 0.36. and 0.72 mol m^{-3}, respectively. For the lowest initial concentration (i.e., 0.045 mol m^{-3}), almost all of the DEP was removed within 900 s of ozonation.

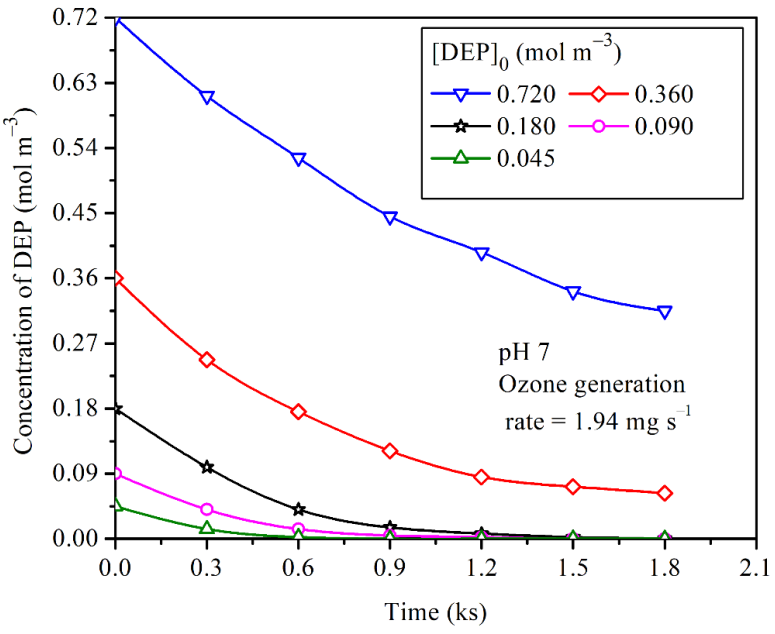

Figure 4.4: Effect of initial concentration of DEP on its removal by the OMBs.

On the other hand, only 38% removal was achieved for 0.72 mol m^{-3} initial concentration of DEP in 900 s. This shows that the OMBs achieved a lesser extent of oxidation of DEP, within a given time, if its initial concentration was higher. An increase in the initial concentration of DEP led to an increase in the concentration of the intermediate compounds formed during the course of ozonation (Tay et al., 2010). Researchers (Jung et al., 2010) have detected about 13 intermediates (e.g., phthalic acid, phthalic anhydride, and 4-hydroxy phthalate) during the ozonation of DEP. They have proposed two degradation pathways (i.e., hydrolysis of the aliphatic chain and hydroxylation resulting from the attack of the hydroxyl radical on the aromatic ring). After the initial hydroxylation and hydrolysis reactions, ozone opened-up the aromatic ring of DEP and formed some acidic compounds such as malonic, succinic, and glutaric acids. Thus, the molecular ozone in the reaction medium and the hydroxyl radicals produced *in situ* were both consumed in the oxidation of DEP and the intermediates produced during the course of reaction.

4.2.5 Effect of ozone generation rate

In this work, the ozonation experiments were conducted with various ozone generation rates to investigate the effect of ozone concentration in the microbubbles on the removal efficiency of DEP. The experimental results shown in Figure 4.5 reveal that the removal rate of DEP increased with increasing ozone generation rate. This is expected because the increase in ozone concentration in the aqueous phase enhanced the direct and indirect reactions of ozone with DEP (Mansouri et al., 2013). From Figure 4.5, it is clearly seen that increasing the ozone generation rate from 1.11 to 2.22 mg s^{-1} significantly improved the removal of DEP from 50 to 99.8% within 900 s of ozonation. However, a much longer

ozonation time was needed to achieve a similar removal when the ozone generation rate was 1.11 mg s^{-1}.

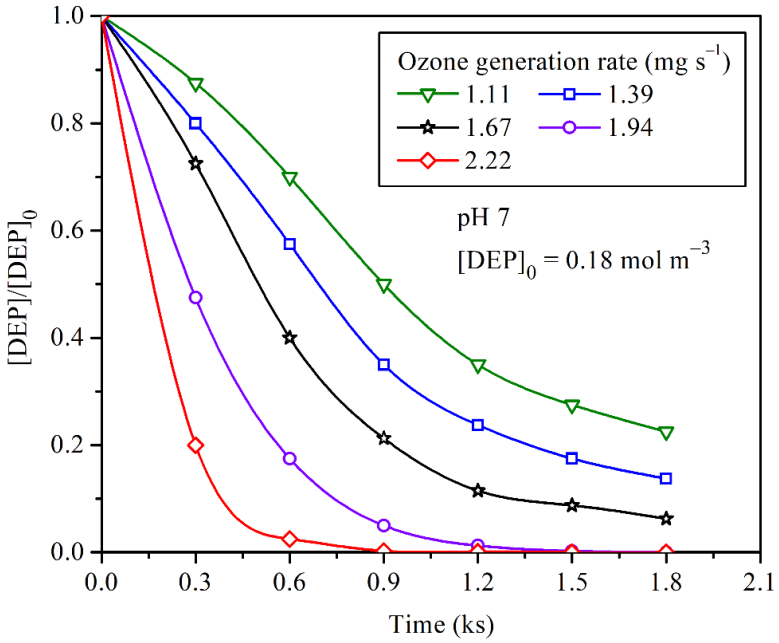

Figure 4.5: The effect of ozone generation rate on the removal of DEP at pH 7.

However, further increase in the ozone generation rate (i.e., beyond 2.2 mg s^{-1}) had a small effect on the oxidation of DEP. These trends are in good agreement with the results reported in the literature (Tay et al., 2010). The concentration of dissolved ozone in the reactor was measured with time. Figure 4.6 depicts the concentration profiles of dissolved ozone in the aqueous phase in the presence of 0.18 mol m^{-3} DEP at two ozone generation rates at pH 7. The steady state concentrations of dissolved ozone were 0.129 and 0.175 mol m^{-3} for the ozone generation rates of 1.11 and 1.94 mg s^{-1}, respectively. The equilibrium concentration of ozone in the aqueous phase can be described by the Henry's law, which is given by Equation (4.1) (Li and Tsuge, 2006).

$$[O_3]^* = \left(\frac{\rho RT}{M}\right)\frac{[O_3]_g}{H} \tag{4.1}$$

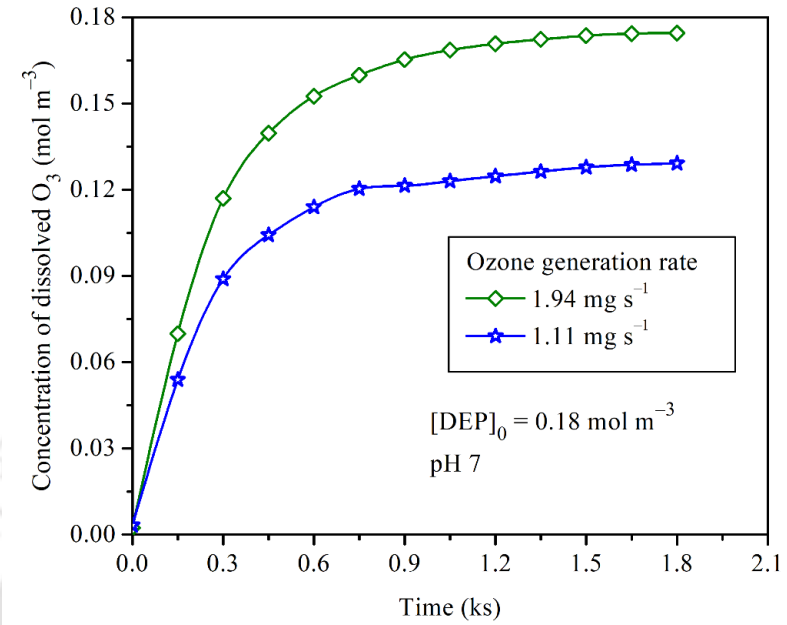

Figure 4.6: Concentration profiles of dissolved ozone in the presence of DEP.

where $[O_3]^*$ is the equilibrium concentration of ozone in the aqueous phase, $[O_3]_g$ is the concentration of ozone in the gas phase, ρ is the density of water, R is the gas constant, T is the temperature, M is the molecular weight of water, and H is the Henry's law constant. The Henry's law constant, H, depends on the temperature and pH of the medium, which are correlated as (Roth and Sullivan, 1981)

$$H = 3.84\times10^7\left[OH^-\right]^{0.035}\exp\left(2428/T\right) \tag{4.2}$$

where $[OH^-]$ is the hydroxide ion concentration. The equilibrium concentration of ozone in the aqueous phase is related to its steady state concentration, $[O_3]_{ss}$, by the Equation (4.3) (Roth and Sullivan, 1981).

$$[O_3]^* = \left(\frac{k_L a + k_d}{k_L a} \right) [O_3]_{ss} \quad (4.3)$$

where k_d is the self-decomposition rate constant of ozone and $k_L a$ is the volumetric mass transfer coefficient of ozone in the reacting system. As the ozone generation rate increased, the steady state concentration of dissolved ozone in the aqueous phase increased. At the low ozone generation rate, the concentration of ozone in the gas mixture was low due to the presence of a large amount of oxygen in the gas (Khuntia et al., 2012b). Hence, the equilibrium concentration of ozone in the aqueous phase was low, which is predicted by Equation (4.1). Furthermore, $k_L a$ increased with increasing ozone generation rate (Khuntia et al., 2012b). Therefore, $[O_3]_{ss}$ increased with increasing $[O_3]^*$ and $k_L a$, as predicted by Equation (4.3).

4.2.6 Reduction of TOC

The overall degree of mineralization of DEP can be determined by analyzing the TOC during the course of reaction. The TOC at any time represents the total concentration of unreacted DEP and the intermediate organic compounds formed from the oxidation of DEP (Oh et al., 2006). The effectiveness of a water treatment technology should be based not only on the efficiency of pollutant degradation but also on the reduction of TOC and the toxicity of the intermediate organic compounds (Na et al., 2012a; Nahum et al., 2013). In order to quantify the mineralization of DEP, the TOC of the aqueous solution before and during the ozonation was monitored with time. All experimental conditions were similar to that of Section 4.2.3. The initial TOC of the solutions was ~23 mg dm^{-3} at 0.18 mol m^{-3} initial concentration of DEP. Figure 4.7 shows the TOC profiles at different pH. It is apparent from Figure 4.7 that the TOC reduction was favored in both neutral and alkaline solutions, although the extent of mineralization was vastly different. At all pH,

the TOC reduction rate was lower than the corresponding DEP removal rate (see Figures 4.3 and 4.7). This was due to the formation of intermediates during the course of ozonation.

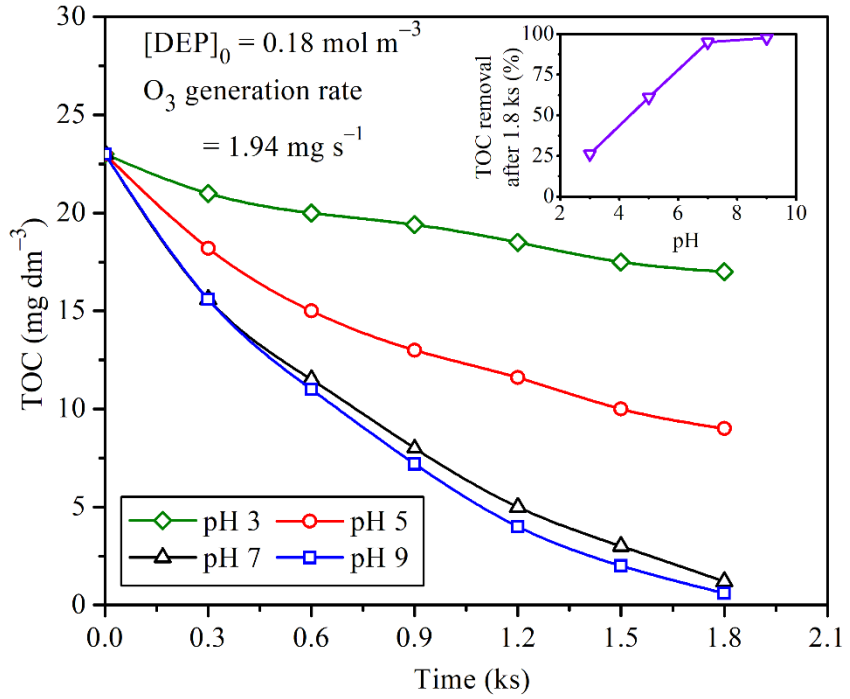

Figure 4.7: Reduction of TOC at different pH.

Complete mineralization of all these compounds needed a longer time. At pH 7, after 600 s of reaction time, less than 50% of the TOC was reduced, while 78% of DEP was removed. In acidic media (i.e., pH 3), only 26% mineralization was achieved, which was very less as compared to 97% at pH 9. In our microbubble-based experimental system, ozone rapidly dissolved in water due to the high pressure inside the microbubbles. Consequently, the microbubbles quickly reduced in size. The pressure inside a microbubble goes on increasing as its size reduces. This ultimately leads to the collapse of the microbubble. The high concentration of dissolved ozone in the aqueous medium leads to the formation of a significant amount of ·OH (Khuntia et al., 2015). The ·OH is

believed to be the key reactive species, which effectively oxidized the intermediate organic compounds. Hou et al. (2016) have reported that direct ozonation was not effective for DEP mineralization, and better removal of TOC was achieved by enhancing the formation of ·OH using the electro-peroxone process.

4.2.7 Effect of addition of H_2O_2

The effect of addition of H_2O_2 on the removal of DEP was investigated by adding 1 to 8 mol m^{-3} H_2O_2 at pH 7. The results shown in Figure 4.8 indicate that a slight enhancement in DEP removal was achieved for 1 and 2 mol m^{-3} doses of H_2O_2. After carrying out ozonation for 1.8 ks, a dose of 2 mol m^{-3} H_2O_2 improved the removal of DEP from 93 to 99%. The improvement was very small above 2 mol m^{-3} dosage of H_2O_2.

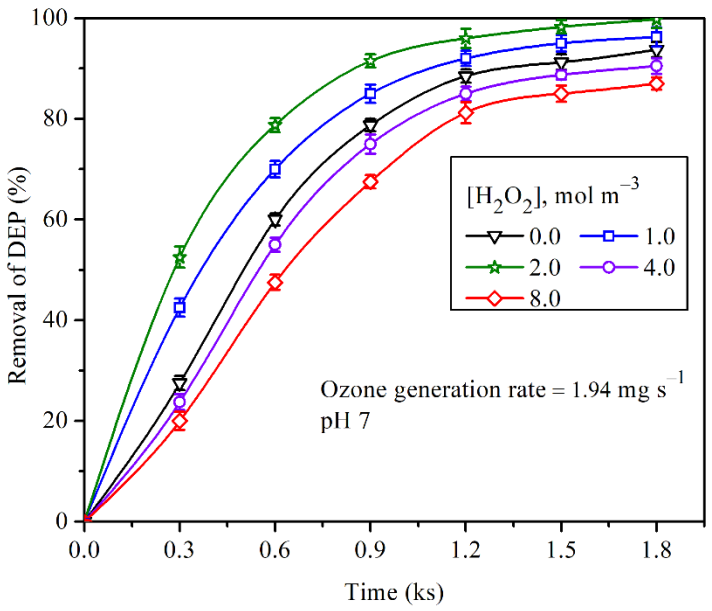

Figure 4.8: Effect of addition of H_2O_2 on DEP degradation.

Addition of H_2O_2 to the ozonation system is expected to promote the decomposition of ozone and enhance the generation of ·OH (Hoigné, 1998; Mansouri et al., 2013; Wen et al., 2011). This would increase the reaction rate, which would enhance

the removal of contaminants significantly. Interestingly, further increase in the dosage of H_2O_2 adversely affected the oxidation of DEP. The removal rate decreased to 90 and 83% for the dosages of 4 and 8 mol m^{-3} H_2O_2, respectively. Huang (2010) has concluded that increasing the H_2O_2/O_3 mole ratio beyond 1:2 did not lead to a pro-rata improvement in the removal rate of the phthalates. It is likely that the excess ·OH produced in the reaction medium recombine, and therefore, lead to a low reaction rate, which is not helpful for the oxidation of the target organic pollutant (Gottschalk et al., 2010). It has been reported (Muruganandham and Swaminathan, 2004) that at high H_2O_2 concentration, H_2O_2 acts as a ·OH quencher, and thus lowers the concentration of ·OH in the aqueous solution. Besides this, H_2O_2 is not only an initiator and promoter of ozonation, but it can also act as an inhibitor of ozone decomposition when its concentration is so high that the reaction between H_2O_2 and O_3 becomes controlled by mass transfer (Beltrán, 2004).

In acidic solutions (i.e., at pH 3 and 5) H_2O_2 reacts very slowly with molecular O_3 (Mansouri et al., 2013). Therefore, a negligible removal of DEP was observed. At pH 7 and 9, the decomposition of ozone was slightly accelerated by H_2O_2, which enhanced the removal of DEP. These findings corroborate the results reported by Mansouri et al. (2013). To investigate the extent of DEP removal by H_2O_2 alone, 2 mol m^{-3} H_2O_2 was added to the aqueous solution containing 0.18 mol m^{-3} DEP, in the presence of air microbubbles. It was found that the removal of DEP was very less after 1.8 ks of reaction time. This implies that DEP is resistant to the degradation by H_2O_2 alone. This is in good agreement with the previous studies (Xu et al., 2007).

The effect of H_2O_2 was studied at different ozone generation rates. Figure 4.9 shows that the addition of 2 mol m^{-3} H_2O_2 enhanced the removal of DEP for all ozone generation rates. Therefore, it is apparent that increasing the ozone generation rate

increased the dissolved ozone concentration in the solution. From Figure 4.9, it is observed that for the same dosage of H_2O_2, its effect became less pronounced at the higher ozone generation rates (i.e., higher dissolved ozone concentration).

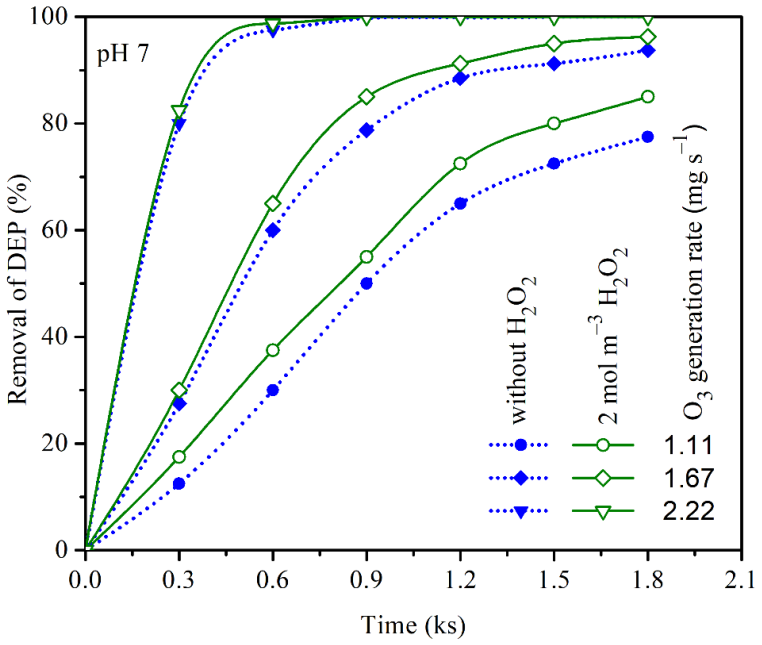

Figure 4.9: Effect of addition of H_2O_2 on DEP degradation at different ozone generation rates.

4.2.8 Estimation of overall kinetic parameters of oxidation of DEP by ozone

In our experimental setup, ozone gradually dissolved in water and reacted with DEP. The rate of transfer of ozone to water was high due to the high residence time of the microbubbles, large gas–liquid interfacial area, and a reasonable solubility of ozone in water (which is much greater than that of oxygen) (Khuntia et al., 2012a). As a result, the concentration of ozone in the aqueous phase went on increasing until the saturation state was asymptotically reached. This usually happened after a few minutes of the commencement of ozonation. The kinetic equation for the reaction between DEP and ozone can be expressed as

$$\frac{\mathrm{d}[\mathrm{DEP}]}{\mathrm{d}t} = -k[\mathrm{DEP}]^m [\mathrm{O_3}]^n \tag{4.4}$$

where k is the overall reaction rate constant, and m and n are the orders of reaction with respect to DEP and ozone, respectively. Ozone reacts directly and indirectly with DEP, and simultaneously undergoes self-decomposition. Several researchers (Beltrán, 2004; Sotelo et al., 1987; Sotelo et al., 1989) have reported that the self-decomposition of ozone in water depends on the pH of the solution, and it follows a first-order kinetics. Therefore, the overall mass balance of ozone contains three terms, i.e., the rate of mass transfer of ozone from the gas to the liquid phase, the self-decomposition of ozone, and the reaction of ozone with DEP. This can be expressed as

$$\frac{\mathrm{d}[\mathrm{O_3}]}{\mathrm{d}t} = k_L a\left([\mathrm{O_3}]^* - [\mathrm{O_3}]\right) - k_d [\mathrm{O_3}] - k[\mathrm{DEP}]^m [\mathrm{O_3}]^n \tag{4.5}$$

Incorporating Equation (4.3) into Equation (4.5) and after rearranging, the following overall mass balance of ozone is obtained.

$$\frac{\mathrm{d}[\mathrm{O_3}]}{\mathrm{d}t} = \left(k_L a + k_d\right)\left([\mathrm{O_3}]_{\mathrm{ss}} - [\mathrm{O_3}]\right) - k[\mathrm{DEP}]^m [\mathrm{O_3}]^n \tag{4.6}$$

The ODEs given by the Equations (4.4) and (4.6) were simultaneously solved by the Runge–Kutta method using Polymath® (version 6.0). The best-fit values of the unknown parameters were obtained by fitting the model to the concentration profiles of DEP and ozone in the reactor. Table 4.1 summarizes these values. The data were fitted well by the model with $r^2 > 0.98$. The values of k_d were calculated in the Section 3.2.8. The fit of the kinetic model to the concentration profiles of ozone and DEP in the reactor at the ozone generation rate of 1.94 mg s^{-1} and pH 7 is shown in Figure 4.10.

As can be seen from Table 4.1, both the overall reaction rate constant, k, and the volumetric mass transfer coefficient of ozone, $k_L a$, slightly increased with increasing pH. The reaction between ozone and DEP followed an overall second-order kinetics, and first-order with respect to both ozone and DEP. These findings corroborate the results reported in the literature (de Oliveira et al., 2011; Hoigné and Bader, 1983).

Table 4.1: Kinetic and mass transfer parameters for the oxidation of DEP by the OMBs (ozone generation rate = 1.94 mg s^{-1}; $[DEP]_0$ = 0.18 mol m^{-3})

pH	$[O_3]_{ss}$ (mol m^{-3})	$k_L a \times 10^3$ (s^{-1})	k [(mol m^{-3})$^{1-m-n}$ s^{-1}]	m (–)	n (–)	r^2 (–)
3	0.202	4.93	0.002	1.2	0.9	0.98
5	0.187	6.14	0.006	1.4	0.7	0.98
7	0.175	6.71	0.024	1.0	0.96	0.99
9	0.158	6.82	0.026	1.0	0.98	0.98

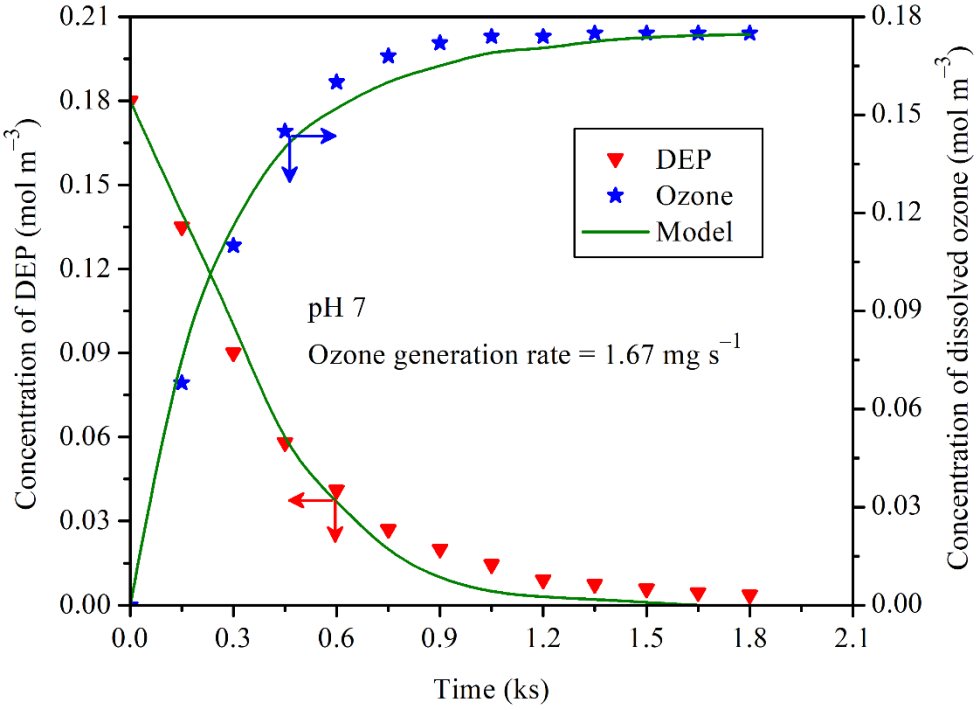

Figure 4.10: Concentration profiles of ozone and DEP in the reactor, and the fit of the kinetic model at pH 7.

4.3 Conclusions

- The OMB-based technology for the oxidation of DEP in the aqueous medium was very effective.
- The use of *t*-BuOH as the hydroxyl radical scavenger confirmed the contribution of ·OH to the degradation of DEP. At neutral and alkaline pH, the reaction between DEP and ·OH was dominant over the direct reaction of DEP with molecular ozone.
- Increase in the ozone generation rate increased the concentration of dissolved ozone in the aqueous phase, which enhanced the oxidation of DEP.
- At pH 7, 94% TOC removal efficiency was achieved. Complete mineralization was achieved at a higher pH and at the ozone generation rate of 1.94 mg s^{-1}. The ·OH generated from ozone is believed to be the key reactive species that effectively oxidized the intermediate compounds formed from DEP during ozonation.
- The rate of oxidation of DEP was enhanced by the addition of a small amount of H_2O_2, which augmented the generation of hydroxyl radicals. However, addition of a large amount of H_2O_2 had an adverse effect on the removal of DEP.
- The oxidation of DEP with ozone followed an overall second-order kinetics. The overall reaction rate constant and the volumetric mass transfer coefficient of ozone slightly increased with pH whereas, the steady state concentration of dissolved ozone in the reactor decreased with increasing pH.

Notations

a	specific gas–liquid interfacial area ($m^2\ m^{-3}$)
[DEP]	concentration of diethyl phthalate in the reactor during the reaction (mol m^{-3})
$[DEP]_0$	initial concentration of diethyl phthalate in the reactor (mol m^{-3})
g	acceleration due to gravity (m s^{-2})
H	Henry's law constant (Pa m^3 mol^{-1})
k	rate constant for the reaction of DEP with ozone [(mol m^{-3})$^{1-m-n}$ s^{-1}]
k_d	self-decomposition rate constant of ozone (s^{-1})
$k_L a$	volumetric mass transfer coefficient of ozone in the reacting system (s^{-1})
m	order of reaction with respect to DEP (–)
M	molecular weight of ozone (g mol^{-1})
n	order of reaction with respect to ozone (–)
$[O_3]$	concentration of ozone during the reaction (mol m^{-3})
$[O_3]^*$	saturation concentration of ozone in water (mol m^{-3})
$[O_3]_g$	concentration of ozone in the gas phase (mol m^{-3})
$[O_3]_{ss}$	steady state concentration of ozone in the aqueous phase (mol m^{-3})
r	correlation coefficient (–)
R	gas constant (J mol^{-1} K^{-1})
t	ozonation time (s)
T	temperature (K)

Greek symbols	
ρ	density of ozone (kg m^{-3})

Abbreviations

DEP	diethyl phthalate
OMBs	ozone microbubbles
TOC	total organic carbon
UV	ultraviolet

References

Beltrán, F.J., **2004**. Ozone Reaction Kinetics for Water and Wastewater Systems, 1st ed. Lewis Publishers, Boca Raton (USA).

de Oliveira, T.F., Chedeville, O., Fauduet, H., Cagnon, B., **2011**. Use of ozone/activated carbon coupling to remove diethyl phthalate from water: influence of activated carbon textural and chemical properties. *Desalination, 276*, 359–365.

Gardoni, D., Vailati, A., Canziani, R., **2012**. Decay of ozone in water: a review. *Ozone Sci. Eng., 34*, 233–242.

Gottschalk, C., Libra, J.A., Saupe, A., **2010**. Ozonation of Water and Waste Water: A Practical Guide to Understanding Ozone and its Applications, 2nd ed. Wiley-VCH, Weinheim (Germany).

Hoigné, J., **1998**. Chemistry of aqueous ozone and transformation of pollutants by ozonation and advanced oxidation processes, in: Hrubec, J. (Ed.), *Quality and Treatment of Drinking Water II*. Springer-Verlag, Berlin (Germany), pp. 83–141.

Hoigné, J., Bader, H., **1983**. Rate constants of reactions of ozone with organic and inorganic compounds in water–I: non-dissociating organic compounds. *Water Res., 17*, 173–183.

Hou, M., Chu, Y., Li, X., Wang, H., Yao, W., Yu, G., Murayama, S., Wang, Y., **2016**. Electro-peroxone degradation of diethyl phthalate: cathode selection, operational parameters, and degradation mechanisms. *J. Hazard. Mater., 319*, 61–68.

Huang, Y. **2010.** Degradation of waterborne contaminants by ozone and hydrogen peroxide. *Doctor of Philosophy Thesis*, Civil & Environmental Engineering, University of Utah, Utah.

Jung, Y.J., Oh, B.S., Kim, K.S., Koga, M., Shinohara, R., Kang, J.W., **2010**. The degradation of diethyl phthalate (DEP) during ozonation: oxidation by-products study. *J. Water Health, 8*, 290–298.

Khuntia, S., Majumder, S.K., Ghosh, P., **2012a**. Microbubble-aided water and wastewater purification: a review. *Rev. Chem. Eng., 28*, 191–221.

Khuntia, S., Majumder, S.K., Ghosh, P., **2012b**. Removal of ammonia from water by ozone microbubbles. *Ind. Eng. Chem. Res., 52*, 318–326.

Khuntia, S., Majumder, S.K., Ghosh, P., **2015**. Quantitative prediction of generation of hydroxyl radicals from ozone microbubbles. *Chem. Eng. Res. Des., 98*, 231–239.

Li, P., Tsuge, H., **2006**. Ozone transfer in a new gas-induced contactor with microbubbles. *J. Chem. Eng. Jpn.*, *39*, 1213–1220.

Mansouri, L., Mohammed, H., Tizaoui, C., Bousselmi, L., **2013**. Heterogeneous catalytic ozonation of diethyl phthalate. *Desalination Water Treat.*, *51*, 6698–6710.

Muruganandham, M., Swaminathan, M., **2004**. Photochemical oxidation of reactive azo dye with UV–H_2O_2 process. *Dyes Pigm.*, *62*, 269–275.

Na, S., Ahn, Y.G., Cui, M., Khim, J., **2012a**. Significant diethyl phthalate (DEP) degradation by combined advanced oxidation process in aqueous solution. *J. Environ. Manage.*, *101*, 104–110.

Na, S., Jinhua, C., Cui, M., Khim, J., **2012b**. Sonophotolytic diethyl phthalate (DEP) degradation with UVC or VUV irradiation. *Ultrason. Sonochem.*, *19*, 1094–1098.

Nahum, M.C., Raúl, O.P., Roberto, L.R., Manuel, S.P., José, R.U., José D., M.D., **2013**. Removal of diethyl phthalate from water solution by adsorption, photo-oxidation, ozonation and advanced oxidation process (UV/H_2O_2, O_3/H_2O_2 and O_3/activated carbon). *Sci. Total Environ.*, *442*, 26–35.

Oh, B.S., Jung, Y.J., Oh, Y.J., Yoo, Y.S., Kang, J.W., **2006**. Application of ozone, UV and ozone/UV processes to reduce diethyl phthalate and its estrogenic activity. *Sci. Total Environ.*, *367*, 681–693.

Roth, J.A., Sullivan, D.E., **1981**. Solubility of ozone in water. *Ind. Eng. Chem. Fundam.*, *20*, 137–140.

Sehested, K., Corfitzen, H., Holcman, J., Fischer, C.H., Hart, E.J., **1991**. The primary reaction in the decomposition of ozone in acidic aqueous solutions. *Environ. Sci. Technol.*, *25*, 1589–1596.

Sehested, K., Holcman, J., Bjergbakke, E., Hart, E.J., **1984**. A pulse radiolytic study of the reaction hydroxyl + ozone in aqueous medium. *J. Phys. Chem.*, *88*, 4144–4147.

Sotelo, J.L., Beltran, F.J., Benitez, F.J., Beltran-Heredia, J., **1987**. Ozone decomposition in water: kinetic study. *Ind. Eng. Chem. Res.*, *26*, 39–43.

Sotelo, J.L., Beltrán, F.J., Benitez, F.J., Beltrán-Heredia, J., **1989**. Henry's law constant for the ozone–water system. *Water Res.*, *23*, 1239–1246.

Staehelin, J., Buehler, R.E., Hoigne, J., **1984**. Ozone decomposition in water studied by pulse radiolysis. 2. Hydroxyl and hydrogen tetroxide (HO_4) as chain intermediates. *J. Phys. Chem.*, *88*, 5999–6004.

Staehelin, J., Hoigne, J., **1982**. Decomposition of ozone in water: rate of initiation by hydroxide ions and hydrogen peroxide. *Environ. Sci. Technol.*, *16*, 676–681.

Tay, K.S., Rahman, N.A., Abas, M.R.B., **2010**. Ozonation of a mixture of dialkylphthalates in aqueous solution. *J. Chem. Technol. Biotechnol.*, *85*, 726–729.

Tomiyasu, H., Fukutomi, H., Gordon, G., **1985**. Kinetics and mechanism of ozone decomposition in basic aqueous solution. *Inorg. Chem.*, *24*, 2962–2966.

von Gunten, U., **2003**. Ozonation of drinking water: part I. Oxidation kinetics and product formation. *Water Res.*, *37*, 1443–1467.

Wen, G., Ma, J., Liu, Z.Q., Zhao, L., **2011**. Ozonation kinetics for the degradation of phthalate esters in water and the reduction of toxicity in the process of O_3/H_2O_2. *J. Hazard. Mater.*, *195*, 371–377.

Xu, B., Gao, N.Y., Sun, X.F., Xia, S.J., Rui, M., Simonnot, M.O., Causserand, C., Zhao, J.F., **2007**. Photochemical degradation of diethyl phthalate with UV/H_2O_2. *J. Hazard. Mater.*, *139*, 132–139.

CHAPTER 5

OXIDATION OF BISPHENOL-A BY OZONE MICROBUBBLES

This chapter presents the use of the ozone microbubbles (OMBs) for oxidation of bisphenol-A (BPA) in water. The effects of the main operational parameters that influence the removal of BPA were investigated. The stoichiometric ratio of ozone consumed to BPA removed, and the ozone utilization efficiency were computed from the experimental results. The degradation efficiency of BPA and its selected major reaction-intermediates (i.e., catechol and hydroquinone) were studied in aqueous solution by the OMBs. The effect of bicarbonate ions and the contribution of hydroxyl radicals on the oxidation of BPA are reported. The extent of mineralization of BPA and its oxidation-intermediates at the optimal conditions are estimated by TOC measurements. The overall kinetic parameters of the reaction between BPA and ozone are reported at different initial concentrations of BPA and pH.

5.1 Introduction

Bisphenol-A is extensively detected in the environment as discussed in the Section 1.6.2. The treatment of BPA is difficult by the conventional wastewater treatment methods because of its ring structure that leads to its low solubility in water and low vapor pressure, enabling the molecules to escape the treatment units (Mutseyekwa et al., 2017). Most of the works based on the catalytic ozonation process have reported that it is effective for the removal of BPA. However, the major drawback of this process is the preparation of the catalyst, which is complicated and expensive. Therefore, the application of the OMBs

would be a very good alternative and efficient method for complete degradation of BPA inasmuch as the reaction between ozone and the organic compound is expected to be accelerated by the use of the microbubbles, and the hydroxyl radicals would be formed *in situ* without using any catalyst.

This work is aimed to examine the effectiveness of OMBs for the oxidation of BPA and its major reaction intermediates. The stoichiometric ratio of ozone consumed to the BPA removed, and the ozone utilization efficiency of the OMBs system were computed from the experimental results. The main operational parameters that influence the oxidation of BPA have been studied in detail. Besides, the effect of bicarbonate and the contribution of the ·OH to the oxidation of BPA have been explored. The extent of mineralization of BPA and its oxidation-intermediates was studied from the TOC measurements. The overall kinetic parameters such as the Hatta number, volumetric mass transfer coefficient, and rate constant of reaction between BPA and ozone have been determined from the experimental results. Since the microbubbles enhance mass transfer as compared to the conventional ozonation process, the OMBs process is expected to provide a better efficiency for the degradation of BPA and mineralization of its oxidation intermediates. At the same time, the amount of ozone required for the oxidation and the loss of ozone can be reduced significantly by this process.

5.2 Results and discussion

5.2.1 Effects of the operational parameters on the removal of BPA

The effectiveness of the OMBs in removing the BPA was investigated under different experimental conditions by varying the pH of the aqueous solution (in the range of 3–11), initial BPA concentration (in the range of 7.81×10^{-3} – 0.25 mol m^{-3}), ozone generation

rate (in the range of 0.56–1.94 mg s^{-1}), *t*-BuOH concentration (in the range of 0.5 – 10 mol m^{-3}), and bicarbonate ion concentration (in the range of 2.0 – 10.0 mol m^{-3}).

5.2.1.1 Effects of pH and hydroxyl radicals

In ozone-based oxidation of the organic pollutants, pH of the solution is considered as a key parameter for the oxidation by molecular ozone as well as that by the ·OH, because pH controls the generation of ·OH and utilization of ozone (Buffle et al., 2006; Elovitz et al., 2000; Hoigné and Bader, 1983). In this work, the effect of initial pH of the solution was investigated at $[BPA]_0$ = 0.125 mol m^{-3} and the ozone generation rate of 1.11 mg s^{-1}. From the experimental results, it is seen that the removal efficiency of BPA by OMBs was improved from 41 to 98% within 600 s of ozonation [Figure 5.1 (a)] as the initial pH was increased from 3 to 7 (i.e., acidic to neutral), which is in agreement with the previous works reported (Garoma and Matsumoto, 2009; Liu et al., 2018). Nevertheless, the removal efficiency of BPA did not show a significant enhancement when the pH was further increased from 7 to 11. It required nearly the same ozonation time (i.e., 700 s) to achieve ~99.9% removal efficiency for the initial pH of 7, 9, and 11. The insignificant effect of alkaline pH during the ozonation may be attributed to the generation of carboxylic acids during the degradation of BPA, which resulted in a slight decrease in the pH of the medium during the oxidation [Figure 5.1 (b)], thereby influencing the BPA removal efficiency.

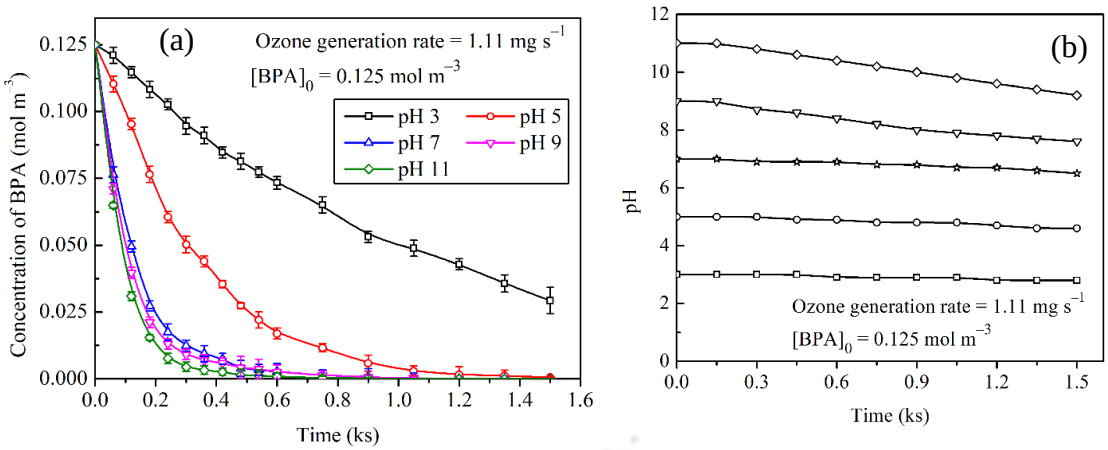

Figure 5.1: (a) Effect of variation of initial pH of the solution on BPA removal and **(b)** variation of pH during the course of ozonation.

Kinetic rate constants for the direct reaction between ozone and BPA have been reported (Kusvuran and Yildirim, 2013) to be 0.13 and 1.6×10^6 mol^{-1} m^3 s^{-1} in strongly acidic and alkaline solutions, respectively, which clearly imply that the electrophilic reaction between BPA and molecular ozone was much more favorable in the alkaline solutions. However, due to the fact that the ozone molecules are consumed by the decomposition reactions in the alkaline solutions, and the non-selective ·OH may react with other ·OH yielding hydrogen peroxide and further-undergoing self-decomposition reactions (Kusvuran and Yildirim, 2013), the improvement in the BPA removal at pH 11 was rather insignificant as compared to that at pH 7 [Figure 5.1 (a)].

Under strongly acidic conditions (e.g., pH 3), BPA removal was not that effective. Nevertheless, the removal efficiency of BPA after 1.5 ks at pH 3 was 76%, which was far better than the results reported (Mutseyekwa et al., 2017) for the conventional ozonation of BPA using millibubbles. This could be due to the enhanced mass transfer of ozone by the microbubbles. It is apparent from Figure 5.2 that there was some contribution from

the indirect reaction between BPA and the hydroxyl radicals, which implies that the OMBs enhanced the generation of hydroxyl radicals under the acidic condition.

As shown in Figure 5.1 (a), the removal efficiency of BPA by the OMBs increased from 76 to 100% within 1.5 ks ozonation time as the initial solution pH was increased from 3 to 11. These results can be explained based on the pH-dependence of the self-decomposition of ozone. It is known that the self-decomposition of ozone is accelerated at a higher solution pH (Sotelo et al., 1987), and it generates more reactive species. Therefore, the increase in the removal efficiency of BPA with the increase in the pH from 3 to 7 could be mainly due to the enhanced self-decomposition of ozone that was enhanced by the microbubbles. Considering the insignificant enhancement in the removal of BPA at pH > 7, the initial pH of 7 was selected as the optimum pH from the practical point of view.

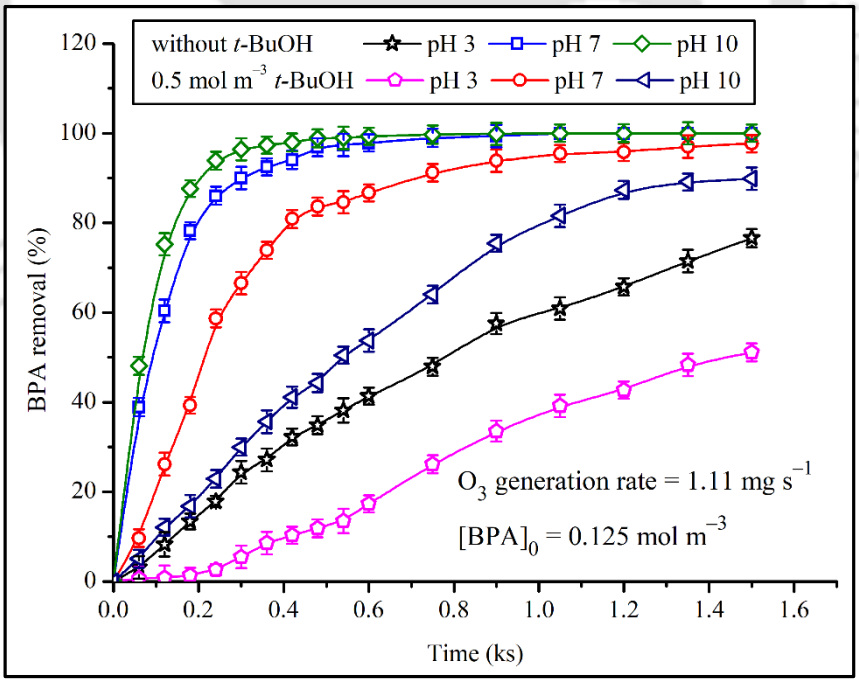

Figure 5.2: Effect of *t*-BuOH on the removal of BPA at different pH.

The role of ·OH in the removal of BPA by the OMBs was examined by using a well-known ·OH inhibitor, i.e., *t*-BuOH. If the ·OH plays a significant role, the degradation of BPA is expected to be substantially hindered in the presence of *t*-BuOH inasmuch as it preferentially scavenges the ·OH. Note that the rate constant for the reaction of *t*-BuOH with ozone is extremely small (i.e., 3×10^{-3} mol^{-1} dm^3 s^{-1}) as compared to that with ·OH (i.e., 6×10^8 mol^{-1} dm^3 s^{-1}) (Hoigné and Bader, 1983). As depicted in Figure 5.2, addition of 0.5 mol m^{-3} *t*-BuOH hindered the removal of BPA in the pH range of 3–11. This is an evidence that both the direct and indirect reactions between the ozone and BPA took place in the pH range up to 11. The effect of 0.5 mol m^{-3} *t*-BuOH was more pronounced in strongly acidic and alkaline solutions. The effect of ·OH at neutral pH was less as compared to pH 3 and 11. The present study confirmed that the OMBs enhanced the mass transfer of ozone, generated the ·OH, and effectively degraded BPA within a shorter time as compared to the conventional ozone-based processes.

5.2.1.2 Effects of ozone generation rate and initial BPA concentration

The concentration of ozone in the aqueous phase during ozonation has a profound effect on the rate of oxidation of the organic compounds. To investigate the effect of ozone concentration (in the gas present in the microbubbles) on the removal efficiency of BPA, the ozonation experiments were conducted with three different ozone generation rates, i.e., 0.56, 1.11, and 1.94 mg s^{-1}, which correspond to 0.283, 0.566, and 1.066 cm^3 s^{-1} volumetric flow rates of ozone in the feed gas, respectively. The experimental results reveal that the removal of BPA was significantly increased as the ozone generation rate (i.e., the ozone concentration in the solution) was increased. It was observed that about 47.2, 90.1, and 99.6% of BPA were removed for 0.56, 1.11, and 1.94 mg s^{-1} OGRs, respectively after 600 s of ozonation [Figure 5.3 (a)]. This is anticipated, because an

increase in the ozone generation rate increased the dissolved ozone concentration in the aqueous solution [Figure 5.3 (b)], which either directly oxidized the BPA, or decomposed to produce the hydroxyl radicals, which in turn reacted with BPA and the intermediate oxidation products.

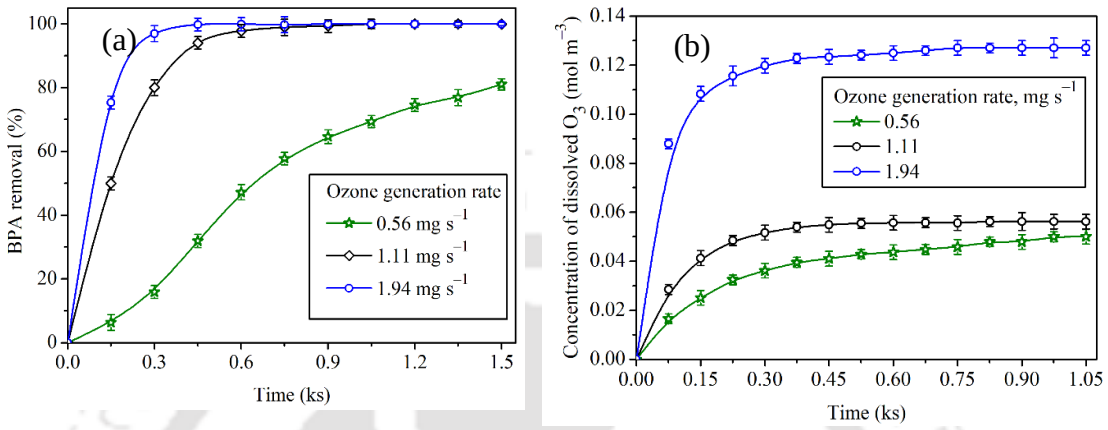

Figure 5.3: Effect of ozone generation rate on **(a)** BPA removal and **(b)** concentration profiles of dissolved ozone in the reactor in the presence of BPA at pH 7 and $[BPA]_0$ = 0.125 mol m^{-3}.

The stoichiometric ratio of moles of ozone consumed per mole of BPA removed during the reaction can be presented as a function of the BPA degraded at a certain ozonation time for different initial concentrations of BPA and ozone generation rates. The stoichiometric ratio (S_R) at the ozonation time *t* was computed by using Equation (5.1) (Garoma and Matsumoto, 2009):

$$S_R = \frac{[O_3]_{abs}}{[BPA]_{rem}} = \frac{\{[O_3]_\infty - ([O_3]_{res} + [O_3]_{exc})\} V_g^{O_3} t}{\{[BPA]_0 - [BPA]\} V_r} \qquad (5.1)$$

where [BPA], $[BPA]_0$, and $[BPA]_{rem}$ are the remaining (unreacted) concentrations of BPA at the reaction time *t*, the initial concentration of BPA, and the number of moles of BPA removed within the ozonation time *t* (all expressed in mol m^{-3}), respectively. $[O_3]_\infty$

, $[O_3]_{abs}$, $[O_3]_{exc}$, and $[O_3]_{res}$ are the total influent concentration of ozone, the number of moles of ozone absorbed by the solution, the excess effluent ozone concentration at reaction time *t*, and the remaining dissolved ozone concentration in the solution at ozonation time *t* (all expressed in mol m^{-3}), respectively. *t* is ozonation time needed to reach the desired removal efficiency, $V_g^{O_3}$ is the volumetric flow rate of ozone, and V_r is the total volume of the reactor. For our ozonation system, $[O_3]_\infty$ and $V_g^{O_3}$ were computed from the Equations (5.2) and (5.3), respectively.

$$[O_3]_\infty = \left(V_g^{O_3}\right)\left(\frac{1}{M}\right)\left(\frac{\rho}{V_r}\right)t \tag{5.2}$$

$$\left(V_g^{O_3}\right) = \left(\dot{G}_{O_3}\right)\left(\frac{RT}{P}\right)\left(\frac{1}{M}\right) \tag{5.3}$$

where *M* is molecular weight of ozone, *P* is the pressure, *T* is the temperature of the aqueous medium, *R* is gas constant, ρ is the density of ozone, and $\dot{G}_{O_3}$ is ozone generation rate. The stoichiometric ratio for the complete removal of BPA was computed from Equation (5.1), and the values are given in Table 5.1. For 0.125 mol m^{-3} initial concentration of BPA, the values of S_R were 0.272, 0.254, and 0.276, for the ozone generation rates of 0.56, 1.11, and 1.94 mg s^{-1}, respectively. Significantly different values of S_R have been reported for the conventional ozonation processes, i.e., 1.5–1.8 (Lee et al., 2003), 7.0–9.5 (Garoma and Matsumoto, 2009), 10.3 (Kusvuran and Yildirim, 2013), and 21.1 (Irmak et al., 2005).

Table 5.1: Summary of the stoichiometric ratios and ozone utilization efficiencies at different ozone generation rates and initial concentrations of BPA

$\dot{G}_{O_3}$ (mg s^{-1})	$V_g^{O_3} \times 10^7$ (m^3 s^{-1})	$[BPA]_0$ (mol m^{-3})	Time* (s)	$[O_3]_\infty$ (mol m^{-3})	$[O_3]_{exc}$ (mol m^{-3})	$[O_3]_{res}$ (mol m^{-3})	$[O_3]_{abs}$ (mol m^{-3})	Stoichiometric ratio (S_R)	Utilization efficiency (%)
0.56	2.83	0.125	2100	1.324	0.131	0.050	1.143	0.272	86.33
1.11	5.66	0.008	360	0.454	0.083	0.133	0.238	0.311	52.42
1.11	5.66	0.125	1050	1.324	0.198	0.056	1.070	0.254	80.82
1.11	5.66	0.250	1500	1.891	0.292	0.042	1.557	0.264	82.34
1.94	10.61	0.125	600	1.419	0.208	0.127	1.084	0.276	76.39

*Ozonation time required for the complete removal of BPA

The range of S_R obtained in this study is noticeably less than most of the values reported for BPA removal using conventional ozonation. The higher values of S_R reported in the literature could be due to the long ozonation times used by these researchers to achieve complete removal of BPA. In such extended ozonation processes, ozone would be consumed by the oxidation intermediates of BPA, resulting in a higher value of S_R. In this study, the ozonation time required for the complete removal of BPA was in the range of 360 – 1500 s, except for the minimum ozone generation rate (i.e., 0.56 mg s^{-1}), which required about 2100 s of ozonation time. The OMBs enhanced the mass transfer of ozone. Since the oxidation of BPA took place in the aqueous phase, a higher concentration of ozone facilitated the reaction. Therefore, the use of the OMBs played a significant role in lowering the S_R.

The concentration of BPA present in the surface water and wastewater varies, and it has been reported that some natural waters contain about 10 mg dm^{-3} BPA (Lee et al., 2003). Thus, it is necessary to evaluate the effect of concentration of BPA on its rate of removal by the OMBs. Figure 5.4 depicts the effect of initial concentration of BPA on its removal by the OMBs at 1.11 mg s^{-1} ozone generation rate and neutral pH. The extent of removal of BPA significantly reduced as the initial concentration of BPA increased, at a given ozone generation rate. The ozonation time required to achieve complete removal of BPA increased with increasing initial concentration of BPA. For instance, for the lowest initial concentration (i.e., 7.81×10^{-3} mol m^{-3}), almost all of the BPA was removed within 360 s of ozonation. On the other hand, for the initial concentrations of 0.125 and 0.25 mol m^{-3}, over 1050 s and 1500 s ozonation times were required, respectively for the complete removal of BPA. This clearly shows that the OMBs achieved a less extent of removal of BPA, within a given time, if its initial concentration was higher.

Keeping other operational parameters constant, as the initial concentration of BPA was increased, the concentration of dissolved ozone in the solution also decreased (Figure 5.4), resulting in the decrease of the molar ratio of ozone to BPA, which resulted in a decreased removal rate of BPA.

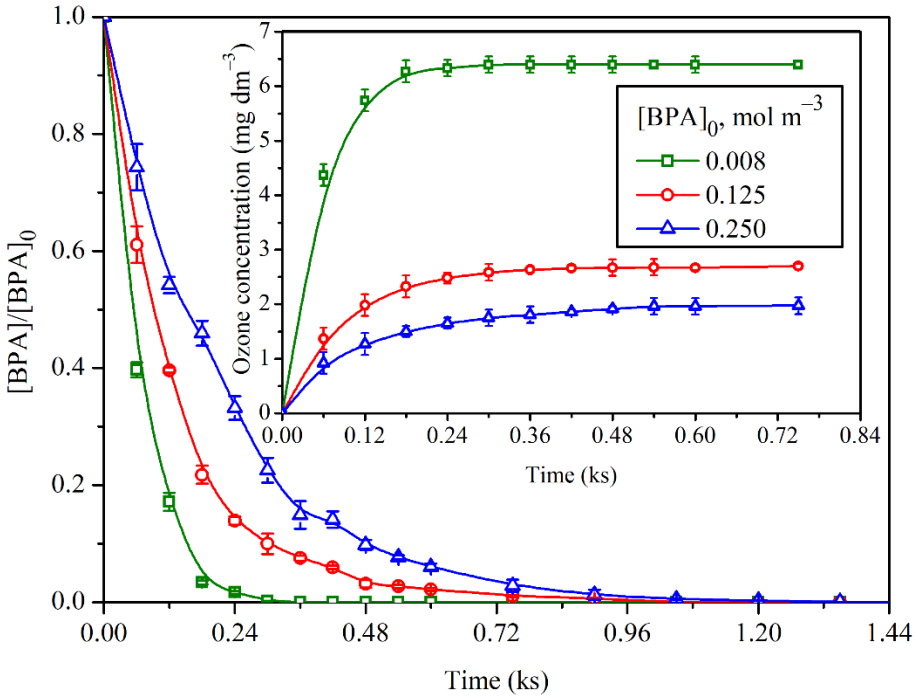

Figure 5.4: Effect of the initial concentration of BPA on the concentration profile of BPA in the reactor. Effect of the initial concentration of BPA on the concentration profile of ozone in the reactor is shown in the inset.

Furthermore, an increase in the initial concentration of BPA led to an increase in the concentration of the intermediate compounds formed during the course of ozonation, which slowed down the removal of BPA, inasmuch as these compounds consumed ozone present in the medium (and hydroxyl radicals) for their further oxidation.

The effectiveness of the microbubble-process was further investigated by determining the utilization efficiency of ozone (η_u) from Equation (5.4), based on the mass balance of ozone in the gas and liquid phases for the ozone generation rates of 0.56, 1.11, and 1.94 mg s^{-1}. The initial concentrations of BPA were 0.008, 0.125, and 0.25 mol m^{-3}. These are summarized in Table 5.1.

$$\eta_u(\%) = \left(\frac{[O_3]_{abs}}{[O_3]_{\infty}} \right) \times 100 \tag{5.4}$$

The range of ozone utilization efficiency for complete removal of BPA (i.e., 52.42 – 86.33%) is considerably higher than the range reported in the literature using catalytic ozonation (i.e., 23.6 – 33.6%) (Zhang et al., 2020). These results confirm that the OMBs improved the utilization of ozone by enhancing the mass transfer of ozone in the aqueous solution and forming the highly reactive hydroxyl radicals. The ozone utilization efficiency decreased with increasing gas flowrate to the reactor, which corroborates the previous works (Li et al., 2009).

5.2.1.3 Effect of bicarbonate ion on BPA removal by the OMBs

The presence of carbonates and bicarbonates in water/wastewater is common, and they may form the reactive carbonate ion radicals by reaction with the hydroxyl radicals (Beltrán, 2004). The carbonate radical anion is a powerful one-electron oxidant that can result from the reaction of a hydroxyl radical with the carbonate or bicarbonate anion (Buxton and Elliot, 1986; Cope et al., 1978), as per the following reactions:

$$\bullet OH + CO_3^{2-} \rightarrow CO_3^{-\bullet} + OH^- \qquad k = 3.9 \times 10^8 \text{ dm}^3 \text{ mol}^{-1} \text{ s}^{-1} \qquad (5.5)$$

$$\bullet OH + HCO_3^- \rightarrow HCO_3^{\bullet} + OH^- \qquad k = 8.5 \times 10^6 \text{ dm}^3 \text{ mol}^{-1} \text{ s}^{-1} \qquad (5.6)$$

$$HCO_3^{\bullet} \rightarrow CO_3^{\bullet} + H^+ \qquad pKa < 0 \qquad (5.7)$$

In this study, the effect of bicarbonate ion on the removal of BPA using OMBs was examined at 1.11 mg s^{-1} ozone generation rate at pH 7. The initial concentration of BPA was 0.125 mol m^{-3}. The sodium bicarbonate concentration was varied in the range of 0.5 – 10.0 mol m^{-3}. Addition of 0.5 mol m^{-3} $NaHCO_3$ had no significant effect (data not shown). A very small effect of the addition of sodium bicarbonate on BPA removal was observed at 10.0 mol m^{-3} $NaHCO_3$ concentration (Figure 5.5). When the carbonate/bicarbonate ions are added to the solution, it is anticipated that the ·OH would react with them to produce the carbonate and/or bicarbonate radicals, which would augment the degradation of the micro-pollutants present in the medium. For instance, it has been reported that the presence of bicarbonate ions enhanced the sonochemical degradation of BPA by a factor of 3.2 (Pétrier et al., 2010). If the bicarbonate ions do not promote the oxidation, they can inhibit the removal of BPA. Nevertheless, from our experimental results, it can be observed that both the promotional and scavenging effects of the bicarbonate ions were rather trivial. This insignificant effect of the bicarbonate ions could be due to the considerably lower rate constants of the reactions of the carbonate and bicarbonate ions with the hydroxyl radical [i.e., 3.9×10^8 and 8.5×10^6 dm^3 mol^{-1} s^{-1}, as shown in Equations (5.5) and (5.6)] than the same of BPA with the hydroxyl radical i.e., 1.0×10^{10} dm^3 mol^{-1} s^{-1} (Gözmen et al., 2003). Consequently, BPA had a better chance of reacting with the hydroxyl radical available in the solution than the

carbonate and bicarbonate ions. The overall rate constant of the reaction of bicarbonate and carbonate ions with ozone (Hoigné et al., 1985) is much less than 0.01 $dm^3\ mol^{-1}\ s^{-1}$, which is significantly lower (i.e., by about a factor of 10^4) than the overall reaction rate constant of BPA with ozone, found in this study (Section 5.2.3.2). It is also lower by a factor of 10^4 to 10^6 $dm^3\ mol^{-1}\ s^{-1}$ in comparison with the rate constants reported in the literature (Deborde et al., 2008; Lee et al., 2003).

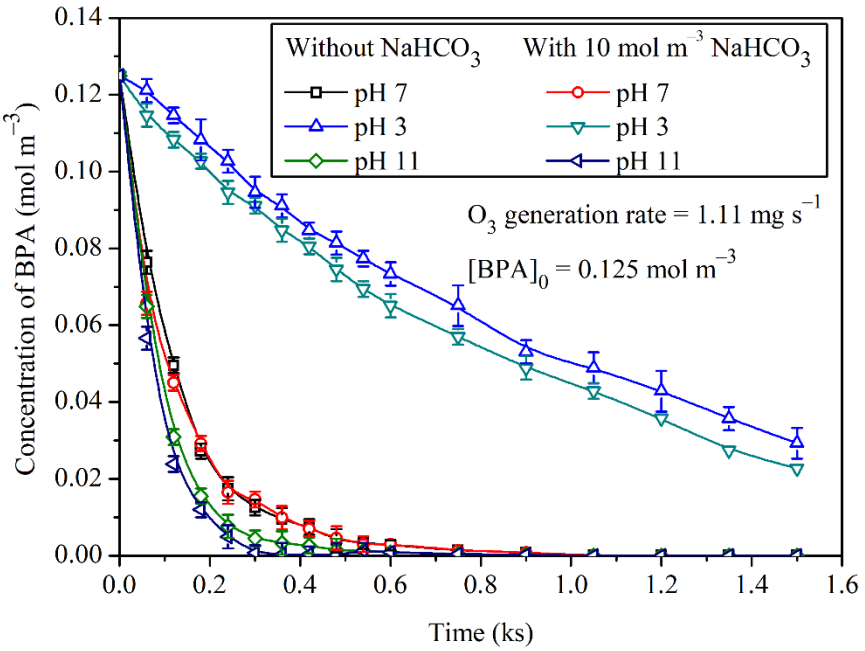

Figure 5.5: Effect of addition of 10 mol m^{-3} $NaHCO_3$ on the removal of BPA by the OMBs.

5.2.2 Extent of mineralization of BPA by the OMBs

The effectiveness of any water/wastewater treatment method should be based not only on its organic pollutant removal efficiency but also on the extent of mineralization of the intermediate organic compounds formed during the course of reaction. The overall degree of

mineralization of BPA can be determined by analyzing the TOC. The TOC at any time represents the total concentration of unreacted BPA and the organic compounds formed during the ozonation (i.e., the reaction intermediates). In order to quantify the mineralization of BPA, the TOC of the aqueous solution before and during the ozonation was monitored with time. Figures 5.6 (a) and 5.6 (b) show the profiles of TOC removal as a function of ozonation time over an initial pH range of 3 – 11 of the aqueous solutions, and at different initial concentrations of BPA, respectively. The rate of TOC removal in the neutral and alkaline conditions was initially slow up to 0.6 ks ozonation time, and then it became faster during 0.6 – 1.8 ks ozonation time. Nonetheless, after 1.8 ks of ozonation, the percentage of mineralization did not change significantly during the rest of the ozonation time, and it took a longer time to remove the remaining TOC. This indicates that the oxidation intermediates of BPA were more resistant to ozonation in the solutions of higher pH. In contrary, in a slightly acidic solution (i.e., pH 5), the rate of TOC removal was very slow during the first 1.2 ks of ozonation time, and then a considerable TOC removal was observed, which led to the complete removal of TOC. Only 19% TOC removal was observed during the first 1.2 ks reaction time, and in the next 1.2 ks (i.e., after 2.4 ks ozonation), more than 99% TOC was removed. It is probable that some oxidation intermediates of BPA were oxidized further in the slightly acidic solutions. This possibility was confirmed by monitoring the extents of removal of two major oxidation intermediates of BPA (i.e., catechol and hydroquinone) formed during the oxidation of BPA by the OMBs at pH 5 and 7 (Figure 5.7).

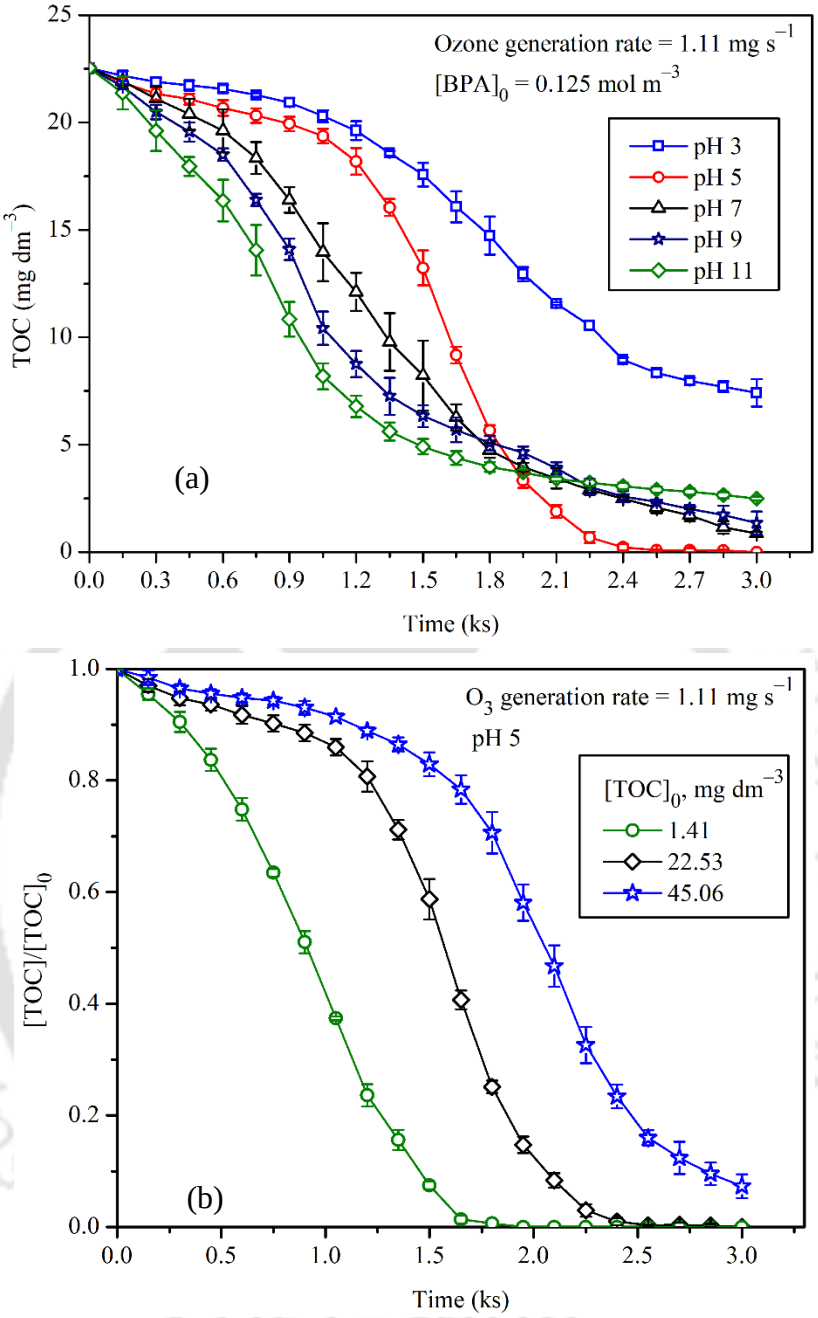

Figure 5.6: TOC removal profiles at **(a)** different (initial) pH of the solution and **(b)** different initial concentrations of BPA.

From Figure 5.7 (b) it is seen that, at pH 7, both catechol and hydroquinone were formed very early and reached their respective maximum concentrations. However, their degradation was very slow and took a longer time. On the other hand, in a slightly acidic medium (i.e., pH 5), both catechol and hydroquinone were formed slowly, and once they reached their maximum concentration, their depletion rate was relatively fast [Figure 5.7 (a)]. This implies that in acidic medium, BPA is relatively more resistant to the OMBs as compared to its oxidation intermediates (i.e., catechol and hydroquinone). The extent of removal of catechol and hydroquinone by the OMBs was separately examined at pH 5 and 7 (Figure 5.8). The results show that both of these compounds were more favorably oxidized in a slightly acidic medium than at the neutral pH.

The ozone contact time ($[O_3]_{CT}$) in the aqueous phase can be written as a function of TOC removal, and it can be determined by using the expression given in Equation (5.8).

$$[O_3]_{CT} = \int [O_3] dt \tag{5.8}$$

$$\frac{[O_3]_{CT}}{[TOC]_{removed}} = \frac{\int [O_3] dt}{[TOC]_0 - [TOC]} \tag{5.9}$$

where $[TOC]_{removed}$ and $[TOC]$ are the TOC removed within ozonation time t, and the concentration of TOC at ozonation time t, respectively. $[TOC]_0$ is the initial TOC. TOC (expressed in mol dm^{-3}) is determined based on the percentage of carbon in BPA, i.e., 78.95% (since 1 mol dm^{-3} BPA contains about 0.7895 mol dm^{-3} TOC). $\int [O_3] dt$ is the area under the curve of the dissolved ozone in the solution versus ozonation time [Figure 5.3 (b)].

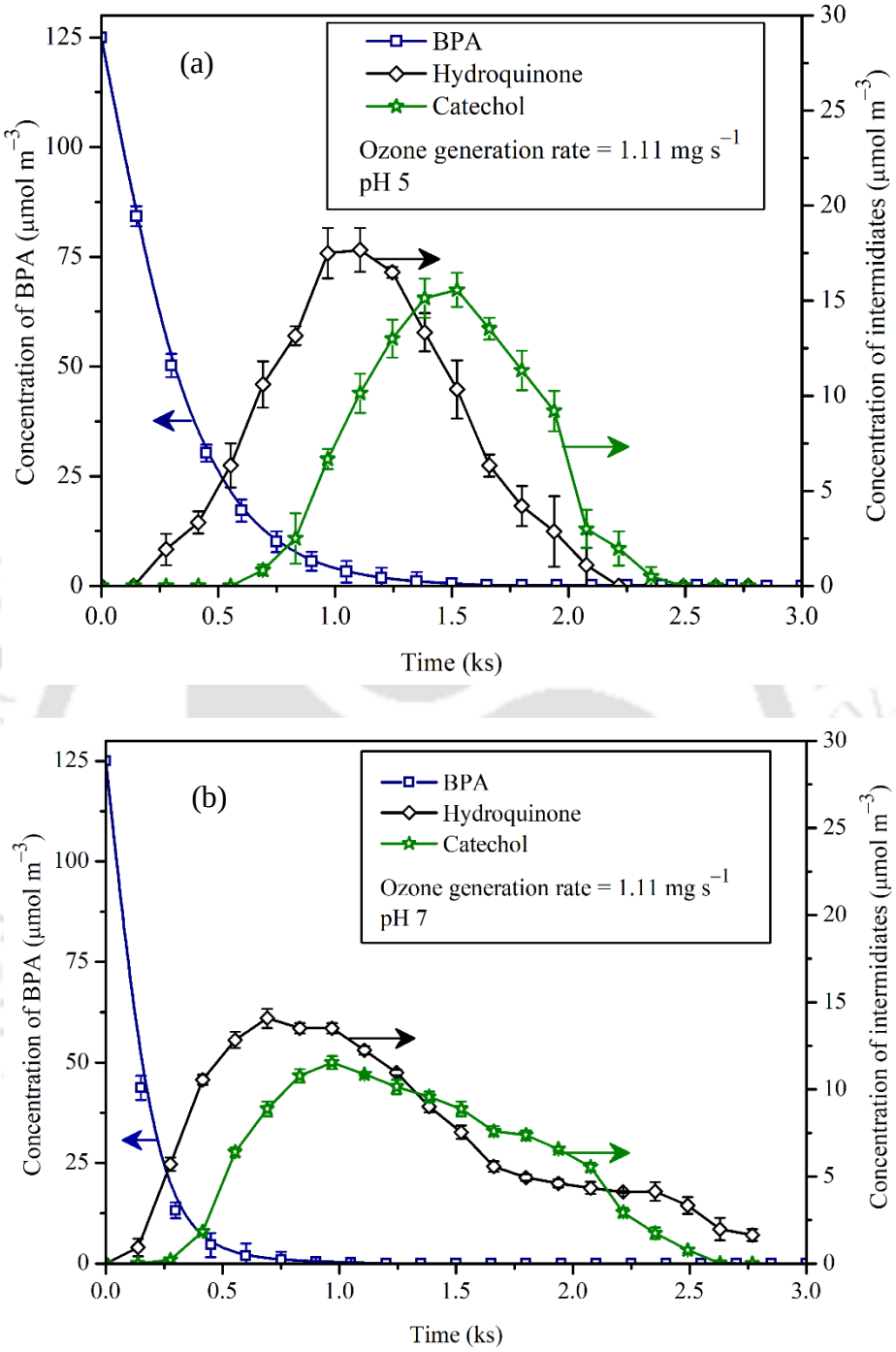

Figure 5.7: Formation and depletion of catechol and hydroquinone during the oxidation of BPA by the OMBs at **(a)** pH 5 and **(b)** pH 7.

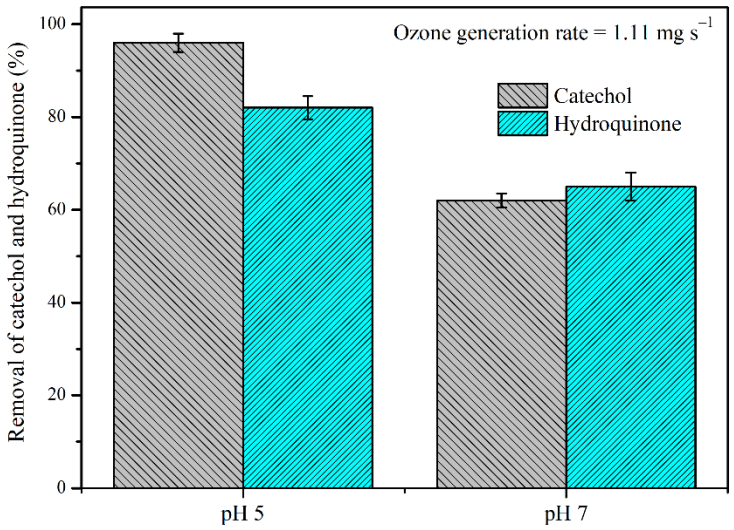

Figure 5.8: Effect of pH on the removal of catechol and hydroquinone by the OMBs at 1.8 ks of ozonation time. The initial concentration of both catechol and hydroquinone was 0.1 mol m^{-3}.

The results show that the value of $[O_3]_{CT}$ increased linearly with TOC removal until 80% of the TOC was removed, and then it increased almost exponentially, as shown in Figure 5.9. This overall increase of aqueous ozone contact time with TOC removal clearly illustrates that the oxidation intermediates of BPA, formed later during the reaction, may be resistant to ozonation.

The quantity, $[O_3]_{CT}/[TOC]_{removed}$ [given in Equation (5.9)] can be used to examine the relationship between $[O_3]_{CT}$ and TOC removal further. The results reveal an increase in $[O_3]_{CT}/[TOC]_{removed}$ with increasing TOC removal during the first 20% of the latter. Then it slightly decreased until 80% of the TOC was removed. Finally, its increase was linear for the final 20% of the TOC removal (Figure 5.9). This supports the findings

presented earlier in this section that at pH 7, the extent of mineralization of BPA was initially slow until 20% of the TOC was removed (i.e., for the first 0.6 ks of the ozonation time). Afterwards (i.e., in the range of 0.6 – 1.8 ks of the ozonation time), the extent of removal was very fast (i.e., 20 – 80% TOC removal), and finally, starting from 1.8 ks up to the rest of the ozonation time, it was hindered [Figure 5.6 (a)].

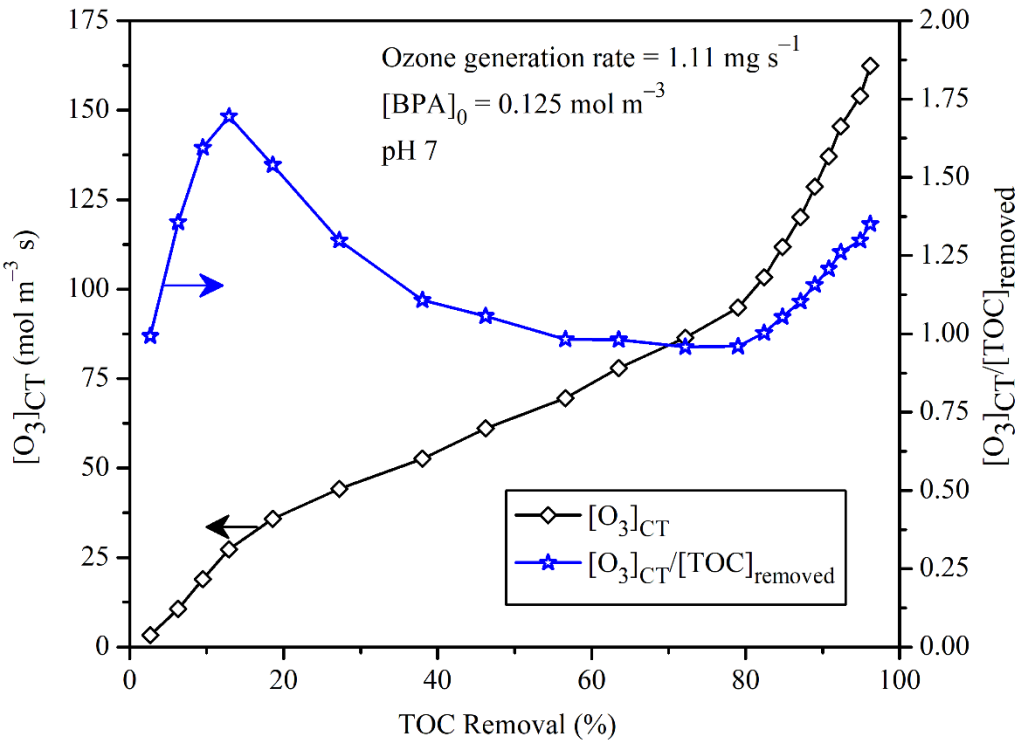

Figure 5.9: Variation of $[O_3]_{CT}$ and $[O_3]_{CT}/[TOC]_{removed}$ with TOC removal.

This indicates that during the slow period of TOC removal, more ozone was consumed by BPA and the oxidation intermediates formed at the early stages, which is reflected by the increase in the stoichiometric ratio, $[O_3]_{CT}/[TOC]_{removed}$. At 0.6 ks ozonation time, about 98% of the BPA was removed [Figure 5.1 (a)]. Therefore, the ozone was mainly consumed by the oxidation intermediates formed in the early stage. This caused

a decrease in the ratio in the middle of the ozonation. The increase in the stoichiometric ratio in the final stage could be due to the oxidation intermediates formed in the later stage of oxidation, which required more ozone for mineralization as compared to BPA and the oxidation intermediates formed in the early stage. This increase in the stoichiometric ratio in the final stage is in agreement with the work of Garoma et al. (2010).

5.2.3 Kinetics of BPA oxidation by the OMBs

It has been reported (Keykavoos et al., 2013; Rivas et al., 2009) that it is not proper to presume a single reaction rate constant during the oxidation of BPA inasmuch as the reaction between ozone and BPA has three main stages. These three stages are fast reaction with a very high reaction rate constant, fast reaction with an intermediate rate constant, and finally, slow reaction with a very low rate constant. Because of these three main stages of reaction, use of a single reaction rate constant is only an approximate way of analyzing the kinetics of the oxidation of BPA by the OMBs. Different kinetic approaches can be considered for each of these three reaction stages.

For the oxidation of BPA by the OMBs in our experimental setup, the complex reaction has been studied through two different approaches. The first approach was a model reaction based on the TOC removal, which included different species with different reactivities towards ozone. Three main stages during the oxidation of BPA were considered. In this approach, it was assumed that only molecular ozone and the hydroxyl radicals are the oxidizing species towards the organic compounds. In the second approach, ozone gradually dissolved in water and reacted with BPA. The effect of self-decomposition of ozone was not ignored, and the overall mass balance of ozone was considered. This is the process that

occurred in our OMB system. Note that, due to the complexity of the aqueous phase reaction, especially for the ozonation process, proposing a general mechanism is difficult. Nevertheless, for understanding the complex reactions during the oxidation of BPA, we have used the two above-mentioned approaches, which are described in Sections 5.2.3.1 and 5.2.3.2.

5.2.3.1 Kinetics based on TOC removal

Kinetic study based on the TOC removal has been considered rarely in ozone-based advanced oxidation of pollutants. Therefore, there are aspects, which have not been considered yet, and they need further attention concerning the TOC kinetics. Ozone self-decomposes in water producing many species such as hydrogen peroxide and hydroxyl radicals. In this kinetic study, a general term, TOC, is treated as a distinct compound. Accordingly, the TOC-content of the solution can undergo two different reactions paths, i.e., with the ozone molecule and the hydroxyl radical. Considering the second-order reaction rate, Equation (5.10) expresses the overall rate equation for the removal of TOC by the ozone molecule and the hydroxyl radical during the ozonation of BPA (Rivas et al., 2009).

$$\frac{\mathrm{d}[\mathrm{TOC}]}{\mathrm{d}t} = -k_{\mathrm{O_3}}[\mathrm{TOC}][\mathrm{O_3}] - k_{\bullet\mathrm{OH}}[\mathrm{TOC}][\bullet\mathrm{OH}] \qquad (5.10)$$

Based on the assumption that the hydroxyl radicals are mainly generated from the ozone decomposition, and their concentration is proportional to the concentration of dissolved ozone in the aqueous solution (Rivas et al., 2009), Equation (5.10) can be simplified to Equation (5.11).

$$-\frac{\mathrm{d[TOC]}}{\mathrm{d}t} = k_{\mathrm{obs}}[\mathrm{TOC}][\mathrm{O_3}] \tag{5.11}$$

where $k_{\mathrm{obs}} = k_{\mathrm{O_3}} + \beta k_{\bullet\mathrm{OH}}$ and $\beta = [\bullet\mathrm{OH}]/[\mathrm{O_3}]$. Integration of Equation (5.11) followed by rearrangement yields Equation (5.12).

$$\ln\left(\frac{[\mathrm{TOC}]_0}{[\mathrm{TOC}]}\right) = k_{\mathrm{obs}} \int_{t_0}^{t} [\mathrm{O_3}]\mathrm{d}t \tag{5.12}$$

Therefore, the observed reaction rate constant (i.e., k_{obs}) can be calculated from the slope of plot of $\ln([\mathrm{TOC}]_0/[\mathrm{TOC}])$ versus $\int_{t_0}^{t} [\mathrm{O_3}]\mathrm{d}t$. The latter was determined by following the procedure explained earlier in Section 5.2.1.4. From Figure 5.10, it is seen that there are three stages of reaction (i.e., from 0 – 0.6, 0.6 – 2.5, and 2.5–3.0 ks of ozonation).

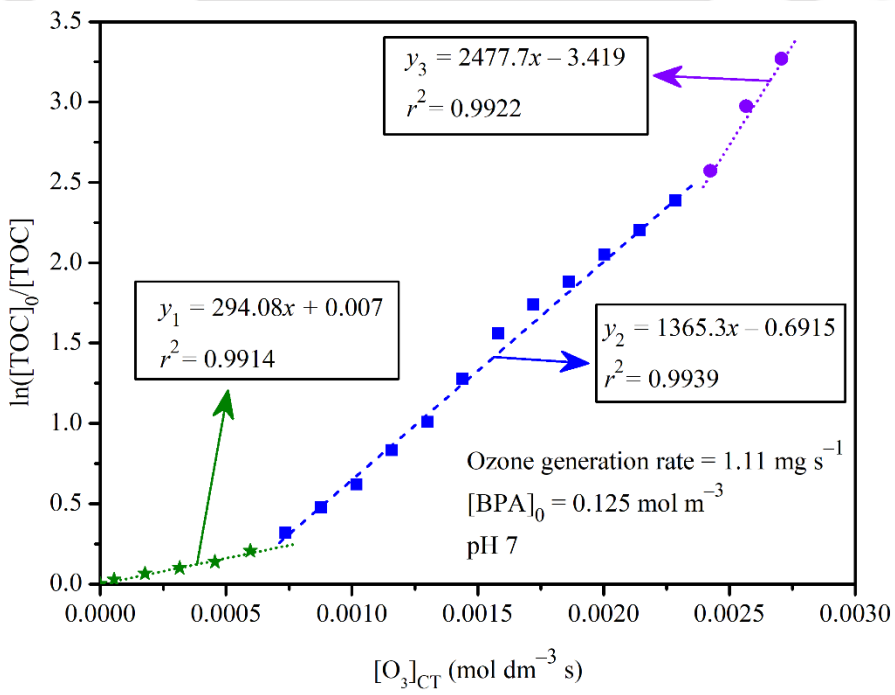

Figure 5.10: Determination of the rate constant for the oxidation of BPA by the OMBs based on the TOC removal.

The corresponding reaction rate constants are 294.1, 1365.3, and 2477.7 $dm^3\ mol^{-1}\ s^{-1}$, respectively. The observed rate constants can provide us a good indication about the kinetic regime during the TOC removal in different stages of the reaction between BPA and ozone. Using similar approaches for determining the kinetics of TOC removal in the non-catalytic ozonation of BPA, the values of the observed rate constant have been reported in the range of 0.7 – 35.6 $dm^3\ mol^{-1}\ s^{-1}$ (Keykavoos et al., 2013; Rivas et al., 2009). The values obtained in this work were fairly higher than these values.

5.2.3.2 Estimation of overall kinetic parameters of oxidation of BPA by ozone

In the batch reactor of our experimental setup, ozone was supplied continuously during the entire course of ozonation. It gradually dissolved in water and reacted with BPA. Equation (5.13) can express the kinetics of the reaction between BPA and ozone.

$$\frac{d[BPA]}{dt} = -k[BPA]^m [O_3]^n \qquad (5.13)$$

where k is the rate constant for the reaction of BPA with ozone, and m and n are the orders of reaction with respect to BPA and ozone, respectively. During the BPA oxidation by the OMBs in the aqueous medium, ozone directly and indirectly reacts with BPA, and simultaneously underwent self-decomposition. Thus, the overall mass balance of ozone [as shown in Equation (5.14)] comprises three terms, i.e., oxidation of BPA by the direct and indirect reactions with ozone, the rate of mass transfer of ozone from the gas to the liquid phase, and the first-order self-decomposition of ozone. The simplified form of this overall mass balance is given by

$$\frac{d[O_3]}{dt} = (k_L a + k_d)\left([O_3]_{ss} - [O_3]\right) - k[BPA]^m [O_3]^n \quad (5.14)$$

The simultaneous ODEs given by Equations (5.13) and (5.14) were solved by the Runge–Kutta method. The concentration profiles of BPA and ozone were fitted to the experimental data using Polymath® (version 6.10) to obtain the best-fit values of the kinetic parameters. The best-fit ($r^2 \geq 0.98$) values of the unknown kinetics parameters are given in Table 5.2. The values of k_d reported in Table 3.1 were used in these computations. The $k_L a$ slightly increased with the increasing $[BPA]_0$ and the pH of the solution. The overall reaction rate constant between BPA and ozone (i.e., *k*) slightly increased with the increasing pH. The oxidation of BPA by ozone followed a first-order with respect to both BPA and ozone, and an overall second-order kinetics. The value of *k* did not significantly vary with the $[BPA]_0$, which shows that it was a true rate constant. Figures 5.13 (a) and 5.13 (b) present the fit of the kinetic model to the concentration profiles of BPA and ozone in the reactor, respectively.

In fluid–fluid reactions, both the chemical reaction and rate of mass transfer are important. To distinguish the role of these terms, a dimensionless parameter called Hatta number (Ha), which indicates the relative importance of these terms in the gas–liquid system (Beltrán, 2004) was computed following the procedure given in Section 3.2.10. For the second-order reaction between BPA and ozone, it can be computed from Equation (5.15), given below.

$$Ha = \frac{\sqrt{k[BPA]_0 D_{O_3}}}{k_l} \quad (5.15)$$

The values of the diffusivity of ozone in water, D_{O_3}, (i.e., 1.89×10^{-9} m^2 s^{-1}) and the mass transfer coefficient, k_l, (i.e., 1.975×10^{-4} m s^{-1}) were calculated for our OMB system in Section 3.2.10. Using these data, Ha was computed from Equation (5.15) at different initial concentrations of BPA. These values and their corresponding values of *k* are reported in Table 5.2. From the experimental results given in Table 5.2, it can be seen that Ha was in the range of 0.01 to 0.54. This shows that the oxidation was in the intermediate reaction regime for the higher initial concentration of BPA (i.e., 0.125 and 0.250 mol m^{-3}), and slow reaction regime for the lower initial concentration of BPA (i.e., 0.008 mol m^{-3}), as per the classification of regimes given by Levenspiel (1999). The low values of Ha obtained in this work confirm that the mass transfer resistance, $(1/k_l)$, was negligible. This implies that the rate of mass transfer was enhanced by the OMBs, which demonstrates the efficiency of the OMB system used for the ozonation of BPA.

Table 5.2: Kinetic and mass transfer parameters (at the ozone generation rate of 1.11 mg s^{-1})

pH	$[BPA]_0$ (mol m^{-3})	$[O_3]_{ss}$ (mol m^{-3})	$(k_La + k_d)$ (s^{-1})	$k_d \times 10^3$ (s^{-1})	$k_La \times 10^2$ (s^{-1})	$k \times 10^{-3}$ [(mol $dm^{-3})^{1-m-n}$ s^{-1}]	m (–)	n (–)	r^2 (–)	Ha (–)
5	0.125	0.064	0.0315	0.12	3.138	0.136	1.0	1.3	0.991	0.029
7	0.008	0.133	0.0264	0.13	2.627	0.252	1.1	1.1	0.985	0.010
7	0.125	0.056	0.0374	0.13	3.727	0.247	1.2	0.9	0.999	0.039
7	0.250	0.042	0.0493	0.13	4.917	0.238	1.3	0.9	0.997	0.054
9	0.125	0.052	0.0461	0.15	4.595	0.412	1.1	0.9	0.986	0.050

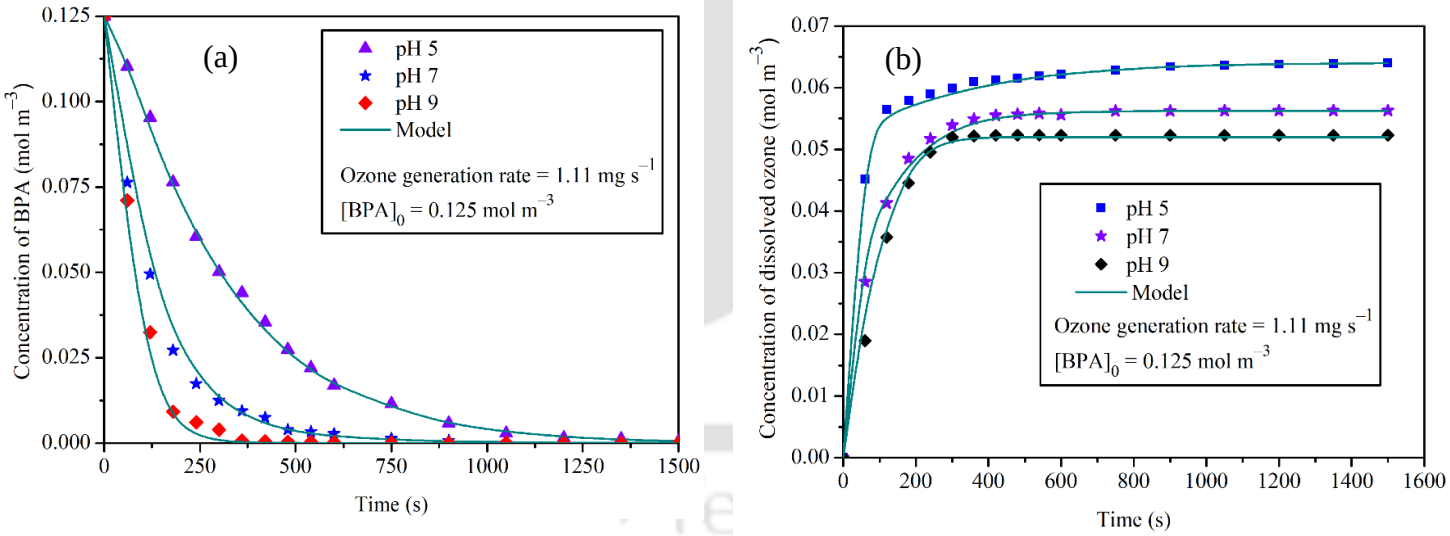

Figure 5.11: Concentration profiles of **(a)** BPA and **(b)** dissolved ozone in the reactor, and the fit of the model.

5.3 Conclusions

The following conclusions were reached based on the experimental studies and the analysis of the results.

- The removal efficiency of BPA by OMBs was improved from 41 to 98% within 600 s of ozonation as the initial pH was increased from 3 to 7. Further increase of pH did not show any significant improvement in the ozonation time (i.e., it did not significantly reduce the ozonation time to achieve the same removal efficiency).
- Addition of 0.5 mol m^{-3} *t*-BuOH hindered the removal of BPA in the pH range 3 to 11, which is an evidence that both the direct and indirect reactions between ozone and BPA took place. The effect of 0.5 mol m^{-3} *t*-BuOH was more pronounced in strongly acidic and alkaline solutions.
- The rate of ozone generation had a significant effect on BPA removal. Increase in the ozone generation rate from 0.56 to 1.94 mg s^{-1} significantly improved the removal of BPA from 47.2 to 99.6% within 600 s at pH 7 and 0.125 mol m^{-3} initial concentration of BPA. This was expected because an increase in the influent ozone generation rate increased the dissolved ozone concentration in the aqueous solution, which directly oxidized BPA and also decomposed to produce reactive hydroxyl radicals, which in turn, reacted with BPA and its oxidation intermediates.
- The stoichiometric ratio of the moles of ozone consumed for complete removal of BPA were determined as 0.228, 0.254, and 0.276 for the ozone generation rates of 0.56, 1.11, and 1.94 mg s^{-1}, respectively at pH 7 and 0.125 mol m^{-3} initial concentration of BPA. The rather small values of the stoichiometric ratios are possibly due to the high rate of mass transfer of ozone into the aqueous phase due to the microbubbles.

- A considerably high range of ozone utilization efficiency (i.e., 52.42 – 82.34%) for complete removal of BPA was achieved.
- Addition of sodium bicarbonate (at 10.0 mol m^{-3} concentration) was found to have an insignificant effect on BPA removal.
- The rate of TO C removal in the neutral and alkaline conditions was initially slow up to 0.6 ks ozonation time. After that, it was faster during 0.6 – 1.8 ks ozonation time. It did not change significantly afterwards. In contrary, at pH 5, the rate of TOC removal was very slow during the first 1.2 ks of ozonation, and then a considerable removal of TOC was observed, which ultimately led to its complete removal.
- The contact time of ozone in the aqueous phase increased linearly with TOC removal up to 80%. It then increased exponentially during the rest 20%. Likewise, the stoichiometric ratio of the aqueous ozone contact time per TOC removed increased during the first 20% of the TOC removal, and it slightly decreased until 80% TOC was removed. Finally, it increased linearly during the remaining 20% TOC removal. During the slow period of TOC removal, the increase in the stoichiometric ratio, $[O_3]_{CT}/[TOC]_{removed}$ reflects that more ozone was consumed by BPA and the oxidation intermediates formed at the early stages.
- Based on the TOC removal, three stages of reaction (i.e., from 0–0.6, 0.6–2.5, and 2.5–3.0 ks of ozonation) were observed, and their corresponding (observed) reaction rate constants were 294.1, 1365.3, and 2477.7 $dm^3\ mol^{-1}\ s^{-1}$, respectively.
- The volumetric mass transfer coefficient of ozone slightly increased with increasing initial concentration of BPA and pH of the solution. The overall reaction rate constant, *k*, slightly increased with increasing pH. The reaction between ozone and BPA followed an overall second-order kinetics, and first-order with respect to both ozone

and BPA. The overall reaction rate constant did not significantly vary with the initial concentration of BPA at pH 7, which indicates that it was a true rate constant.

- Very low values of the Hatta number (i.e., 0.01–0.054) showed that the reaction was in the intermediate and slow reaction regimes. This proves that the mass transfer resistance was negligible, which implying that the rate of mass transfer was enhanced by the OMBs.

Notations

a	specific gas–liquid interfacial area ($m^2\ m^{-3}$)
[BPA]	unreacted concentration of BPA at reaction time t (mol m^{-3})
$[BPA]_0$	initial concentration of BPA (mol m^{-3})
$[BPA]_{rem}$	number of moles of BPA removed within ozonation time t (mol)
D_{O_3}	diffusivity of ozone in water ($m^2\ s^{-1}$)
$\dot{G}_{O_3}$	ozone generation rate (g s^{-1})
Ha	Hatta number (–)
K	rate constant for the reaction of BPA with ozone [(mol $dm^{-3})^{1-m-n}\ s^{-1}$]
k'	pseudo-first-order rate constant for the reaction of BPA with ozone (s^{-1})
k_d	self-decomposition rate constant of ozone (s^{-1})
k_l	mass transfer coefficient (m s^{-1})
k_La	volumetric mass transfer coefficient of ozone in the reacting system (s^{-1})
$(k_La)_0$	volumetric mass transfer coefficient of ozone in the non-reacting system (s^{-1})
k_{obs}	observed reaction rate constant ($dm^3\ mol^{-1}\ s^{-1}$)
M	order of reaction with respect to BPA (–)
M	molecular mass of ozone (g mol^{-1})
N	order of reaction with respect to ozone (–)
[·OH]	concentration of hydroxyl radical in the solution at time t (mol m^{-3})
$[O_3]$	concentration of ozone during the reaction (mol m^{-3})
$[O_3]_\infty$	total influent concentration of ozone at ozonation time t (mol m^{-3})
$[O_3]^*$	saturation concentration of ozone in water (mol m^{-3})

$[O_3]_{abs}$	number of moles of ozone absorbed by the solution within ozonation time *t* (mol)
$[O_3]_{CT}$	ozone contact time (mol m^{-3} s)
$[O_3]_{exc}$	excess effluent ozone concentration at reaction time *t* (mol m^{-3})
$[O_3]_{res}$	residual dissolved ozone concentration in the solution at reaction time *t* (mol m^{-3})
$[O_3]_{ss}$	steady state concentration of ozone in the aqueous phase (mol m^{-3})
P	pressure (Pa)
R	correlation coefficient (–)
R	gas constant (J mol^{-1} K^{-1})
S_R	stoichiometric ratio (–)
T	ozonation time needed to reach the desired removal efficiency (s)
T	temperature (K)
[TOC]	concentration of total organic carbon at ozonation time *t* (mol dm^{-3})
$[TOC]_0$	initial total organic carbon (mol dm^{-3})
$[TOC]_{removed}$	total organic carbon removed within ozonation time *t* (mol dm^{-3})
$V_g^{O_3}$	volumetric flow rate of ozone (m^3 s^{-1})
V_r	total volume of the OMBs reactor (m^3)

Greek symbols

η_u	utilization efficiency of ozone
P	density of ozone (kg m^{-3})

Abbreviations

BPA	bisphenol-A
OMBs	ozone microbubbles
TOC	total organic carbon
UV	ultraviolet

References

Beltrán, F.J., **2004**. Ozone Reaction Kinetics for Water and Wastewater Systems, 1st ed. Lewis Publishers, Boca Raton (USA).

Buffle, M.O., Schumacher, J., Meylan, S., Jekel, M., von Gunten, U., **2006**. Ozonation and advanced oxidation of wastewater: Effect of O_3 dose, pH, DOM and HO•-scavengers on ozone decomposition and HO• generation. *Ozone Sci. Eng., 28*, 247–259.

Buxton, G.V., Elliot, A.J., **1986**. Rate constant for reaction of hydroxyl radicals with bicarbonate ions. *Int. J. Radiat. Appl. Instrum. C Radiat. Phys. Chem., 27*, 241–243.

Cope, V.W., Huffman, M.Z., Chen, S.N., **1978**. Reactivity of the carbonate radical toward metal complexes in aqueous solution. *J. Phys. Chem., 82*, 2665–2669.

Deborde, M., Rabouan, S., Mazellier, P., Duguet, J.-P., Legube, B., **2008**. Oxidation of bisphenol A by ozone in aqueous solution. *Water Res., 42*, 4299–4308.

Elovitz, M.S., von Gunten, U., Kaiser, H.-P., **2000**. Hydroxyl radical/ozone ratios during ozonation processes. II. The Effect of temperature, pH, alkalinity, and DOM properties. *Ozone Sci. Eng., 22*, 123–150.

Garoma, T., Matsumoto, S., **2009**. Ozonation of aqueous solution containing bisphenol A: effect of operational parameters. *J. Hazard. Mater., 167*, 1185–1191.

Garoma, T., Matsumoto, S.A., Wu, Y., Klinger, R., **2010**. Removal of bisphenol A and its reaction-intermediates from aqueous solution by ozonation. *Ozone Sci. Eng., 32*, 338–343.

Gözmen, B., Oturan, M.A., Oturan, N., Erbatur, O., **2003**. Indirect electrochemical treatment of bisphenol A in water via electrochemically generated Fenton's reagent. *Environ. Sci. Technol., 37*, 3716–3723.

Hoigné, J., Bader, H., **1983**. Rate constants of reactions of ozone with organic and inorganic compounds in water–I: non-dissociating organic compounds. *Water Res., 17*, 173–183.

Hoigné, J., Bader, H., Haag, W., Staehelin, J., **1985**. Rate constants of reactions of ozone with organic and inorganic compounds in water–III. Inorganic compounds and radicals. *Water Res., 19*, 993–1004.

Irmak, S., Erbatur, O., Akgerman, A., **2005**. Degradation of 17β-estradiol and bisphenol A in aqueous medium by using ozone and ozone/UV techniques. *J. Hazard. Mater.*, *126*, 54–62.

Keykavoos, R., Mankidy, R., Ma, H., Jones, P., Soltan, J., **2013**. Mineralization of bisphenol A by catalytic ozonation over alumina. *Sep. Purif. Technol.*, *107*, 310–317.

Kusvuran, E., Yildirim, D., **2013**. Degradation of bisphenol A by ozonation and determination of degradation intermediates by gas chromatography–mass spectrometry and liquid chromatography–mass spectrometry. *Chem. Eng. J.*, *220*, 6–14.

Lee, J., Park, H., Yoon, J., **2003**. Ozonation characteristics of bisphenol A in water. *Environ. Technol*, *24*, 241–248.

Levenspiel, O., **1999**. Chemical Reaction Engineering, 3rd ed. Wiley, New York (USA).

Li, P., Tsuge, H., Itoh, K., **2009**. Oxidation of dimethyl sulfoxide in aqueous solution using microbubbles. *Ind. Eng. Chem. Res.*, *48*, 8048–8053.

Liu, Z., Wardenier, N., Hosseinzadeh, S., Verheust, Y., De Buyck, P.-J., Chys, M., Nikiforov, A., Leys, C., Van Hulle, S., **2018**. Degradation of bisphenol A by combining ozone with UV and H_2O_2 in aqueous solutions: mechanism and optimization. *Clean Technol. Environ. Policy*, *20*, 2109–2118.

Mutseyekwa, M.E., Doğan, Ş., Pirgalıoğlu, S., **2017**. Ozonation for the removal of bisphenol A. *Water Sci. Technol.*, *76*, 2764–2775.

Pétrier, C., Torres-Palma, R., Combet, E., Sarantakos, G., Baup, S., Pulgarin, C., **2010**. Enhanced sonochemical degradation of bisphenol-A by bicarbonate ions. *Ultrason. Sonochem.*, *17*, 111–115.

Rivas, F.J., Encinas, Á., Acedo, B., Beltrán, F.J., **2009**. Mineralization of bisphenol A by advanced oxidation processes. *J. Chem. Technol. Biotechnol.*, *84*, 589–594.

Sotelo, J.L., Beltran, F.J., Benitez, F.J., Beltran-Heredia, J., **1987**. Ozone decomposition in water: kinetic study. *Ind. Eng. Chem. Res.*, *26*, 39–43.

Zhang, H., He, Y., Lai, L., Yao, G., Lai, B., **2020**. Catalytic ozonation of bisphenol A in aqueous solution by Fe_3O_4-MnO_2 magnetic composites: performance, transformation pathways and mechanism. *Sep. Purif. Technol.*, *245*, 116–449.

CHAPTER 6

A COMPARATIVE STUDY ON THE REMOVAL OF DIMETHYL SULFOXIDE FROM WATER USING MICROBUBBLES AND MILLIBUBBLES OF OZONE

In this chapter, the potential of the ozone microbubbles (OMBs) for the oxidation of dimethyl sulfoxide (DMSO) is investigated, and the results are compared with those of the conventional ozone millibubbles (OMLBs). Ozone utilization and the stoichiometric ratio of ozone consumed to DMSO removed were computed and compared. The effectiveness of OMBs and OMLBs in terms of the extent of mineralization of DMSO was investigated and compared. Formation and depletion of the two main oxidation intermediates of DMSO (i.e., $DMSO_2$ and MSA) were investigated for both OMBs and OMLBs. The overall kinetic parameters of the reaction between DMSO and ozone have been determined from the experimental results, and their values have been compared.

6.1 Introduction

Removal of DMSO by conventional wastewater treatment techniques is not practicable due to the generation of volatile and noxious intermediate gases, as discussed in Section 1.6.3. In recent times, ozone-based microbubble-aided technology has attracted much attention as a new potential candidate for effective oxidation of DMSO in water/wastewater without producing noxious intermediate gases. The aim of the present work was to investigate the potential of the OMBs for the oxidation of DMSO in detail, and compare the results with those of the conventional ozonation process using

millibubbles (i.e., OMLBs). The main operational parameters that influence the removal of DMSO have been studied. In addition, the contribution of ·OH to the removal of DMSO has been investigated for both OMBs and OMLBs. Ozone utilization and the stoichiometric ratio of ozone consumed to DMSO removed were computed and compared. Formation and depletion of the two main oxidation intermediates of DMSO (i.e., $DMSO_2$ and MSA) were investigated for both OMBs and OMLBs. The overall kinetic parameters of the reaction between DMSO and ozone and their variation with the pH of the medium have been determined from the experimental results, and the results have been compared.

6.2 Results and discussion

6.2.1 Determinations of stoichiometric ratio and ozone utilization efficiency

Ozone consumption and ozone utilization efficiency are the vital parameters for evaluating the oxidation performance of the ozone-based AOPs. These parameters need to be determined and optimized for high ozone utilization, that would involve high mass transfer of ozone and a large amount of generation of ·OH. From the mass balance, the amount of ozone absorbed during ozonation, which refers to the total ozone transferred to the aqueous solution per unit reactor volume, can be determined from Equation (6.1) (Marce et al., 2016).

$$[O_3]_{abs} = \int_0^{t_d} \left(\frac{V_g^{O_3}}{V_r} \right) \{ [O_3]_{\infty} - ([O_3]_{eff} + [O_3]_{res}) \} dt \qquad (6.1)$$

where $[O_3]_{\infty}$, $[O_3]_{abs}$, $[O_3]_{eff}$, and $[O_3]_{res}$ are the total influent concentration of ozone, the number of moles of ozone absorbed by the solution, the excess effluent ozone

concentration, and the concentration of dissolved ozone remaining in the solution at the desired ozonation time, t_d (all expressed in mol m^{-3}), respectively. $V_g^{O_3}$ is the volumetric flow rate of ozone (m^3 s^{-1}), and V_r is the total volume of the reactors (m^3). In our experimental setup, all parameters in the integral of Equation (6.1) can be directly determined at the desired ozonation time (t_d). Accordingly, Equation (6.1) can be integrated, and $[O_3]_{abs}$ can be computed from Equation (6.2) (Garoma and Matsumoto, 2009).

$$[O_3]_{abs} = \frac{\{[O_3]_{\infty} - ([O_3]_{eff} + [O_3]_{res})\}\left(V_g^{O_3}\right)t_d}{V_r} \tag{6.2}$$

In both the experimental setups for the OMBs and OMLBs, $[O_3]_{\infty}$ and $V_g^{O_3}$ can be computed from Equation (5.2) and Equation (5.3), respectively (Section 5.2.1.2). The stoichiometric ratio of the moles of ozone consumed per mole of DMSO removed during the reaction can be presented as a function of the DMSO removed at the desired ozonation time. The stoichiometric ratio (S_R) at t_d was computed by using Equation (6.3).

$$S_R = \frac{[O_3]_{abs}}{[DMSO]_{rem}} \tag{6.3}$$

$$[DMSO]_{rem} = [DMSO]_0 - [DMSO] \tag{6.4}$$

where $[DMSO]$, $[DMSO]_0$, and $[DMSO]_{rem}$ are the remaining unreacted concentration of DMSO at t_d, the initial concentration of DMSO, and the number of moles of DMSO removed within t_d (all expressed in mol m^{-3}), respectively. For both OMBs and OMLBs, Equation (6.3) computes the stoichiometric ratio for the complete removal of DMSO at different pH of the medium, and the values are given in Tables 6.1 and 6.2, respectively.

Table 6.1: Summary of the stoichiometric ratios and ozone utilization efficiencies at different pH and initial concentrations of DMSO for the OMBs (at the ozone generation rate of 1.67 mg s^{-1})

pH	$[DMSO]_0$ (mol m^{-3})	Time* (s)	$[O_3]_\infty$ (mol m^{-3})	$[O_3]_{exc}$ (mol m^{-3})	$[O_3]_{res}$ (mol m^{-3})	$[O_3]_{abs}$ (mol m^{-3})	S_R (–)	η_u (%)
5	1.5	1200	2.27	0.49	0.119	1.661	0.056	73.2
7	1.5	1200	2.27	0.56	0.086	1.624	0.055	71.5
9	1.5	1080	2.04	0.37	0.069	1.601	0.049	78.5
7	0.5	720	1.36	0.34	0.124	0.896	0.055	65.9
7	2.5	1800	3.40	0.67	0.041	2.689	0.082	79.1

*Ozonation time required for the complete removal of DMSO

Table 6.2: Summary of the stoichiometric ratios and ozone utilization efficiencies at different pH and initial concentrations of DMSO for the OMLBs (at the ozone generation rate of 1.67 mg s^{-1})

pH	$[DMSO]_0$ (mol m^{-3})	Time* (s)	$[O_3]_\infty$ (mol m^{-3})	$[O_3]_{exc}$ (mol m^{-3})	$[O_3]_{res}$ (mol m^{-3})	$[O_3]_{abs}$ (mol m^{-3})	S_R (–)	η_u (%)
5	1.5	6480	12.26	8.7	0.026	3.534	0.648	28.8
7	1.5	4680	8.85	5.2	0.019	3.631	0.481	41.0
9	1.5	3600	6.81	3.5	0.015	3.295	0.335	48.4
7	0.5	3240	6.13	4.4	0.024	1.706	0.469	27.8
7	2.5	7200	13.62	7.2	0.008	6.374	0.779	46.8

*Ozonation time required for the complete removal of DMSO

For 1.5 mol m^{-3} initial concentration of DMSO, the values of S_R were 0.056, 0.055, and 0.049, at pH 5, 7, and 9, respectively for the OMBs. On the other hand, the corresponding values of S_R for the OMLBs were 0.648, 0.481, and 0.335 at the same

initial concentration of DMSO. From these results, it is apparent that the ozone consumption was ten times lower for the OMBs. The higher values of S_R for the OMLBs could be due to the long ozonation time required to achieve complete removal of DMSO. In such extended ozonation processes, ozone may be consumed by the oxidation intermediates of DMSO, resulting in a higher value of S_R. For the OMBs, the ozonation time required for the complete removal of DMSO was in the range of 0.72 – 1.8 ks, whereas the same was in the range of 3.24 – 7.2 ks for the OMLBs. The OMBs enhanced the mass transfer of ozone. Since the oxidation of DMSO took place in the aqueous phase, a higher concentration of ozone facilitated the oxidation of DMSO. Therefore, the OMBs played a significant role in lowering the value of S_R.

The effectiveness of both processes was further investigated by determining the utilization efficiency of ozone (η_u) from Equation (5.4), based on the mass balance of ozone in the gas and liquid phases. The values of η_u are summarized in Tables 6.1 and 6.2. The range of ozone utilization efficiency for complete removal of DMSO by the OMBs (i.e., 65.9 – 79.1%) is substantially higher than that for the OMLBs (i.e., 27.8–48.4%). From these results, it is clear that the OMBs considerably improved the utilization of ozone by enhancing its mass transfer in the aqueous solution and forming the highly reactive hydroxyl radicals. The values of the ozone utilization efficiency obtained in this work for the OMBs are in accordance with those reported by Li et al. (2009). As the microbubbles enhanced mass transfer more than that by the millibubbles, the OMB process is anticipated to improve the oxidation of DMSO and its intermediates. At the same time, the amount of ozone required for oxidation and the loss of ozone could be reduced significantly by the OMBs.

6.2.2 Effects of the initial concentration of DMSO and ozone generation rate on the removal of DMSO

Both the initial concentration of DMSO and ozone generation rate (which is equivalent to the concentration of ozone in the feed gas) had a significant effect on the removal of DMSO by the OMBs and OMLBs. It is observed from Figure 6.1 that increase in the initial concentration of DMSO from 0.5 to 2.5 mol m^{-3} had an adverse effect on its removal by both the OMBs and OMLBs. Therefore, it is apparent that the concentration of the intermediates increased with the increasing concentration of DMSO, which resulted in a higher consumption of the ozone present in the aqueous medium (as shown in Tables 6.1 and 6.2), as well as the ·OH. Consequently, this slowed the rate of removal of DMSO.

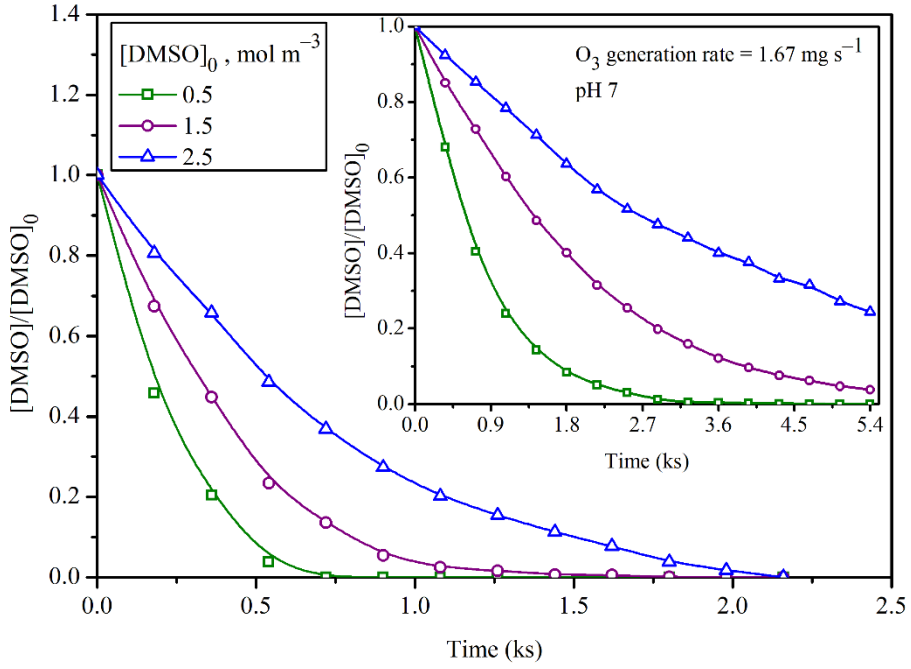

Figure 6.1: Effect of initial concentration of DMSO on its removal by the OMBs and OMLBs (inset).

At pH 7 and ozone generation rate of 1.67 mg s^{-1}, when the initial concentration of DMSO increased from 0.5 to 2.5 mol m^{-3}, the stoichiometric ratio of moles of ozone

consumed to DMSO removed increased from 0.055 to 0.082 for the OMBs, and from 0.469 to 0.779 for the OMLBs, (see Tables 6.1 and 6.2). Nevertheless, as the initial concentration of DMSO increased, the utilization efficiency of ozone was improved for both the OMB and OMLB processes. On the other hand, increase in the ozone generation rate from 0.56 to 2.78 mg s^{-1} profoundly improved the oxidation of DMSO for both the OMBs and OMLBs (Figure 6.2). This is expected because an increase in the ozone generation rate increased the dissolved ozone concentration in the aqueous medium, which either directly oxidized the DMSO or produced the ·OH, which reacted with DMSO and the intermediates produced during the course of ozonation.

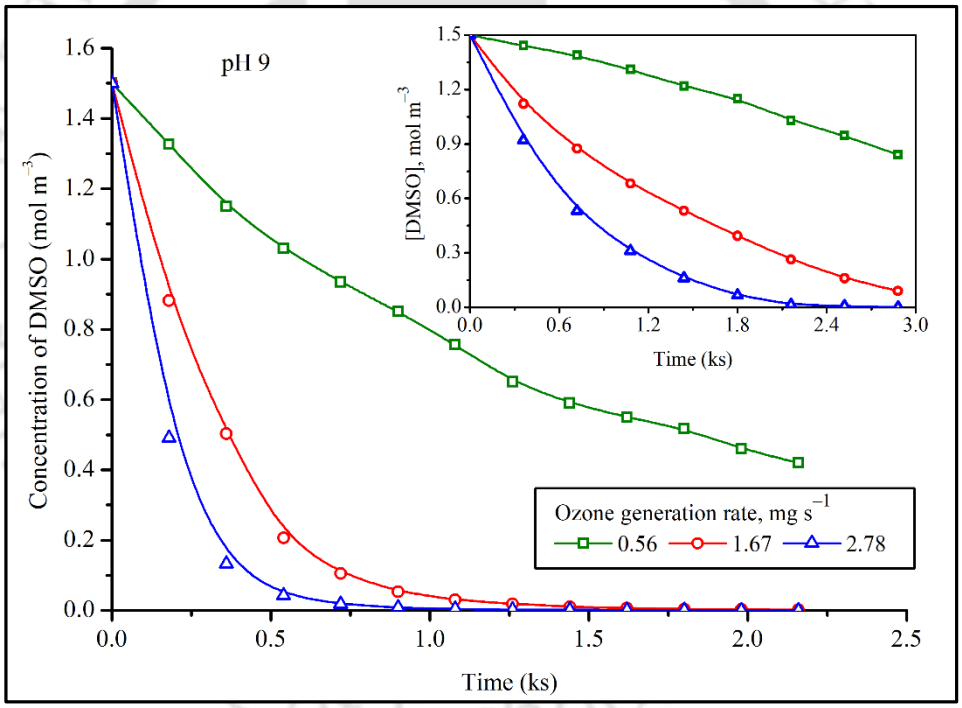

Figure 6.2: Effect of ozone generation rate on the removal of DMSO by the OMBs and OMLBs (inset).

6.2.3 Effects of the pH of the medium and reactions with the hydroxyl radicals

Experiments were conducted with both the OMBs and OMLBs at the ozone generation rate of 1.67 mg s^{-1} and 1.5 mol m^{-3} initial concentration of DMSO in the pH range of 5 to 9. From Figure 6.3 (a), it is observed that the variation in the pH had a rather trivial

effect on the oxidation of DMSO by the OMBs. Slight improvements were observed at pH 5 and 9 as compared to pH 7. The removal of DMSO was slightly increased with the pH of the solution for the OMLBs. The decrease in the pH of the medium during the course of ozonation, as shown in Figure 6.3 (b), could be due to the formation of acidic intermediates. The decrease in the pH of the solutions was more pronounced for the OMLB process.

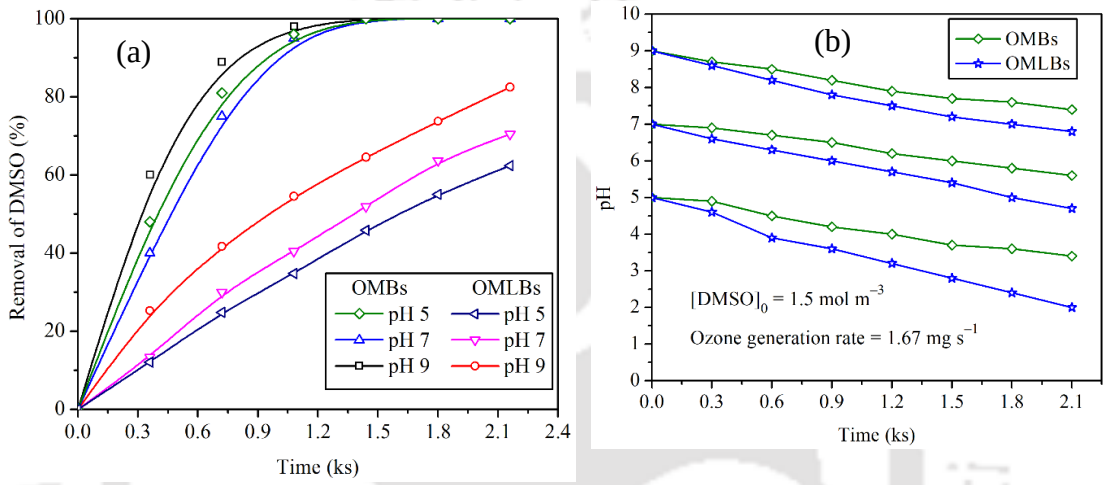

Figure 6.3: (a) Effect of pH of the medium and **(b)** variation of pH during the course of ozonation.

To examine the effect of the indirect oxidation of DMSO by the ·OH, experiments were conducted by using H_2O_2, which is a promoter for this reaction. Experiments were also conducted with *t*-BuOH, which is a scavenger of the ·OH. For oxidation of DMSO by the OMBs, the optimal ratio of $[H_2O_2]/[DMSO]_0$ was 1.0:1.3. The removal efficiency did not change if the H_2O_2 concentration was lower, but it decreased if the concentration was higher [Figure 6.4 (a)]. These observations signify that the contribution of ·OH from H_2O_2 was insignificant as compared to the existing concentration of ·OH in the aqueous medium when the concentration of H_2O_2 was low. On the other hand, when the latter was

high, the available ·OH was consumed by the reaction with H_2O_2 itself (Koito et al., 1998). This result is in agreement with the previous works (Koito et al., 1998), and corroborate our work on the removal of DEP and DMP by the OMBs reported in Sections 3.2.6 and 4.2.7, respectively.

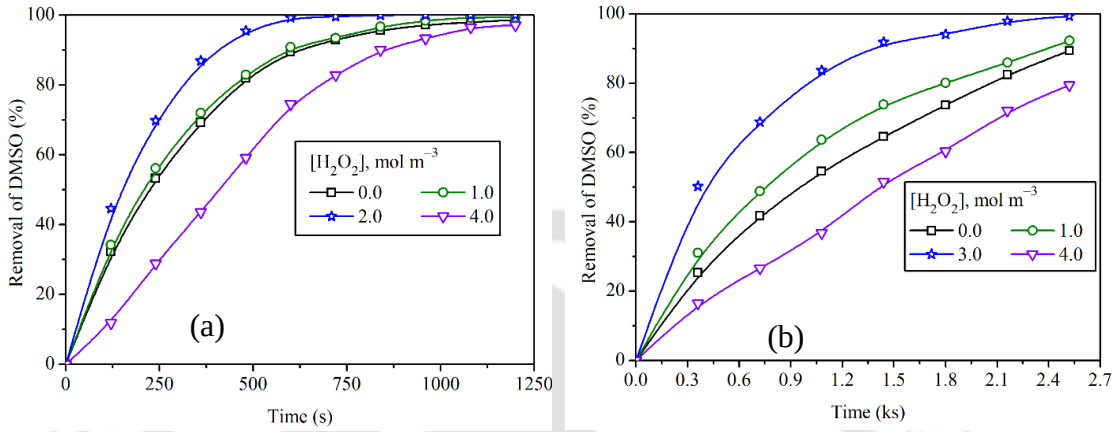

Figure 6.4: Effects of H_2O_2 on the removal of DMSO by the **(a)** OMBs and **(b)** OMLBs (at $[DMSO]_0$ = 1.5 mol m^{-3}, ozone generation rate =1.67 mg s^{-1}, and pH 9).

For the OMLBs, the $[H_2O_2]/[DMSO]_0$ ratio was 1:2. A similar trend was observed for the high concentration of H_2O_2 [Figure 6.4 (b)]. However, a low concentration of H_2O_2 had also shown a positive effect on the removal of DMSO. Therefore, for 1.5 mol m^{-3} DMSO, a dosage of 0 – 3 mol m^{-3} H_2O_2 had a positive effect on the removal of DMSO for the OMLB system. Further increase of the dosage of H_2O_2 had a negative effect on the oxidation efficiency of DMSO, similar to that observed for the OMBs. Figure 6.5 depicts the contribution of ·OH on the oxidation of DMSO and its reaction intermediates by both OMBs and OMLBs at pH 5 and 9. From Figure 6.5 (a), it can be observed that the contribution of ·OH was significant at pH 5 and 9 for the OMBs. However, for the OMLBs, no significant effect was observed at pH 5, while some effect was observed at pH 9. The significant and insignificant effects of ·OH at pH 5 for the

OMBs and OMLBs, respectively, imply that the formation of ·OH was enhanced by the microbubbles, and hardly any ·OH was generated by the OMLBs at this pH.

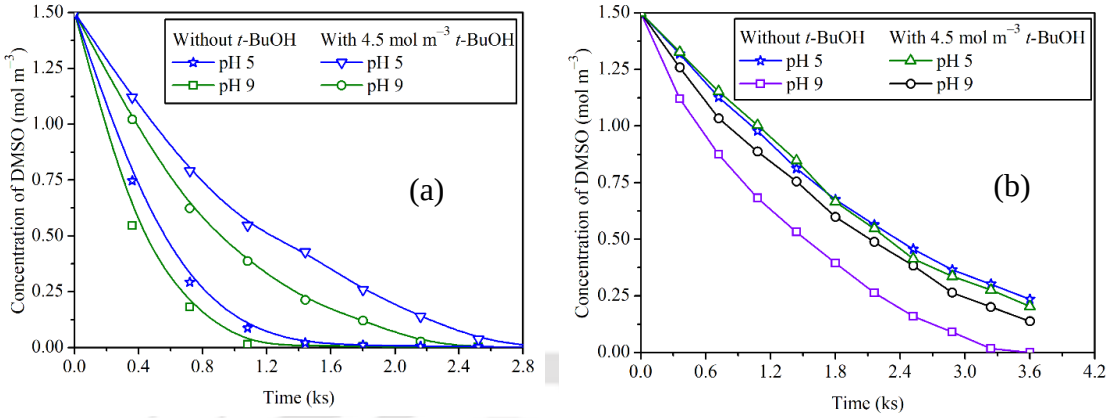

Figure 6.5: Effect of addition of *t*-BuOH on the oxidation of DMSO by the **(a)** OMBs and **(b)** OMLBs (at $[DMSO]_0 = 1.5$ mol m^{-3} and ozone generation rate =1.67 mg s^{-1}).

6.2.4 Formation and depletion of the oxidation intermediates of DMSO

It has been reported that DMSO is oxidized promptly by chemical oxidation (such as the AOPs), and becomes dimethyl sulfone [$DMSO_2$, i.e., $(CH_3)_2 SO_2$], as shown by Equation (6.5) (Baldoni-Andrey et al., 2005; Koito et al., 1998). In this oxidation process, no noxious compound is generated. Nevertheless, an additional method is needed to oxidize the $DMSO_2$ further, due to its stability against chemical oxidation. This was discussed in Section 1.6.3.

$$CH_3–SO–CH_3 \xrightarrow{[O]} CH_3–SO_2–CH_3 \qquad (6.5)$$

In this work, the formation and decay of the two major oxidative intermediates of DMSO were monitored for the experimental condition of $[DMSO]_0 = 1.5$ mol m^{-3}, ozone generation rate =1.67 mg s^{-1}, and pH 9. It was observed that $DMSO_2$ was formed during both the processes (Figure 6.6). Nevertheless, the concentration of $DMSO_2$ formed by the

OMBs was very less, and it started depleting after reaching the peak concentration at about 1.8 ks of ozonation time. In contrary to this, for the OMLBs, $DMSO_2$ started forming late, i.e., after 1.2 ks of ozonation time, and its concentration went on increasing for more than 5.4 ks of ozonation time. Besides, the simultaneous formation of MSA was observed for the OMBs after about 600 s of ozonation time, which went on increasing until the formation of $DMSO_2$ reached its maximum, and then its concentration started depleting slowly. This shows that MSA was more resistant to the OMBs, and needed a longer reaction time to be removed totally. It has been reported (Koito et al., 1998; Scaduto, 1995) that DMSO could be directly decomposed to MSA by the ·OH in AOPs where oxidation mainly takes place through the reaction with the ·OH, and the MSA could be further degraded easily by the conventional biological treatment without generating any harmful reaction intermediate.

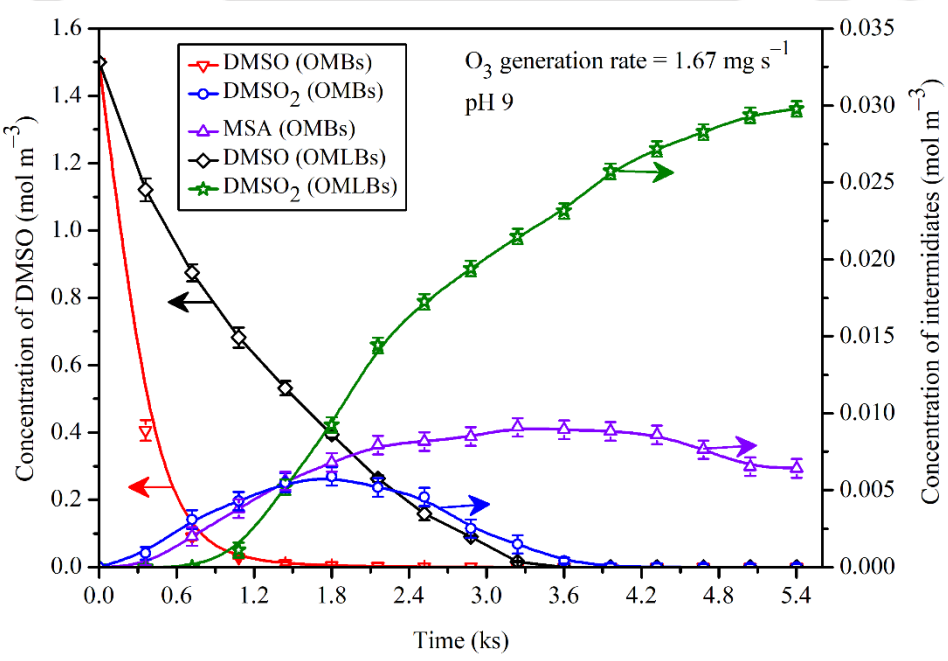

Figure 6.6: Comparison of reactions taking place in the OMB and OMLB systems in terms of formation and depletion of the two main oxidation intermediates of DMSO (i.e., $DMSO_2$ and MSA).

For the OMLBs, formation of MSA was not detected. The proposed oxidation mechanism in the OMLB system is shown in Figure 6.7 (b). This route (i.e., the oxidation of DMSO by conventional ozonation), is in agreement with the work of Chou and Chang (2007) and Equation (6.5). From our experimental results, it is evident that the MSA was formed through two paths in the OMB system [Figure 6.7 (a)]. The first path is the prompt conversion of DMSO to MSA by the reaction with ·OH without formation of the intermediate, $DMSO_2$. The other path is via the formation of $DMSO_2$ by the oxidation of DMSO by molecular ozone, followed by further oxidation of $DMSO_2$ to MSA by the ·OH present in the solution.

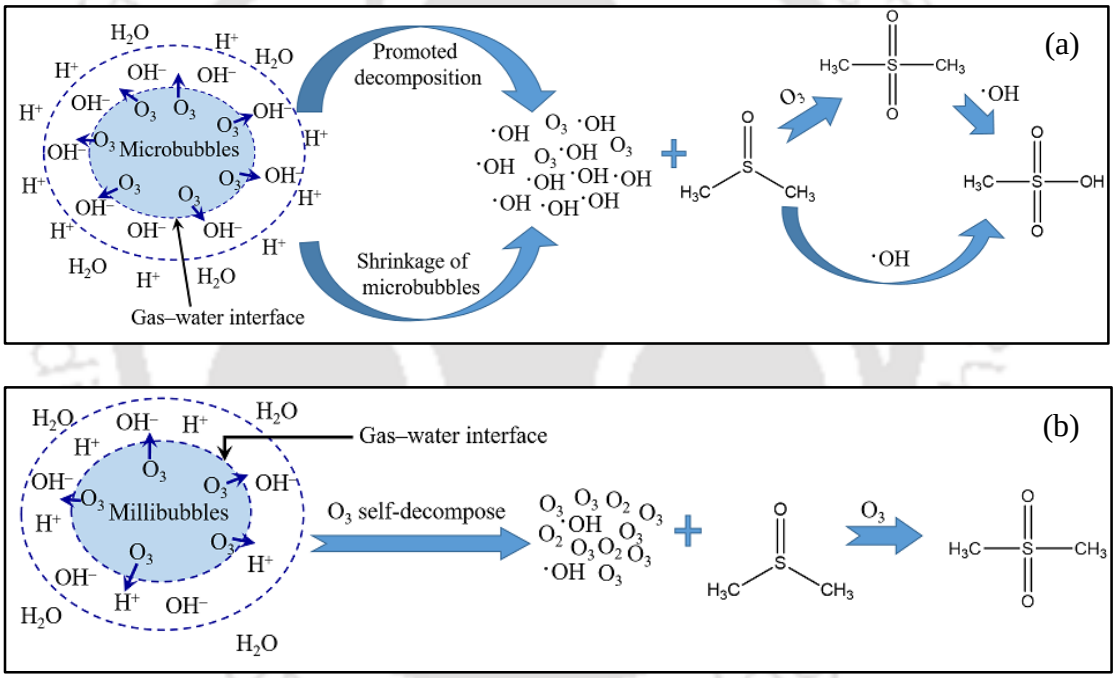

Figure 6.7: Proposed mechanisms of DMSO degradation by **(a)** OMBs and **(b)** OMLBs.

As shown in Figure 6.7 (a), microbubbles promoted the self-decomposition of ozone to the ·OH due to their negative surface charge (as a result of the hydroxyl ions accumulating at the microbubble surface), which promoted the self-decomposition of

ozone and formed the ·OH (Liu et al., 2020). Besides, ·OH were also generated by the self-shrinkage and collapse of the microbubbles (Chu et al., 2008b; Khuntia et al., 2012a). The path of self-decomposition of ozone in the millibubble system is different from that of the microbubble system. Due to the instability of ozone, it quickly decomposed to oxygen, and a small amount of ·OH was formed when the solution was highly alkaline. The amount of ·OH formed was less for the millibubble system.

6.2.5 Extent of mineralization of DMSO by the OMBs and OMLBs

In order to assess the efficiency of the OMBs and OMLBs towards the degradation of DMSO and their respective extents of mineralization, the ozonation was studied at different pH of the aqueous solution. Figure 6.8 (a) depicts the TOC removal profiles by both ozonation processes as a function of ozonation time at different pH of the medium. For OMBs, it was observed that the TOC removal was slightly more favorable at pH 5 as compared to pH 7 and 9 [Figure 6.8 (a)]. This can be attributed to the favorable oxidation of the intermediates in the acidic medium. This possibility was checked by separately carrying out the oxidation of $DMSO_2$ in water by the OMBs at pH 5 and 9. Figure 6.8 (b) depicts that the oxidation of $DMSO_2$ was slightly more favored at pH 5 than at pH 9. Moreover, a huge difference between the removal rates of DMSO and its corresponding TOC were observed, particularly for the OMLBs. For the OMLBs, after 2.16 ks of ozonation, the removal of DMSO was 62.5, 70.4, and 78.4% at pH 5, 7, and 10, respectively, and the corresponding TOC removal were 1.9, 5.5, and 8.9% [Figure 6.8 (c)]. The better DMSO removal efficiencies as compared to the corresponding TOC removal at all pH show that the oxidation of DMSO could be achieved via the direct oxidation by the ozone molecules. In contrast, TOC reduction (i.e., further oxidation of the reaction intermediates) was mainly achieved through the indirect oxidation by the

·OH. The low TOC reduction at all pH suggests that the available concentration of the ·OH was not enough to degrade the intermediates produced during the ozonation of DMSO.

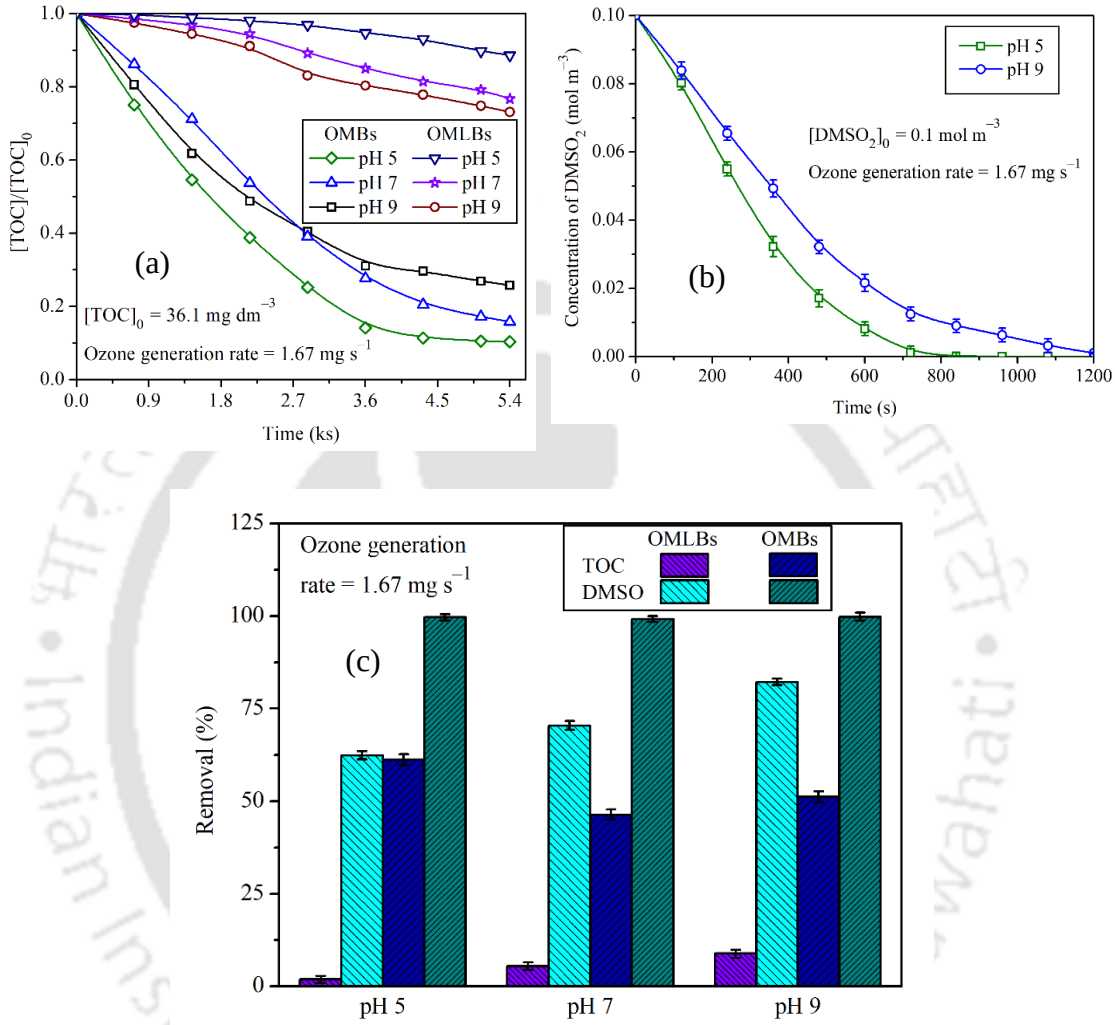

Figure 6.8: (a) TOC removal profiles at different pH, **(b)** oxidation of $DMSO_2$ in water by the OMBs, and **(c)** comparison of the OMB and OMLB processes in terms of DMSO and TOC removal efficiencies at 2.16 ks of ozonation time.

The overall removal efficiency of DMSO in the alkaline solution was better than that in the acidic solution for the OMLBs. These results corroborate the literature (Wu et al., 2007). For conventional ozonation, the direct reaction by molecular ozone was

predominant in the acidic medium, whereas indirect oxidation by ·OH was predominant in the alkaline medium (Glaze and Kang, 1989).

Furthermore, the contribution of ·OH on the TOC removal was further investigated by using a promoter (H_2O_2) and an inhibitor (*t*-BuOH) of the ·OH. Coupling H_2O_2 with both the ozonation systems (i.e., OMBs and OMLBs) had a significant effect on the TOC reduction by augmenting the generation of ·OH. However, the impact was more pronounced for the OMLBs [Figure 6.9 (a)]. The addition of the ·OH scavenger (i.e., *t*-BuOH) also proved that the indirect reaction was the main pathway for the mineralization of DMSO and its oxidative intermediates [Figure 6.9 (b)].

The effectiveness of the four processes (i.e., sole OMLBs, OMLBs coupled with H_2O_2, sole OMBs, and OMBs coupled with H_2O_2) was compared in terms of the DMSO removal and the extent of mineralization. Longer ozonation time (i.e., 5.4 ks) was considered for comparison. At this extended ozonation time, all four processes were equally effective for the complete removal of DMSO. Nevertheless, a wide variation was observed in terms of the TOC removal [Figure 6.9 (c)]. The sole-OMLBs-process exhibited a very poor efficiency for TOC removal, whereas the sole-OMB-process was more effective for TOC removal than the OMLB/H_2O_2 process.

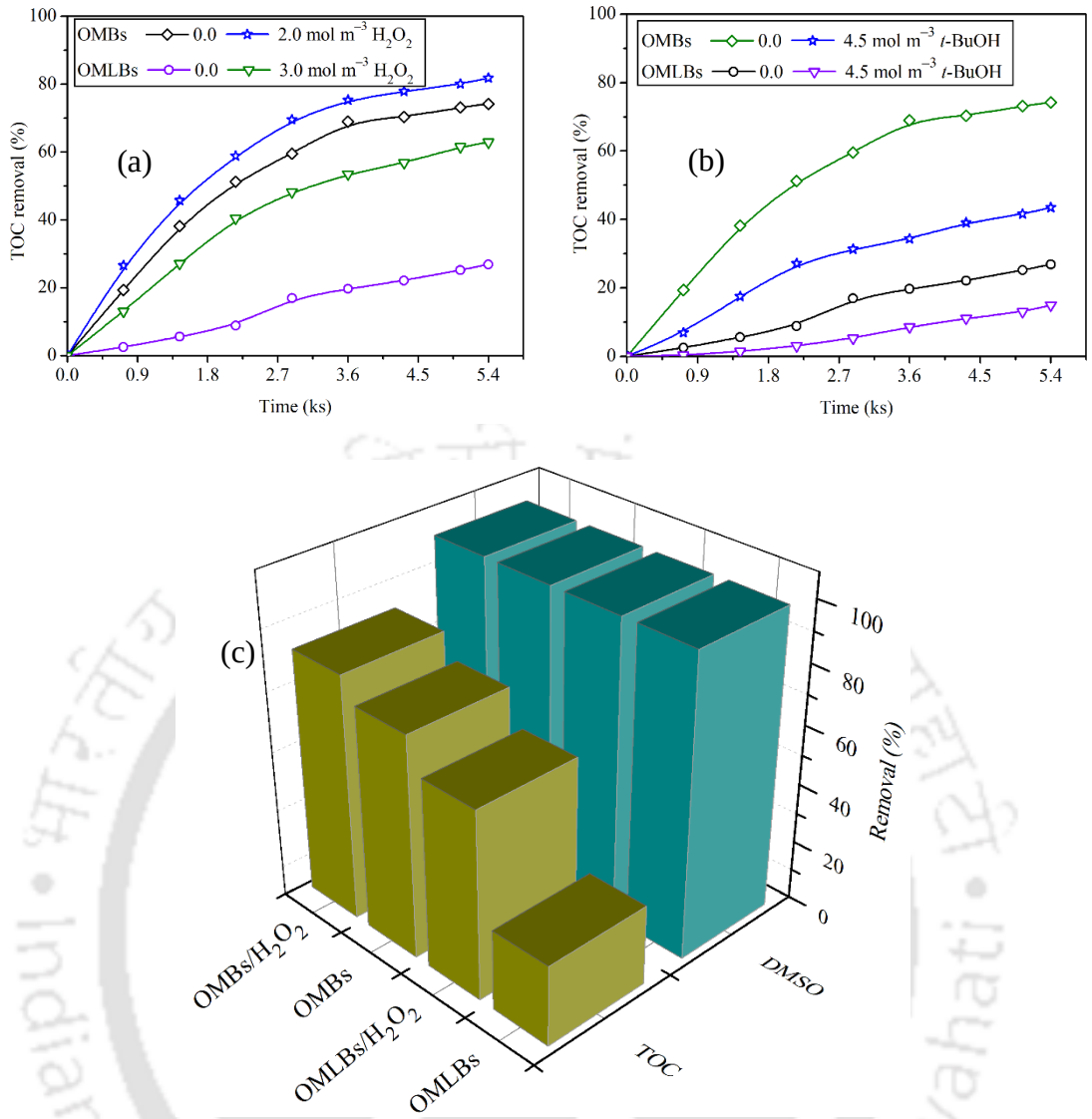

Figure 6.9: Effects of addition of **(a)** H_2O_2 and **(b)** *t*-BuOH on the TOC removal by the OMBs and OMLBs, and **(c)** the comparison of four processes in terms of the removal of DMSO and TOC at 5.4 ks of ozonation time (at the ozone generation rate of 1.67 mg s^{-1}, pH 9, and $[DMSO]_0$ = 1.5 mol m^{-3}).

6.2.6 Overall kinetics for the oxidation of DMSO by the OMBs

For the experimental setup using OMBs, the kinetic parameters of the overall reaction between DMSO and ozone were determined from the experimental results by using a mass balance. In the batch reactor of our experimental setup, ozone was supplied

continuously during the entire ozonation. It gradually dissolved in water and reacted with DMSO. Equation (6.6) can expresses the kinetics of the reaction between DMSO and ozone.

$$\frac{\mathrm{d[DMSO]}}{\mathrm{d}t} = -k[\mathrm{DMSO}]^m [\mathrm{O_3}]^n \tag{6.6}$$

During the oxidation of DMSO by the OMBs, the overall mass balance of ozone contains three terms, i.e., the rate of reaction of DMSO with ozone (directly and indirectly), the rate of mass transfer of ozone from the gas to the liquid phase, and the first-order self-decomposition of ozone. In such a system, where ozone gradually dissolves in the aqueous solution, simultaneously undergoes self-decomposition, and reacts with DMSO, Equation (6.7) gives the general mass balance.

$$\frac{\mathrm{d}[\mathrm{O_3}]}{\mathrm{d}t} = (k_L a + k_d)\left([\mathrm{O_3}]_{\mathrm{ss}} - [\mathrm{O_3}]\right) - k[\mathrm{DMSO}]^m [\mathrm{O_3}]^n \tag{6.7}$$

The two simultaneous ODEs [i.e., Equations (6.6) and (6.7)] were solved by the Runge–Kutta method using Polymath® (version 6.10). The best-fit values ($r^2 > 0.98$) of the kinetic parameters obtained by fitting the experimental data are presented in Table 6.3. The fit of the kinetic model to the concentration profiles of DMSO and ozone is shown in Figure 6.10 at different pH of the medium. The values of k_d used in these computations were taken from Table 3.1. The overall rate constant for the reaction of DMSO with ozone (k) increased with the pH of the medium to some extent. The oxidation of DMSO by ozone followed a first-order kinetics with respect to both DMSO and ozone, and an overall second-order kinetics (Table 6.3). The volumetric mass transfer coefficient of ozone $(k_L a)$ slightly increased in the acidic and alkaline solutions. The enhancement factor was

computed from the ratio of the volumetric mass transfer coefficients in the reacting and non-reacting systems (see Section 3.2.9).

Table 6.3: Kinetic and mass transfer parameters for the oxidation of DMSO by the OMBs (at the ozone generation rate of 1.67 mg s^{-1} and $[DMSO]_0$ = 1.5 mol m^{-3})

pH	$[O_3]_{ss}$ (mol m^{-3})	k_La (s^{-1})	$k \times 10^{-3}$ [(mol dm^{-3})$^{1-m-n}$ s^{-1}]	m (–)	n (–)	r^2 (–)	E (–)
5	0.119	0.0137	0.1376	1.12	0.89	0.993	7.10
7	0.086	0.0159	0.1378	1.22	0.84	0.989	7.28
9	0.069	0.0215	0.1382	1.21	0.97	0.992	5.85

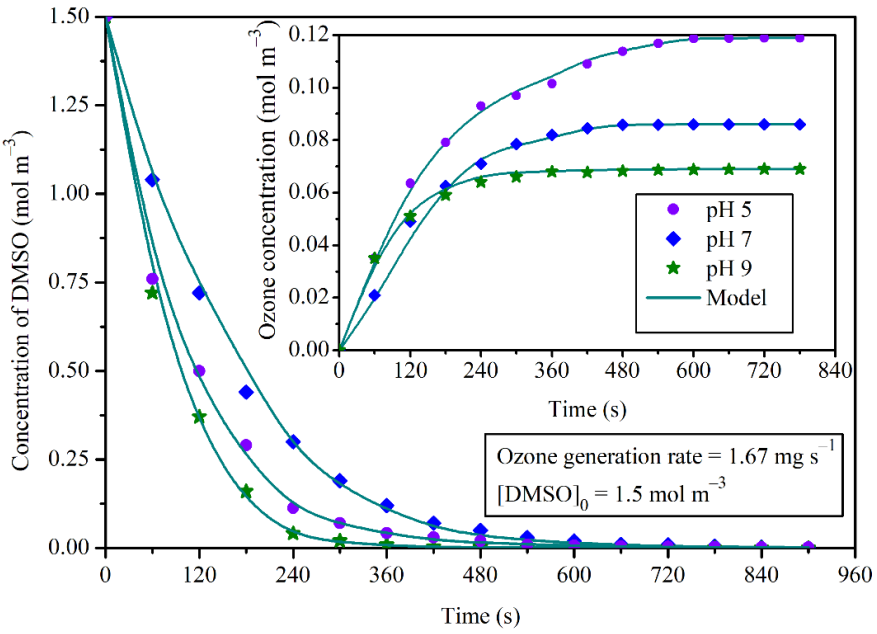

Figure 6.10: Concentration profiles of DMSO and dissolved ozone (inset) in the reactor, and the fit of the model. The legends are the same for both the systems.

6.2.7 Overall kinetic study for the oxidation of DMSO by the OMLBs

On the contrary to the OMBs, oxidation of DMSO by OMLBs did not fit the second-order reaction model. Assuming the first-order kinetics, the reaction rate between DMSO and ozone is given by Equation (6.9) (Li et al., 2009).

$$\frac{\mathrm{d[DMSO]}}{\mathrm{d}t} = -k_L a \left(\frac{D_{\mathrm{DMSO}}}{D_{\mathrm{O_3}}} [\mathrm{DMSO}] \right) \tag{6.9}$$

where D_{DMSO} and $D_{\mathrm{O_3}}$ are the diffusivities of DMSO and ozone in water, respectively. Assuming that these diffusivities and $k_L a$ remain constant during the ozonation, by re-arranging and integrating Equation (6.9), we get.

$$\ln\left(\frac{[\mathrm{DMSO}]_0}{[\mathrm{DMSO}]} \right) = \left(k_L a \frac{D_{\mathrm{DMSO}}}{D_{\mathrm{O_3}}} \right) t = k_{\mathrm{obs}} t \tag{6.10}$$

where

$$k_L a = k_{\mathrm{obs}} \left(\frac{D_{\mathrm{O_3}}}{D_{\mathrm{DMSO}}} \right) \tag{6.11}$$

If there is a linear relationship between $\ln\left(\frac{[\mathrm{DMSO}]_0}{[\mathrm{DMSO}]} \right)$ and the ozonation time t, k_{obs} may be determined from the slope of the line (Figure 6.11). At the temperature of the aqueous solution in the reactor (i.e., 298 K), the value of $D_{\mathrm{O_3}}$ is 1.89×10^{-9} m^2 s^{-1} (see Section 3.2.10). The value of D_{DMSO} is 6.1×10^{-10} m^2 s^{-1} (Vishnyakov et al., 2001). The values of k_{obs} and the corresponding values of $k_L a$ computed from Equation (6.11) are given in Table 6.4.

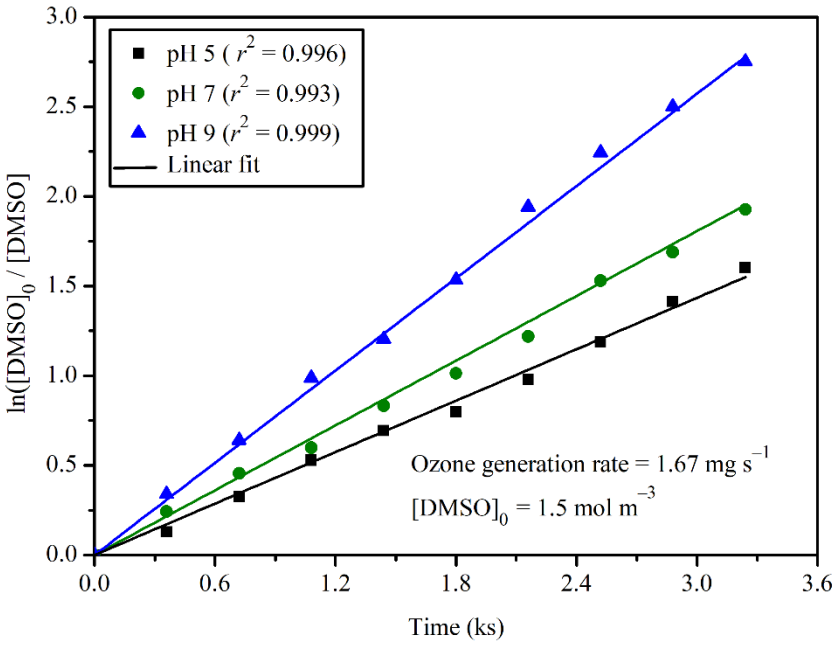

Figure 6.11: Fit of the first-order kinetics for the reaction between DMSO and ozone in the OMLB system.

Table 6.4: Kinetic and mass transfer parameters for the oxidation of DMSO by the OMLBs (at the ozone generation rate of 1.67 mg s^{-1} and $[DMSO]_0$ = 1.5 mol m^{-3})

pH	$[O_3]_{ss}$ (mol m^{-3})	$k_{obs} \times 10^3$ (s^{-1})	$k_L a \times 10^3$ (s^{-1})	r^2 (–)	$k_d \times 10^3$ (s^{-1})	$(k_L a)_0 \times 10^3$ (s^{-1})	E (–)
5	0.026	0.283	0.88	0.996	0.212	0.46	1.22
7	0.019	0.593	1.84	0.993	0.362	0.79	1.49
9	0.015	1.986	6.15	0.999	0.488	1.18	3.35

6.2.8 Mass transfer of ozone by the millibubbles

In this section, studies on the mass transfer of ozone in the millibubble systems is reported for a non-reacting system (i.e., in the absence of DMSO). The concentration profiles of dissolved ozone in water for the OMLB system at different pH of the solution are depicted

in Figure 6.12 (a). The saturation concentration of dissolved ozone ($[O_3]_{ss}$) decreased with increasing pH of the solution. This is because ozone decomposes into the ·OH rapidly in the alkaline medium, which reduces the $[O_3]_{ss}$ in the solution. Nevertheless, the alkaline condition may result in a higher gradient in the ozone concentration between the two phases (i.e., gas and liquid), which is the main driving force for the mass transfer of ozone (Xiong et al., 2019).

Equation (6.12) can be used for our thoroughly-mixed semi-batch reactor to estimate the $(k_L a)_0$ (Khuntia et al., 2012b).

$$\frac{d[O_3]}{dt} = [(k_L a)_0 + k_d]([O_3]_{ss} - [O_3]) \tag{6.12}$$

This mass balance equation can be integrated with the initial condition (i.e., at $t = 0$, $[O_3]_{ss} = 0$), which gives Equation (6.13).

$$\ln\left(\frac{[O_3]_{ss}}{[O_3]_{ss} - [O_3]}\right) = [(k_L a)_0 + k_d]\, t \tag{6.13}$$

Therefore, if the plot of $\ln\left(\frac{[O_3]_{ss}}{[O_3]_{ss} - [O_3]}\right)$ versus t is a straight line passing through the origin [as shown in Figure 6.12 (b)], the slope of this line would give $[(k_L a)_0 + k_d]$ (Khuntia et al., 2012b). For the OMLB system, the value of k_d is determined later in this section. The values of $(k_L a)_0$, which are given in Table 6.4, are in agreement with the earlier reports (Kukuzaki et al., 2010). As shown later in this section, k_d increased with the pH of the medium, thereby enhancing the rate of mass transfer of ozone [i.e., increased $(k_L a)_0$].

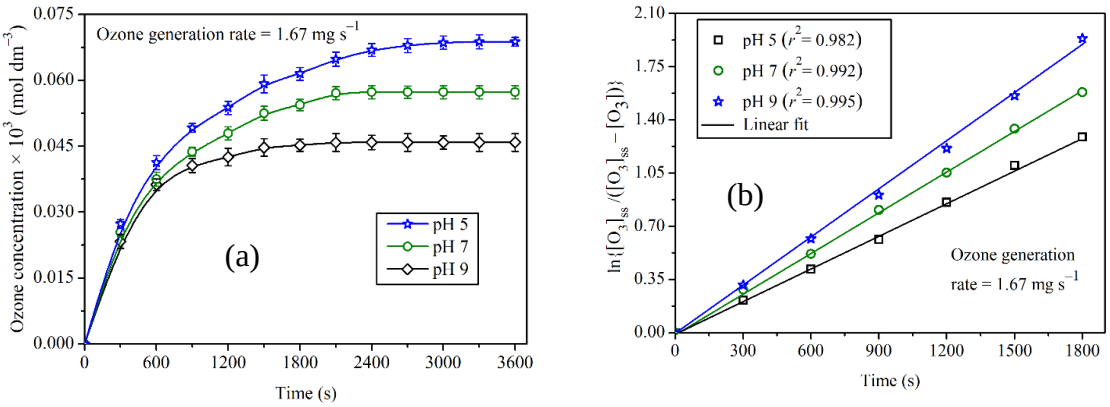

Figure 6.12: (a) Concentration profile of dissolved ozone in the reactor of the OMLB system and **(b)** determination of the volumetric mass transfer coefficient of ozone in the OMLB system in the absence of DMSO.

The values of k_d for the non-reacting OMB system have been reported in Section 3.2.8. k_d for the OMLB system was determined by following a similar procedure. Several works have reported that the self-decomposition of ozone in water follows a first-order kinetics, and it mainly depends on the pH of the medium (Beltrán, 2004; Sotelo et al., 1987; Sotelo et al., 1989). Equation (3.1) gives the rate equation for the self-decomposition reaction (Gao et al., 2005; Kukuzaki et al., 2010; Rosal et al., 2006). Therefore, if the plot of $\ln\left(\frac{[O_3]_{ss}}{[O_3]}\right)$ versus t is a straight line passing through the origin (as shown in Figure 6.13), the slope of this line would give k_d. The fit of the first-order kinetic model to the experimental data is shown in Figure 6.13. The values of k_d, given in Table 6.4, show that they increased with the pH of the medium, corroborating with the literature (Sotelo et al., 1987) and our earlier work using the OMBs (Section 3.2.8).

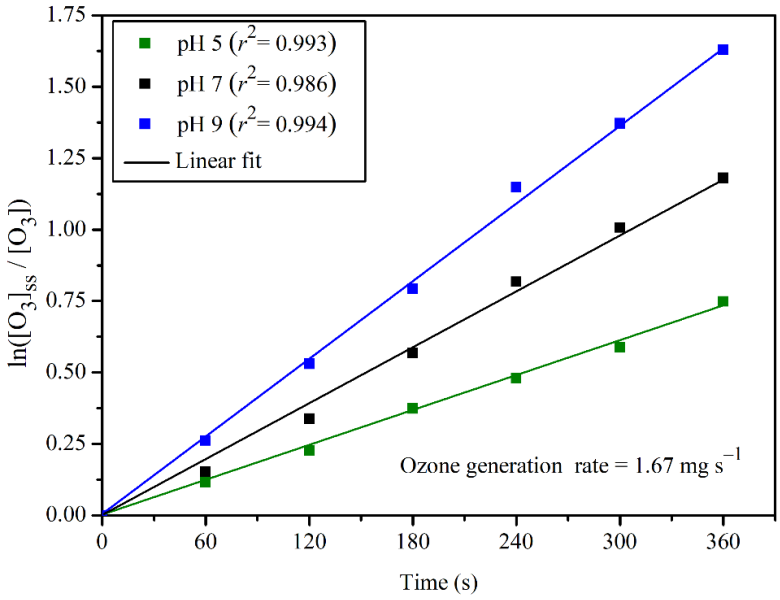

Figure 6.13: The fit of the first-order kinetic model to the experimental data for determining the self-decomposition rate constant of ozone in water by the millibubbles.

Table 6.5 presents a summary of the values of k_d reported in the literature. The values of k_d obtained in this study fall within the range of the values given in Table 6.5, and they are slightly higher than our earlier results for the OMBs (Table 3.1). As the microbubbles improve the stability of ozone in the solution, OMBs are more persistent in the solution as compared to the OMLBs. Ozone is less stable in the OMLB system, and it quickly decomposes to oxygen, resulting in the higher values of k_d. It has been reported (Hu and Xia, 2018) that the average half-life for the OMLB system was ~60 s, whereas it was ~600 s for the OMB system.

The volumetric ozone transfer rate (VOTR), which was obtained from the product of the volumetric mass transfer coefficient and the steady state concentration of ozone (i.e., $\text{VOTR} = k_L a\left([\text{O}_3]_{ss}\right)$ (Chu et al., 2008a; Khuntia et al., 2012a) at different pH of the solutions, were higher for the OMB system. This is shown in Figure 6.14. This result is

in agreement with the work of Chu et al. (2008a), who have reported that the microbubble generators exhibited a higher gas transfer rate as compared to conventional bubble diffusers. As the effectiveness of ozonation is dependent on the ozone transfer rate from gas to liquid phase and the concentration of dissolved ozone in the aqueous solution (Panda and Mathews, 2008), the higher VOTR and $k_L a$ obtained in this work demonstrate the effectiveness of the OMB system for the ozonation of DMSO.

Table 6.5: Reported values of the self-decomposition rate constant of ozone (k_d) in water

$k_d \times 10^3$ (s^{-1})	Reactor type	pH	Reference
0.04	Karman contactor (static mixer)	7	Gao et al. (2005)
0.21 – 0.42	Glass vessel (bubble column)	2.5 – 9	Sotelo et al. (1987)
0.21 – 0.54	Gas-inducing reactor	2.6 – 7	Hsu et al. (2002)
0.42	Shirasu porous glass (ozone–water membrane contactor)	Unspecified	Kukuzaki et al. (2010)

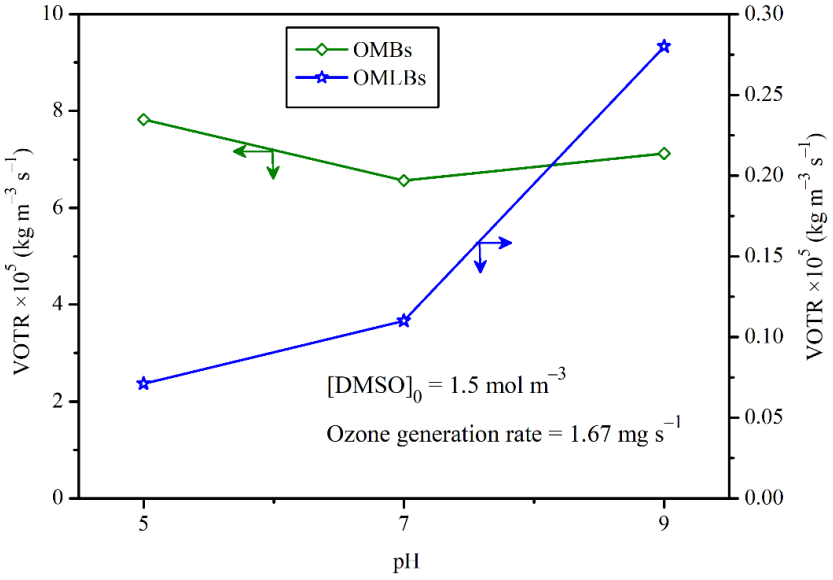

Figure 6.14: Volumetric ozone transfer rate in the presence of DMSO for the OMB and OMLB systems.

6.3 Conclusions

The following conclusions were reached based on the experimental studies and the analysis of the results.

- DMSO present in water was effectively removed by the OMBs, and a longer time was required for the OMLBs.
- Keeping other operational parameters (i.e., initial concentration of DMSO, ozone generation rate, and initial pH of the medium) constant for both the OMB and OMLB systems, the latter needed a longer time for the complete removal of DMSO, and consequently, a higher consumption of ozone. Therefore, a higher stoichiometric ratio of ozone consumed to DMSO removed (i.e., a ratio of 10) was obtained for the OMLBs.
- Higher ozone utilization efficiencies (i.e., 65 – 79%) were observed for the OMBs, whereas, the same for the OMLBs was only 21 – 48%.
- The addition of H_2O_2 slightly increased the rate of removal of DMSO by augmenting the generation of the ·OH radicals. However, a large dosage of H_2O_2 had an adverse effect on the rate of removal of DMSO for both ozonation systems. The optimal ratio (i.e., $[H_2O_2]/[DMSO]_0$) was 2.0 and 3.0 for the OMBs and OMLBs, respectively.
- For the OMBs, the contribution of ·OH was significant at pH 5 and 9, indicating that the microbubbles enhanced the generation of ·OH both in the acidic and alkaline solutions. Addition of *t*-BuOH proved that there was no contribution of ·OH at pH 5 for the OMLB system, and very little effect was observed at pH 9.
- The degradation of DMSO to MSA was achieved via two possible pathways. The first pathway was the direct conversion by the reaction with the ·OH. In the second pathway, DMSO was first converted to $DMSO_2$ by direct oxidation with the ozone

molecule, and then $DMSO_2$ was further oxidized to MSA by the ·OH. During the ozonation using the OMLBs, hardly any formation of MSA was observed.

- OMLBs displayed a very poor efficiency in TOC removal. In terms of TOC removal efficiency, the order of effectiveness was as follows: OMLBs < OMLBs/H_2O_2 < OMBs < OMBs/H_2O_2.
- Oxidation of DMSO by ozone followed the second-order kinetics for the OMB system, and the first-order kinetics was observed for the OMLB system. Higher values of the volumetric mass transfer coefficient of ozone, enhancement factor, and volumetric ozone transfer rate were observed for the OMBs than the OMLBs.
- In general, it can be concluded that the OMBs were more efficient than the OMLBs in terms of ozone utilization efficiency, efficient removal of DMSO within a short ozonation time, and TOC removal.

Notations

a	specific gas–liquid interfacial area ($m^2\ m^{-3}$)
[DMSO]	unreacted concentration of DMSO in the reactor at reaction time, t (mol m^{-3})
$[DMSO]_0$	initial concentration of DMSO in the reactor (mol m^{-3})
$[DMSO]_{rem}$	number of moles of DMSO removed within desired ozonation time, t_d (mol)
D_{DMSO}	diffusivity of DMSO in water ($m^2\ s^{-1}$)
D_{O_3}	diffusivity of ozone in water ($m^2\ s^{-1}$)
E	enhancement factor (–)
k	rate constant for the reaction of DMSO with ozone [(mol $dm^{-3})^{1-m-n}\ s^{-1}$]
k_d	self-decomposition rate constant of ozone (s^{-1})
k_La	volumetric mass transfer coefficient of ozone in the reacting system (s^{-1})
$(k_La)_0$	volumetric mass transfer coefficient of ozone in the non-reacting system (s^{-1})
k_{obs}	observed reaction rate constant ($dm^3\ mol^{-1}\ s^{-1}$)
m	order of reaction with respect to DMSO (–)
n	order of reaction with respect to ozone (–)
$[O_3]$	concentration of ozone during the reaction (mol m^{-3})
$[O_3]_\infty$	total influent concentration of ozone at the desired ozonation time t_d (mol m^{-3})

$[O_3]_{abs}$	number of moles of ozone absorbed by the solution within the desired ozonation time, t_d (mol)
$[O_3]_{exc}$	excess effluent ozone concentration at reaction time, t (mol m^{-3})
$[O_3]_{res}$	residual dissolved ozone concentration in the solution at desired ozonation time, t_d (mol m^{-3})
$[O_3]_{ss}$	steady state concentration of ozone in the aqueous phase (mol m^{-3})
r	correlation coefficient (–)
S_R	stoichiometric ratio (–)
t_d	ozonation time needed to reach the desired removal efficiency (s)
$[TOC]_0$	initial amount of the total organic carbon (mg dm^{-3})
$V_g^{O_3}$	volumetric flow rate of ozone (m^3 s^{-1})
V_r	total volume of the reactor (m^3)

Greek symbols	
η_u	utilization efficiency of ozone

Abbreviations	
DMSO	dimethyl sulfoxide
$DMSO_2$	dimethyl sulfone
MSA	methane sulfonic acid
OMBs	ozone microbubbles
OMLBs	ozone millibubbles
TOC	total organic carbon
UV	ultraviolet

VOTR	volumetric ozone transfer rate

References

Baldoni-Andrey, P., Commarieu, A., Plisson-Saune, S., **2005**. Treatment of Wastewater Containing Dimethyl Sulfoxide (DMSO), in: Lichtfouse, E., Schwarzbauer, J., Robert, D. (Eds.), *Environmental Chemistry: Green Chemistry and Pollutants in Ecosystems*. Springer Berlin Heidelberg, Berlin (Germany), pp. 615–620.

Beltrán, F.J., **2004**. Ozone Reaction Kinetics for Water and Wastewater Systems, 1st ed. Lewis Publishers, Boca Raton (USA).

Chou, M.S., Chang, K.L., **2007**. Oxidation of aqueous dimethyl sulfoxide (DMSO) using UV, O_3, and UV/O_3. *Ozone Sci. Eng.*, *29*, 391–397.

Chu, L.B., Xing, X.H., Yu, A.F., Sun, X.L., Jurcik, B., **2008a**. Enhanced treatment of practical textile wastewater by microbubble ozonation. *Process Saf. Environ. Prot.*, *86*, 389–393.

Chu, L.B., Yan, S.T., Xing, X.H., Yu, A.F., Sun, X.L., Jurcik, B., **2008b**. Enhanced sludge solubilization by microbubble ozonation. *Chemosphere*, *72*, 205–212.

Gao, M., Hirata, M., Takanashi, H., Hano, T., **2005**. Ozone mass transfer in a new gas–liquid contactor – Karman contactor. *Sep. Purif. Technol.*, *42*, 145–149.

Garoma, T., Matsumoto, S., **2009**. Ozonation of aqueous solution containing bisphenol A: effect of operational parameters. *J. Hazard. Mater.*, *167*, 1185–1191.

Glaze, W.H., Kang, J.W., **1989**. Advanced oxidation processes. Description of a kinetic model for the oxidation of hazardous materials in aqueous media with ozone and hydrogen peroxide in a semibatch reactor. *Ind. Eng. Chem. Res.*, *28*, 1573–1580.

Hsu, Y.C., Chen, T.Y., Chen, J.H., Lay, C.W., **2002**. Ozone transfer into water in a gas-inducing reactor. *Ind. Eng. Chem. Res.*, *41*, 120–127.

Hu, L., Xia, Z., **2018**. Application of ozone micro-nano-bubbles to groundwater remediation. *J. Hazard. Mater.*, *342*, 446–453.

Khuntia, S., Majumder, S.K., Ghosh, P., **2012a**. Microbubble-aided water and wastewater purification: a review. *Rev. Chem. Eng.*, *28*, 191–221.

Khuntia, S., Majumder, S.K., Ghosh, P., **2012b**. Removal of ammonia from water by ozone microbubbles. *Ind. Eng. Chem. Res.*, *52*, 318–326.

Koito, T., Tekawa, M., Toyoda, A., **1998**. A novel treatment technique for DMSO wastewater. *IEEE Trans. Semicond.*, *11*, 3–8.

Kukuzaki, M., Fujimoto, K., Kai, S., Ohe, K., Oshima, T., Baba, Y., **2010**. Ozone mass transfer in an ozone–water contacting process with Shirasu porous glass (SPG)

membranes – a comparative study of hydrophilic and hydrophobic membranes. *Sep. Purif. Technol., 72*, 347–356.

Li, P., Tsuge, H., Itoh, K., **2009**. Oxidation of dimethyl sulfoxide in aqueous solution using microbubbles. *Ind. Eng. Chem. Res., 48*, 8048–8053.

Liu, Y., Wang, S., Shi, L., Lu, W., Li, P., **2020**. Enhanced degradation of atrazine by microbubble ozonation. *Environ. Sci. Water Res. Technol., 6*, 1681–1687.

Marce, M., Domenjoud, B., Esplugas, S., Baig, S., **2016**. Ozonation treatment of urban primary and biotreated wastewaters: impacts and modeling. *Chem. Eng. J., 283*, 768–777.

Panda, K.K., Mathews, A.P., **2008**. Mass transfer of ozone in a novel *in situ* ozone generator and reactor. *J. Environ. Eng., 134*, 860–869.

Rosal, R., Rodríguez, A., Zerhouni, M., **2006**. Enhancement of gas–liquid mass transfer during the unsteady-state catalytic decomposition of ozone in water. *Appl. Catal. A, 305*, 169–175.

Scaduto, R.C., **1995**. Oxidation of DMSO and methanesulfinic acid by the hydroxyl radical. *Free Radical Biol. Med., 18*, 271–277.

Sotelo, J.L., Beltran, F.J., Benitez, F.J., Beltran-Heredia, J., **1987**. Ozone decomposition in water: kinetic study. *Ind. Eng. Chem. Res., 26*, 39–43.

Sotelo, J.L., Beltrán, F.J., Benitez, F.J., Beltrán-Heredia, J., **1989**. Henry's law constant for the ozone–water system. *Water Res., 23*, 1239–1246.

Vishnyakov, A., Lyubartsev, A.P., Laaksonen, A., **2001**. Molecular dynamics simulations of dimethyl sulfoxide and dimethyl sulfoxide−water mixture. *J. Phys. Chem. A, 105*, 1702–1710.

Wu, J.J., Muruganandham, M., Chen, S.H., **2007**. Degradation of DMSO by ozone-based advanced oxidation processes. *J. Hazard. Mater., 149*, 218–225.

Xiong, X., Wang, B., Zhu, W., Tian, K., Zhang, H., **2019**. A review on ultrasonic catalytic microbubbles ozonation processes: properties, hydroxyl radicals generation pathway and potential in application. *Catalysts, 9*, 10–28.

CHAPTER 7

SUMMARY AND SCOPE OF FUTURE WORKS

This chapter presents the brief summary of the thesis, and scope and suggestions for future works.

7.1 Summary of the work

The removal of DMP, DEP, BPA, and DMSO from water using ozone microbubbles were studied in an experimental setup with a reactor of 20 dm^3 capacity. Experiments were performed under various reaction conditions to examine the effects of the initial concentration of the pollutants, pH of the medium, and ozone generation rate. The role of hydroxyl radicals in the oxidation of the target pollutants was studied using *t*-butyl alcohol as the hydroxyl radical scavenger. The effect of addition of H_2O_2 and sodium bicarbonate also examined in the OMB system. The extent of mineralization of the target pollutants was studied from the TOC measurements. The stoichiometric ratio of ozone consumed to the pollutant removed, and the ozone utilization efficiency of the OMBs system were computed from the experimental results. The enhancement factor, Hatta number, volumetric mass transfer coefficient, and the rate constant of the reaction between the pollutants and ozone were determined. The potential of the OMBs for the oxidation of DMSO was investigated in detail, and the results were compared with those of the conventional ozonation using the OMLBs.

DMP, DEP, BPA, and DMSO present in water were effectively removed by the OMBs. The OMB system needed a shorter ozonation time for complete removal of the

targeted pollutant. Lower values of the stoichiometric ratio were obtained, possibly due to the high rate of mass transfer of ozone into the aqueous phase in the OMB system. A considerably high range of ozone utilization efficiency was achieved for the complete removal of the pollutants. The optimal addition of H_2O_2 increased the rate of removal of the pollutants by augmenting the generation of the hydroxyl radicals. A better TOC removal efficiency was observed in the OMB system as compared to the conventional ozonation. In terms of the TOC removal efficiency, the effectiveness was in the following order: OMLBs < OMLBs/H_2O_2 < OMBs < OMBs/H_2O_2. Very low values of the Hatta number were obtained, which proves that the mass transfer resistance was negligible, implying that the rate of mass transfer was enhanced by the OMBs. Higher ozone volumetric mass transfer coefficient, enhancement factor, and volumetric ozone transfer rate were obtained for the OMBs as compared to the OMLBs.

7.2 Scope and suggestions for future works

In future, the following works can be carried out for the practical use of the process:

- Experiments can be conducted at different temperatures to verify the effect of temperature. Different types of vessels, suitable for practical use, can be used as reactors.
- The detailed reaction mechanisms can be studied by analyzing more oxidation intermediates and reaction pathways.
- Catalysts such as metal ions can be used with the OMBs to enhance the generation of the hydroxyl radicals.
- Based on the remarkable properties of the boron-doped diamond electrodes (i.e., large overvoltage for water electrolysis, high chemical and electrochemical

stability, and high current yield for the generation of the hydroxyl radicals *in situ*), they can be used along with the OMBs to improve the oxidation of the organic pollutants.

Research publications

Referred journals

[1] Jabesa, A., Ghosh, P., **2016**. Removal of diethyl phthalate from water by ozone microbubbles in a pilot plant. *J. Environ. Manage.*180, 476–484.

[2] Jabesa, A., Ghosh, P., **2017**. Removal of dimethyl phthalate from water by ozone microbubbles. *Environ. Technol.*, 38, 2093–2103.

[3] Jabesa, A., Ghosh, P., **2021**. A comparative study on the removal of dimethyl sulfoxide from water using microbubbles and millibubbles of ozone. *J. Water Process Eng.*, 40, 101937.

[4] Jabesa, A., Ghosh, P., **2021**. Oxidation of bisphenol-A by ozone microbubbles: effects of operational parameters and kinetics study. *Environ. Technol., Innov.* (Manuscript submitted, ETI-D-21-00994).

Conference

[1] Jabesa, A., Ghosh, P., Degradation study of dimethyl phthalate using ozone microbubbles, Indian Chemical Engineering Congress (CHEMCON 2015), Indian Institute of Technology Guwahati, 27–30 December, 2015 (*Poster presented*).

Appendix A1

Sample uncertainty analysis

Equation (A1.1) gives the mean value ($\bar{x}$) of the experimentally measured data.

$$\bar{x} = \frac{1}{N}\sum_{i=1}^{N} x_i \tag{A1.1}$$

where N is the total number of measurements and x_i is the measured value. The standard deviation (STD) of the measured data was computed from Equation (A1.2).

$$STD = \sqrt{\frac{\sum_{i=1}^{N}(x_i - \bar{x})^2}{N-1}} \tag{A1.2}$$

The relative standard deviations (i.e., % RSD) of the measured data was computed from Equation (A1.3).

$$\text{RSD (\%)} = \left(\frac{\text{STD}}{\bar{x}}\right)\times 100 \tag{A1.3}$$

The standard and relative uncertainties of the measured data were estimated from Equations (A1.4) and (A1.5), respectively.

$$\text{Standard uncertainty} = \frac{\text{STD}}{\sqrt{N}} \tag{A1.4}$$

$$\text{Relative uncertainty} = \frac{1}{\bar{x}}\left(\frac{\text{STD}}{\sqrt{N}}\right)\times 100 \tag{A1.5}$$

The mean, standard deviation, relative standard deviation, and standard and relative uncertainties of the measured peak areas of BPA by UFLC, and their respective retention times are shown in Tables A1.1 and A1.2, respectively.

Table A1.1: Sample uncertainty analysis for the measurement of BPA using UFLC

$[BPA]_0$ (μmol m^{-3})	UFLC peak area (μV s)					% RSD	Standard uncertainty	Relative uncertainty (%)
	Trial 1	Trial 2	Trial 3	$\bar{x}$	STD			
0.0004	11239.0	11501.6	11393.8	11378.1	131.98	1.160	76.20	0.67
0.0044	55285.0	55794.8	55160.9	55413.5	335.92	0.606	193.95	0.35
0.0438	409605.0	410632.5	402589.7	407609.1	4377.12	1.074	2527.13	0.62
0.0876	767071.0	762116.4	765064.7	764750.7	2492.20	0.326	1438.87	0.19
0.1314	1150606.5	1143174.5	1147597.0	1147126.0	3738.30	0.326	2158.31	0.19

Table A1.2: Sample uncertainty analysis of the retention time for the measurement of BPA using UFLC

$[BPA]_0$ (μmol m^{-3})	UFLC retention time (s)					% RSD	Standard uncertainty	Relative uncertainty (%)
	Trial 1	Trial 2	Trial 3	$\bar{x}$	STD			
0.0004	311.6	315.8	313.9	313.8	2.10	0.67	1.21	0.39
0.0044	312.0	312.1	311.6	311.9	0.25	0.08	0.14	0.05
0.0438	313.1	312.9	314.0	313.3	0.56	0.18	0.32	0.10
0.0876	311.5	312.8	315.9	313.4	2.18	0.70	1.26	0.40
0.1314	313.8	311.4	313.1	312.8	1.23	0.39	0.71	0.23

Appendix A2

Cost estimation of the ozone microbubble setup

The estimated capital and running cost of the OMB setup is given below. The summary of capital costs of the main units is given in Table A2.1. The main operation cost of this experimental setup would be the cost of electricity, which is summarized in Table A2.2.

Table A2.1: Capital cost of the OMB experimental setup

Item	Cost (INR)
Microbubble generator	4,51,500
Ozone generation system (oxygen concentrator, ozone generator, ozone destructor, step-down transformer, and voltage stabilizer)	2,51,990
Water circulatory bath	2,00,000
Total cost	9,03,490

Table A2.2: Operational cost of the OMB experimental setup

Item	Power consumption (W)	Hours/month*	Electricity consumption (kWh)
Microbubble generator	450	125**	56.25
Oxygen concentrator	350	120	42.00
Ozone generator	205	120	24.60
Step-down transformer	300	120	36.00
Water circulatory bath	230	120	27.60
Total units (kWh)			186.45

*Average operating hours; **Includes 5 hours for cleaning

In 2020, the cost of electricity for one unit in Assam state is 6.95 INR. Therefore, the estimated total operating cost of the OMB system for purifying 1200 dm^3 water per month is 1296 INR.